AD-A155 605 PERMEATION OF MIXED PENETRANTS THROUGH GLASSY POLYMER 1/3
MEMBRANES(U) NORTH CAROLINA STATE UNIV AT RALEIGH
R T CHERN ET AL. 15 MAR 85 ARO-17773.15-CH
UNCLASSIFIED DAAG29-81-K-0039 F/G 11/9 NL

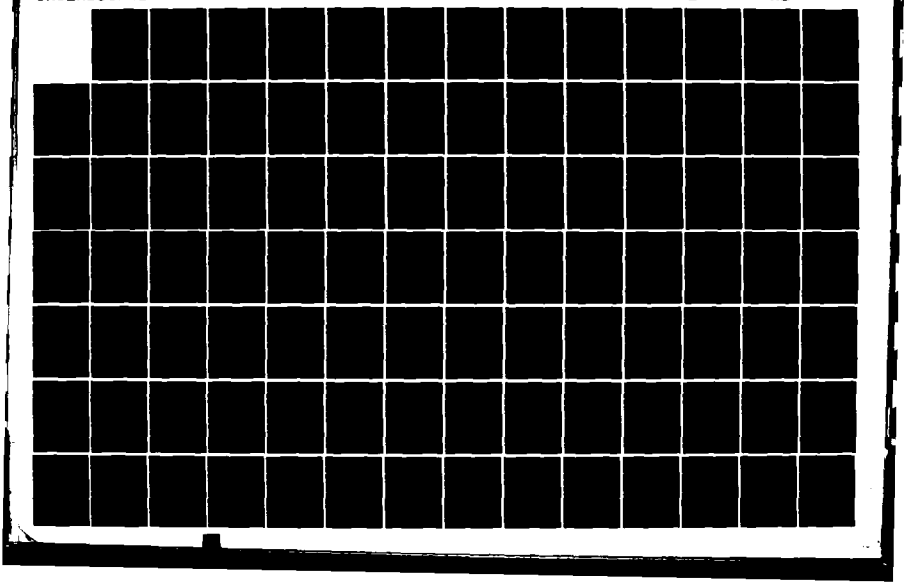

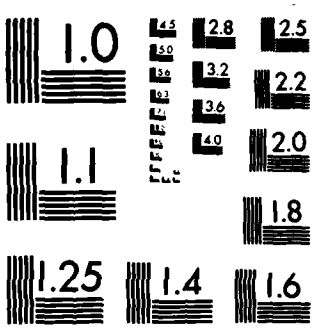

MICROCOPY RESOLUTION TEST CHART
NATIONAL BUREAU OF STANDARDS-1963-A

UNCLASSIFIED
SECURITY CLASSIFICATION OF THIS PAGE (When Data Entered)

MASTER COPY - FOR REPRODUCTION PURPOSES

AD-A155 605

DTIC FILE COPY

REPORT DOCUMENTATION PAGE

READ INSTRUCTIONS BEFORE COMPLETING FORM

1. REPORT NUMBER: ARO 17773.15-CH	2. GOVT ACCESSION NO.: N/A
3. RECIPIENT'S CATALOG NUMBER: N/A	
4. TITLE (and Subtitle): Permeation of Mixed Penetrants Through Glassy Polymer Membranes	5. TYPE OF REPORT & PERIOD COVERED: Final Report 2/81 - 1/85
	6. PERFORMING ORG. REPORT NUMBER:
7. AUTHOR(s): Chern, Rey T.; Hopfenberg, Harold B.; Stannett, Vivian T.	8. CONTRACT OR GRANT NUMBER(s): DAAG29-81-K-0039
9. PERFORMING ORGANIZATION NAME AND ADDRESS: North Carolina State University, Raleigh, NC 27695	10. PROGRAM ELEMENT, PROJECT, TASK AREA & WORK UNIT NUMBERS:
11. CONTROLLING OFFICE NAME AND ADDRESS: U. S. Army Research Office, Post Office Box 12211, Research Triangle Park, NC 27709	12. REPORT DATE: 3/15/1985 13. NUMBER OF PAGES: 243
14. MONITORING AGENCY NAME & ADDRESS (if different from Controlling Office)	15. SECURITY CLASS. (of this report): Unclassified 15a. DECLASSIFICATION/DOWNGRADING SCHEDULE:

16. DISTRIBUTION STATEMENT (of this Report)

Approved for public release; distribution unlimited.

DTIC ELECTE JUN 25 1985 D A

17. DISTRIBUTION STATEMENT (of the abstract entered in Block 20, if different from Report)

NA

18. SUPPLEMENTARY NOTES

The view, opinions, and/or findings contained in this report are those of the author(s) and should not be construed as an official Department of the Army position, policy, or decision, unless so designated by other documentation.

19. KEY WORDS (Continue on reverse side if necessary and identify by block number)

- permeation
- membrane
- gas separation
- dual mode model
- polyimide
- fluorination
- glassy polymer
- sorption
- diffusion

20. ABSTRACT (Continue on reverse side if necessary and identify by block number)

This report summarizes the results of research activities supported by the Army Research Office grant DAAG29-81-K-0039. Three important areas were investigated: (1) Selective permeation of mixed gaseous penetrants in glassy polymers; (2) Transport of a reactive penetrant in polymers; and (3) Effects of chemical modification resulted from exposure to reactive penetrants on the permeability of the polymer to permanent gases.

(Cont.)

DD FORM 1 JAN 73 1473 EDITION OF 1 NOV 65 IS OBSOLETE

UNCLASSIFIED
SECURITY CLASSIFICATION OF THIS PAGE (When Data Entered)

20.

The results of the first study indicated that the penetrants in a gaseous mixture compete with each other for diffusion paths provided by the microvoid sorption sites existing typically in a glassy polymer when the polymer was vitrified. The permeability to a given penetrant in a mixture is depressed from its pure-component value simply due to the competition effect.

In the second area, we found that polyimide, often quoted for its chemical stability, is susceptible to attack by a strong nucleophile, ammonia. Numerical solutions for a multiple-reaction/diffusion model were reported for describing the penetration of this reactive penetrant into Kapton polyimide films. We further found that the permeability of the ammonia-treated polyimide film to a series of permanent gases is greatly reduced compared with that of the pristine film. This reduction in permeability is caused by a substantial decrease in the diffusivity rather than in the solubility of the penetrant.

Finally, through ESCA and permeability measurements, we demonstrated that high-temperature fluorination of polyethylene, which gives a relatively well-defined surface fluorinated layer, is controlled by the diffusion rate of fluorine. On the other hand, room temperature fluorination tends to be reaction-controlled and results in a distribution of fluorine atoms throughout the thickness of the film. This latter process was demonstrated to be ineffective in improving the barrier properties of both HDPE and LDPE to a series of liquid penetrants with cohesive energy ranging from 8 to 9 $(cal/cm^3)^{1/2}$.

PERMEATION OF MIXED PENETRANTS THROUGH GLASSY POLYMER MEMBRANES

FINAL REPORT

R. T. CHERN, H. B. HOPFENBERG, AND V. T. STANNETT

March 15, 1985

U. S. ARMY RESEARCH OFFICE

GRANT NUMBER: DAAG29-81-K-0039

NORTH CAROLINA STATE UNIVERSITY
RALEIGH, NC 27695

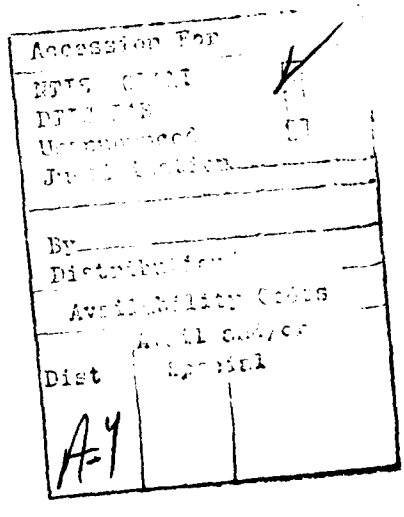

APPROVED FOR PUBLIC RELEASE;
DISTRIBUTION UNLIMITED

85 06 6 107

THE VIEW, OPINIONS, AND/OR FINDINGS CONTAINED IN THIS REPORT ARE THOSE OF THE AUTHORS AND SHOULD NOT BE CONSTRUED AS AN OFFICIAL DEPARTMENT OF THE ARMY POSITION, POLICY, OR DECISION, UNLESS SO DESIGNATED BY OTHER DOCUMENTATION.

FOREWORD

This report summarizes the results of research activities supported by the Army Research Office grant DAAG29-81-K-0039. The research objectives outlined in the original proposal were: (1) To design equipment for characterizing the permeability and selectivity of glassy polymers to pure and mixed gases; (2) To provide a data base for mixed-gas permeabilities in glassy polymers; and (3) To test the validity of the proposed "generalized dual-mode" model. This research is expected to lay the ground work for describing the transport behavior of gaseous penetrants, pure or mixed, in glassy polymeric materials.

We have achieved these goals by completing a systematic study on the permeation of CO_2, CH_4 and CO_2/CH_4 mixture in a rigid glassy polymer, Kapton polyimide; and the permeation of CO_2 in the presence of water vapor and isopentane vapor, respectively, in a tough but less rigid glassy polymer, Lexan polycarbonate. The results of these studies indicate that penetrants in a gaseous mixture compete with each other for diffusion paths provided by the microvoid sorption sites existing typically in a glassy polymer when the polymer was vitrified. Manifestation of this competition effect results in the commonly observed "anomaly" for the permeability of glassy polymers to mixed penetrants.

Specifically, the permeability to a given penetrant in a mixture is depressed from its pure-component value simply due to the competition effect. If the penetrants involved have large differences in their

condensibility, the more condensible one tends to swamp the microvoids such that the permeability to the other component is greatly reduced even if the partial pressure of the more condensible penetrant is relatively low. The observed depression of CO_2 permeability in the presence of water or isopentane is a manifestation of this effect although there appears to be complications in addition to the model prediction in the case of water/CO_2 system. These findings have significant implications in describing the selective permeation of polymeric media to gaseous penetrants.

In the course of our studies, we realized that even a rigid, tough polyimide oftenly quoted for its chemical stability is susceptible to attack by a strong nucleophile, ammonia. In order to describe the penetration of ammonia into the Kapton polyimide film, numerical solutions for a multiple-reaction/diffusion model have been obtained. We further find that the permeability of the ammonia-treated film to a series of gases is greatly reduced compared with that of the pristine film. This reduction in permeability is caused by a substantial decrease in the diffusivity of the penetrant in the ammonia-treated films rather than in the solubility of the penetrant, as our data demonstrated. These findings support the feasibility of improving the barrier properties of polymeric materials through minor chemical modification by exposing the polymer to reactive penetrants. These results also lead us to investigate a commercial process, namely the fluorination of polyethylene for improved barrier property to various liquid penetrants, as described below.

Through ESCA and permeability measurements, we found that high-temperature fluorination results in a relatively well-defined surface fluorinated layer, which is controlled by the diffusion rate of fluorine. On the other hand, fluorination of polyethylene films at room temperature tends to be reaction-controlled which results in a distribution of fluorine atoms throughout the thickness of the film. This latter process was demonstrated to be ineffective in improving the barrier properties of both HDPE and LDPE to a series of liquid penetrants with cohesive energy ranging from 8 to 9 $(cal/cm^3)^{1/2}$. We found that the fluorination process alters both the diffusivity and solubility of those penetrants in polyethylene. However, it also tends to decrease the crystallinity of the semicrystalline polymer, which will serve to increase the permeability. As a result, we infer that a concentrated fluorine population on the surface layer is more effective in changing the cohesive energy of the polymer, and there exists an optimal amount of fluorination for barrier property improvement even in the case of high-tempearature fluorination.

As demonstrated by this study, the transport of simple molecules in glassy polymers can be described satisfactorily by the proposed model. However, progressively more complex behavior is expected to arise as more interactive and even reactive penetrants are used. We believe that more involved models which account for the stress field induced by the imbibition of penetrants, and the viscoelasticity of the polymer may be required for describing the transport of larger and more interactive penetrants including some of the chemical warfare agents.

PROBLEMS STUDIED

Three major areas are investigated under the support of this research grant. All are related to the transport of small molecules in polymeric materials. The objectives include barrier-property modification and selective permeation of gaseous penetrants through polymers. The following is a summary of the specific problems studied:

(1) Measurement and modeling of the permeation of superatmospheric pure and mixed gases through glassy polymeric films. Materials used include: CO_2, CH_4, CO_2/CH_4 mixture, CO_2/H_2O mixture, CO_2/isopentane mixture, Lexan polycarbonate, and Kapton polyimide.

(2) Modeling of the diffusion and permeation of interactive and reactive penetrants in glassy polyimide films. Ammonia, a strong nucleophile and water, a strong hydrogen-bonding molecule are the penetrants.

(3) Characterization of the effects of both hot- and cold-fluorination on the barrier properties of high density polyethylene, and the difference between the two processes in terms of the chemical changes in polyethylene caused by the fluorination step.

SUMMARY OF THE MOST IMPORTANT RESULTS

(1) Derived state-of-the-art mathematical models for multicomponent transport of gases in glassy polymers at low and intermediate concentrations (<5 wt%).

(2) Performed confirmatory experiments to demonstrate the basic validity of the theories derived and to suggest areas in which additional work should be done to extend the theories, such as the transport of large, bulky molecules.

(3) Demonstrated that a model based on multiple penetrant-polymer reactions coupled with diffusion is required to describe the degradation of Kapton polyimide in the presence of ammonia. Numerical solutions of the proposed model are obtained using a finite difference technique.

(4) Showed that, although a minor change in the glass transition temperature results from disruption of up to 15% of the imide rings in Kapton by ammonia, the barrier properties of Kapton polymimide to SO_2, CO_2, CH_4, Ar amd O_2 gases are profoundly improved.

(5) Developed a simple, inexpensive permeation cell for testing permeation properties of rubbery polymers to liquids.

(6) Demonstrated by ESCA and permeation testing that the diffusion of fluorine controls the fluorination of polyethylene at high temperatures. This causes a fairly well-defined laminate structure to form and causes significant increases in the barrier properties of polyethylene to penetrants with solubility parameters in the range of 8 to 9 $(cal/cm^3)^{1/2}$.

(7) Demonstrated that reaction controls the fluorination at room temperature, which results in a distribution of fluorination throughout the polyethylene film. This cold fluorination is much less effective for building good barrier properties than the hot fluorination where the fluorine atoms are reacted primarily in the surface region of the film.

The detailed technical information is included in the awarded theses and the thirteen papers published in various technical journals and a handbook. The thesis abstracts, the reprints of the published papers and the accepted manuscripts are included in this report for reference. Only the "table of contents" for publication no. 12 is included due to its large volume.

PUBLICATIONS SUPPORTED BY THIS GRANT

1. Koros W. J., Chern R. T., Stannett V. T. and Hopfenberg H. B., "A Model for Permeation of Mixed Gases and Vapors in Glassy Polymers", J. Polym. Sci., Phys. Ed., Vol.19, 1513(1981).

2. Iler L.R., Laundon R.C. and Koros W.J., "Characterization of Penetrant Interactions in Kapton Polyimide Using A Gravimetric Sorption Technique", J. Appl. Polym. Sci., 27, 1163(1982).

3. Chern R. T., Koros W. J., Hopfenberg H. B. and Stannett V. T., "Reversible Isopentane-Induced Depression of Carbon Dioxide Permeation through Polycarbonate", J. Polym. Sci., Phys. Ed., Vol.21, 753(1983).

4. Chern R. T., Koros W. J., Sanders E. S. and Chen S. H. and Hopfenberg H. B. , "Implications of the Dual-Mode Sorption and Transport Models for Mixed Gas Permeation", ACS Symposium Series, No. 223, 47(1983).

5. Chern R. T., Koros W. J., Sanders E. S. and Yui R., "Second Component Effects in Sorption and Permeation of Gases in Glassy Polymers", J. Membr. Sci., 15, 157(1983).

6. Chern R. T., Koros W. J., Yui R., Hopfenberg H. B. and Stannett V. T., "Selective Permeation of CO_2 and CH_4 Through Kapton Polyimide: Effects of Penetrant Competition and Gas Phase Nonideality", J. Polym. Sci., Phys. Ed., Vol. 22, No. 6, 1061(1984).

7. Al-Hussaini H.S.A., Koros W.J., Howard M. and Hopfenberg H.B., "A Simple Apparatus for Measurement of Liquid Permeabilities through Polymeric Films", Ind. Eng. Chem. Prod. Res. Dev., 23, 2, 317(1984).

8. Patton C.J., Felder R.M. and Koros W.J., "Sorption and Transport of Benzene in Poly(ethylene Terephthalate)", J. Appl. Polym. Sci., 29, 1095(1984).

9. Iler L.R., Koros W.J., Yang D.K. and Yui R., "Sorption and Transport of Physically and Chemically Interacting Penetrants in Kapton Polyimide", in Polyimide, vol. 1, Mittal K.L., Ed., Plenum , 443, 1984.

10. Chern R. T., Koros W. J., Hopfenberg H. B. and Stannett V. T., "Material Selection for Membrane-Based Gas Separations", ACS Symposium 269, Material Science of Synthetic Membranes, Ed. by Lloyd D.R., 1985.

11. Yang D.K., Koros W.J., Hopfenberg H.B. and Stannett V.T., "Sorption and Transport Studies of Water in Kapton Polyimide-Part I.", accepted by J. Appl. Polym. Sci..

12. Koros W.J. and Chern R.T., "Membrane Processes- Gas Separations", Chapter 20, in "Handbook of Separation Process Technology", accepted and to be published by John Wiley & Sons.

13. Chern R. T., Koros W. J. and Fedkiw P. S., "Simulation of A Hollow Fiber Gas Separator: The Effects of Process and Design Variables", accepted by Ind. Eng. Chem. Process Des. Dev..

MANUSCRIPTS IN PREPARATION

1. Yang D.K., Koros W.J., Hopfenberg H.B. and Stannett V.T., "Sorption and Transport Studies of Water in Kapton Polyimide-Part II.", submitted to J. Appl. Polym. Sci..

2. Chern R.T., Hsieh Y.C., Hopfenberg H.B., Stannett V.T., Koros W.J., and Uragami T., "Effects of Ammonolysis on the Sorption and Diffusion of Permanent Gases in Kapton Polyimide", to be submitted to J. Polym. Sci., Polym. Phys. Ed.

3. Chern R.T., Koros W.J., Paul D.R. and Sanders E., "A Compliation of Gas Solubilities in Glassy Polymers based on the Dual-Mode Analysis", to be submitted to J. Chem. Eng. Data.

4. Chern R.T. and Koros W.J., "Selective Permeation of CO_2/CH_4 mixture through Kapton Polyimide", to be submitted to J. Polym. Sci., Polym. Letters.

PARTICIPATING SCIENTIFIC PERSONNEL AND ADVANCED DEGREES AWARDED

Principal Investigators

1. Koros W.J., Professor (1981-1983)
2. Chern R.T., Assistant Professor (1983-)
3. Hopfenberg H.B., Professor
4. Stannett V.T., Professor

Research Assistants

1. Chern R.T., Ph.D., 1983, currently employed as an assistant professor in the Chemical Engineering Department at NC State University
2. Yang D.K., Ph.D., 1984, currently employed as a research associate in the Material Engineering Department at NC State University
3. Iler L.R., MS, 1984, currently employed as a process engineer at Sumitomo Electric Research Triangle, Inc.
4. Yui R., MS, 1984, currently employed as a process engineer at Texas Instrument Co. in Dallas, Texas.
5. Hsieh Y.C., MS, (expected May 1985)
6. Sheu F.R., Ph.D. candidate

THESIS ABSTRACTS

ABSTRACT

CHERN, REY TORN Measurement and Modeling of Mixed Gas Permeation In Glassy Polymers(Under the direction of WILLIAM J. KOROS and HAROLD B. HOPFENBERG).

A theoretical and experimental study of the permeabilities of glassy polymers to both pure and mixed gases is presented in this dissertation.

The permeabilities of 0.3 mil Kapton H polyimide films to pure CO_2, pure CH_4 and mixtures of these two penetrants were measured at three system temperatures(35, 45 and 60°C) as the gas phase pressure was varied systematically between 30 and 600 psia. The pure gas permeabilities decreased with increasing gas pressure and were demonstrated to be amenable to the interpretation of the dual mobility model. For the 32.2% CO_2 in CH_4 mixture, the permeabilities of both CO_2 and CH_4 were lower than their respective pure component values at the corresponding partial pressures. For the 10.37% CO_2 in CH_4 mixture, similar behaviors were observed except that CO_2 permeabilities were slightly higher than the corresponding pure gas values.

The permselectivity of Kapton H to CO_2 over CH_4 dropped as the gas phase pressure was increased and it decreased even more dramatically as the system temperature was increased from 35 to 60°C.

The presence of small mole fractions of condensable vapors such as water and isopentane was found to cause significant depressions in the permeabilities of Kapton H and Lexan polycarbonate to carbon dioxide.

A generalized dual mobility model was developed for the analysis and interpretation of the experimental results. This model was derived based on the postulate that the observed pressure and composition dependencies of the permeabilities are caused by the combined effects of competition between penetrants for a limited microvoid sorption capacity in the glassy polymer and thermodynamic nonideality of the gas phase. A comparison between model predictions and experimental data suggests that mechanisms other than the proposed simple competition may be also operative which act to lower further the individual permeabilities more than the model predictions.

A computer program was developed for simulating the performance of a single hollow fiber membrane gas separator under isothermal conditions. The effects of various process variables such as feed pressure, feed flow rate and feed composition were investigated.

ABSTRACT

ILER, LEWIS RAYMOND. Sorption and Transport of Anhydrous Ammonia in Kapton Poly(ether-diimide). (Under the direction of WILLIAM J. KOROS.)

Measurements of the kinetics and equilibria of NH_3 sorption in 0.1-mil Kapton poly(ether-diimide) films using a highly sensitive quartz spring microbalance are reported at 30, 45, and 60°C for pressures up to 0.80 atmospheres. Sorption/desorption kinetics at 30°C indicated that initial NH_3 exposure to these 0.1-mil etched films resulted in a small undesorbable ammonia component attributed to strong NH_3/polymer interactions, thereby complicating the interpretation of both solubility and kinetic data. However, extremely short exposure times were needed to satisfy sorptive equilibrium in these ultra-thin films, minimizing any substantial polymer/penetrant interactions. For all three temperatures studied, concave curvature of the sorption isotherm to the pressure axis was observed. The so-called "dual mode sorption model" satisfactorily described these equilibrium isotherms. Residual solvent or perhaps unimidized polyamic acid residues present in the 0.1-mil etched films may be responsible for the abnormal Langmuir affinity constant relationship observed as a function of temperature.

NH_3 sorption kinetics in as-received 0.5-mil Kapton films exhibited significant deviations from simple Fickian behavior at 30°C. A large fraction of the initially sorbed ammonia remained in the film after extended periods under vacuum at 30°C indicating significant polymer/penetrant interactions. Infrared analysis of the NH_3-treated film revealed the presence of new carbonyl and nitrogen-hydrogen

stretching peaks, nonexistent in the as-received film. These observations suggest that the sorbed ammonia reacts chemically with a portion of the imide linkages present in the polymer film. The scission reaction appears to involve nucleophilic attack of the backbone imide linkages by ammonia, resulting in the formation of both primary and secondary amides. Rapid attack of NH_3 with uncyclized carboxylic acid groups is believed to be responsible for a small portion of the irreversibly sorbed NH_3 component. These uncyclized carboxylic acid groups arise in the as-received polymer films due to incomplete polyimide curing and are present in small but significant concentrations. The diffusion coefficient of desorption lies approximately 30 times lower than the expected NH_3 mobility determined from strictly size-dependent factors based on diffusion coefficient values of other penetrants in Kapton. The low NH_3 diffusivity value can be explained on the basis of an additional activation energy contribution of approximately 2 kcal/mole, which arises from the need to overcome strong specific NH_3/Kapton interactions prior to executing a diffusional jump, and is of a reasonable order of magnitude for hydrogen bonding interactions.

The general equations for the kinetics of the successive processes of diffusion of a reagent into a film followed by an irreversible chemical reaction were applied to describe actual ammonia uptake in these thin Kapton films. A pseudo first-order chemical reaction expression describes the ammonolysis reaction during relatively short exposure times at both low and high NH_3 pressures in 0.3-mil Kapton films. Significant deviations from the simple pseudo first-order reaction kinetics occur at low extents of imide reaction (6 to 10% bond disruption),

consistent with the existence of a distribution of imide reactivities brought about during the final polyimide solid state curing step. A second-order kinetic expression satisfactorily describes intermediate sorption data but deviates significantly from actual ammonia uptake at much longer times. A model incorporating diffusion and a simplified distribution of reactivities is proposed to describe the sorption data over extended time periods, up to the point at which the ammonolysis reaction asymptotically approaches zero.

The kinetics and equilibria of SO_2, a relatively noninteractive penetrant, in both as-received and NH_3-treated 0.3-mil Kapton polyimide films were measured at 30°C for pressures up to 0.70 atm. The curved isotherms were well described by the dual mode sorption model and were not superimposable before and after ammonia treatment of the polyimide film. Although the resulting sorption/desorption kinetics were Fickian in nature, the apparent mobility of SO_2 in the NH_3-modified film was reduced substantially, due presumably to an increase in the apparent activation energy associated with diffusion as a result of specific SO_2/amide interactions.

Based on infrared analysis of the NH_3-exposed Kapton, heating the polymer sample under vacuum at elevated temperatures caused reformation of most of the originally disturbed imide structures with attendant evolution of ammonia as a condensation product as well as slight chain scission. The NH_3-treated sample regained a portion of its mechanical integrity upon annealing but was more brittle and slightly darker in color than the as-received film.

ABSTRACT

AL-HUSSAINI, HAITHAM SAYED AHMAD. Penetrant Permeation through Fluorinated and Untreated Polyethylene Films. (Under the direction of WILLIAM J. KOROS and H. B. HOPFENBERG.)

The permeabilities of seventeen solvents through 20-mil films of untreated and partially fluorinated high-density and low-density polyethylene (HDPE, LDPE) were measured at 40°C to determine the effectiveness of fluorination for improving the barrier properties of these polymers. Electron spectroscopy for chemical analysis (ESCA) was used to determine the effects of cold and hot fluorination on HDPE and LDPE. Also, ESCA was used in conjunction with plasma etching to determine the effects of the gas phase fluorine concentration and fluorination time on the chemical structure of the treated film.

A novel permeation cell was designed to carry out the permeation measurements based upon a weight loss method. The design is based on two symmetrically opposed metal o-rings integral to the top and bottom sealing surfaces. The cell contains a drilled blind female nut, a male nut and a gland. The measurements were carried out in a controlled-temperature environment with an air distribution system to ensure zero activity of the penetrant at the outside of the film, by sweeping away the penetrant at the outside surface of the film immediately after it diffuses through the film.

The permeabilities measured fall between 1.38×10^{-7} and 54.2×10^{-7} (cc (STP) cm)/cm^2 sec for HDPE and between 2.5×10^{-6} and 35.2×10^{-6} (cc (STP) cm)/cm^2 sec for LDPE. The solvents used have

solubility parameters falling between 7.0 and 9.93 $(cal/cc)^{1/2}$. The permeabilities through HDPE and LDPE did not correlate with the solubility parameters of these solvents. A much more improved correlation was obtained for HDPE and LDPE when the permeabilities were correlated with the nonpolar permachor, suggested by Salame. The permachor parameter incorporates the effect of penetrant size and shape as well as the effect of solubility parameter. The permeability data for the highest level of fluorination fall between 4.0×10^{-8} and 22.6×10^{-7} for HDPE and between 1.4×10^{-6} and 29.1×10^{-6} (cc (STP) cm)/cm^2 sec.

Cold fluorination of LDPE and HDPE was shown to be less effective than hot fluorination for improving film barrier properties. ESCA analysis shows that for the cold-treated case, fluorination resulted in a gradual fluorine concentration profile through the polymer matrix. On the other hand, for the hot-fluorinated case, a well-defined fluorinated layer was formed after fluorination with depths not exceeding a few hundred angstroms inside the polymer.

DSC analysis of cold-treated and untreated HDPE showed a 7% drop in the crystallinity of the treated film. The reduction in crystallinity in the cold-treated sample presumably offsets the effectiveness of the surface-fluorinated layer's barrier contribution. This offsetting effect presumably arises due to producing additional amorphous regions through which permeation can occur.

ABSTRACT

YANG, DYI-KANG Sorption and Transport studies of water in Kapton Polyimide (Under the Direction of WILLIAM J. KOROS and VIVIAN T. STANNETT)

Sorption isotherms and diffusion coefficients for water, measured by gravimetric sorption on a quartz microbalance, in 0.3 mil and 2 mil Kapton polyimide films at 30°, 45° and 60°C are reported. A permeation study of water in Kapton using the modified Daynes-Barrer technique at these three different temperatures is also reported.

Evidence of chemical interaction of water with Kapton was found by gravimetric and infrared techniques, thereby complicating the interpretation of both thermodynamic and kinetic data. Because the time to reach sorption equilibrium is much shorter in a 0.3 mil film than in a 2 mil film, even assuming that the intrinsic reactivity is the same for the two markedly different thicknesses of film, different kinetic responses are anticipated and were, in fact, observed depending simply on which sample thickness was studied. Using 0.3 mil Kapton, sorption equilibria could be studied with a minimum interference from the chemical reaction. This information was then used to aid in the interpretation of the 2 mil Kapton sorption where more reaction could occur prior to achievement of sorption equilibrium.

For the 0.3 mil Kapton/H_2O system, the sorption equilibria and kinetics are well described by the so-call "dual mode" sorption and transport models at low activities. At high penetrant activities, clustering of water appears to occur based on a Zimm-Lundberg analysis and the fact that the diffusion coefficient for water decreases with increasing external vapor activity. The temperature effect on the diffusion coefficients at infinite dilution and the dual mode sorption parameter k_D, b and C_H' are presented and discussed. The diffusion coefficient for water ranges from $4x10^{-10}$ to $2.4x10^{-9}$ cm^2/sec for temperatures ranging from 30^o to 60^oC. The magnitude of the activation energy of diffusion coefficient at infinite dilution, 5.43 Kcal/g-mole, is smaller than the corresponding activation energy in more flexible chain polymers, perhaps reflecting the fact that rather small backbone motions are required to permit diffusion of water through the Kapton matrix. The existence of unimidized polyamic acid residues and/or a trace solvent residue are presumedly responsible for the form of the temperature dependence of the Henry's law parameter, k_D, and the Langmuir affinity parameter, b.

The predictions of the dual mode model for the isoteric enthalpy of sorption are presented and compared to the values determined from graphical analysis of the sorption isotherms which was performed independently without reference to the dual mode sorption model.

A larger amount of water is irreversibly sorbed into the polymer at the high sorption temperature compared to the lower temperature even after protracted evacuation. This irreversible uptake and the history dependence of the sorption kinetic data at high temperatures and vapor activities appear to be primarily the result of small amount of hydrolysis of unimidized groups present in the sample. A subtle microstructural change in the structure of Kapton, the formation of many polar groups and oligomers due to hydrolysis are all believed to cause the observed increase of solubility and the depression of diffusion coefficient, respectively. The permeability of water through Kapton ranges from 5.2 ~ 3.7 x 10^{-8} [cc(STP) cm/cm^2-sec-cmHg] over the temperature range from 30^{o} to 60^{o}C. The permeability exhibits a slightly negative apparent activation energy equal to E_p, -1.622 Kcal/g-mole. This effect presumabaly results from the rather small diffusional activation energy and the substantial negative enthalpy of sorption of water in the polyimide. The essentially Fickian behavior of water diffusion in Kapton at 30^{o}C prior to the occurrence of substantial reaction is confirmed by the form of sorption kinetic data and the coincidence of the experimental and predicted time lag calculated using Frisch's method for concentration dependent diffusion coefficients. The kinetic data of sorption in a "passivated" film in which most of the highly reactive groups bave been consumed are also well-fitted by the Fickian model. The effective diffusion coefficient (D_{eff}), calculated from steady state permeation data and equilibrium

sorption data were found to be in the range 1.5×10^{-9} to 1.4×10^{-8} cm^2/sec for the temperature range 30^{o} to $60^{o}C$.

ABSTRACT

YUI, ROBERT EDWIN. Sorption and Transport of Various Gases in Kapton Polyimide. (Under the direction of WILLIAM J. KOROS.)

The sorption equilbria of carbon dioxide and methane were measured at 45 and 60°C in 0.3 mil Kapton polyimide. The transient and steady state permeation of carbon dioxide through 0.3 mil Kapton was measured at 35°C. Also, steady state permeation was measured for helium and a helium/benzene mixture through 0.3 mil Kapton at 30°C.

The observed sorption isotherms were nonlinear and concave to the absicssa (i.e., pressure axis) which is characteristic of the typical behavior of a gas/glassy polymer system.

Atypical of the "usual" gas/glassy polymer system was the absence of initial penetrant-induced conditioning. During initial methane isotherms, after carbon dioxide or a temerature change, the sorption level slightly decreased at the higher pressures (i.e., above ca. 18 atm). It was proposed that this is a manifestation of redistribution of "volume packets." This effect was apparently "erased" during the subsequent isotherms.

The Langmuir capacity, from carbon dioxide and methane measurements, projected a T_g far below the reported value for Kapton (ca. 400°C). Also, the prediction of the sorbed molar volume of a

penetrant in the glassy state of a polymer (assuming equally available unrelaxed volume and no size exclusion effects) indicated that Kapton ought to treated differently from other relatively more flexible glassy polymers. Also attributed to the extraordinary stiffness of Kapton was the decrease of the initial sorption levels of methane (only) at high pressures.

The permeation of carbon dioxide through Kapton is explainable by the dual mode sorption and partial immobilization models up to 180 psia. At this pressure and above, and 35 ^{o}C, plasticization occurs. Predicted time lags agree with the experimental ones-even above 180 psia. The agreement above 180 psia supports a mathematical observation of the time lag being a weaker function of the concentration than the diffusion coefficient.

The helium permeation apparently is in agreement with the dual mode model, however, without the requisite sorption parameters a definite confirmation is not possible.

APPENDICES: REPRINTS AND MANUSCRIPTS OF PUBLICATIONS

A Model for Permeation of Mixed Gases and Vapors in Glassy Polymers

W. J. KOROS, R. T. CHERN, V. STANNETT, and H. B. HOPFENBERG,
Department of Chemical Engineering, North Carolina State University, Raleigh, North Carolina 27650

Synopsis

A model is discussed which explains reported complex effects of feed composition and pressure on component permeabilities in high-pressure gas separators based on glassy polymer membranes. A special form of Fick's law which accounts for the fact that penetrants in glassy polymers sorb into and diffuse through two different molecular environments provides the basis for the analysis of gas mixture permeation. Potential deviations from the theory are discussed in terms of separable solubility- and mobility-related effects.

INTRODUCTION

Permselective membranes provide an attractive approach for separating small gas molecules such as hydrogen and helium from larger molecules such as carbon oxides and nitrogen.[1-9] Depending on the polymer used, the ratio of permeabilities of these small molecules to the permeabilities of the larger molecules can vary from less than 0.5 to over 300.[5] Currently, there is no indisputable explanation for the existence of such a wide range of selectivities. It is known, however, that the polymers which exhibit the most attractive selectivities for small molecules, such as H_2 and He, compared to larger molecules, such as CO_2, CO, N_2, and CH_4, are stiff-chain glassy polymers. Glassy polymers exhibit more complex equilibrium sorption and transport behavior than do rubbery polymers, which have a rather low ability to discriminate between large and small molecules on the basis of permeability.[5]

For rubbery polymers, in the absence of plasticization, the constituents of a multicomponent gas mixture permeate essentially independently of one another.[10,11] The solubilities and diffusivities measured for the pure components can therefore be used directly in mixed-gas calculations; i.e., cross terms in the general flux expression[12] can be neglected. In the interest of simplicity, a similar approach will be used for glassy polymers; however, the fact that penetrants in glassy polymers sorb into and diffuse through two different molecular environments must still be accounted for, even in such an ideal case, to explain the reported data for mixtures. It is known, for instance, that the presence of a "slow" gas (CO or CH_4) can *reduce* the permeability of a "fast" gas[2,3,8]; conversely, the presence of a fast (H_2 or He) gas can increase the permeability of a slow gas.[8] Finally, the presence of a small amount of water or hydrocarbon vapor in the mixed gas feed can reduce both fast and slow gas permeabilities by as much as 20–60%,[2] with a net result that the observed separation factor can be increased or decreased slightly (10–20%) but is usually not too dramatically altered.[2,13]

Models which describe the sorption equilibria and transport processes in

Journal of Polymer Science: Polymer Physics Edition, Vol. 19, 1513–1530 (1981)
© 1981 John Wiley & Sons, Inc.
CCC 0098-1273/81/101513-18$01.80

gas/glassy polymer systems will be shown to be consistent with the data and qualitative observations that have been reported for high-pressure gas separators. Understanding and manipulation of the phenomenon of superselectivity should be of considerable value in guiding the selection, processing, and in-use conditions for various applications. The present work focuses primarily on steady-state transport; however, the parameters which arise from analysis of the pressure-dependent permeabilities can be used to treat transient transport situations as well.[14] Although it is not of primary importance in terms of gas separation, the transient-state transport of mixed penetrants in glassy environments is very important in such applications as designing gas barriers for food packaging, steam stripping of toxic monomers from glassy polymers, and the migration of residuals into package contents. The approach outlined in the present paper is the first step toward a rational treatment of these more complicated problems.

BACKGROUND

Considerable literature exists in the area of gas separations using rubbery polymers.[15-24] Until recently, the low fluxes associated with glassy polymer membranes have precluded their use. Now, asymmetric and thin supported membranes in hollow fiber configurations provide high flux capabilities[2,5] without sacrificing the outstanding permselectivity of glassy membranes.

Unrelaxed Volume in Glassy Polymers—Effects on Sorption and Transport of Small Molecules

A number of approaches to modeling the sorption and transport of pure components in glassy polymers have been successful.[5,25,30] One of the most widely known and used approaches is the so-called "dual-mode sorption, partial immobilization" model which takes into account the unique nonequilibrium nature of glassy polymers.[14,29] The presence of unrelaxed molecular-scale gaps, frozen into glassy polymers during quenching from the rubbery state or casting from solution, produces sorption isotherms which are concave to the pressure axis and permeabilities which decrease as the upstream pressure increases. Both effects are attributable to the finite amount of unrelaxed volume at each temperature. As this volume becomes saturated at high pressure, the apparent solubility decreases (i.e., C versus p becomes concave to the pressure axis). The permeability, which is equal to the product of a solubility- and a mobility-related term, can also decrease with increasing upstream pressure for glassy polymers if the aforementioned decrease in apparent solubility is not offset by a corresponding increase in the effective average mobility.

The unrelaxed volume $V_g - V_f$, shown schematically in Figure 1, decreases as the glass transition temperature is approached. Presumably, chain segments bordering on unrelaxed gaps are most likely to begin moving first. As these boundary chain segments execute increasingly larger amplitude vibrations and eventually convolutions, they encroach on the previously frozen "gap" territory represented as $V_g - V_f$ in Figure 1. This encroachment no longer permits a sorbed molecule to experience a microvoid environment. Presumably the smallest gaps are eliminated first, and the additional sorption capacity due to the existence of the microvoid environment is progressively reduced with cor-

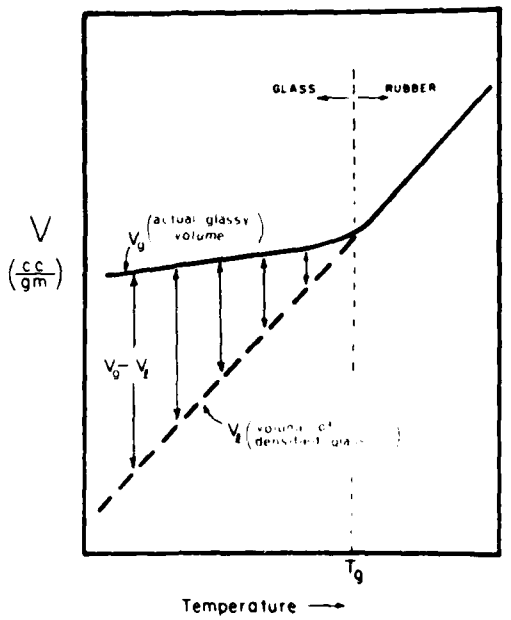

Fig. 1. Hypothetical unrelaxed volume $V_g - V_f$ in glassy polymers as a function of temperature

responding reduction in $V_g - V_f$ as T_g is approached. Finally, above T_g all chains have sufficient mobility to preclude the existence of any semipermanently fixed gaps. Consistent with the disappearance of the unrelaxed volume at T_g, sorption isotherms become straight and can be described by Henry's law (C/p is constant at a fixed temperature), and the permeability becomes independent of pressure.

Sorption of Pure and Mixed Gases in Glassy Polymers

As noted above, sorption isotherms for pure gases in glassy polymers are generally concave to the pressure axis.[5,31-38] At a fixed temperature, the magnitude of the deviation from a linear Henry's law sorption relation for a given sorbate is largely a function of the tendency of the sorbate molecule to exist in the condensed state. The relative tendencies of various sorbates to exist in the condensed state can be characterized conveniently by their respective critical temperatures or Lennard–Jones potential-well depths. For example, the sorption isotherm for helium in polycarbonate exhibits negligible curvature even up to 20 atm,[34] while CO_2 and other gases and even hydrocarbon vapors[35] show marked concavity to the pressure axis at low and intermediate pressures. These isotherms tend to become linear at higher pressures in the absence of plasticization [see Figs. 2(a) and 2(b)].

The observed negative deviations from a linear relation between sorbed concentration and the surrounding penetrant pressure are believed to be related to the presence of unrelaxed volume distributed throughout the glassy polymer. In the absence of penetrant-induced swelling, the sum of these packets of volume comprises a finite "excess" capacity for sorption which can be saturated at suf-

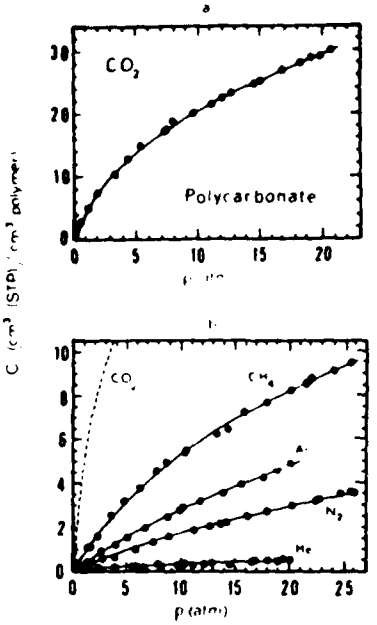

Fig. 2. Sorption isotherms for various gases in polycarbonate at 35°C.

ficiently high pressures, the ...ved volume can be considered analogous to the Langmuir case ... zeolites and charcoals.[39] The sorption isotherm data can be ... alled dual-mode sorption model, for which

$$C = k_D p + C'_H b p/(1 + bp) \quad (1)$$

where k_D is the ... ch characterizes sorption in the "normal" molecular dissolved ... mer ... ed earlier. The parameter b is the Langmuir affinity constant which char... erizes the tendency of a given penetrant to sorb in the Langmuir mode. The affinity constants for "noncondensable" penetrants such as helium and hydrogen are small, while more easily condensable polar and polarizable penetrants tend to have significantly larger affinity constants.[34] The parameter C'_H, the Langmuir capacity constant, characterizes the total sorption capacity of the lower-density regions (unrelaxed gaps) in a glassy polymer for a particular penetrant. The unrelaxed gap volume is essentially a constant for a given polymer at a given temperature.[40] The primary factor, therefore, in determining the di...erence in the Langmuir capacity constant for different penetrants (say, He, N_2, CO_2, and H_2O) is the value of the sorbed density of the penetrant at the point of complete saturation of the Langmuir sites. For materials such as CO_2 and H_2O which are below or only slightly above their critical temperature at the temperature of measurement, there is evidence that the penetrant exists at roughly the same density as it would as a pure liquid below its critical point.[37,39,41] For highly supercritical gases such as He and N_2, the indication is that the saturation density in the Langmuir sites is low, so that even when the unrelaxed gap volume is full, the amount of gas in this mode is small. This fact, coupled with the low affinity constants observed for such gases, ac-

counts for the low level of sorption and minor curvature in the sorption isotherm of helium at pressures as high as 20 atm.

Extension of the dual-mode theory to include multicomponent mixtures of penetrants based on pure-gas measurements is straightforward.[42] The *primary* effect for a mixture is simple competition by the various penetrants for the fixed unrelaxed volume fraction in the polymer. Such an effect may cause significant *depression* in sorption of both gases in a binary mixture whereas in a rubbery polymer in the absence of plasticizing effects the solubility of a given penetrant is essentially independent of other components present. Extension of dual-mode theory to a binary mixture of gases A and B gives the following expression for the concentrations of A and B as a function of the partial pressures, p_A and p_B, of the two components[42]:

$$C_A = k_{DA}p_A + C'_{HA}b_Ap_A/(1 + b_Ap_A + b_Bp_B) \quad (2)$$

and

$$C_B = k_{DB}p_B + C'_{HB}b_Bp_B/(1 + b_Ap_A + b_Bp_B) \quad (3)$$

The meanings of the various parameters in eqs. (2) and (3) are consistent with those defined in eq. (1): e.g., k_{DA} is the Henry's law parameter for component A in the mixture, etc. (for definitions of these and other parameters used in this paper see the List of Symbols). All of the parameters in eqs. (2) and (3) can be measured for the pure components and used directly for the mixture, assuming that plasticizing effects on k_D and penetrant-penetrant interaction influences on both the Langmuir affinity constants b_i and the saturation densities of the components are negligible.

Pure-Gas Permeation in Glassy Polymers

Independent transport[34,44] and pulsed nuclear magnetic resonance[38] studies indicate that penetrant molecules in the two distinct molecular environments (Henry's law and Langmuir) have different inherent mobilities. The so-called "dual mobility" or "partial immobilization" model accounts for this fact by expressing Fick's law as

$$N = -D_D\frac{\partial C_D}{\partial x} - D_H\frac{\partial C_H}{\partial x} \quad (4)$$

where N is the total diffusive flux [cm³(STP)/cm² s], and C_D and C_H are the local concentrations of the penetrant in the Henry's law and Langmuir environments, respectively. The coefficients D_D and D_H characterize diffusion due to local concentration gradients in the two environments. Both diffusion coefficients are assumed to be functions of temperature but not of concentration. This model predicts that the permeability of a pure gas measured with an upstream driving pressure p_2 and a zero downstream pressure p_1 is given by the expression

$$P = k_DD_D\,[1 + FK/(1 + bp_2)] \quad (5)$$

where $F = D_H/D_D$ and $K = C'_Hb/k_D$ are convenient dimensionless groups. Independent gas sorption measurements of k_D, b, and C'_H allow determination of D_D and F by plotting P versus $1/(1 + bp_2)$.[14,34] Equation (5) has been shown to describe permeation data well for a variety of gases in a number of glassy polymers.[34,43-45]

Typical permeation data for two markedly different gases (He and CO_2) are shown in Figure 3.[34] Over the pressure range 1–20 atm, the permeability of helium decreases by only 6%, while that of CO_2 decreases by 27%. This effect is due primarily to the fact that the pressure-dependent term in eq. (5) is relatively unchanged over the pressure range 1–20 atm for helium, owing to the small affinity constant of this gas ($b = 0.0121$ atm^{-1}), while the pressure-dependent term changes considerably for CO_2 because of the larger affinity constant ($b = 0.2618$ atm^{-1}) of this more condensable gas.

THEORY

Generalization of the Dual-Mobility Model for Steady-State Permeation of Gas Mixtures

In the following treatment, attention is first focused on the steady-state permeation of two gases A and B which arises due to partial-pressure driving forces $p_{A2}-p_{A1}$ and $p_{B2}-p_{B1}$ existing between the upstream and the downstream faces of the membrane (a subscript 2 refers to the upstream side of the membrane and a subscript 1 refers to the downstream side of the membrane). Finally, an expression is presented for the important case where a third component (contaminant) is present in addition to the binary system.

At the steady state, the constant flux N_{SSA} of component A through a membrane of thickness l is given by[5]

$$N_{SSA} = P_A(p_{A2} - p_{A1})/l \tag{6}$$

or, equivalently,

$$P_A = N_{SSA}l/(p_{A2} - p_{A1}) \tag{7}$$

Thus the problem of predicting the permeability P_A of component A reduces

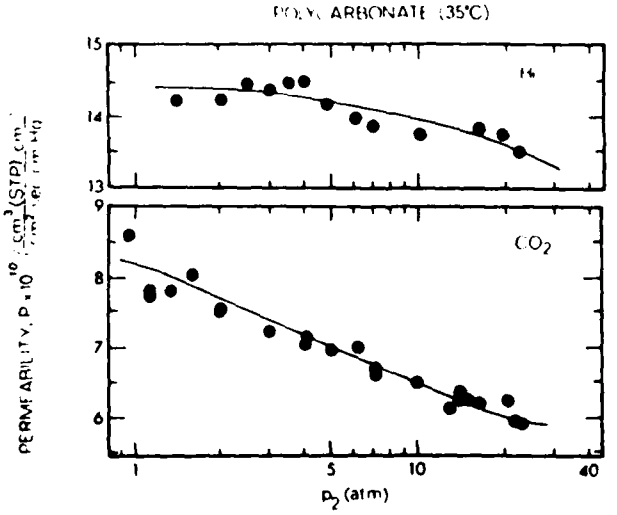

Fig. 3. Permeabilities of helium and CO_2 in polycarbonate at 35°C as functions of upstream pressure.

simply to one of deriving an expression for the steady-state flux of component A in terms of the various partial pressures and the solubility and mobility coefficients. The flux expression for component A in the absence of cross product terms can be written

$$N_A = -D_{DA}\frac{\partial C_{DA}}{\partial x} - D_{HA}\frac{\partial C_{HA}}{\partial x} \tag{8}$$

Consistent with eq. (4), C_{DA} and C_{HA} are the local concentrations of penetrant A in the Henry's law and Langmuir environments, respectively. An equivalent but mathematically more convenient way of writing the partial immobilization model for component A is[14]

$$N_A = -D_{DA}\frac{\partial C_{MA}}{\partial x} \tag{9}$$

where $C_{MA} \equiv C_{DA} + F_A C_{HA}$ and $F_A \equiv D_{HA}/D_{DA}$. Since, at the steady state, N_A is a constant equal to N_{SSA}, we have

$$\int_l^0 N_{SSA}\,dx = -lN_{SSA}$$

$$= -\int_{C_{MA1}}^{C_{MA2}} D_{DA}\,dC_{MA} = -D_{DA}(C_{MA2} - C_{MA1}) \tag{10}$$

The assumption of local equilibrium at all points in the polymer (i.e., local equality of chemical potentials of component A in the two environments) permits expressing C_{HA} in terms of C_{DA} as[42]

$$C_{HA} = \frac{C_{DA}K_A}{1 + \alpha_A C_{DA} + \alpha_B C_{DB}} \tag{11}$$

where $\alpha_A \equiv b_A/k_{DA}$, $\alpha_B \equiv b_B/k_{DB}$ and $K_A \equiv C_{HA}b_A/k_{DA}$. Substituting for C_{MA2} and C_{MA1} in eq. (10), we have

$$N_{SSA} = \frac{D_{DA}}{l}\left[C_{DA2} + \frac{F_A K_A C_{DA2}}{1 + \alpha_A C_{DA2} + \alpha_B C_{DB2}} - C_{DA1} - \frac{F_A K_A C_{DA1}}{1 + \alpha_A C_{DA1} + \alpha_B C_{DB1}}\right] \tag{12}$$

Since $C_{DA} = k_{DA}p_A$, and $C_{DB} = k_{DB}p_B$, we have the following expression for P_A, the steady-state permeability of component A:

$$P_A = D_{DA}k_{DA}\left(1 + \frac{F_A K_A p_{A2}/(p_{A2} - p_{A1})}{1 + b_A p_{A2} + b_B p_{B2}} - \frac{F_A K_A p_{A1}/(p_{A2} - p_{A1})}{1 + b_A p_{A1} + b_B p_{B1}}\right) \tag{13}$$

In all of the cases which will be dealt with in the present discussion, the experiments will be assumed to be performed with a negligible downstream partial pressure of components A and B, so eq. (13) reduces to

$$P_A = D_{DA}k_{DA}[1 + F_A K_A/(1 + b_A p_{A2} + b_B p_{B2})] \tag{14}$$

or, in terms of the mole fraction y_A of component A in the feed and total feed pressure p_T:

$$P_A = D_{DA}k_{DA}[1 + F_A K_A/[1 + b_B p_T + y_A p_T(b_A - b_B)]] \tag{15}$$

In situations where the downstream partial pressures are not zero, eq. (13) can be used with relatively little difficulty.

To facilitate parameter estimation, it is most convenient to use an experimental setup with $p_{A1} = p_{B1} = 0$, and henceforth all derivations will assume such a mode of operation. According to the report by Pye et al.,[2] for a carrier gas-type system with $p_{A1} = 0$ (rapid carrier flow past the downstream membrane face) the permeability determined should be the same as that measured by manometric methods with a vacuum downstream.

Similar expressions for the permeability of component B may be derived in terms of its sorption and transport parameters:

$$P_B = D_{DB}k_{DB}[1 + F_BK_B/(1 + b_Ap_{A2} + b_Bp_{B2})] \tag{16}$$

or, in terms of y_A and p_T,

$$P_B = D_{DB}k_{DB}[1 + F_BK_B/[1 + b_Bp_T + y_Ap_T(b_A - b_B)]] \tag{17}$$

For the case where $p_{A1} = p_{B1} = 0$, the separation factor $\beta_{A,B}$ defined by eq. (18) reduces simply to the ratio of permeabilities of component A to component B,[46]

$$\beta_{A,B} \equiv \frac{x_A/x_B}{y_A/y_B} \simeq \frac{P_A}{P_B} \tag{18}$$

where x_A and x_B are the mole fractions of components A and B in the downstream permeant, and y_A and y_B are the mole fractions of components A and B on the high-pressure feed side of the membrane. Therefore, substituting in eq. (18) from eqs. (15) and (17) we find

$$\beta_{A,B} = (D_{DA}k_{DA}/D_{DB}k_{DB})[1 + F_AK_A + b_Bp_T + y_Ap_T(b_A - b_B)] / [1 + F_BK_B + b_Bp_T + y_Ap_T(b_A - b_B)] \tag{19}$$

If a third component E is present at a partial pressure p_{E2} in the feed, the above equations can be modified simply as shown below:

$$P_A = D_{DA}k_{DA}[1 + F_AK_A/(1 + b_Ep_{E2} + b_Ap_{A2} + b_Bp_{B2})] \tag{20}$$

$$P_B = D_{DB}k_{DB}[1 + F_BK_B/(1 + b_Ep_{E2} + b_Ap_{A2} + b_Bp_{B2})] \tag{21}$$

$$\beta_{A,B} = (D_{DA}k_{DA}/D_{DB}k_{DB})(1 + b_Ep_{E2} + F_AK_A + b_Ap_{A2} + b_Bp_{B2}) / (1 + b_Ep_{E2} + F_BK_B + b_Ap_{A2} + b_Bp_{B2}) \tag{22}$$

Expressions analogous to eqs. (20)–(22) can clearly be obtained for any number of additional components in the feed. The terms in parentheses containing p_{E2} are constants as long as the partial pressure of component E is maintained constant. If component E is a material such as water with a high affinity constant b_E, the term b_Ep_E may be so large that it dominates the observed behavior of P_A, P_B, and $\beta_{A,B}$, even though the partial pressure p_{E2} may be much less than p_{A2} or p_{B2}.

Two detailed case studies will now be considered with specific reference to actual reported gas separation data which illustrate the power and utility of the expressions presented in eqs. (14)–(22).

Case Study I: Binary mixture of a "fast" gas and a "slow" gas (He and CO_2) in polycarbonate at 35°C

Helium, the "fast" (higher permeability) gas in this case exhibits little inherent pressure dependence in permeability over the range of pressures up to 20 atm due to its low affinity constant. Carbon dioxide, the "slow" (lower permeability) gas exhibits significant inherent pressure dependence in its permeability over the range of pressures up to 20 atm due to its higher affinity constant (see Fig. 3). The pertinent sorption and transport parameters for these two gases are presented in Table I.[34] By substituting the appropriate parameters into eqs. (15), (17), and (19) for gas A (helium) and gas B (CO_2), the results presented in Figures 4(a) and 4(b) can be calculated. Similar trends are predicted for other gas pairs, e.g., He/N_2, although the magnitude of the pressure effect on the two permeabilities is roughly half as large in this case, owing to the less-pronounced dual-mode character of N_2 compared to CO_2, which is apparent in Figure 2. Even in this case, however, a reduction of nearly 15% is expected for the two components in some cases. The separation factor for the He/N_2 case is not a significant function of pressure since the permeability of each component is reduced, on a percentage basis, by an approximately equal amount over the pressure range 1-20 atm.

It is clear from Figure 4(b) that polycarbonate is not particularly attractive as a separation membrane for helium and carbon dioxide since the separation factor varies from 1.62 in the limit as $y_A \to 1$ and $p_f \to 0$ to 1.82 as $y_A \to 0$ and $p_f = 20$ atm. The system He/CO_2 in polycarbonate is considered here not because of practical significance for gas separations but because the trends which it illustrates are typical of other more important systems which have been described in the literature (e.g., H_2 and CO in Kapton) for which model parameters are not yet available.

The approximate magnitude of the separation factor in eq. (19) is determined largely by the ratio of the product $D_D k_D$ for the two components. On the other hand, the magnitude of the percentage change in $\beta_{A,B}$ over a given pressure range is determined by the change in the ratio of the two terms containing F's, K's, and b's inside the parentheses in eq. (19). This latter effect is adequately illustrated in Figure 4(b), in which the percentage increase in the separation factor is approximately 11% between 1 and 20 atmospheres for He/CO_2 mixtures with low mole fractions of the fast gas, helium. Equation (19) predicts that the separation factor could either increase or decrease with increasing upstream pressure, depending on the relative values of $F_A K_A$ and $F_B K_B$. These two composite parameters can be determined independently by pure-gas sorption and transport measurements as was done for the He/CO_2 system.

TABLE I
Dual Mode Parameters for He and CO_2 in Polycarbonate at 35°C (Koros et al. ref. 34)

Gas	k_D $\left(\frac{\text{cm}^3\text{(STP)}}{\text{cm}^3\text{ polymer atm}}\right)$	b (atm^{-1})	C_H' $\left(\frac{\text{cm}^3\text{(STP)}}{\text{cm}^3\text{ polymer}}\right)$	K	$D_D \times 10^8$ (cm^2/s)	$D_H \times 10^8$ (cm^2/s)	F
Helium (A)	0.914	0.0171	0.313	0.26	550	744	1.33
CO_2 (B)	0.6852	0.2618	18.805	7.19	6.22	0.49	0.078

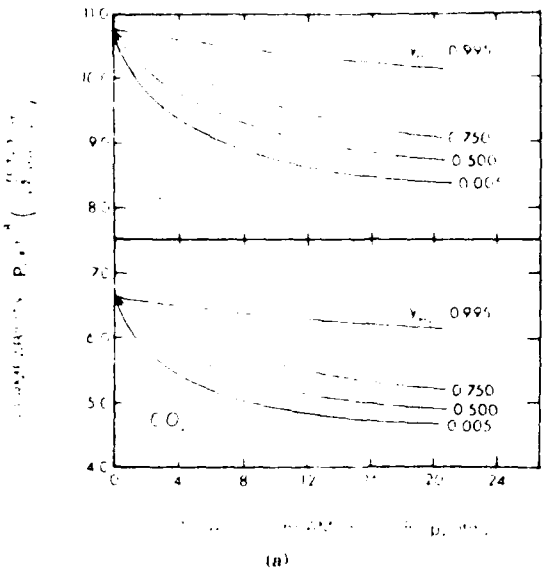

(a)

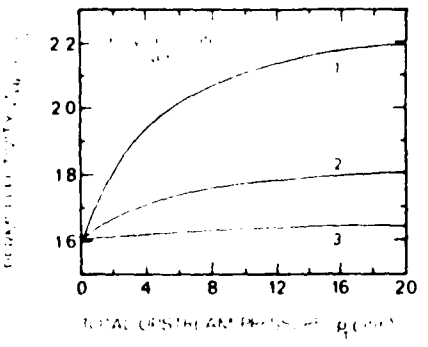

(b)

Fig. 4. (a) Permeabilities of helium and CO_2 in mixed-gas feeds for various mole fractions of helium in the feed gas as a function of total upstream gas pressure. The downstream pressure is assumed to be negligibly small, i.e., eqs. (15) and (16) apply. (b) Predicted permselectivities of polycarbonate at 35°C for helium relative to CO_2 as a function of total upstream pressure for the case of a negligible downstream pressure. Curve 1: for a 50/50 mixture of He/CO_2 with β_{He/CO_2} (= permeability of pure helium)/(permeability of pure CO_2), where both permeabilities were calculated at their corresponding partial pressures at the stated total pressure, e.g., at a total system pressure of 10 atm, the permeability of each component was calculated at 5 atm. Curves 2 and 3 correspond to feed compositions of $y_{He} = 0.005$ and $y_{He} = 0.995$, respectively. Both curves 2 and 3 were calculated from the model [eq. (19)].

The tendency of the predicted separation factor in Figure 4(b) to increase with increasing driving pressure is consistent with the actual separation factor observed in a study of Kapton by McCandless[3] for a 50/50 H_2/CO mixture. It was reported that the actual separation factor at approximately 40°C increased by 36% (from 31.2 up to 42.5) when the driving pressure differential was increased from 50 to 300 psi. The values of the separation factors shown in Figure 4(b) calculated from eq. (19) at high upstream pressures are significantly less than

those calculated for a 50/50 mixture of the gases by taking the ratios of the respective pure-gas permeabilities [see curve 1 in Fig. 4(b)].

McCandless noted that "There is some interaction between components of the binary mixture during permeation which effectively decreases the permeability of H_2 relative to CO." His observations are also consistent with the report by Antonson et al.[8] that "the fast gas was 'slowed down' by the slow gas and the slow gas was 'speeded up' by the fast gas." Moreover, both of these separate qualitative observations are consistent with the predictions of the theory represented by eqs. (15)–(19) and illustrated by the results in Figures 4(a) and 4(b). The permeability of helium decreases as the mole fraction of CO_2 present in the feed increases at a fixed total pressure. The "slowdown" effect noted by both McCandless and Antonson is clearly the most pronounced at the higher pressures in Figure 4(a) and can amount to as much as 20% in some cases. In simple terms, one can explain the effect by noting that helium in the Langmuir mode had a higher mobility than helium in the Henry's law mode ($D_H > D_D$) and as the mole fraction of CO_2 in the feed increases it excludes helium from access to its higher-mobility environment.

Also consistent with Antonson's general observation, the presence of the fast gas, He, tends to speed up the slow gas, CO_2. The permeability of CO_2 in Figure 4(a) is the highest at each pressure for mixtures where the mole fraction of helium in the feed is the highest (e.g., $y_A = 0.995$). This effect occurs because $b_A < b_B$, which causes the term $y_A p_T(b_A - b_B)$ to be a negative contributor to the denominator in eq. (17), thereby actually increasing the permeability P_B as y_A increases, consistent with the above observations.

Case Study II: Effect of introduction of a low partial pressure of a contaminant (H_2O) with a high affinity constant in the feed stream

Another interesting set of data on mixture permeation in highly selective glassy polymers was reported by Pye et al.[2] These investigators note that a partial pressure of only 15 mm(Hg) of water vapor in the feed of a 50/50 molar mixture of H_2 and CH_4 at 1 atm upstream pressure significantly depressed the permeabilities of both H_2 and CH_4. In this case CH_4 acts as the slow gas, analogous to CO_2 in the previous case study. The effects of introducing a trace contaminant such as water in the feed stream can be illustrated by extending the previous case study with helium and CO_2. Although data are not available for dual-mode sorption parameters for water in polycarbonate, it is often found that the Langmuir affinity constant of a given penetrant is quite similar in different polymers [e.g., CO_2 has affinity constants at 30–35°C in poly(ethylene terephthalate) (PET), poly(acrylonitrile) (PAN), polycarbonate (PC), poly(methyl methacrylate) (PMMA), and poly(ethyl methacrylate) (PEMA) in the range of 0.2 ± 0.07 atm^{-1} (refs. 34, 39, 41, 43)]. Ranade et al.[47] indicate that the affinity constant of water in PAN at 35°C is 243.2 atm^{-1}, while CO_2 in the same sample had an affinity constant of only 0.16 atm^{-1}. The highly condensable nature of H_2O is presumably responsible for its high affinity for Langmuir sorption. If one assumes that the affinity constant of water in polycarbonate is, to a first approximation, equal to that in PAN, the previous results for the binary mixture of He/CO_2 can be extended to treat the effects of water contaminant present at a constant partial pressure in the feed. The expressions for the permeabilities

of component A (He) and component B (CO_2) and the separation factor β_{He,CO_2} in the presence of a constant 35% RH at 35°C [15 mm(Hg) partial pressure of water] in the feed (so $b_F p_F = 4.8$) can be shown to be given by the following expressions in units of [cm³(STP) cm]/(cm² s atm):

$$P_{He} = 7.97 \times 10^{-8}[1 + 0.3458/[(1 + 4.8) + 0.2618p_T^* - 0.2497p_T^* y_A^*]]$$

$$P_{CO_2} = 4.26 \times 10^{-8}[1 + 0.5604/[(1 + 4.8) + 0.2618p_T^* - 0.2497p_T^* y_A^*]]$$

$$\beta_{He,CO_2} = 1.87\,(6.15 + 0.2618p_T^* - 0.2497p_T^* y_A^*) / (6.36 + 0.2618p_T^* - 0.2497p_T^* y_A^*)$$

In the above expressions, y_A^* is the mole fraction of component A (He) in the feed at a total pressure p_T^* expressed on a dry basis (exclusive of the small amount of water present). Since the partial pressure of water is so low in this case (p_{F2} = 0.02 atm) it is a good approximation to say that $y_A^* = y_A$ and $p_T^* = p_T$ for feed pressures above 1 atm, which are the cases of real interest here.

The plots of the expressions for permeabilities and separation factors for pressures of one atmosphere and above are shown in Figure 5 for various dry-basis mole fractions corresponding to the curves in Figure 4. Comparison of the sets of data in the two figures indicates that the pressure dependences of the permeabilities and separation factors are essentially eliminated because the water largely excludes the other components from the Langmuir mode. The separation factor β_{He,CO_2} is not affected adversely by the presence of the water contaminant, and actually *increases* from 1.62 for an uncontaminated 50/50 He/CO_2 feed to 1.80 for the water-contaminated 50/50 He/CO_2 feed (dry basis) at one atmosphere. On the other hand, the fluxes of *both* components at 1 atm are predicted to be *reduced significantly* (30% for CO_2 and 20% for He) in the case of the

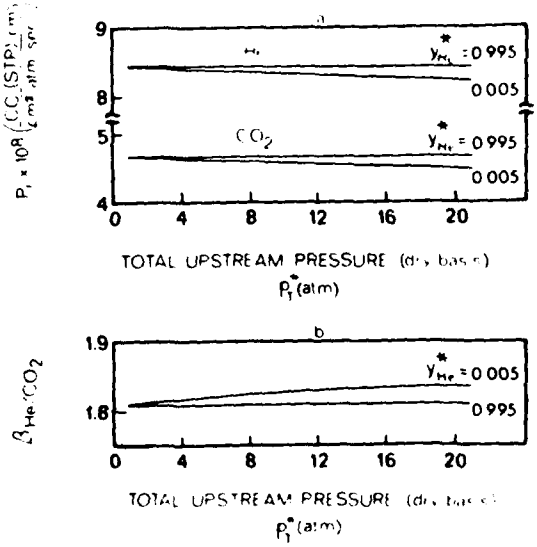

Fig. 5. Predicted permeabilities for helium and CO_2 (a) and permselectivities (b) of polycarbonate at 35°C for helium relative to CO_2 as a function of total upstream pressure (dry basis) in the presence of 15 mm(Hg) of water vapor in the upstream feed stream. The downstream pressure is assumed to be negligibly small, i.e., eqs. (20)–(22) apply.

contaminated feed with only 15 mm(Hg) of water vapor present. For the He/N_2 binary system, which was also discussed briefly in Case Study I, it is predicted that the fluxes of both components drop by over 20% in the presence of 15 mm(Hg) H_2O vapor for an upstream pressure of 1 atm. Such considerations are important and indicate that significant reduction in production rate can occur, although permeant purity is not compromised by the presence of condensable contaminants in the feed. The higher the affinity constant b_E of the extra component, the more potent it is in depressing the fluxes of the other mixture constituents.

The predicted reductions in permeabilities discussed above for the He/CO_2 system are satisfyingly consistent with the observations of Pye et al.[2], which are summarized in Table II below. As noted earlier, these investigators introduced a partial pressure of 15 mm(Hg) of water into a stream of 50/50 H_2/CH_4 at 1 atm (referred to as "wet" in Table II) and compared their results with those for an uncontaminated 50/50 H_2/CH_4 stream at 1 atm (referred to as "dry" in Table II). Note that the H_2 permeability decreased by as much as 59%, while the CH_4 permeability decreased by as much as 56% owing to the presence of the water vapor. Since reductions in the permeabilities for the two components tended to be correlated (as expected from the theory presented) the ratio of the permeabilities, and hence the separation factor, is not very much different in the wet and dry cases. Pye et al.[2] pointed out that the permeability reductions noted above are *reversible*; that is when the contaminant moisture is removed from the feed stream, the normal dry permeabilities are again observed. They also note that it is possible to introduce the same sort of contaminant blocking action using small amounts of hydrocarbon contaminants such as pentane. Such highly condensable materials are also expected to have large affinity constants and to compete for the available gap volume in exactly the same way that was discussed previously for water. In such a case, the effect on the observed separation factor is expected to be small; however quite significant reductions in productivity can occur if permeability reductions of as much as 60% can be expected (as reported for polymer C in Table II) due to the trace water contamination.

Pye and co-workers appreciated qualitatively what caused the blocking action and correctly suggested that the reduction in permeability was due to water (or hydrocarbon) sorption "effectively reducing the microvoid content of the film and the available diffusion paths for the nonreactive gases." The rather remarkable insight of these workers says in qualitative terms what eqs. (20)–(22)

TABLE II
Permeabilities and Permeability Ratios at 30°C for Various Stiff-Chain Polymers[a]

Polymer[a]	P_{H_2}[b] Dry	P_{H_2}[b] Wet	Reduction due to H_2O contaminant	P_{CH_4}[b] Dry	P_{CH_4}[b] Wet	Reduction due to H_2O contaminant	P_{H_2}/P_{CH_4} Dry	P_{H_2}/P_{CH_4} Wet	Reduction due to H_2O contaminant
A	3557	2817	21%	13.2	11.1	16%	270	254	6%
B	7637	6160	19%	68.2	57.0	16%	112	108	3%
C	3168	1274	59%	7.5	3.3	56%	422	386	9%

[a] A prepared by reaction of 4,4′-hexafluoroisopropylidenediphthalic anhydride with 1,3-diamino benzene. B prepared by reaction of 4,4′-hexafluoroisopropylidenediphthalic anhydride with 1,5-diaminonaphthalene. C prepared by reaction of 4,4′-hexafluoroisopropylidenediphthalic anhydride with 3,5-diamino benzoic acid.

[b] $P = (B = 10^{-10}$ cm^2 (STP)/cm^2/s/cmHg)

say quantitatively, and their data are consistent with the predictions of the simple theory proposed here.

Investigation of Possible Deviations from Simple Dual-Mode Permeation Behavior

As noted earlier, the use of pure-gas sorption and diffusion coefficients in the expressions for the permeabilities of components of the mixture implies that the various materials permeate independently except for the competition for unrelaxed gap volume. On the basis of the preceding case studies and review of observations of various trends in the data, it seems that the simple theory reflects current experience remarkably well. If quantitative deviations from the simple model are observed, they can be analyzed in terms of two classes of effects as shown in Table III. The solubility-related effects can be treated independently by performing sorption measurements for component A ($C_A|p_B$) at fixed partial pressure of component B. Equation (2) can be written in the form

$$C_A|p_B = k_{DA}p_A + C_{HA}b'_A p_A/(1 + b'_A p_A) \tag{23}$$

where $b'_A = b_A/(1 + b_B p_B)$, which is a constant at fixed partial pressure of component B. Since all parameters in eq. (23) can, in principle, be determined from sorption measurements on the pure gases, a direct comparison of the predictions of eq. (23) with the actual concentration of component A measured at constant partial pressure of component B should be possible. Moreover, the nonlinear least-squares technique employed for determination of the pure-component parameters[34] can be used to independently assign values to the parameters k_{DA}, C_{HA}, and b'_A using the concentration data for component A measured at a constant partial pressure of component B. If there are no significant deviations from the theory due to items listed as solubility-related factors in Table III, it should be found that

$$(k_{DA})|p_B = k_{DA}$$
$$(C_{HA})|p_B = C_{HA}$$
$$b'_A = (b_A)|p_B = b_A/(1 + b_B p_B)$$

where the parameters on the right-hand side of the above equations are those determined from pure-gas sorption. Any solubility-related deviations from the theory can therefore be distinguished from mobility-related effects.

Mobility-related deviations from the theory can be treated in a similar fashion by rewriting eq. (14) for the situation where p_{B2} is held constant:

$$P_A|p_{B2} = D_{DA}k_{DA}\left(1 + \frac{F_A(C_{HA}b_A/k_{DA})}{1 + b_A p_{A2} + b_B p_{B2}}\right) \tag{24}$$

TABLE III
Possible Sources of Deviation From Simple Dual-Mode Permeation Behavior

a. Solubility related
(i) alteration of k_D of one component due to the presence of the second component
(ii) alteration of b of one component due to the presence of the second component
(iii) alteration of C_H of one component due to the presence of the second component
b. Mobility related
(i) alteration of D_D of one component due to the presence of the second component
(ii) alteration of D_H of one component due to the presence of the second component

or

$$P_A|p_{B2} = D_{DA}k_{DA}\left(1 + \frac{F_A(C'_{HA}b'_A/k_{DA})}{1 + b'_A p_{A2}}\right) \tag{25}$$

and hence

$$P_A|p_{B2} = D_{DA}k_{DA}\left(1 + \frac{F_A K'_A}{1 + b'_A p_{A2}}\right) \tag{26}$$

where $b'_A = b_A/(1 + b_B p_{B2})$ and $K'_A = C'_{HA}b'_A/k_{DA}$, which is consistent with the earlier treatment of solubility effects. A similar expression can, of course, be written for the permeability of component B measured at a constant partial pressure of component A in the feed.

The interesting fact suggested by eq. (26) is that even though the presence of a second component reduces the apparent affinity constant b'_A and consequently K'_A because of the competition for available gap volume, the overall form of the permeability expression (at constant p_{B2}) is unchanged. In the absence of deviations from the theory due to items listed as mobility-related factors in Table III, the values of D_{DA} and D_{HA} obtained from the slope and intercept of a plot of $P_A|p_{B2}$ versus $1/(1 + b'_A p_{A2})$ should be identical to the D_{DA} and D_{HA} obtained for the pure-component case. The values of b'_A and K'_A will, of course, be known independently from sorption measurements at a fixed value of p_{B2}.

CONCLUSIONS

Permeation data for mixed gases in glassy polymer membranes indicate that such penetrants do not permeate entirely independently of one another. This is a substantially different situation from the corresponding case for rubbery polymers in the absence of plasticization. A very low partial pressure of a condensable species such as water in the feed stream to a gas separator can significantly *reduce* the permeability of a given constituent relative to its permeability as a pure component.

A special form of Fick's law which accounts for the fact that penetrants in glassy polymers sorb into and diffuse through two quite different molecular environments leads to a model which is consistent with the reported complex effects of feed composition and pressure on component permeabilities in high-pressure gas separators. The model explains the observed depression in permeabilities of gas penetrants in terms of the much greater affinities of condensable vapors toward the unrelaxed volume between chain segments in a glassy polymer; consequently, permeation of the gas due to transport through this molecular environment is greatly reduced. The straightforward procedure for separating possible solubility- and mobility-related deviations from the model predictions can provide useful insight into the physics of the glassy state.

The authors gratefully acknowledge the support of this work by NSF Grant No. CPE-79-18200.

LIST OF SYMBOLS

Symbols	Definitions	Common Units
b_i	Langmuir affinity constant of component i	atm^{-1}
b_A^*	$= b_A/(1 + b_B p_B)$, apparent Langmuir affinity constant for component A observed in the presence of a constant partial pressure of component B	atm^{-1}
C_i	concentration of penetrant i in the polymer	$\frac{cm^3(STP)}{cm^3\ polymer}$
C_{H_i}	Langmuir capacity constant of component i	$\frac{cm^3(STP)}{cm^3\ polymer}$
C_{D_i}	local concentration of penetrant i in the Henry's law environment	$\frac{cm^3(STP)}{cm^3\ polymer}$
C_{H_i}	local concentration of penetrant i in the Langmuir environment	$\frac{cm^3(STP)}{cm^3\ polymer}$
C_{M_i}	$C_{D_i} + F_i C_{H_i}$	$\frac{cm^3(STP)}{cm^3\ polymer}$
D_{D_i}	diffusion coefficient of component i in the Henry's law environment	cm^2/s
D_{H_i}	diffusion coefficient of component i in the Langmuir environment	cm^2/s
F_i	D_{H_i}/D_{D_i}	dimensionless
k_{D_i}	Henry's law constant of component i in the polymer	$\frac{cm^3(STP)}{cm^3\ polymer\ atm}$
K	$C'_H b/k_D$	dimensionless
K_A^*	$C'_{H_A} b_A^*/k_{D_A}$	dimensionless
l	membrane thickness	cm
N_i	diffusive flux of component i	$\frac{cm^3(STP)}{cm^2\ s}$
N_{SS_i}	steady-state flux of component i	$\frac{cm^3(STP)}{cm^2\ s}$
p	pressure	atm
p_A, p_B	partial pressures of A, B	atm
p_1	total upstream pressure	atm
P_i	permeability of component i	$\frac{cm^3(STP)\,cm}{s\ cm^2\ atm}$
T_g	Glass transition temperature	°C
$V_g - V_i$	theoretical unrelaxed volume of glassy polymers	$\frac{cm^3}{g}$
x	distance from the upstream side of the polymer film	cm
x_i	mole fraction of component i in the downstream side	dimensionless
y_i	mole fraction of component i in the upstream side	dimensionless
ω_i	$= b_i/k_{D_i}$	$\frac{cm\ polymer}{cm^3(STP)}$
$\beta_{A/B}$	$= (x_A/x_B)/(y_A/y_B)$, separation factor for a given membrane	dimensionless

superscript*	indicates "dry basis" when written x_i^*, y_i^*, or p_i^*
subscript 1	indicates downstream conditions in permeation experiment
subscript 2	indicates upstream conditions in permeation experiment
subscripts A, B, E	different components in a multicomponent mixture

References

1. D. G. Pye, H. H. Hoehn, and M. Panar, *J. Appl. Polym. Sci.*, **20**, 287 (1976).
2. D. G. Pye, H. H. Hoehn, and M. Panar, *J. Appl. Polym. Sci.*, **20**, 1921 (1976).
3. F. P. McCandless, *Ind. Eng. Chem. Proc. Des. Dev.*, **11**, 470 (1972).
4. L. Pilato, L. Litz, B. Hargitay, R. C. Osborn, A. Farnham, J. Kawakami, P. Fritze, and J. McGrath, *Polym. Prepr. Am. Chem. Soc. Div. Polym. Chem.*, **16**, 42 (1975).
5. V. T. Stannett, W. J. Koros, D. R. Paul, H. K. Lonsdale, and R. W. Baker, *Adv. Polym. Sci.*, **32**, 69 (1979).
6. R. J. Gardner, R. A. Crane, and J. F. Hannan, *Chem. Eng. Prog.*, **73**, 78 (1977).
7. D. L. MacLean and T. E. Graham, *Chem. Eng.*, **87**(4), 54 (1980).
8. C. R. Antonson, R. C. Gardner, C. F. King, and D. Y. Ko, *Ind. Eng. Chem. Proc. Des. Dev.*, **16**, 463 (1977).
9. *Chem. Eng. News*, Vol. 58, No. 20, 57 (1980).
10. T. Graham, *Philos. Mag.*, **32**, 401 (1866).
11. N. Yi-Yan, R. M. Felder, and W. J. Koros, *J. Polym. Sci. Polym. Phys. Ed.*, to appear.
12. C. Tanford, *Physical Chemistry of Macromolecules*, Wiley, New York, 1961, p. 352.
13. J. M. Van Gelder, Simple Separation Systems for Hydrogen Recovery, technical information bulletin, Monsanto Co., St. Louis, 1980.
14. D. R. Paul, and W. J. Koros, *J. Polym. Sci. Polym. Phys. Ed.*, **14**, 675 (1976).
15. D. R. Paul, *Ind. Eng. Chem. Proc. Des. Dev.*, **20**, 1921 (1976).
16. N. N. Li, R. B. Long, and E. J. Henley, *Ind. Eng. Chem.*, **57**, 18 (1965).
17. C. E. Rogers, M. Fels, and N. N. Li, in *Recent Developments in Separation Science*, N. N. Li, Ed., Chemical Rubber, Cleveland, 1972, Vol. III, p. 107.
18. S. T. Hwang, C. K. Choi, and K. Kammermeyer, *Sep. Sci.*, **9**, 461 (1974).
19. S. A. Stern, in *Membrane Separation Processes*, P. Meares, Ed., Elsevier, New York, 1976, Chap. 8.
20. K. Kammermeyer, in *Progress in Separation and Purification*, E. S. Perry, Ed., Interscience, New York, 1968, Vol. I, p. 335.
21. S. A. Stern, and W. Walawender, *Sep. Sci.*, **4**, 129 (1969).
22. S. Hwang, and K. Kammermeyer, *Membranes in Separations*, Wiley, New York, 1975.
23. S. A. Stern, in *Industrial Processing with Membranes*, Interscience, New York, 1972.
24. K. Kammermeyer, *Ind. Eng. Chem.*, **49**, 1685 (1957).
25. J. S. Vrentas, and J. L. Duda, *J. Appl. Polym. Sci.*, **22**, 2325 (1978).
26. R. M. Barrer, J. A. Barrie, and J. Slater, *J. Polym. Sci.*, **27**, 177 (1958).
27. A. S. Michaels, W. R. Vieth, and J. A. Barrie, *J. Appl. Phys.*, **34**, 1, 13 (1963).
28. V. Stannett, in *Diffusion in Polymers*, J. Crank and G. S. Park, Eds., Academic, New York, 1968, Chap. 2.
29. J. H. Petropoulos, *J. Polym. Sci., Part C*, **41**, 79 (1973).
30. W. R. Vieth, and K. J. Sladek, *J. Colloid Sci.*, **20**, 1014 (1965).
31. P. J. Fenelon, in *Permeability of Plastic Films and Coatings to Gases, Vapors and Liquids*, H. B. Hopfenberg, Ed., Plenum, New York, 1974, p. 285.
32. W. R. Vieth, J. M. Howell, and J. H. Hseih, *J. Membr. Sci.*, **1**, 177 (1976).
33. W. R. Vieth and J. A. Eilenberg, *J. Appl. Polym. Sci.*, **16**, 945 (1972).
34. W. J. Koros, A. H. Chan, and D. R. Paul, *J. Membr. Sci.*, **2**, 165 (1977).
35. J. A. Barrie, M. Williams, and K. Munday, *Polym. Eng. Sci.*, **20**, 20 (1980).
36. A. H. Chan and D. R. Paul, *J. Appl. Polym. Sci.*, **24**, 1539 (1979).
37. A. H. Chan and D. R. Paul, *Polym. Eng. Sci.*, **20**, 87 (1980).
38. R. A. Assink, *J. Polym. Sci. Polym. Phys. Ed.*, **13**, 1665 (1975).
39. W. J. Koros and D.R. Paul *J. Polym. Sci. Polym. Phys. Ed.*, **16**, 1947 (1978).
40. W. J. Koros and D. R. Paul, *Polym. Eng. Sci.*, **20**, 14 (1980).

41. W. J. Koros and G. N. Smith, *J. Appl. Polym. Sci.*, to appear
42. W. J. Koros, *J. Polym. Sci. Polym. Phys. Ed.*, **18**, 981 (1980)
43. G. S. Huvard, Ph.D. thesis, North Carolina State University, 1978
44. W. J. Koros and D. R. Paul, *J. Polym. Sci. Polym. Phys. Ed.*, **16**, 2171 (1978)
45. A. H. Chan, W. J. Koros, and D. R. Paul, *J. Membr. Sci.*, **3**, 117 (1978)
46. S. A. Stern, P. J. Gareis, T. F. Sinclair, and P. H. Mohr, *J. Polym. Sci.*, **7**, 2035 (1963).
47. G. Ranade, V. Stannett, and W. Koros, *J. Membr. Sci.*, to appear

Received December 16, 1980
Accepted April 13, 1981

Characterization of Penetrant Interactions in Kapton* Polyimide Using a Gravimetric Sorption Technique

L. R. ILER, R. C. LAUNDON, and W. J. KOROS, *Department of Chemical Engineering, North Carolina State University, Raleigh, North Carolina 27650*

Synopsis

Sorption of pure anhydrous ammonia and pure sulfur dioxide in Kapton polyimide has been measured at 30 and 35°C at subatmospheric pressures using a McBain quartz spring balance. The sulfur dioxide sorption and desorption was well described by the Fickian transport model; however, the ammonia sorption exhibited significant deviations from Fickian behavior. A substantial fraction of the initially sorbed ammonia remained in the film after extended periods under vacuum at 35°C. Infrared analysis of the treated film revealed the presence of new carbonyl and nitrogen–hydrogen stretching peaks characteristic of primary and secondary amides. These observations suggest that the ammonia reacts chemically with some of the imide linkages. Based on infrared analysis of the ammonia-exposed Kapton, heating the sample under vacuum at 120°C caused re-formation of most of the originally disturbed imide structures, with attendant evolution of ammonia as a condensation product.

INTRODUCTION

Gas separators based on permselective glassy polymer membranes offer an economical means for recovering valuable components from mixed gas streams. Choice of the correct polymer permits almost total blockage of the transfer of undesirable gaseous molecules while allowing the desired species to diffuse rapidly through the membrane.[1] In the synthesis of ammonia, the process stream from the reactor contains high concentrations of nitrogen and hydrogen along with other gases such as argon and ammonia in small, but significant, concentrations.[1] Gas permeators can be used to salvage hydrogen from the reactor purge gas stream, while preventing the accumulation of inerts in the system. Inside the separator, the hydrogen molecules sorb into polymeric hollow fibers, diffuse from a high-pressure region surrounding the fiber to a low-pressure region within the bore of the fiber, and are then recycled to the reactor.[2] After exposure to the process stream for a long period of time, the ability of the membrane to separate hydrogen from the mixed gas stream may decrease if the polymer is attacked by the components of the stream.

The present study focuses on a possible new polymer for gas separation service in demanding process environments such as the ammonia example cited above. Kapton, an aromatic poly(ether-imide) developed by du Pont, has been found to be resistant to both chemical and thermal attack. Furthermore, Kapton is a matrix polymer for use in novel graphite-reinforced composites which offer outstanding properties for important aerospace applications.[3] The sorption, transport and possible chemical attack of ammonia in this polymer is therefore

* Trademark of E. I. du Pont

Journal of Applied Polymer Science, Vol. 27, 1163-1175 (1982)
© 1982 John Wiley & Sons, Inc
CCC 0021-8995/82/041163-13$02.30

of interest in several areas and motivated the choice of this polymer/penetrant pair as the focus of the present study.

Koros et al.[4] and Patton[5] have studied sorption of SO_2 in Kapton at 35°C, and Sacher and Susko[6] have studied H_2O in Kapton between 20 and 55°C. Similar data for SO_2 were measured in the present study to substantiate the experimental techniques employed here. Whereas data existed for comparison with the SO_2/Kapton work, no previous studies of ammonia sorption in this polymer have been reported. Pulsed NMR data for ammonia interactions with polystyrene have, however, been reported by Assink, who observed normal sorption/desorption behavior in that system.[7]

SORPTION KINETICS OF GASES IN POLYMERS

Sorption kinetics of gases and vapors at low activities in polymers generally obey Fick's law given by

$$N = -D\frac{\partial C}{\partial x} \tag{1}$$

where N is the diffusive flux, C is the local concentration, D is the diffusion coefficient of the penetrant in the polymer, and x is the coordinate direction in which transport is occurring.[8] Although the diffusion coefficient may be concentration dependent, it is known that as long as eq. (1) applies in each local region of the polymer, an effective average diffusion coefficient can be used in the standard infinite series solution for an approximate description of the sorption and desorption process. In such cases, the effective diffusion coefficient D_{AV} appropriate for describing transport processes over a range of concentrations from C_1 to C_2 can be conveniently defined according to

$$D_{AV} = \frac{\int_{C_1}^{C_2} D(c)\,dC}{\int_{C_1}^{C_2} dC} \tag{2}$$

and evaluated from the "short time" solution of the infinite series expression given in eq. (3) for uptake into (or desorption from) a slab of thickness l:

$$\frac{M_t}{M_\infty} = 4\left(\frac{Dt}{l^2}\right)^{1/2}\left[\frac{1}{\pi^{1/2}} + 2\sum_{n=1}^{\infty}(-1)^n \text{ierfc}\left(\frac{nl}{2(Dt)^{1/2}}\right)\right] \tag{3}$$

where M_t and M_∞ are the mass sorbed (or desorbed) at time t and at "infinite" time, respectively. For values of $M_t/M_\infty \leq 0.5$, this equation can be approximated well by neglecting the infinite series contribution.[8] Alternatively, one can evaluate M_t/M_∞ at the half-point of either sorption or desorption and thereby calculate a separate effective diffusion coefficient from the sorption run (D_s) and the desorption run (D_d)[8]:

$$D_s = \frac{0.0492l^2}{(t_{1/2})_s} \tag{4a}$$

$$D_d = \frac{0.0492l^2}{(t_{1/2})_d} \tag{4b}$$

where $(t_{1/2})_s$ and $(t_{1/2})_d$ correspond to respectively the time for sorbing and desorbing one half of the penetrant which eventually is sorbed (or desorbed) in the run under consideration. Conventionally, in cases where the diffusion coefficient is dependent on concentration, one generally equates the average of the diffusion coefficients determined in the sorption and desorption runs to D_{AV}

$$D_{AV} = \frac{D_d + D_s}{2} \tag{5}$$

This technique was applied by Koros et al.[4] for SO_2 sorption in Kapton at 35°C. To verify our experimental techniques and equipment operation, we performed a similar characterization of our Kapton sample.

It is known that, in a given polymer, diffusion coefficients are strongly dependent on the molecular size of the penetrant molecule considered. A correlation between the Lennard–Jones collision diameter and the diffusion coefficients of various penetrants in a given polymer is well established.[8] Therefore, the diffusion coefficient of ammonia in Kapton can be estimated using reported diffusion coefficients in Kapton of water and sulfur dioxide which bracket ammonia in terms of molecular size. The semilogarithmic plot of D vs. the Lennard–Jones collision diameter shown in Figure 1 using the SO_2 data from Patton[5] and the water data from Sacher and Susko[6] at 30°C suggests that an average diffusion coefficient, corresponding to eq. (5), should have a value of approximately 1.24×10^{-9} cm^2/s. Therefore, it was anticipated that an easily measurable response for ammonia sorption would be observed with a half-time for sorption calculated from eq. (4a) of approximately 4.19 min (or 2.05 min$^{1/2}$) in a 1-mil film and 1.05 min (or 1.02 min$^{1/2}$) in a 1/2-mil film.

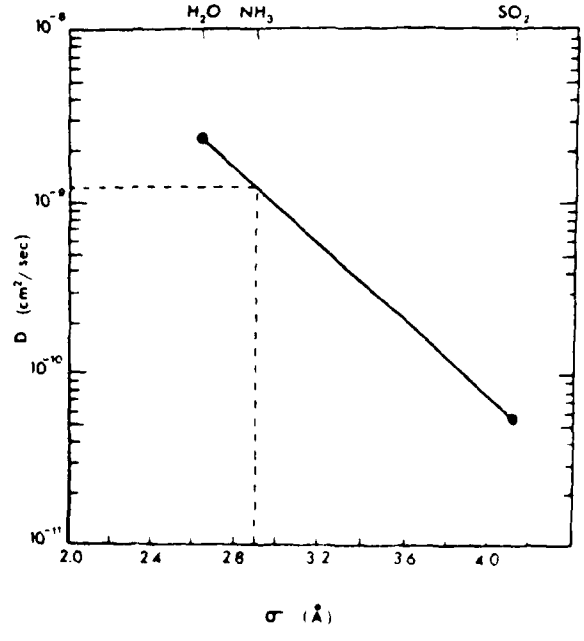

Fig. 1. Estimation of the diffusivity of NH_3 in Kapton polyimide at 30°C using the Lennard-Jones collision diameter as a characteristic size correlation parameter.

EXPERIMENTAL

Materials

The Kapton poly(ether-imide) used in the present study was kindly supplied by the E. I. du Pont Company, Circleville, Ohio.

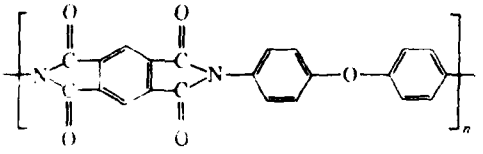

Kapton poly(ether-imide)

Measurements by precision micrometry indicated film thicknesses of 1 ± 0.01 and 0.5 ± 0.01 mil, respectively, for the two different samples studied. Both the SO_2 and anhydrous ammonia used as penetrants in sorption experiments were obtained from Air Products and Chemicals, Inc., Raleigh, NC, at a purity of 99.9%. The gases were used as received without further treatment.

Apparatus

A McBain quartz spring balance was constructed following the design described by Hopfenberg et al.[9] With this sytem, a direct gravimetric measure of penetrant uptake within the polymer as a function of time can be determined by observing changes in spring extension. To collect data, a polymer sample is suspended from a calibrated quartz spring within a constant temperature and pressure sorption cell. The mass of the penetrant sorbed by the polymer film is then determined by measuring spring extension with a cathetometer.

The sorption cell and supporting apparatus are shown in Figure 2. A quartz spring with a maximum capacity of 100 mg, corresponding to a maximum extension of approximately 200 mm, was hung from the cell cap. Using calibration weights, a spring constant of 0.500 ± 0.006 mg/mm extension was obtained. The polymer sample was then hung at the base of the spring. A glass reference fiber was hung parallel to the spring to compensate for small shifts in the spring support position which may occur during the experiment. A precision microscope, capable of detecting spring deflections as small as 0.005 mm, was used to observe spring extension. Thus, deflections represented by masses as small as 2.5 μg were detectable.

The sorption cell was maintained at a constant temperature by circulating an ethylene glycol mixture from a bath through a fluid jacket enclosing the cell. Aluminum foil was wrapped around portions of the cell and grounded to reduce static attraction between the cell wall and the polymer film. A large vapor reservoir was used to increase the total volume of the sorption system, thereby eliminating measurable fluctuations in pressure within the sorption cell.

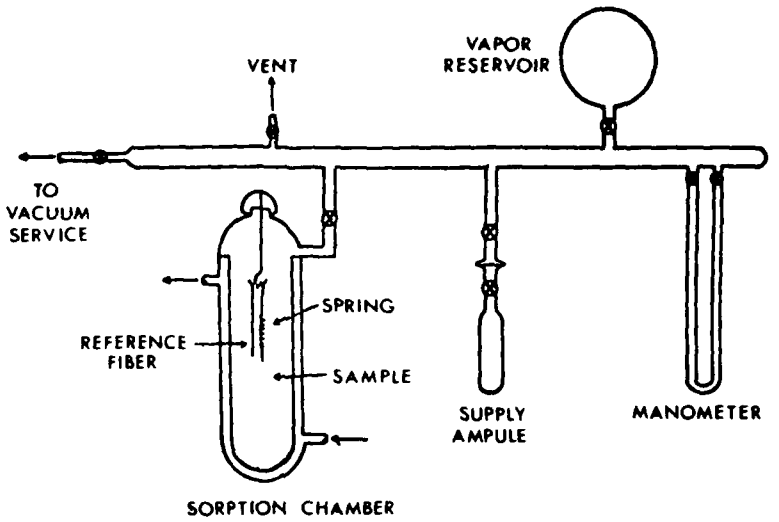

Fig. 2. McBain balance apparatus used for gravimetric determination of vapor sorption data.

Procedures

A Kapton sample of known weight was hung from the quartz spring and degassed for 24 h. An apparently, constant weight of the degassed sample was obtained within 10h. The system, excluding the sorption cell, was pressurized with penetrant to an empirically determined value that would give the desired sorption pressure when the stopcock to the sorption cell was opened. At time zero, penetrant was admitted into the sorption cell, and the spring extension was measured as a function of time. The system pressure was monitored during the experiment and was permitted to vary no more than ±5 mm Hg. System pressure was adjusted by either introducing more penetrant or by raising or lowering the heating tape temperature in the exterior lines. To begin a desorption experiment, the valve connecting the sorption cell to the vacuum line was opened, and the contraction of the spring was observed as a function of time.

RESULTS AND DISCUSSION

SO_2 Sorption Kinetics

A typical normalized sorption/desorption cycle for sulfur dioxide in ½-mil Kapton is shown in Figure 3 as a plot of M_t/M_∞. For the sorption cycle, M_t is the mass of penetrant sorbed at any time t, and M_∞ is the mass of penetrant sorbed at equilibrium. For the desorption cycle, M_t and M_∞ refer to the mass of penetrant desorbed at time t and at equilibrium, respectively. As shown in the figure, penetrant uptake initially varies linearly with $t^{1/2}$, consistent with Eq. (3) for values of $M_t/M_\infty < 0.5$, and eventually becomes concave to the time axis. Molecules initially sorb into the polymer at a rapid rate due to the large concentration gradient at the film surface; and as the concentration gradient diminishes, the rate of penetrant uptake slows and eventually reaches a saturation point at equilibrium. The sorption and desorption processes are well

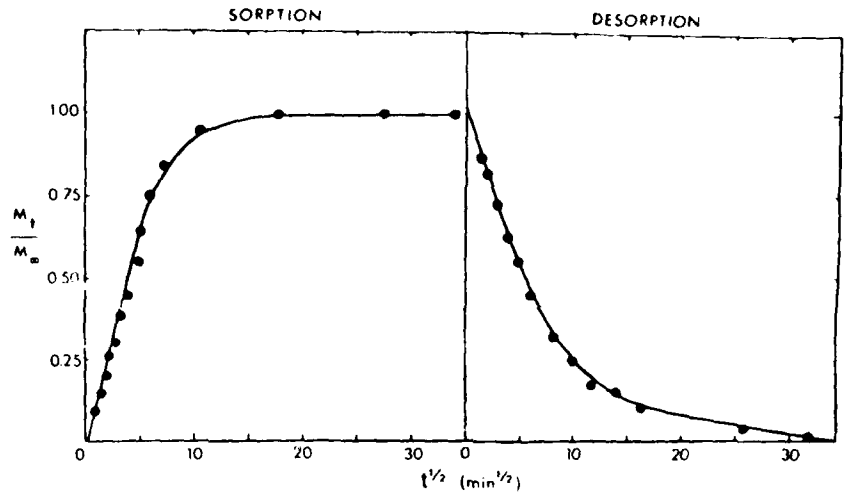

Fig. 3. Sorption/desorption kinetic runs for a ½-mil Kapton polyimide film at 35°C and at a SO_2 pressure of 0.33 atm.

described by Fick's law; the lines drawn through the sorption and desorption curves were calculated using eq. (3) with the respective value of $D_s = 6.75 \times 10^{-11}$ cm^2/s and $D_d = 4.37 \times 10^{-11}$ cm^2/s, determined using Eqs. (4a) and (4b). It was expected that sorption/desorption curves for ammonia in Kapton would be similar in shape to those for SO_2 but, as discussed earlier, would show that ammonia sorbs and desorbs roughly 20 times faster on a normalized basis (M_t/M_∞) because of its smaller relative molecular size.

Ammonia Sorption/Desorption Kinetics

Using the system described previously, with 1-mil-thick Kapton as the polymer and ammonia as the penetrant, the sorption experiment shown in Figure 4 was made at 35°C. The resulting sorption curve was significantly more protracted than was expected for a small penetrant like ammonia, which is not much larger than water in terms of collision cross section (Fig. 1). Another Kapton film (½-mil-thick) was loaded into the cell, and a similar response at 30°C was discovered for this film also. Figure 5 shows that the approach to equilibrium was not complete even after two weeks, although the sorption half-time at 30°C was calculated from eq. (4a) using the ammonia D estimated in Figure 1 to be only 1.05 min for ammonia in a ½-mil film of Kapton.

Such a protracted process in the case of a small penetrant such as ammonia suggests that simple Fickian sorption as described by eq. (3) was not adequate to explain the observed data.[10] It was originally suspected that a physical relaxation of the polymer chains was occurring and causing the extremely slow uptake and was responsible for the observed deviations from Fickian uptake kinetics. If the deviations arose due to strictly physical interactions, one would expect that during a corresponding desorption run, the amount of gas desorbed should nevertheless equal the amount sorbed when the surrounding desorption bath pressure was essentially zero (i.e., $< 10^{-3}$ torr). As shown in Figure 5, only about one-half of the ammonia which was sorbed into the polymer was removed

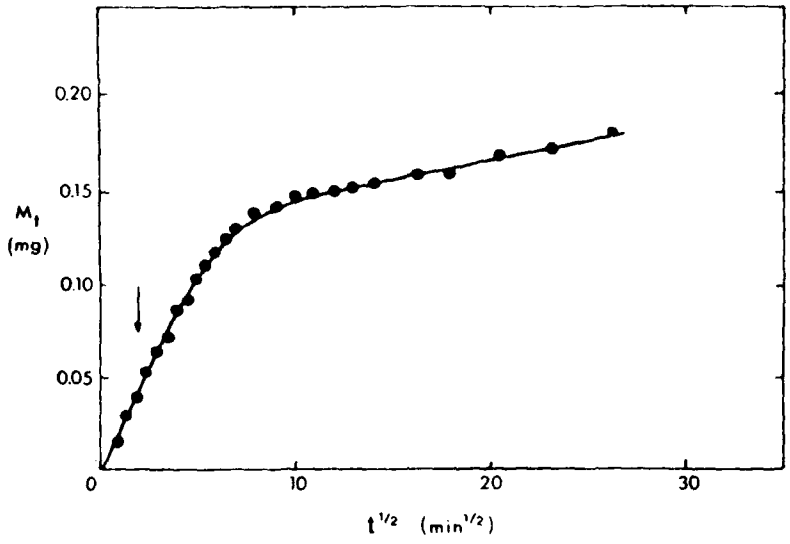

Fig. 4. NH_3 sorption kinetics in a 1-mil Kapton film at 35°C and at an NH_3 pressure of 0.29 atm. Arrow marks the expected sorption half-time for ammonia in 1-mil Kapton at 30°C on the basis of simple size dependent diffusion calculated from eq. (4a) using the value for D estimated from Fig. 1. One would expect the diffusion coefficient of ammonia to be even larger under the 35°C test conditions than at 30°C, so the half-time might be expected to be even shorter than indicated by the arrow. The kinetics are therefore being protracted by some complex factors.

even after prolonged pumping (>12 days, not shown in Fig. 5). Using the information from the sorption cycle, it is reasonable to assume that the ammonia might be chemically attacking the polymer and thereby becoming a nondesorbable component of the sample.

The most likely point of ammonia attack on the polymer is at the imide linkage, with resultant formation of primary and secondary amides:

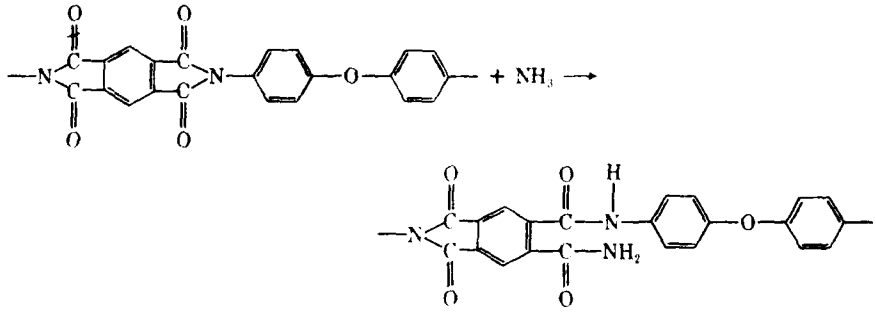

One method of determining whether such an attack takes place is through the use of infrared spectroscopy. Amide groups will become apparent as new carbonyl peaks in the range 1630–1700 cm^{-1}, and nitrogen–hydrogen stretching will appear in the region 3200–3500 cm^{-1}.[11] Infrared spectra for both the as-received sample and the exposed sample corresponding to the sorption run in Figure 5 are presented in Figures 6 and 7. Clearly, the presence of the new carbonyl and nitrogen–hydrogen stretching peaks supports the postulated attack of ammonia at the imide linkage.

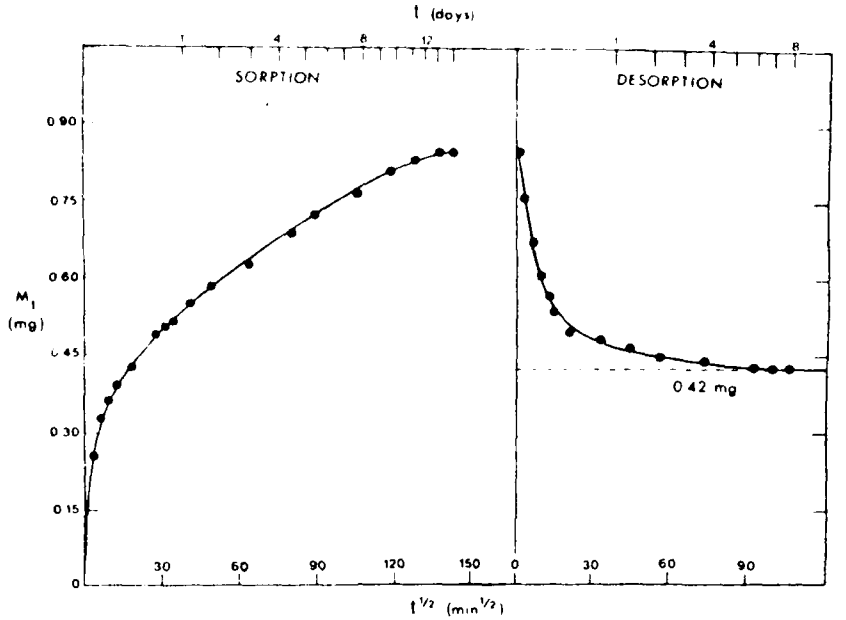

Fig. 5. Sorption/desorption kinetic runs for a ½-mil Kapton polyimide film at 30°C and at an NH_3 pressure of 0.36 atm. Note that at equilibrium 0.42 mg of the penetrant remained in the polymer sample after protracted desorption under vacuum.

During the desorption cycle, the sorbed ammonia in the Kapton sample is quickly removed, as shown in Figure 5; hence the rate of reaction of ammonia falls rapidly. If one neglects the small extent of reaction which occurs during the desorption process and replots the data in the form (M_t/M_∞) consistent with eq. (3), the plot shown in Figure 8 results. Application of eq. (4b) to the data in Figure 8 yields a value of the diffusion coefficient for ammonia equal to 2.35×10^{-11} cm^2/s. The dashed line through the data points in Figure 8, calculated from eq. (3) using the above value of D, describes the process quite well up to a value of $M_t/M_\infty = 0.6$. The tendency of the model equation to deviate from the data at long times is characteristic of systems in which the diffusion coefficient increases with increasing local penetrant concentration. In the final phases of desorption, the lower diffusion coefficient associated with the low level of penetrant remaining in the film causes the protracted desorption process. If one compares the effective diffusion coefficient estimated from Figure 1 strictly on the basis of size-dependent factors, it is obvious that the diffusion coefficient lies approximately 50 times lower than the expected mobility determined from strictly size-dependent factors.

The activation energy E_d for diffusion in polymeric media is generally associated with the energy required to produce a sufficiently large gap between chains to permit the passage of a penetrant.[12] Diffusion coefficients decrease sharply with increasing penetrant size due to the fact that more energy must be available to cause formation of a large gap to permit passage of a large penetrant than to cause formation of a small gap to permit passage of a small penetrant. This fact can be seen from consideration of Eq. (6):

$$D = D_0 \exp\left(\frac{-E_d}{RT}\right) \tag{6}$$

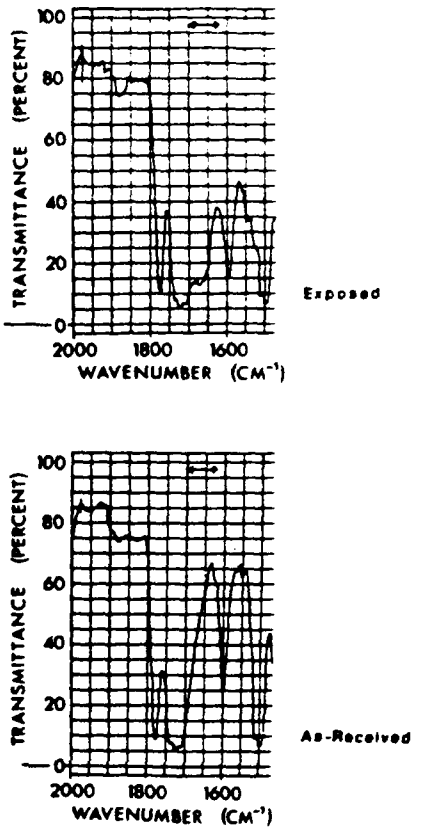

Fig. 6. Infrared spectra of the as-received and the NH_3-exposed Kapton polyimide samples. Note the increased absorbance in the 1630–1700 cm^{-1} range consistent with the reaction shown between NH_3 and the imide structure.

Although additional factors enter into determination of D_0 and hence D, the above discussion regarding E_d still deals with the major issues in simple size-dependent diffusion.[12] The above discussion, which assumes that E_d is associated simply with generation of a hole into which the penetrant can move, implies that if a hole opens next to a penetrant, no additional activation energy is required to permit the penetrant to execute the diffusional jump into the hole. In cases of strongly interacting penetrant/polymer systems, such an assumption is not necessarily correct, and one may expect that the effective activation energy is the sum of the polymer-related activation contribution E_1 and the penetrant-related activation contribution E_2, i.e., $E_d = E_1 + E_2$.

If one neglects, as a first approximation, differences in D_0 between a weakly interacting penetrant (whose D should be given by the correlation line in Fig. 1) and a strongly interacting penetrant such as ammonia, an estimate of the $\Delta E_d = (E_1 + E_2) - E_1$ between the two cases can be evaluated:

$$\ln\left[\frac{D_{NH3}}{D_{Fig.1}}\right] = \frac{-[E_1 + E_2 - E_1]}{RT} \tag{7a}$$

$$\Delta E_d = 2.4 \text{ kcal/mol} \tag{7b}$$

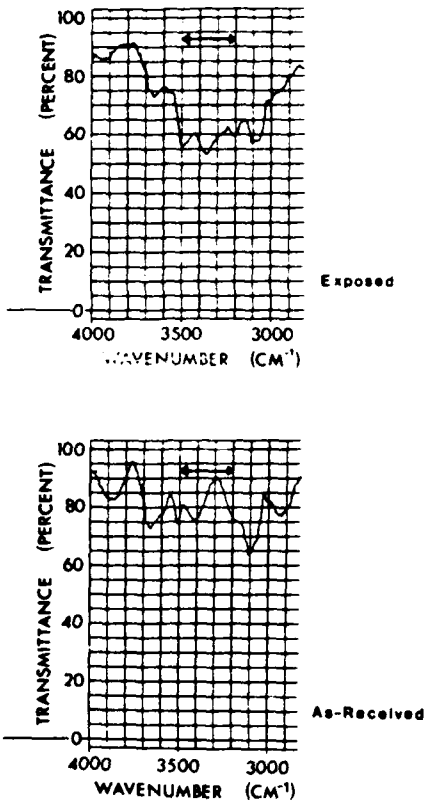

Fig. 7. Infrared spectra of the as-received and the NH_3-exposed Kapton polyimide samples. Note the increased absorbance in the 3200–3500 cm^{-1} range consistent with the reaction shown between NH_3 and the imide structure.

One can therefore explain the observed lower value of the NH_3 diffusion coefficient compared to the prediction from Figure 1 on the basis of an additional activation contribution of slightly over 2 kcal/mol. This additional contribution arises from the need to overcome strong specific NH_3–Kapton interactions prior to executing a diffusional jump and is of a reasonable order of magnitude for hydrogen bonding interactions. To demonstrate this effect completely, one should compare the diffusion coefficient and activation energy of NH_3 in Kapton to another less strongly interacting penetrant of the same approximate size (e.g., neon, σ = 2.82 Å).

Sample Heat Treatment

The sample corresponding to the sorption/desorption runs in Figure 5 was removed from the sorption cell and heated under vacuum at 120°C for 72 h. It was found that the IR spectrum of the heat-treated sample again approached that of the as-received Kapton, suggesting that the disrupted imide linkages reform at elevated temperatures with the elimination of NH_3. This observation is consistent with the fact that the standard technique for producing such imide

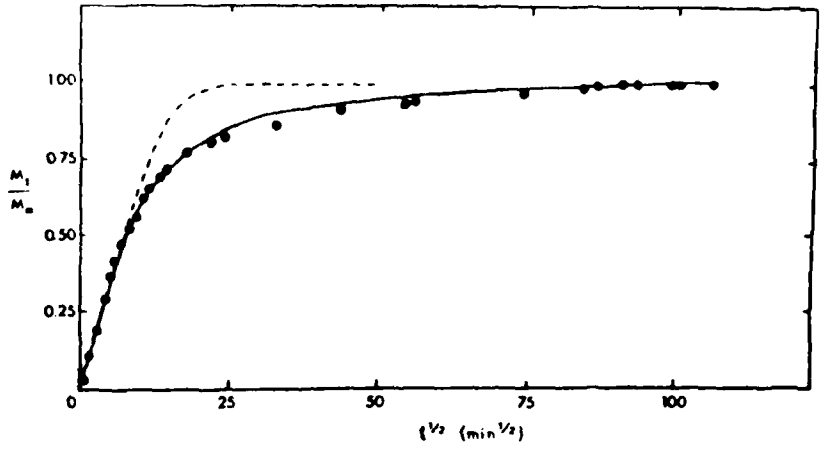

Fig. 8. Desorption kinetic run for 0.5-mil Kapton polyimide film at 30°C and at a NH_3 pressure of 0.36 atm. Using the diffusion coefficient calculated from eq. (4b), the dashed line represents Fickian desorption.

linkages involves condensing pyromellitic dianhydride with bis(4-aminophenyl) ether. The first step, to the polyamic acid intermediate, occurs readily at room temperature:

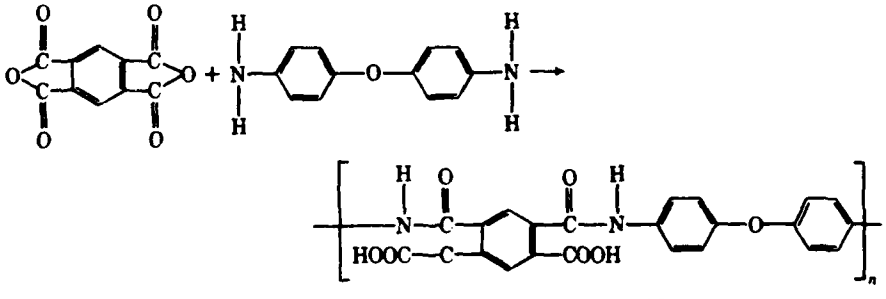

polyamic acid

Upon heating above 150°C, the amic acid dehydrates by cyclization to form the insoluble polyimide[13]:

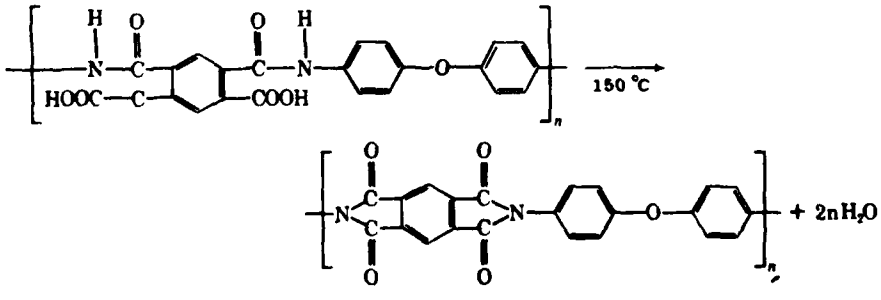

Presumably, in the present case, the recyclization process at 120°C simply gives

rise to ammonia as the condensation product rather than water as in the amic acid case:

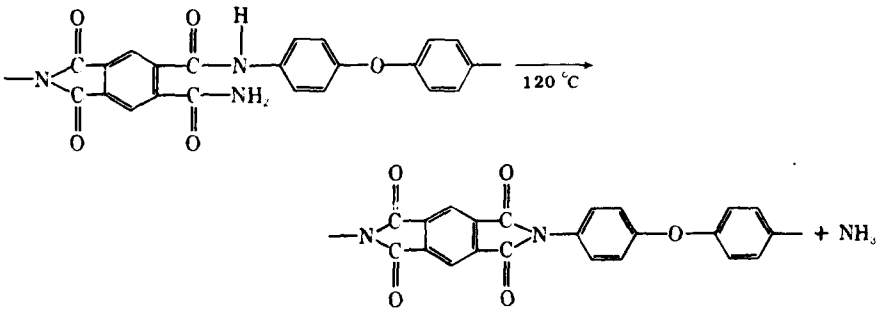

CONCLUSIONS

Ammonia has been shown to interact chemically with Kapton at 35°C. The point of attack appears to be the imide group present in the chain backbone. Over a two-week period, approximately 17% of the imide structures were reacted under the conditions studied.

It is likely that many polymers formed by the reaction of amine-ended monomers and carbonyls have a similar propensity to undergo ammonia attack. This fact could be of considerable importance, since many of the exotic, high-temperature polymers use amine-ended monomers as starting materials. The susceptibility of these polymers to ammonia attack may be considered an "Achilles' heel" for such otherwise robust material. It is also possible that other basic and, to a lesser degree, acidic compounds may react with the imide structure of Kapton. Imide structures tend to be quite stable in neutral aqueous environments but are known to be susceptible to attack by either basic or strongly acidic compounds. This fact might be of considerable importance in graphite-reinforced applications where the bonding between matrix and filler is critical.

Further research, involving the use of pulsed NMR and Raman spectroscopy, could be useful to investigate the molecular environment experienced by the sorbed ammonia and further aid in distinguishing the fraction of sorbed molecules that are physically dissolved from those that have undergone a specific chemical reaction with Kapton. The diffusion coefficient estimated for ammonia in Kapton suggests the existence of strong physical as well as weak chemical interactions between this penetrant/polymer pair. To completely model the coupled processes of diffusion and reaction over the range of practical importance, the concentration dependence of this diffusion coefficient and the temperature dependence of both the diffusion and reaction rate coefficients needs to be evaluated. This work is currently under way.

The authors gratefully acknowledge the financial support of this project by Army Research Office under Grant Number DAAG29-81-K-0039.

References

1. R. J. Gardner, R. A. Crane, and J. F. Hannan, *CEP*, 73(10), 76 (1977).
2. Composite Membrane Key to Gas Separators, *C&EN*, 57 (May 1980).
3. R. E. Fornes, J. D. Memory, and N. Naranong, *J. Appl. Polym. Sci.*, to appear.
4. W. J. Koros, C. J. Patton, R. M. Felder, S. J. Fincher, *J. Polym. Sci. Phys. Ed.*, **18**, 1485 (1980).
5. C. J. Patton, Dual Mode Sorption and Transport of Condensable Penetrants in Glassy Polymers, M.S. thesis, North Carolina State University, Raleigh, NC, 1980.
6. E. Sacher and J. R. Susko, *J. Appl. Polym. Sci.*, **23**, 2355 (1979).
7. R. A. Assink, *J. Polym. Sci. Polym. Phys. Ed.*, **13**, 1665 (1975).
8. J. Crank and G. S. Park, Eds., *Diffusion in Polymers*, Academic, London, 1968, Chaps. 1 and 2.
9. C. H. M. Jacques and H. B. Hopfenberg, *Polym. Eng. Sci.*, **14**, 441 (1974).
10. A. R. Berens and H. B. Hopfenberg, *J. Polym. Sci. Phys. Ed.*, **17**, 1757 (1979).
11. R. Zbinden, *Infrared Spectroscopy of Polymers*, Academic, New York, 1964.
12. G. J. Van Amerongen, *Rubber Chem. Technol.*, **37**, 1065 (1964).
13. N. Platzer, *Ind. Eng. Chem.*, **61**(5), 10 (1969).

Received July 20, 1981
Accepted August 6, 1981

Reversible Isopentane-Induced Depression of Carbon Dioxide Permeation through Polycarbonate

R. T. CHERN, W. J. KOROS, H. B. HOPFENBERG, and V. T. STANNETT, *Department of Chemical Engineering, North Carolina State University, Raleigh, North Carolina 27650*

Synopsis

Permeability data are reported for carbon dioxide in Lexan polycarbonate at 35°C. Measurements were made for both pure carbon dioxide and for a mixed feed consisting of carbon dioxide with a 117.8-torr (0.155-atm) partial pressure of isopentane. The effects of varying upstream CO_2 driving pressure from 1 up to 20 atm were studied. The permeability to CO_2 is reduced significantly in the presence of isopentane; however, the fractional depression of the CO_2 permeability due to the isopentane at low driving pressures is much more significant than at high CO_2 driving pressures. The well-known pressure dependence of carbon dioxide permeabilities in glassy polymers, therefore, is largely diminished by introducing isopentane to the pure carbon dioxide feed. These observations are consistent with a model for transport in glassy polymers which explains the observed trends in terms of competition between the two penetrants for microvoid sorption sites existing in the nonequilibrium glassy polymer. Exclusion of carbon dioxide from microvoid sorption sites by the more condensable isopentane preempts transport through the microvoid regions, resulting in the observed depression of the CO_2 permeability.

INTRODUCTION

Glassy polymer membranes offer unusually high selectivities compared to rubbery polymers for separating small molecules such as hydrogen and helium from large molecules.[1] Experimental data indicate, however, that the permeabilities of individual gases in a mixture, in many cases, are quite different from those obtained from pure-gas measurements.[1,2] Consequently, separation factors taken as the ratios of pure-component permeabilities of the respective penetrants can be significantly different from those measured directly with actual mixed gas feeds.

The transport of pure gases in glassy polymers is satisfactorily described by the so-called dual-mobility or *partial-immobilization model*.[3] This model contends that there are two different sorption populations associated with different molecular environments in the polymer. The total sorption concentration in the two populations is described well by superposition of a Henry's-law term and a Langmuir term. The Langmuir mode of sorption is believed to be associated with preexisting gaps between unrelaxed polymer chain segments in the nonequilibrium glassy polymer, and therefore only exists below the glass transition temperature. Conversely, the Henry's-law mode of sorption exists both above and below the glass transition of the polymer and presumably is associated with sorption of penetrant between chain segments which have relaxed to essentially their equilibrium packing density. Permeation involves both sorption in and diffusion through the two distinct molecular environments. The mobility

Journal of Polymer Science: Polymer Physics Edition, Vol. 21, 753–763 (1983)
© 1983 John Wiley & Sons, Inc.
CCC 0098-1273/83/050753-11$02.10

of penetrant executing diffusional jumps within and between these two molecular environments can be different, thereby introducing an interesting form of concentration dependence of the effective diffusion coefficient, even in the absence of plasticization.[4]

On the basis of this model, Koros et al.[5] proposed that, in the absence of plasticization, competition among penetrants for the limited excess volume in the glassy polymer is the main cause for several previously unexplained effects of feed composition on the performance of permeators for separation of gas mixtures.[2,6] Pye et al.[6] reported data for several glassy polyimides which are qualitatively consistent with this hypothesis. A generalized dual-mobility model was developed by Koros et al.[5] to deal with these effects. For example, when the downstream pressure is negligible, the permeability to a component A in a binary gas mixture was shown to be given by

$$P_A = k_{DA}D_{DA}[1 + F_AK_A/(1 + b_Ap_A + b_Bp_B)] \quad (1)$$

The definitions of the various parameters in eq. (1) are presented in the Nomenclature section. The parameters in eq. (1) can be obtained simply from pure-gas sorption and permeability measurements. According to eq. (1), the presence of a penetrant B with a very high affinity constant ($b_B \gg b_A$) can substantially reduce the permeability of A. This depression can occur even if the partial pressure of component B is considerably smaller than that of component A in the feed stream. In this paper, we present a model system designed to treat explicitly the premises of this hypothesis.

EXPERIMENTAL

An evaporator containing liquid isopentane was added to the feed line of the system originally designed by Huvard for the study of carbon dioxide permeation in polyacrylonitrile.[7] For runs involving mixed penetrant feeds, the refrigerated evaporator permitted saturation of the CO_2 feed stream with isopentane at any chosen temperature prior to introduction to the permeation cell. The low flow rate of gas (10 cm^3/min at room temperature and pressure), and the use of a glass wool demister section eliminated entrainment of liquid isopentane. The thermostat temperature was controlled at -17.0 ± 0.1°C to yield a partial pressure of isopentane of 117.8 ± 0.7 torr (0.155 ± 0.0009 atm)[8] in the feed stream. A coil-type heat exchanger (¼-in.-o.d., 10-ft-long stainless-steel 316 tube) was used to bring the gas temperature up to 35°C before the feed gas entered the permeation cell.

The manometric permeation system employed in this study permits measurement of the flux of penetrant by monitoring the pressure increase in a fixed downstream volume (660 cm^3) using a precise (±1% of reading) capacitance manometer (MKS Baratron 221). The downstream receiver pressure was always at $\leq 2 \times 10^{-3}$ atm whereas the upstream driving pressure ranged from 1 to 20 atm. The assumption of an effectively zero downstream pressure was, therefore, well satisfied. The permeation measurements were carried out at 35.0 ± 0.2°C. Coleman-grade carbon dioxide (99.99% pure) was supplied by Air Products and Chemicals, Inc., Allentown, PA. Certified-grade isopentane (99.2% pure) was supplied by Fischer Scientific Corp., Pittsburgh, PA. The 4-mil Lexan polycarbonate film used in this study was supplied by G.E. Corp., Pittsfield, MA.

By the procedures outlined in Appendix A, using the data reported by both Barrie et al.[9] and Koros et al.,[10] the permeability of polycarbonate to isopentane at 35°C and 0.155 atm is estimated to be ca. 7×10^{-12} cm^3(STP)cm/(cm^2 s cmHg). On the other hand, the permeability of pure carbon dioxide at the lowest pressure studied is 6.28×10^{-10} cm^3(STP)cm/(cm^2 s cmHg). For the present study, the partial pressure of isopentane was maintained at 0.155 atm and the lowest CO_2 partial pressure was 5.294 atm. Under these conditions, the flux of carbon dioxide through the Lexan film will then be approximately 3100 times that of isopentane under steady-state permeation conditions. Even if the competition effect mentioned previously lowered the permeability of carbon dioxide to one-half its pure-component value, the contribution of isopentane at steady state to the overall flux is less than 0.1% and can be neglected in considering the overall diffusive flux.

The time required to reach apparent steady-state CO_2 permeation for the 4-mil film used in the present study was on the order of 1.5–2 h for both the pure and mixed feed cases. After achievement of apparent steady-state permeation, the downstream receiving volume was evacuated and the apparent permeability was rechecked at least one or two more times to verify that the flux was indeed constant after the 2-h period.

Based on the transport model described earlier,[5] a numerical non-steady-state permeation analysis was performed using parameters for the CO_2/polycarbonate system reported earlier.[4] The calculations indicate that essentially steady-state CO_2 permeation behavior is to be anticipated in the 4-mil Lexan film at 35°C after less than 2 h in both the pure and mixed feed situations. These model calculations hold as long as local sorption equilibrium of all mixture components is attained rapidly at the two membrane faces, even if the isopentane flux is far from steady state. These model predictions are consistent with the observations noted above; however, the relatively thick film used in the present study (4 mils) precluded the possibility of waiting for steady-state permeation of isopentane to confirm unequivocally all details of the model predictions. On the basis of the estimated magnitudes of the transport parameters for isopentane (Appendix A) one would expect that the establishment of steady-state permeation for isopentane would require approximately nine months at 35°C in a 4-mil polycarbonate film. An analysis of the non-steady-state behavior of such mixed penetrant systems will be described in detail in another article. However, a brief discussion of the time lag which reflects the time required to reach steady-state permeation is included in Appendix B.

RESULTS AND DISCUSSION

The permeability to CO_2, both in the absence and in the presence of the 0.155-atm isopentane partial pressure, is plotted as a function of feed pressure in Figure 1. Curve 1 represents the data in the presence of isopentane, while Curve 2 represents the corresponding permeabilities of carbon dioxide in the same Lexan film in the absence of the isopentane contaminant. The permeability of the polycarbonate film to pure CO_2 was essentially the same before and after exposure to the low partial pressure of isopentane. This indicates that no significant permanent change in the polycarbonate film was effected by exposure to the low partial pressure of isopentane. It is apparent that the depression effect

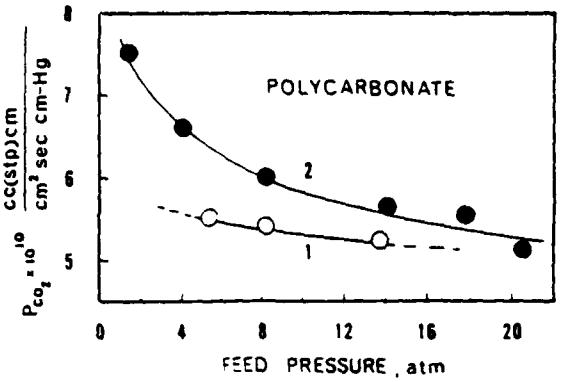

Fig. 1. Permeability of CO_2 in polycarbonate at 35°C in the presence (1) and absence (2) of a 117.8-mmHg partial pressure of isopentane in the upstream feed to the cell.

of isopentane on the carbon dioxide permeability is large at low pressures (ca. 20% at $p_{CO_2} = 5$ atm) and gradually diminishes as the driving pressure of carbon dioxide increases, becoming negligible when $p_{CO_2} \geq 20$ atm.

According to eq. (1), if carbon dioxide is designated as A and isopentane as B, then for the pure-component CO_2 case, we have

$$P_A = k_{DA} D_{DA} [1 + F_A K_A/(1 + b_A p_A)] \tag{2}$$

In such a case, the permeability of pure carbon dioxide is a linear function of $1/(1 + b_A p_A)$ with an intercept of $k_{DA} D_{DA}$ and a slope equal to $k_{DA} D_{DA} F_A K_A$. This relationship is verified in Figure 2 for the case where pure carbon dioxide is used

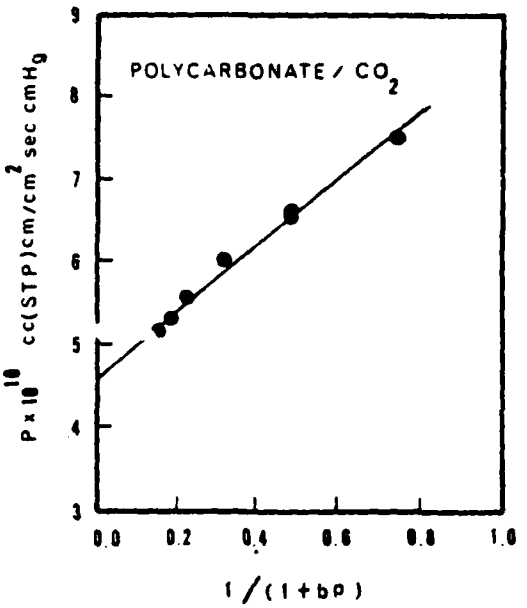

Fig. 2. Permeability of pure CO_2 at 35°C plotted according to eq. (2).

TABLE I
Sorption Parameters for Carbon Dioxide in Polycarbonate at 35°C

	C'_H [cm³(STP)/cm³]	b (atm⁻¹)	k_D [cm³(STP)/cm³ atm]
Koros et al.[10]	18.805	0.2618	0.6852
Sanders[11]	17.61	0.2563	0.6751

as the feed. The plot also provides the parameters $k_D D_D$ and FK for carbon dioxide. The sorption parameters of carbon dioxide were determined from sorption data provided by this laboratory[11] and are reproduced in Table I; the parameters reported by Koros et al.[10] are also included for comparison. On the other hand, the affinity constant of isopentane b_B is not currently available. Although a direct test of the validity of eq. (1) is therefore not possible, eq. (1) can be rearranged to give eq. (3), which permits a test of the accuracy of the general form of eq. (1) under conditions in which p_B is held constant:

$$\frac{k_{DA}D_{DA}}{P_A - k_{DA}D_{DA}} = \frac{1 + b_B p_B}{F_A K_A} + \frac{b_A p_A}{F_A K_A} \tag{3}$$

Plotting the left-hand side of eq. (3) against p_A one should find a straight line with an intercept of $(1 + b_B p_B)/F_A K_A$ and a slope equal to $b_A/F_A K_A$ by applying linear regression analysis. Since b_B is the only unknown, it is then possible to calculate the value of b_B using the intercept of this plot. The plot shown in Figure 3 using the data in Table I and Figure 1 yields a good straight line and indicates a value of b_B equal to 13.97 atm⁻¹. The linearity of the plot provides satisfying consistency with the theory presented previously. The value of the slope in eq. (3) determined from this figure (0.245 atm⁻¹) is sensitive to experi-

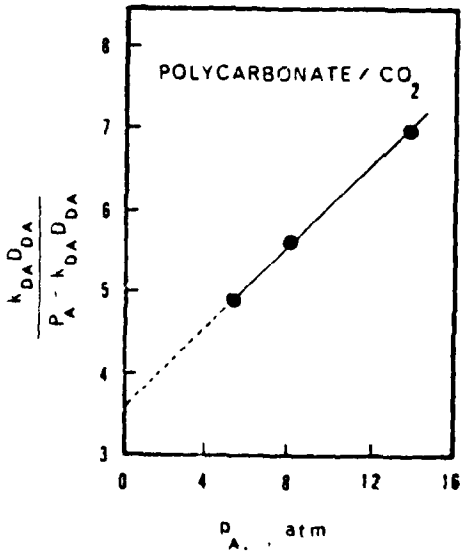

Fig. 3. Data from Fig. 1 plotted according to eq. (3) for estimation of the affinity constant of isopentane in polycarbonate at 35°C.

mental uncertainty in the mixed gas data; however, its value is satisfyingly consistent with the corresponding value calculated independently from pure-component CO_2 data (0.291 $atm^{-1} = b_A/F_A K_A$).

The affinity constants for various fixed gases in Lexan polycarbonate can be correlated well using the Lennard–Jones potential-well depth of the respective gases as shown in Figure 4. The affinity constant estimated in the present study for isopentane along with the value for *n*-propane reported by Barrie et al.[9] are also included in this figure. No experimental data are available for ϵ/k for isopentane; therefore the value was estimated using the predictive methods summarized by Reid et al.[12] The differences in the predicted values of ϵ/k are reflected by the uncertainty band in Figure 4. Depending on the correct value of ϵ/k for isopentane, one might conclude that $\ln(b)$ either correlates linearly with ϵ/k or tends to increase more than linearly. The affinity constant reported by Barrie for *n*-propane would tend to suggest a higher-order dependency on ϵ/k since the value of b for *n*-propane lies substantially above the line drawn through the data for fixed gases. Direct sorption measurement of the affinity constant for isopentane will be performed in the future for comparison to the indirect estimate reported here on the basis of transport measurements.

CONCLUSIONS

Carbon dioxide permeability was reduced by up to 20% compared to the pure-component case by the presence of a partial pressure of isopentane in the feed of only 0.155 atm at a total pressure of 5 atm. The predictions of the generalized dual-mobility model for mixed penetrants agree well with the experimental data reported here. The sorption affinity constant of isopentane in Lexan estimated through eq. (3) is reasonably consistent with a value predicted by a correlation between Lennard–Jones potential-well depth and the affinity con-

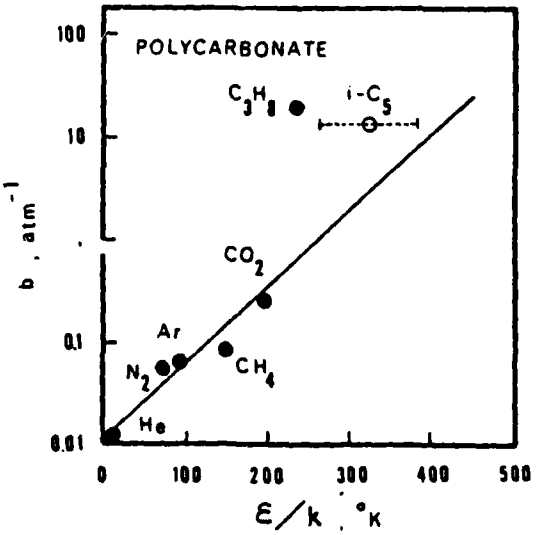

Fig. 4. Affinity constants of penetrants in polycarbonate at 35°C plotted vs. the Lennard–Jones potential-well depth ϵ/k.

stants of several penetrants. This correlation was established previously through direct sorption measurements with various penetrants in Lexan polycarbonate at 35°C. The present work then provides additional, albeit indirect, support for the validity of the proposed model for mixed penetrant sorption and transport in glassy polymers. Direct and more comprehensive verification of the model is currently under way using several gases and vapors in a number of polymers.

The authors gratefully acknowledge the support of this work by combined grants from the National Science Foundation, Grant No. CPE-79-18200, and the Army Research Office, Grant No. DAAG29-81-K-0039. Also, the help of Mr. E. S. Sanders in collecting the sorption data for CO_2 in polycarbonate is acknowledged.

APPENDIX I: ESTIMATION OF THE PERMEABILITY OF POLYCARBONATE TO ISOPENTANE AT 35°C AND 0.155 atm DRIVING PRESSURE

The value of the permeability of polycarbonate to isopentane (component B) can be calculated from eq. (A1) if values of the appropriate sorption and transport parameters are available, viz.,

$$P_B = k_{DB}D_{DB}[1 + F_BK_B/(1 + b_Ap_A + b_Bp_B)] \tag{A1}$$

or

$$P_B = k_{DB}D_{DB} + D_{HB}C'_{HB}b_B/(1 + b_Ap_A + b_Bp_B) \tag{A2}$$

The maximum value of P_B will correspond to the case $p_A = 0$, so that

$$(P_B)_{max} = k_{DB}D_{DB} + D_{HB}C'_{HB}b_B/(1 + b_Bp_B) \tag{A3}$$

where $p_B = 0.155$ atm in all cases for the present study. Experimental values of the required dual-mode parameters (D_{DB}, D_{HB}, k_{DB}, $C'_{HB}b_B$, b_B) were not available. Therefore, an estimation scheme was developed based on empirical linear correlations between the logarithms of these parameters and physical properties of several gases which have been studied previously.[9,10]

Linear correlations of $\log D_D$ and $\log D_H$ as functions of penetrant diameter are presented in Figure 5. In the correlation, the Lennard–Jones collision diameter was used for all gases except CO_2. It was shown earlier[10] that the transport parameters D_D and D_H for CO_2 are more appropriately correlated with the zeolite sieving dimension for this penetrant, presumably because of its highly linear and, therefore, asymmetric structure. Linear regression of the data yielded the correlation coefficients reported in Table II and values of D_{DB} and D_{HB} equal to 3×10^{-12} and 1.89×10^{-13} cm²/s, respectively.

Linear correlations of k_D and C'_Hb are shown in Figures 6 and 7 as functions of the penetrant Lennard–Jones potential-well depth. A similar correlation is presented above for the penetrant affinity constant, b (Fig. 4). As noted earlier, some uncertainty exists in the value of ϵ/k for iso-

TABLE II
Linear Correlation Coefficients of the Various Correlations of Log(X) vs. Y

X	Y	Correlation coefficient[a]
$D_D \times 10^8$	σ	−0.994
$D_H \times 10^8$	σ	−0.962
$k_D \times 10^2$	ϵ/k	0.960
C'_Hb	ϵ/k	0.989
b	ϵ/k	0.989

[a] The square of the correlation coefficient is defined to be the ratio of the regression sum of squares to the total sum of squares.

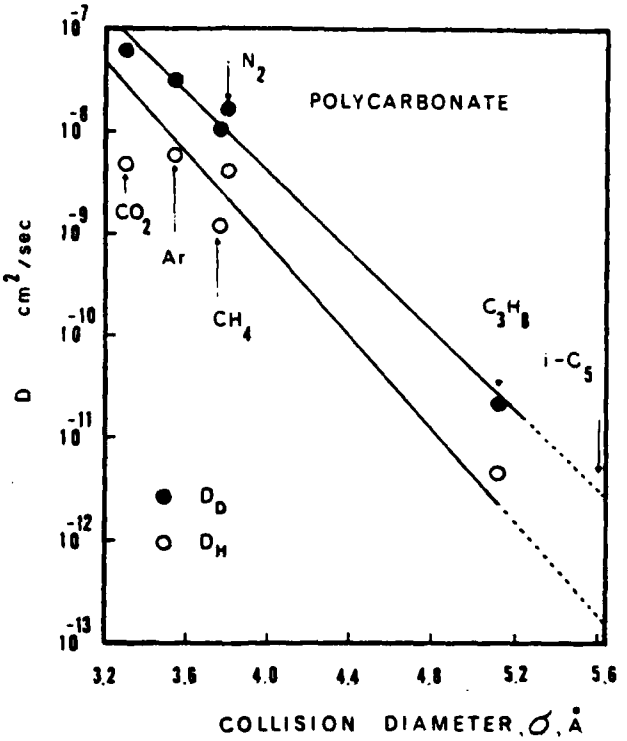

Fig. 5. Correlation of diffusion coefficients D_D and D_H vs. penetrant collision diameters.

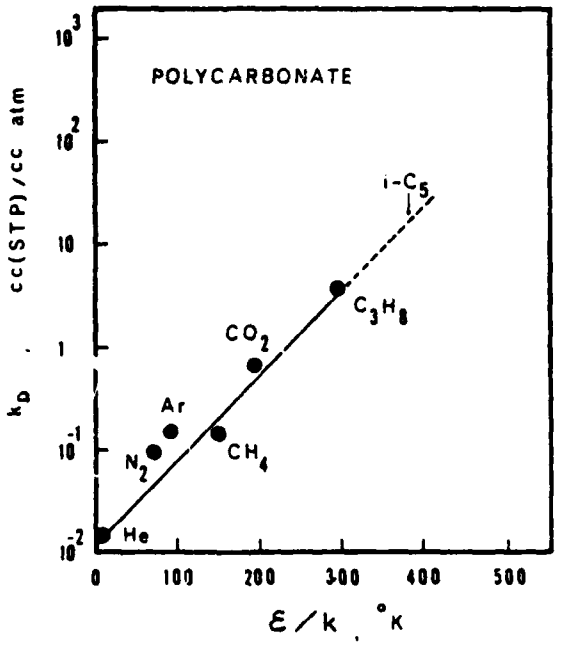

Fig. 6. Correlation between k_D and ϵ/k. The arrow indicates the estimated parameter value for isopentane.

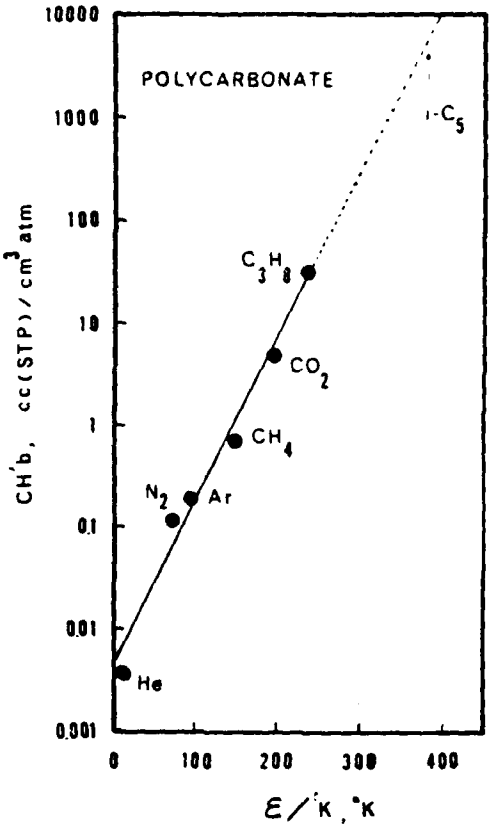

Fig. 7. Correlation between $C'_H b$ and ϵ/k. The arrow indicates the estimated parameter value for isopentane.

pentane since data are not reported for this penetrant. The largest value of ϵ/k calculated by the various estimation techniques[12] provide conservatively large estimates of the composite parameters $C'_H b$ and the Henry's-law parameter for isopentane. The estimates of k_D and $C'_H b$ for isopentane from Figures 6 and 7 are 58.38 and 5693 cm³(STP)/cm³ atm, respectively. Using these estimates along with the value of $b_B = 13.97$ atm^{-1} estimated earlier, one predicts a value of isopentane permeability equal to $\simeq 7 \times 10^{-12}$ cm³(STP)cm/(cm² s cmHg) for the case in which there is an upstream isopentane pressure of 117.8 torr. The extraordinarily low permeability to isopentane under the conditions imposed in this system will produce a negligibly small contribution to the massive CO_2 flux to the downstream chamber.

APPENDIX II: THE TIME LAG OF COMPONENT A IN THE PRESENCE OF COMPONENT B

According to the dual-mobility model, the equation of continuity for component A in a flat membrane can be written as[3]

$$\frac{\partial C_A}{\partial t} = \frac{\partial}{\partial x} D_{DA} \frac{\partial C_{MA}}{\partial x} \tag{B1}$$

where $C_{MA} \equiv C_{DA} + F_A C_{HA}$ is a convenient variable comprised of a combination of the so-called "dissolved" (C_{DA}) and "Langmuir" populations (C_H). The parameter F_A is equal to the ratio of the diffusion coefficient of species A in the Langmuir environment (D_{HA}) to the diffusion coefficient of species A in the dissolved environment (D_{DA}). Following Frisch,[13] integration of eq. (B1) at time

t with respect to x assuming zero concentration at the downstream face gives

$$\int_{x'}^{l} \frac{\partial C_A}{\partial t} dx = -N_A(l,t) - D_{DA} \frac{\partial C_{MA}}{\partial x}\bigg|_{x'}$$

and

$$\int_0^l \int_{x'}^{l} \frac{\partial C_A}{\partial t} dx\, dx' = -N_A(l,t)l - \int_{C^*_{MA}}^{0} D_{DA}\, dC_{MA} \tag{B2}$$

Assuming instantaneous equilibrium is attained and maintained at the membrane surfaces, then, C^*_{MA} (the value of C_{MA} at $x = 0$) is equal to its steady-state value for all times greater than zero, and we have

$$\int_0^l \int_{x'}^{l} \frac{\partial C_A}{\partial t} dx\, dx' = -N_A(l,t)l + lN_A^{SS} \tag{B3}$$

where $N_A(l,t)$ is the flux of A at the downstream face at time t, and

$$N_A^{SS} = \frac{1}{l} \int_0^{C^*_{MA}} D_{DA}\, dC_{MA}$$

is the steady-state flux of A. Integration of eq. (B3) with respect to time, followed by integration by parts gives

$$\frac{l}{A} Q_A(t) = \frac{l}{A} Q_A^{SS} - \int_0^l x'[C_A(x',t) - C_A(x',0)]dx \tag{B4}$$

where

$$Q_A(t) = A \int_0^t N_A(l,t)dt,$$

$$Q_A^{SS} = A \int_0^t N_A^{SS}\, dt$$

and A is the diffusion area. As t approaches infinity, $Q_A(t)$ approaches $AN_A^{SS}(t - \theta_A)$, where θ_A is the time lag for component A.[13]

Consequently, for the case treated here in the absence of concentration dependence of F_A and D_{DA} and for an initially degassed film [$C_A(x,t = 0) = 0$], eq. (B4) simplifies to

$$\theta_A = \frac{1}{lN_A^{SS}} \int_0^l xC_A^{SS}(x)dx \tag{B5}$$

This equation indicates that the value of θ_A, and hence the time required to reach steady-state permeation of component A, is independent of the time to approach steady-state permeation for component B as long as the boundary conditions do not vary with time and the partial immobilization model describes transport. Moreover, consistent with eq. (11), although N_A^{SS} and $C_A^{SS}(x)$ may both be substantially suppressed by competition from component B for the Langmuir environment, θ_A may be relatively insensitive to the presence of the second component in the feed stream. This conclusion is consistent with our experimental observations in the present study with mixtures which suggested that steady-state permeation was achieved over time scales similar to that for pure component CO_2.

Nomenclature

- A Area available for diffusion
- b_i Affinity constant of component i for the polymer (atm^{-1})
- $C_A(x,t)$ Total concentration of component A in polymer at time t and distance x from the upstream face
- C_{MA} $= C_{DA} + F_A C_{HA}$
- D_D Diffusion coefficient of the Henry's-law species (cm^2/s)
- D_H Diffusion coefficient of the Langmuir species (cm^2/s)
- F Ratio of Langmuir and Henry's-law diffusion coefficients
- k_D Henry's-law constant [cm^3 gas (STP)/cm^3 polymer atm]
- K $C'_H b/k_D$ where C'_H is the capacity of Langmuir mode [cm^3 gas (STP)/cm^3 polymer]

$N_A(l,t)$ Flux of component A at the downstream face at time t
N_A^{SS} Steady-state flux of component A
p_i Upstream driving pressure for penetrant i (atm)

$$Q(t) = A\int_0^t N_A(l,t)dt$$

$$Q_A^{SS} = A\int_0^t N_A^{SS}\,dt$$

P_i Permeability of component i [cm^3(STP)cm/cm^2 s cmHg]
ϵ/k Lennard–Jones potential-well depth (K)
σ Collision diameters of the penetrants in Lennard–Jones potential equation (Å)
θ_A Time-lag value for component A (s)

References

1. V. T. Stannett, W. J. Koros, D. R. Paul, H. K. Lonsdale, and R. W. Baker, *Adv. Polym. Sci.*, **32**, 69 (1979).
2. F. P. McCandless, *Ind. Eng. Chem. Proc. Res. Dev.*, **11**, 470 (1972).
3. D. R. Paul and W. J. Koros, *J. Polym. Sci. Polym. Phys. Ed.*, **14**, 675 (1976).
4. W. J. Koros, D. R. Paul, and A. A. Rocha, *J. Polym. Sci. Polym. Phys. Ed.*, **14**, 687 (1976).
5. W. J. Koros, R. T. Chern, V. T. Stannett, and H. B. Hopfenberg, *J. Polym. Sci. Polym. Phys. Ed.*, **19**, 1513 (1981).
6. D. G. Pye, H. H. Hoehn, and M. Panar, *J. Appl. Polym. Sci.*, **20**, 287 (1976).
7. G. S. Huvard, V. T. Stannett, W. J. Koros, and H. B. Hopfenberg, *J. Membr. Sci.*, **6**, 185 (1980).
8. R. H. Perry and C. H. Chilton, *Chemical Engineer's Handbook*, 5th ed., McGraw-Hill, New York (1973) Chap. 3.
9. J. A. Barrie, K. Munday, and M. Williams, *Polym. Prepr. Am. Chem. Soc. Div. Polym. Chem.*, **39**, 187 (1978).
10. W. J. Koros, A. H. Chan, and D. R. Paul, *J. Membr. Sci.*, **2**, 165–190 (1977).
11. E. S. Sanders, personal communications.
12. R. C. Reid, J. M. Prausnitz, and T. K. Sherwood, *The Properties of Gases and Liquids*, 3rd ed., McGraw-Hill, New York (1977), Chap. 2, p. 24 and Appendix C, p. 678.
13. H. L. Frisch, *J. Phys. Chem.*, **61**, 93 (1957).

Received April 27, 1982
Accepted November 17, 1982

Journal of Membrane Science, 15 (1983) 157–169
Elsevier Science Publishers B.V., Amsterdam — Printed in The Netherlands

"SECOND COMPONENT" EFFECTS IN SORPTION AND PERMEATION OF GASES IN GLASSY POLYMERS*

R.T. CHERN, W.J. KOROS, E.S. SANDERS and R. YUI

Department of Chemical Engineering, North Carolina State University, Raleigh, North Carolina 27650 (U.S.A.)

(Received October 13, 1982; accepted December 26, 1982)

Summary

Data for CO_2 permeability through Kapton polyimide at 60°C are reported for upstream pressures up to 240 psia (16.33 atm) in the presence and absence of water vapor in the feed. The carbon dioxide flux was depressed by the presence of the water vapor. This phenomenon is analyzed in terms of the dual mode sorption and transport models. Together with other recent sorption and permeation data, this study suggests that competition of mixed penetrants for sorption sites and transport pathways associated with unrelaxed volume in glassy polymers is a general feature of gas/glassy polymer systems. The permselectivity of a membrane to a mixture of penetrants is strongly related to its ability to maintain a size and shape differentiating matrix, that is, to remain essentially unplasticized under operating conditions. Under such conditions, competition among penetrants for excess volume will be a generally important consideration for modeling gas permeation in permselective membranes.

Introduction

General considerations

High membrane permselectivity is generally associated with a rigid chain backbone of the constituent polymer, providing sieving on a molecular scale [1,2]. At sufficiently high driving pressure (i.e., at high sorbed penetrant concentration), plasticization of the polymer is expected to flexibilize the discriminating matrix with a reduction in the permselectivity of the membrane. Although this can occur at sufficiently high sorbate concentrations for essentially all glassy materials, selection of a membrane material with a high glass transition temperature and extraordinary inherent backbone rigidity should minimize such deleterious effects.

Often the ratio of pure component permeabilities at an arbitrary pressure for the two components is used as an indication of the potential selectivity of

*Paper presented at the IUPAC Symposium on Interrelations between Processing, Structure and Properties of Polymeric Materials, August 29—September 2, 1982, Athens, Greece.

0376-7388/83/$03.00 © 1983 Elsevier Science Publishers B.V.

a candidate membrane. While this approach offers a useful approximation, the actual selectivity and productivity (flux) observed in the mixed gas case may be surprisingly different from those predicted on the basis of pure component data. In the words of Pye et al. [3], the permeability of a membrane to a component A may be reduced due to the sorption of a second component B in the polymer which "... effectively reduces the microvoid content of the film and the available diffusion paths for the non reactive gases". The present paper will offer additional experimental and theoretical insight into this interesting effect.

Unrelaxed volume

The unrelaxed volume shown schematically in Fig. 1 corresponds to the difference between the actual glassy sample specific volume, V_g, and the equilibrium densified specific volume, V_l, achieved after extensive annealing. Differences in the amount of this excess volume in various samples of the same polymer, related to differences in processing histories, will be reflected

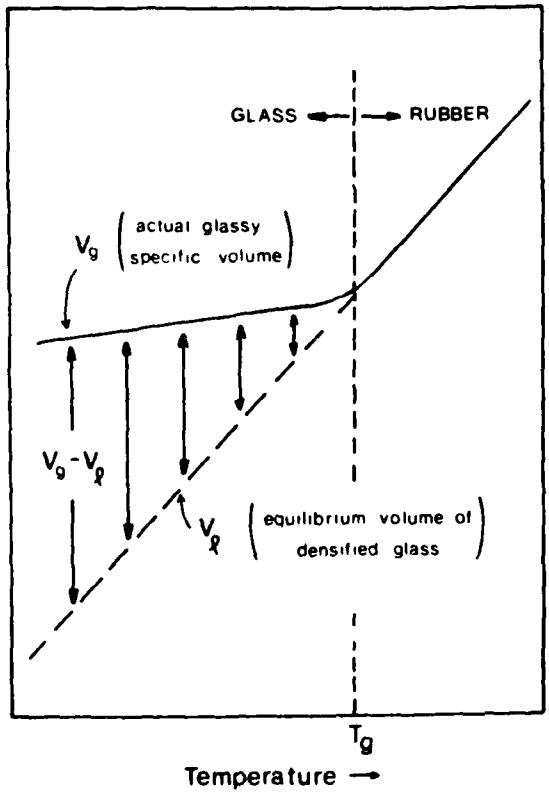

Fig. 1. Schematic representation of the excess volume ($V_g - V_l$) of a glassy polymer.

as differences in the sorption and transport properties of the samples. The deviation of the actual volume from the equilibrium volume is a direct manifestation of the nonequilibrium nature of the glassy state and enters directly in current model descriptions of sorption and transport [1].

Sorption and permeation of pure gases

The sorption of a pure gas in a glassy polymer is described very satisfactorily by the dual mode sorption model [1,4–6]. The model attributes the distinct shape of such isotherms to the fact that uptake of gas in the glass occurs simultaneously in two molecularly distinct environments. The first contribution, C_D, generally referred to as the dissolved or the Henry's law component, is present not only in glasses, but also rubbers and even low molecular weight liquids.

The second contribution to sorption in a glass, C_H, is not present in rubbery polymers or low molecular weight liquids. This term, typically referred to as the Langmuir component, is associated with uptake of the penetrant by regions comprising the unrelaxed volume, $(V_g - V_l)$, introduced in the discussion of Fig. 1. This additional mode of sorption is believed to contribute to many of the unusual transport behaviors observed for gas/glassy polymer systems.

The dual mode sorption model is generally written as shown in eqn. (1):

$$C = k_D p + \frac{C'_H b p}{1 + bp} \tag{1}$$

where k_D, C'_H, and b are generally referred to as the Henry's law constant, the Langmuir capacity constant and the Langmuir affinity constant, respectively [1].

The corresponding equation for the steady state permeability of a pure component in glassy polymers is described satisfactorily by the dual mobility or partial immobilization model [6,7]. When the downstream receiver pressure is zero, the permeability is given by eqn. (2) [6]:

$$P = k_D D_D \left(1 + \frac{FK}{1 + bp}\right) \tag{2}$$

where D_D is the diffusion coefficient of the penetrant in the Henry's law environment, F is the ratio of the diffusion coefficient of the penetrant in the microvoid environment to that in the Henry's law environment ($F = D_H/D_D$), and $K = C'_H b/k_D$ is a useful collection of the sorption parameters introduced above. The first term in eqn. (2) describes transport related to the Henry's law environment, while the second term is related to the Langmuir environment. The values of D_D and D_H are usually taken to be constant. This assumption has been shown to be adequate for describing the permeabilities of a number of glassy polymers to permanent gases [8–11]. Stern [12] has further generalized the model to account for concentration dependence of the transport coefficients under conditions for which plasticization becomes important.

Mixed component sorption and transport

Arguments similar to those presented above for pure components have been extended to generalize the expressions given in eqns. (1) and (2) to account for mixed penetrants as shown below [13,14]:

$$C_A = k_{DA} p_A + \frac{C'_{HA} b_A p_A}{1 + b_A p_A + b_B p_B} \tag{3}$$

$$P_A = k_{DA} D_{DA} \left(1 + \frac{F_A K_A}{1 + b_A p_A + b_B p_B}\right) \tag{4}$$

In the above expressions, "A" refers to the component of primary interest while "B" refers to a second, competing component.

The permeability of a polymer to a penetrant depends on the multiplicative contribution of a solubility and a mobility term. These two factors may be functions of local penetrant concentration in the general case. Robeson [15] has presented data for CO_2 permeation in polycarbonate in which both solubility and diffusivity are reduced due to antiplasticization caused by the presence of the strongly interacting 4,4'-dichloro diphenyl sulfone. On the other hand, sorption of a less strongly interacting penetrant, such as a hydrocarbon, may affect primarily only the solubility factor without significantly changing the inherent mobility of the penetrant in either of the two modes. Flux reduction in this latter context occurs simply because the concentration driving force of penetrant A is reduced. This results from the exclusion of A by component B from Langmuir sorption sites which were previously available to penetrant A in the absence of B.

Consistent with the preceding discussion concerning flux reduction by relatively non interacting penetrants, the sorption data shown in Fig. 2 clearly illustrate the progressive exclusion of CO_2 from Langmuir sorption sites in poly(methyl methacrylate) (PMMA), as ethylene partial pressure is increased in the presence of an essentially constant CO_2 partial pressure of 1.53 ± 0.04 atm [16]. The tendency of the CO_2 sorption shown in Fig. 2 to decrease monotonically with ethylene pressure provides impressive support for the competition concept on which eqns. (3) and (4) are based. Permeation data are not available for this system to determine if changes in the values of D_D and D_H occur in the mixed penetrant situation; however, for the case of the relatively non-interacting ethylene, any such effects are expected to be minor.

The data shown in Fig. 3 illustrate the reduction of permeability of polycarbonate to CO_2 caused by competition between isopentane and CO_2 for Langmuir sorption sites [17]. The flux depression shown in Fig. 3 was found to be reversible, with the permeability returning to the pure CO_2 level after sufficient evacuation of the isopentane-contaminated membrane. Even at the low isopentane partial pressure considered (0.1539 atm), the tendency is clear for the CO_2 permeability to be depressed from its pure component level toward the limiting value ($P_A = k_{DA} D_{DA}$), corresponding to complete exclusion

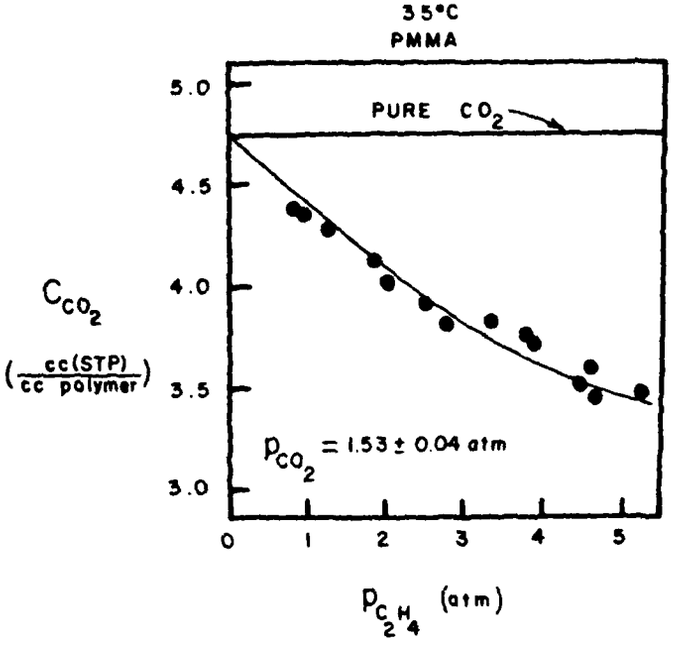

Fig. 2. The effect of C_2H_4 partial pressure on the sorption level of CO_2 in PMMA at 35°C.

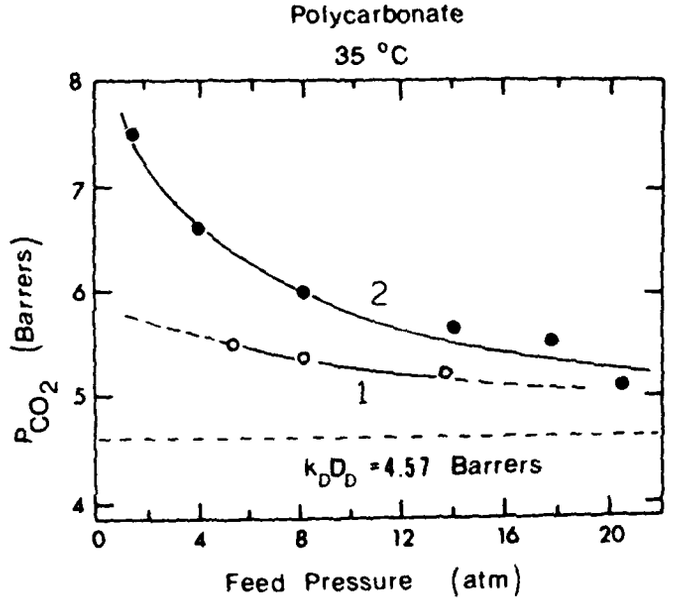

Fig. 3. Permeability of Lexan polycarbonate to CO_2 at 35°C as a function of CO_2 partial pressure. (1): in the presence of 117 mmHg isopentane; (2): pure CO_2.

of CO_2 from the Langmuir environment. Further increases in the isopentane partial pressure in the feed should eventually complete the depression of CO_2 permeability to its limiting value of 4.57 Barrers* unless plasticizing effects set in at the higher isopentane levels. This suggests, for example, that the effective CO_2 permeability at 2 atm could be reduced by as much as 36% due to small amounts of such hydrocarbons in the feed stream.

The lines drawn through the data in Fig. 3 were calculated from eqns. (2) and (4) for the pure and mixed penetrant feed situations, respectively, using the same model parameters in both cases [17]. The satisfactory fit of the data suggests that D_D and D_H for CO_2 in the mixed feed case are not affected measurably by the presence of the relatively non-interacting isopentane. For the case of CO_2 flux depressions by water in Kapton which will be discussed later, it appears that water affects not only the CO_2 solubility due to simple competition, but also to a slight degree the CO_2 mobility compared to that of pure dry CO_2.

Experimental

Materials

The 0.3 mil Kapton film used in the present study was kindly supplied by the E.I. DuPont Company, Circleville, Ohio. After being mounted in the permeation cell, the film was conditioned at 60°C and 300 psia CO_2 from the feed side for roughly 24 hours. However, it was found later that this step does not change the permeability of the film, presumably because of the rigid molecular structure of Kapton. This finding supports the presumption that a rigid-chain membrane forming polymer with high T_g is free from the conditioning effects observed for less rigid glassy polymers such as polycarbonate and polysulfone. This property may be important for retaining high membrane selectivity as the feed temperature or pressure increases. The CO_2 used in our permeation studies was obtained from Airco, Inc., Raleigh, North Carolina and had a purity of over 99.99%. Deionized and degassed water was used as a flux depressing agent and was introduced into the feed stream using a precisely temperature-controlled gas saturator (±0.05°C) which has been described earlier [17].

Equipment

The permeation equipment consisted of a well-thermostated (±0.1°C) pick-up gas flow system using nitrogen (>99.99% pure) as the carrier gas at the downstream membrane surface. The pickup gas flow rate was adjusted to maintain the penetrant concentrations below 2000 ppm and was fed to a Varian 3700 gas chromatograph for evaluation of CO_2 steady state permeabilities. Long term permeation runs were performed to guarantee the establishment of steady state. It was found, however, that steady state permeation for CO_2 was established through the thin films in roughly one hour. At least four replicate measurements were made for use in permeability calculations at each condition, which vary at most ±0.5% from the average values.

*1 Barrer = 10^{-10} (cm³(STP)-cm)/(cm²-sec-cmHg).

Carbon dioxide permeabilities were determined at 60°C as functions of upstream CO_2 pressure for the pure component case and in the presence of water as a competing species. The same film sample was used in all experiments. It was found that the flux depression effects due to the presence of water vapor were completely reversible after prolonged evacuation and conditioning under 18 atm CO_2 pressure on the feed side of the contaminated film, thereby indicating no permanent changes occurred in the film during the measurements. These observations are consistent with those of Pye et al. [3].

Results and discussion

Pure component data

Pure component CO_2 permeability data in Kapton at 60°C are presented in Fig. 4 as a function of upstream CO_2 partial pressure. The downstream CO_2 partial pressure was always less than 2 mmHg (2.632×10^{-3} atm) and could therefore be neglected in all permeability calculations compared with the superatmospheric upstream pressure. The permeability of Kapton to CO_2 at 60°C shows a 16% drop between 20 psia (1.36 atm) and 260 psia (17.69 atm) while in polycarbonate at 35°C, CO_2 permeability decreases by more than 30% over the same range of pressures. The transport parameters were

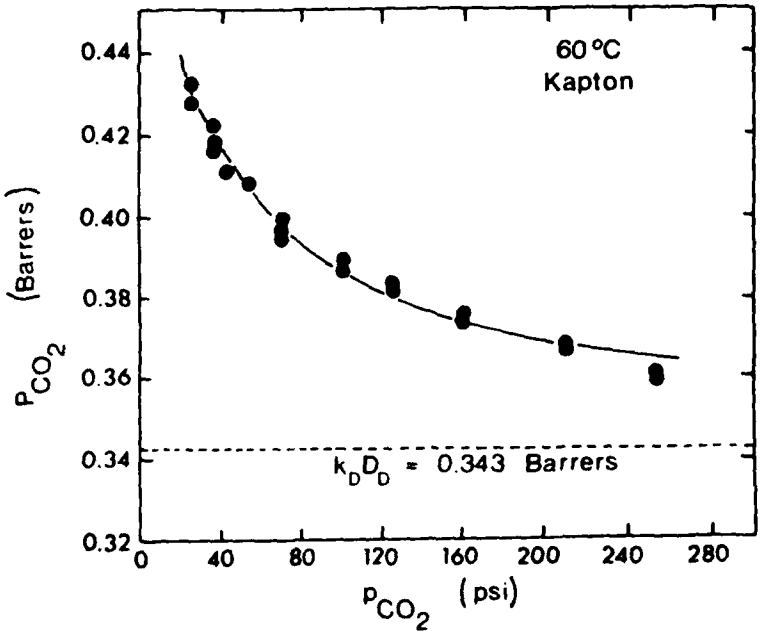

Fig. 4. Permeability of Kapton polyimide to CO_2 at 60°C.

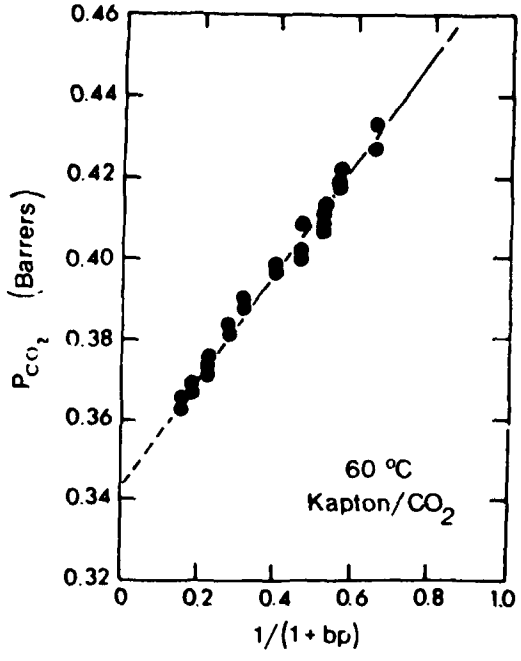

Fig. 5. Permeability of Kapton to CO_2 at 60°C plotted according to eqn. (2).

TABLE 1

Sorption parameters for CO_2 in Kapton at 60°C

Parameter	Value	Standard error	95% Confidence interval
$k_D \left(\frac{\text{cm}^3\ (\text{STP})}{\text{cm}^3\ \text{polymer-atm}} \right)$	0.3806	0.0541	0.2695 ~0.4917
$C'_H \left(\frac{\text{cm}^3\ (\text{STP})}{\text{cm}^3\ \text{polymer}} \right)$	12.4805	1.4768	9.4503 ~15.5101
b (atm^{-1})	0.2966	0.0607	0.1720 ~0.4211
$K = C'_H b/k_D$	[illegible]	–	–

evaluated by linear least squares analysis of a plot of permeability as a function of $1/(1 + bp)$ as shown in Fig. 5 [6], using the sorption parameters given in Table 1. The sorption parameters were evaluated using a precision sorption cell, the operation of which has been described in detail in the past [18,19]. The line through the data in Fig. 4 was calculated from eqn. (2) using the

TABLE 2

Transport parameters for CO_2 in Kapton at 60°C

Parameter	Value
D_D (cm²/sec)	6.85×10^{-9}
D_H (cm²/sec)	0.276×10^{-9}
$F = D_H/D_D$	0.0404

sorption parameters in Table 1 in conjunction with the transport parameters, D_D and F, reported in Table 2. The linearity of the plot in Fig. 5 and good description of the permeability data in Fig. 4 demonstrate the suitability of the model for the pure component data. The data reported in Table 1 indicate that K in eqn. (2) is large, so the relative insensitivity of permeability to upstream pressure in Kapton arises from the low value of $F = D_H/D_D$ for this rigid-backbone polymer.

CO_2/H_2O mixed penetrant feeds

The CO_2 permeability of Kapton at 60°C is plotted in Fig. 6 as a function of upstream CO_2 driving pressure for two different relative humidities (5.5% and 9.3% R.H.) in the feed stream. Consistent with qualitative expectations based on eqn. (4), the flux depressing effect of water tends to be most serious at low pressures where water successfully competes with CO_2 for the un-

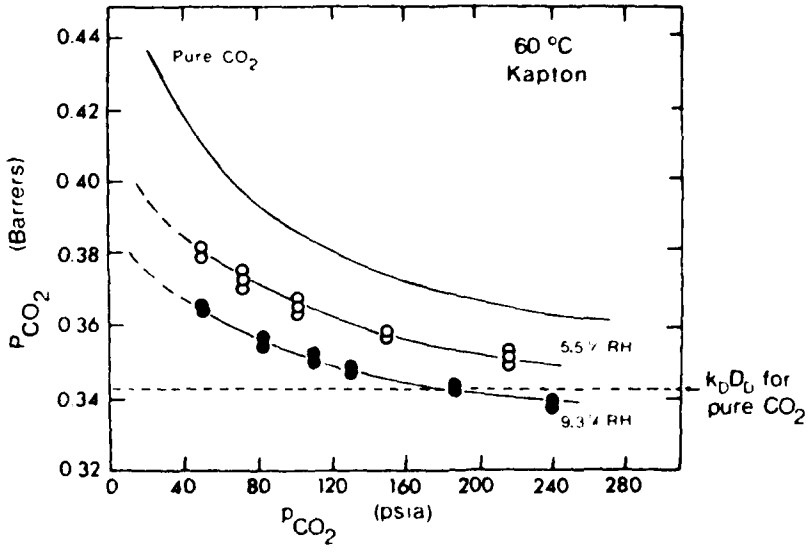

Fig. 6. Depression of the permeability of Kapton to CO_2 at 60°C caused by a small amount of water vapor.

relaxed volume comprising the Langmuir environment. The general tendency for the CO_2 permeability to asymptotically approach the limit $k_D D_D$ is also consistent with eqn. (4) as the second term in brackets related to the Langmuir environment, becomes small as the pressure increases.

At high relative humidities, CO_2 would tend to be progressively excluded from the Langmuir mode of permeation with a maximum depression of 17% in CO_2 production rate compared to the rate in the absence of competition. In the case of polycarbonate, which shows a much more pronounced pressure dependence in permeability, due to its larger value of $F = D_H/D_D$ (0.075 as compared to 0.0404 for Kapton), total exclusion of CO_2 from the Langmuir mode would result in 35% reduction compared to the pure component case.

Pye et al. [3] have measured the effects of small partial pressures of water and pentane on the fluxes of H_2 and CH_4 through a series of stiff-chain polyimides. Consistent with the results in the present study for CO_2, these investigators discovered flux depressions ranging from 21% to 59% for H_2 and CH_4 due to the presence of water vapor (about 50% R.H.) in the feed at 35°C. Sorption of a high affinity vapor such as water tends to lower the sorption of both CH_4 and H_2. Consistent with this expectation, Pye et al. found that although the component fluxes were reduced seriously (21—59%), the ratio of the permeabilities of the two components varied by only 6—9% [1,3].

In the absence of actual data for the Langmuir affinity constant ($b_{H,O}$) for water in Kapton at 60°C, a quantitative test of eqn. (4) is not possible. Earlier sorption measurements for water in polyacrylonitrile (PAN) yielded values for the Langmuir affinity parameter as a function of temperature [20]. At 60°C, the affinity constant is equal to 60 atm^{-1} for water in PAN. Earlier [14], it was noted that the value of the affinity constant of a given penetrant does not appear to be a strong function of the polymer type being considered; therefore, one might reasonably assume that b = 60 atm^{-1} applies for water in Kapton also.

The dotted lines in Fig. 7 represent the CO_2 permeability versus pressure calculated from eqn. (4) at the two relative humidities studied using the pure component CO_2 sorption and transport parameters reported in Tables 1 and 2 and the estimated affinity constant for water (b = 60 atm^{-1}). The additional decrease in observed permeability may be attributed to a reduction in D_D as relative humidity increases. Such an effect is, in fact, consistent with the reports of Lim et al. [21] that a small amount of humidity can cause an increase in the modulus (antiplasticization) of Kapton.

Consistent with such an interpretation, a 3.8% and a 6.2% reduction in the effective value of D_D at 5.5% and 9.3% R.H., respectively, provides a good fit to the data leaving all other pure component CO_2 parameters unchanged. Such an effect is consistent with the observations of Robeson [15] mentioned earlier, in which combined solubility and mobility reductions can occur due to both volume filling and specific penetrant/polymer interactions. The generalized dual mobility model is clearly able to identify and characterize, quantitatively, the magnitude of each of the two contributing factors.

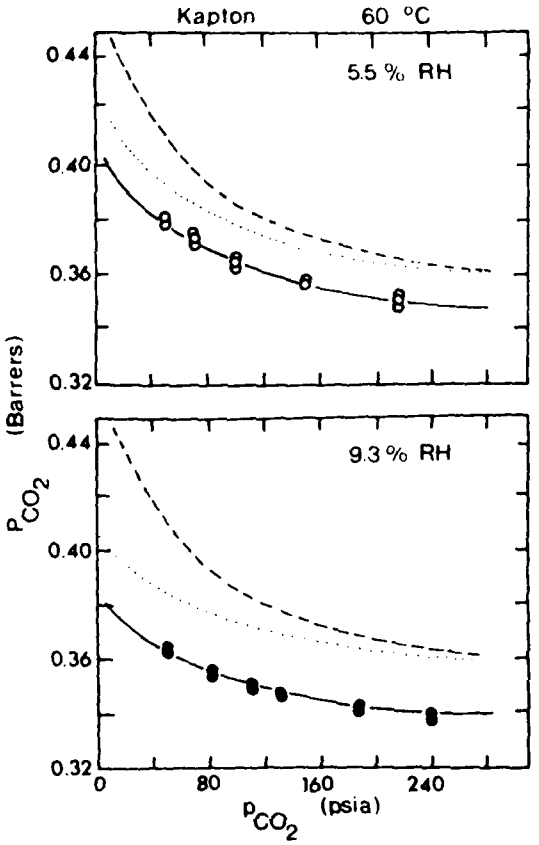

Fig. 7. Depression of CO_2 permeability caused by antiplasticization in addition to simple dual mode competition effects; (– – – –): pure CO_2; (· · · ·): model prediction assuming simple competition, eqn. (4); (——): model prediction accounting for antiplasticization of Kapton by H_2O.

Conclusions

The confluence of current views of the glassy state with several recent sorption and transport studies for mixed penetrants in glassy polymers provides a complementary framework useful to both areas. Specifically, the concept of unrelaxed volume is useful in rationalizing physical property behavior such as impact strength and physical ageing, as well as the sorption and permeation behaviors discussed here. The dual mode sorption and transport model provides a valuable basis for both qualitative and quantitative analysis of gas permeation in the preplasticizing regime. Although plasticizing effects are likely to be of considerable importance at very high pressures in gas separators with the present generation of membrane materials, one might

anticipate that the next generation of materials based on very high T_g, highly rigid backbone polymers such as Kapton, will minimize sensitivity to such deleterious effects. If such stiff-chain materials can be formulated into useful membranes, phenomena associated with dual mode sorption and transport will be of primary importance over the full range of operating pressures. Such plasticization-resistant membranes might even maintain reasonable selectivity in liquid/liquid permeation separations such as pervaporation.

Acknowledgements

The authors gratefully acknowledge support of this work under NSF Grant No. CPE-79-18200 and ARO Grant No. DAAG29-81-K-0039. The authors also acknowledge the continued encouragement and valuable advice offered by Dr. J.H. Petropoulos in the development of a rational quantitative treatment of diffusion in glassy materials. His ideas, some of them unpublished, have been critically important in our work. Also the assistance of Mrs. Leslie Edgerton in typing the manuscript is acknowledged.

List of symbols

b_i	Affinity constant of component i for the polymer (atm^{-1})
D_D	Diffusion coefficient of the Henry's law species (cm^2/sec)
D_H	Diffusion coefficient of the Langmuir species (cm^2/sec)
F	Ratio of Langmuir and Henry's law diffusion coefficients
k_D	Henry's law constant ((cm^3 gas (STP))/(cm^3 polymer-atm))
K	$C'_H b/k_D$
C'_H	Langmuir capacity coefficient ((cm^3 gas (STP))/(cm^3 polymer))
p_i	Upstream driving pressure for penetrant i (atm)
P_i	Permeability of i (Barrer)
R.H.	Relative humidity
V_g	Specific volume of the glassy polymer (cm^3/g)
V_l	Specific volume of the densified liquid (cm^3/g)

References

1 V.T. Stannett, W.J. Koros, D.R. Paul, H.K. Lonsdale and R.W. Baker, Adv. Polym. Sci., 32 (1979) 69.
2 R.M. Barrer and J.A. Barrie, J. Polym. Sci., 23 (1957) 331.
3 D.G. Pye, H.H. Hoehn and M. Panar, J. Appl. Polym. Sci., 20 (1976) 287.
4 A.S. Michaels, W.R. Vieth and J.A. Barrie, J. Appl. Phys., 34 (1963) 1.
5 D.R. Paul and W.J. Koros, J. Polym. Sci., Polym. Phys. Ed., 14 (1976) 675.
6 W.J. Koros and D.R. Paul, J. Polym. Sci., Polym. Phys. Ed., 16 (1978) 1947.
7 J.H. Petropoulos, J. Polym. Sci., A-2, 8 (1970) 1797.
8 W.J. Koros, A.H. Chan and D.R. Paul, J. Membrane Sci., 2 (1977) 165.
9 P. Masi, D.R. Paul and J.W Barlow, J. Polym. Sci., Polym. Phys. Ed., in press.
10 A.J. Erb and D.R. Paul, J. Membrane Sci., 8 (1981) 11.

11 W.J. Koros and D.R. Paul, Polym. Eng. Sci., 20(1) (1980) 14.
12 S.A. Stern and V. Saxena, J. Membrane Sci., 7 (1980) 47.
13 W.J. Koros, J. Polym. Sci., Polym. Phys. Ed., 18 (1980) 981.
14 W.J. Koros, R.T. Chern, V.T. Stannett and H.B. Hopfenberg, J. Polym. Sci., Polym. Phys. Ed., 19 (1981) 1513.
15 L.M. Robeson, Polym. Eng. Sci., 9(4) (1969) 277.
16 E.S. Sanders, W.J. Koros, H.B. Hopfenberg and V.T. Stannett, Mixed gas sorption in glassy polymers: Equipment design considerations and preliminary results, J. Membrane Sci., 13 (1983) 161.
17 R.T. Chern, W.J. Koros, H.B. Hopfenberg and V.T. Stannett, The effects of low partial pressures of isopentane on the permeability of polycarbonate to CO_2, J. Polym. Sci., Polym. Phys. Ed., in press.
18 W.J. Koros and D.R. Paul, J. Polym. Sci., Polym. Phys. Ed., 14 (1976) 1903.
19 W.J. Koros and G.N. Smith, J. Appl. Polym. Sci., 26 (1981) 159.
20 G. Ranade, V.T. Stannett and W.J. Koros, J. Appl. Polym. Sci., 25 (1980) 2179.
21 T.T. Lim, Ph.D. Thesis, Rutgers University, 1967.

3

Implications of the Dual-Mode Sorption and Transport Models for Mixed Gas Permeation

R. T. CHERN, W. J. KOROS, E. S. SANDERS, S. H. CHEN, and H. B. HOPFENBERG

North Carolina State University, Department of Chemical Engineering, Raleigh, NC 27650

The concept of unrelaxed volume in glassy polymers is used to interpret sorption and transport data for pure and mixed penetrants. A review of recent sorption and permeation data for mixed penetrants indicates that competition for sorption sites associated with unrelaxed gaps between chain segments is a general feature of gas/glassy polymer systems. This observation provides convincing support for the use of the Langmuir isotherm to describe deviations from simple Henry's law sorption behavior.

The observed flux depressions of a component in a mixture, relative to its pure component value at an equivalent partial pressure driving force, derives from the above sorption competition mechanism which influences the effective concentration gradient driving diffusion across the membrane. The competition among penetrants for excess volume described above should be an important consideration for modeling essentially all permselective gas separation membranes. Significant plasticizing effects may mitigate flux reductions caused by the above competitive effects at high pressures in plasticization-prone polymers, but would also lead to selectivity losses which are highly undesirable. The permeation behavior of stiff-chain, plasticization-resistant polymers which are likely to comprise the next generation of gas separation polymers will be appropriately treated by the model discussed here.

0097-6156/83/0223-0047$07.75/0
© 1983 American Chemical Society

High membrane permselectivity is generally associated with a rigid chain backbone of the constituent polymer, providing sieving on a molecular scale (1,2). At high upstream driving pressure (i.e., at high sorbed penetrant concentration), plasticization of the polymer may reduce the permselectivity of the membrane. Although plasticization will occur at sufficiently high sorbed concentrations for essentially all glassy materials, selection of a membrane material with a very high glass transition temperature and extraordinary inherent backbone rigidity should minimize effects associated with plasticization.

Often the ratio of pure component permeabilities at an arbitrary pressure for the components of interest is used as an indication of the potential selectivity of a candidate membrane. While this approach offers a useful approximation, the actual selectivity and productivity (flux) observed in the mixed gas case may be surprisingly different than predicted on the basis of the pure component data. As shown in Figure 1, prior to the onset of plasticizing, the presence of a second component B can depress the observed permeability of a component A relative to its pure component value at a given upstream driving pressure of component A. In the words of Pye et al. (3), the permeability of a membrane to a component A may be reduced due to the sorption of a second component B in the polymer which ". . . effectively reduces the microvoid content of the film and the available diffusion paths for the non reactive gases". The present paper will offer additional experimental and theoretical insight into this interesting effect that is characteristic of glassy polymers.

Unrelaxed Volume - Relation To Sorption And Transport Properties Of Glassy Polymers

The concept of "unrelaxed volume", $V_g - V_\ell$, illustrated in Figure 2 may be used to interpret sorption and transport data in glassy polymers exposed to pure and mixed penetrants. The extraordinarily long relaxation times for segmental motion in the glassy state lead to trapping of nonequilibrium chain conformations in quenched glasses, thereby permitting miniscule gaps to exist between chain segments. These gaps can be redistributed by penetrant in so-called "conditioning" treatments during the initial exposure of the polymer to high pressures of the penetrant (4). Following such initial exposure to penetrant, settled isotherms characterized by concavity to the pressure axis at low pressures and a tendency to approach linear high pressure limits are observed as shown in Figure 3. Reference to penetrant-induced conditioning effects have been made continuously since the very earliest investigations of penetrant/glassy polymer sorption

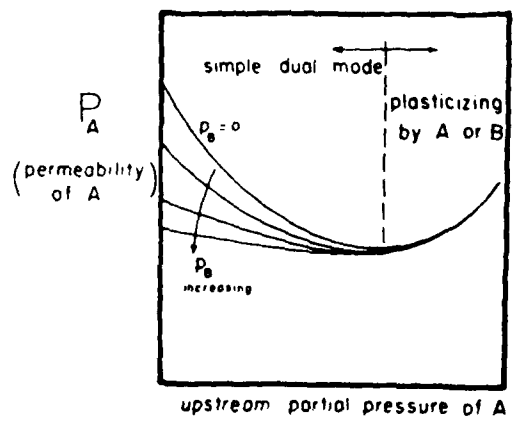

Figure 1. Permeability of a glassy polymer to penetrant A in the presence of varying partial pressures of penetrant B.

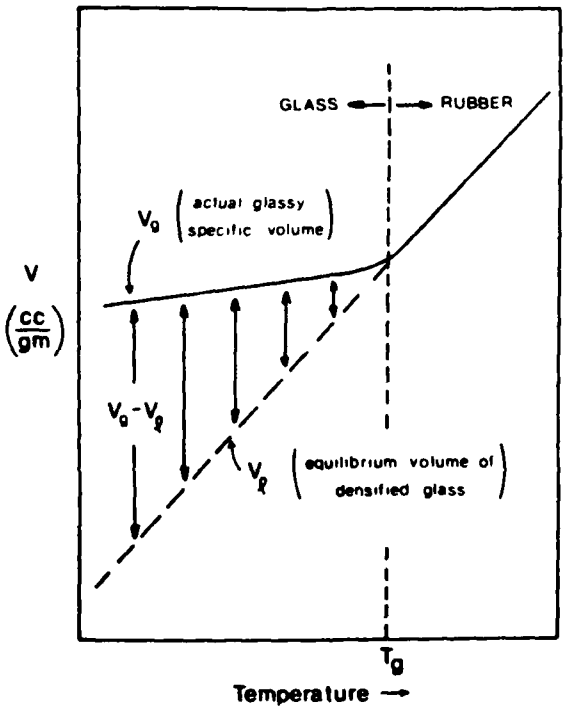

Figure 2. Schematic representation of the unrelaxed volume, $V_g - V_f$, in a glassy polymer. Note that the unrelaxed volume disappears at the glass transition temperature, T_g.

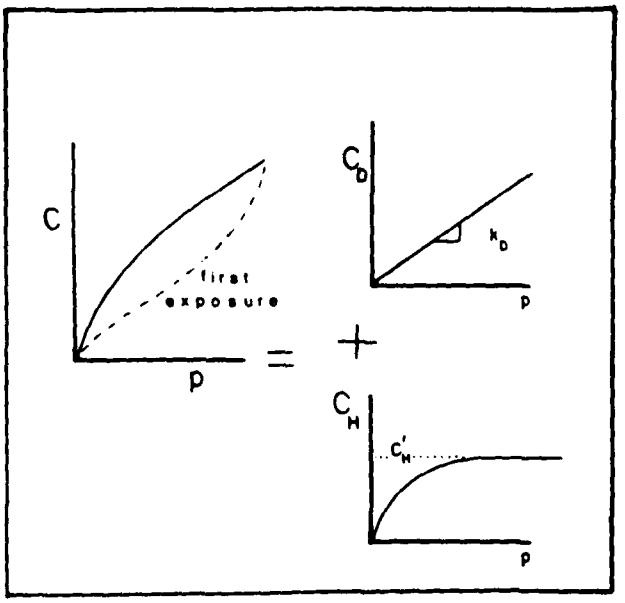

Figure 3. Schematic representation of the dual mode sorption concept.

behavior (2,4,5,6). If one "overswells" the polymer with a highly sorbing penetrant such as a high activity vapor and then removes the penetrant, the excess volume which is introduced will tend to relax quickly at first, followed by a very slow, long term approach toward equilibrium (6).

At extremely high gas conditioning pressures, substantial swelling of the polymer sample can occur with a resultant increase in the value of V_g-V_ℓ (5). For the case of conditioning with gases such as CO_2 at pressures less than 30 atm, however, consolidation in the absence of penetrant following the conditioning treatment is typically unmeasurable since penetrant sorption uptake is not very extensive (< 4-5% by weight) (4,5). As a result, in such cases redistribution of the originally present intersegmental gaps may be the primary process occurring during the first exposure of the polymer to high pressures of penetrant as shown in Figure 3 (4).

An interpretation of the observed conditioning behavior that occurs during the primary penetrant exposure in the absence of large swelling effects may be couched in terms of coalesence of packets of the original intersegmental gaps. Redistribution of chain conformations, consistent with optimal accomodation of the penetrant in the unrelaxed volume between chain segments may permit this process during the conditioning treatment. This rearrangement would tend to produce a more or less densified matrix with a small volume fraction of essentially uniformly distributed molecular scale gaps or "holes" throughout the matrix. In such a situation, one can appreciate the meaning of two slightly different molecular environments in the glass in which sorption of gas may occur. Consider first the limiting case in which a highly annealed, truly equilibrium densified glass characterized by "V_ℓ" in Figure 2 is exposed to a given pressure of a penetrant. In this case, all gaps are missing, but there will clearly still be a certain characteristic sorption concentration (C_D) typical of true molecular dissolution in the densified glass, similar to that observed in low molecular weight liquids or rubbers (above Tg). Next, consider a corresponding conditioned nonequilibrium glass (illustrated by "V_g" in Figure 2) containing unrelaxed volume in which the surrounding matrix has been more or less densified by the coalesence of gaps to form molecular scale berths for penetrant. A local equilibrium requirement leads to an average local concentration of penetrant held in the uniformly distributed molecular scale gaps (C_H) in equilibrium with the "dissolved" concentration (C_D) at any given external penetrant pressure or activity. This simple physical model can be described analytically up to reasonably high pressues (generally for pressures less than or equal to the maximum conditioning pressure employed (4)) in terms of the sum of Henry's law for C_D and a Langmuir isotherm for C_H.

$$C = C_D + C_H \quad (1)$$

$$C = k_D p + \frac{C_H' b p}{1 + bp} \quad (2)$$

where k_D is the Henry's law constant that characterizes sorption of penetrant in the densified regions which comprise most of the matrix. The parameter b characterizes the affinity of the penetrant for the interchain gap regions in the polymer. The parameter C_H' is the Langmuir sorption capacity of the glassy matrix and can be interpreted directly in terms of Figure 2 in which the unrelaxed volume, $V_g - V_\ell$, corresponds to the summation of all of the molecular scale gaps in the glass. As shown in Figure 4, the Langmuir capacity of glassy polymers tends to approach zero in the same way that $V_g - V_\ell$, approaches zero at the glass transition temperature (see Figure 2). This qualitative observation can be extended to a quantitative statement in cases for which the effective molecular volume of the penetrant in the sorbed state can be estimated. As a first approximation, one may assume that the effective molecular volume of a sorbed CO_2 molecule is 80 $Å^3$ in the range of temperature from 25°C to 85°C. This molecular volume corresponds to an effective molar volume of 49 cc/mole of CO_2 molecules and is similar to the partial molar volume of CO_2 in various solvents, in several zeolite environments, and even as a pure subcritical liquid (See Table 1) (4,8). The implication here is not that more than one CO_2 molecule exists in each molecular scale gap, but rather that the effective volume occupied by a CO_2 molecule is roughly the same in the polymer sorbed state, in a saturated zeolite sorbed state and even in a dissolved or liquid-like state since all of these volume estimates tend to be similar for materials that are not too much above their critical temperatures. With the above approximation, the predictive expression given below for C_H' can be compared to independently measured values for this parameter from sorption measurements.

$$C_H' \left[= \frac{V_g - V_\ell}{V_g} \right] \rho^* \quad (3)$$

where ρ^* is the equivalent density of CO_2 (~1/49 mole/cc) discussed above. The comparison of measured (4,9-11) and predicted C_H''s calculated from Eq (3) using reported dilatometric parameters (12-15) for the various glassy polymers is shown in Figure 5. The correlation is clearly impressive.

Application of Eq (3) to highly supercritical gases is somewhat ambiguous since the effective molecular volume of sorbed gases under these conditions is not easily estimated. A

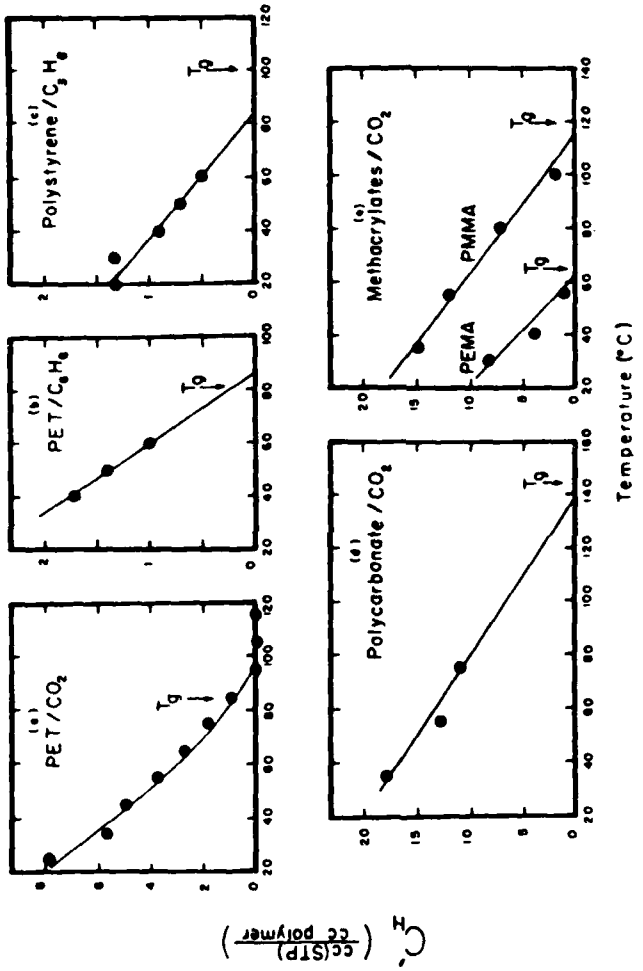

Figure 4. Langmuir sorption capacity, C'_H, as a function of temperature for several polymer/penetrant systems. Note that C'_H disappears near T_g. (Reproduced with permission from Ref. 7. Copyright John Wiley & Sons, 1981.)

Table 1: Effective Molar or Partial Molar Volume of CO_2 in Various Environments at 25°C.

Environment	Molar or Partial Molar Volume (cc/mole)	Ref
Carbon Tetrachloride	48.2	8
Chlorobenzene	44.6	8
Benzene	47.9	8
Acetone	44.7	8
Methyl Acetate	44.5	8
4A or 5A Zeolite at saturation of capacity	52.4	4

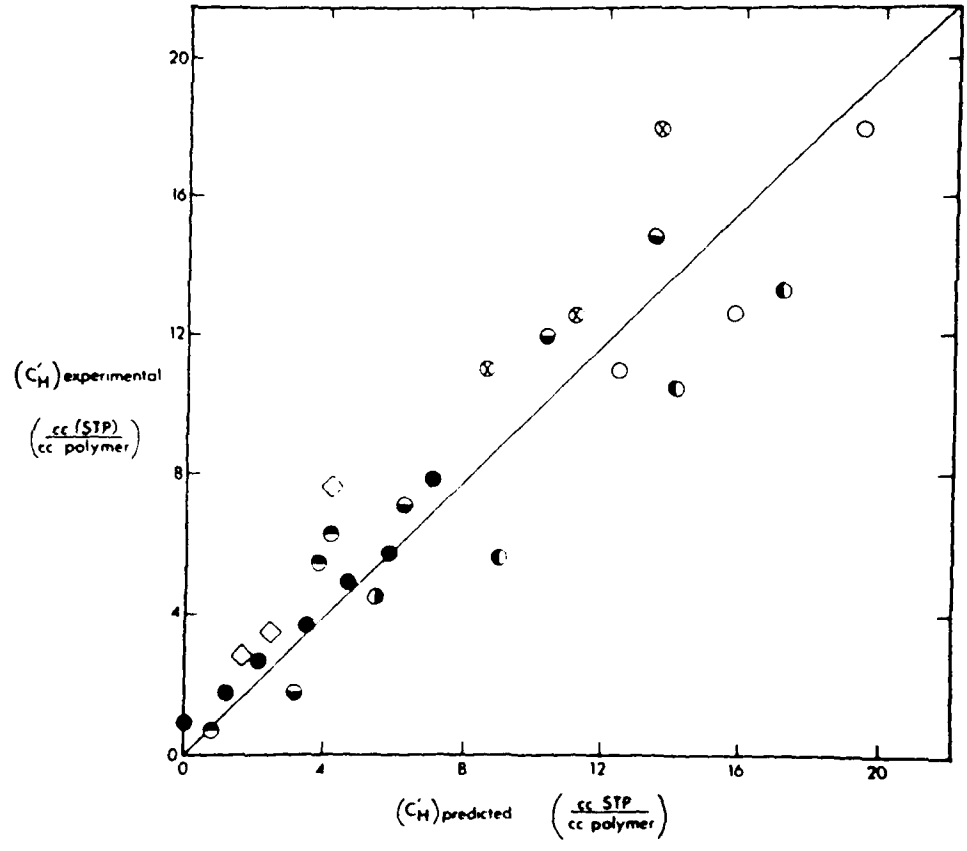

Figure 5. Quantitative comparison of experimentally measured values of C'_H for CO_2 in various polymers with the predictions of Equation 3. [● poly(ethylene terephthalate) at 25, 35, 45, 55, 65, 75, and 85 °C], [● poly(benzyl methacrylate) at 30 °C], [◐ poly(phenyl methacrylate) at 35, 50, and 75 °C], [◊ poly-(acrylonitrile) at 35, 55, and 65 °C], [O ⊗ polycarbonate at 35, 55, and 75 °C: the O symbols refer to predictions using dilatometric coefficien[illegible]om Ref. 14; the ⊗ symbols refer to predictions using coefficients from Ref. 15]. [◒ poly(ethyl methacrylate) at 30, 40, and 55 °C], [● poly(methyl methacrylate) at 35, 55, 80 and 100 °C].

similar problem exists in a priori estimates of partial molar volumes of supercritical components even in low molecular weight liquids (16). The principle upon which Eq (3) is based remains valid, however, and while the total amount of unrelaxed volume may be available for a penetrant, the magnitude of C_H' depends strongly on how condensible the penetrant is, since this factor determines the relative efficiency with which the component can utilize the available volume.

Transport. A companion transport model that also acknowledges the fact that penetrant may execute diffusive jumps into and out of the two sorption environments expresses the local flux, N, at any point in the polymer in terms of a two part contribution (17-20):

$$N = - D_D \frac{\partial C_D}{\partial x} - D_H \frac{\partial C_H}{\partial x} \tag{4}$$

where D_D and D_H refer to the mobility of the dissolved and Langmuir sorbed components, respectively. It is typically found that D_D is considerably larger than D_H except for non condensible gases such as helium (14). The above expression can be written in terms of Fick's law with an effective diffusion coefficient, $D_{eff}(C)$, that is dependent on local concentration:

$$N = - D_{eff}(C) \frac{\partial C}{\partial x} \tag{5}$$

The dual mobility model expresses the concentration dependency of $D_{eff}(C)$ in terms of the local concentration of dissolved penetrant, C_D, as shown in Eq (6):

$$D_{eff}(C) = D_D \left[\frac{1 + \frac{FK}{(1 + \alpha C_D)^2}}{1 + \frac{K}{(1 + \alpha C_D)^2}} \right] \tag{6}$$

where $F \equiv D_H/D_D$, $K \equiv C_H'b/k_D$ and $\alpha \equiv b/k_D$. This model explains concentration dependency of the local diffusion coefficient such as that shown for CO_2 in poly(ethylene terephthalate) (PET) in Figure 6 (21) in terms of a progressive increase in the fraction of the local concentration present in the higher mobility Henry's law environment as the local Langmuir capacity saturates at increasingly higher pressures.

The points in Figure 6 were evaluated from the phenomenological permeability and sorption concentration data

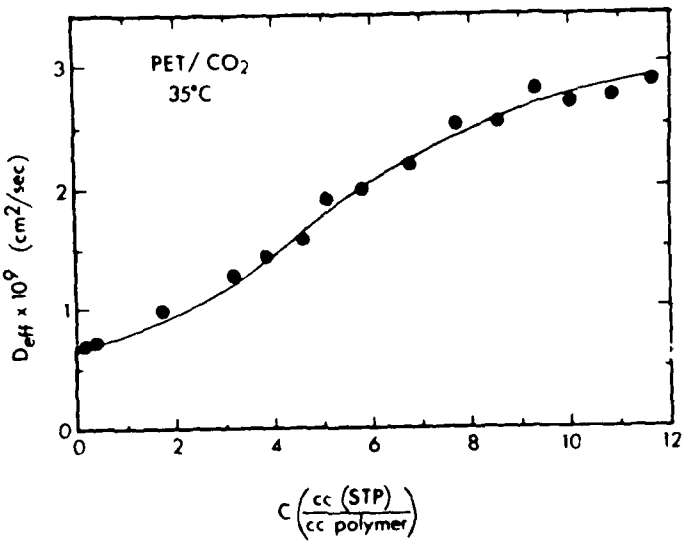

Figure 6. Local effective diffusion coefficient, $D_{eff}(C)$, for carbon dioxide in poly(terephthalate) at 35 °C.

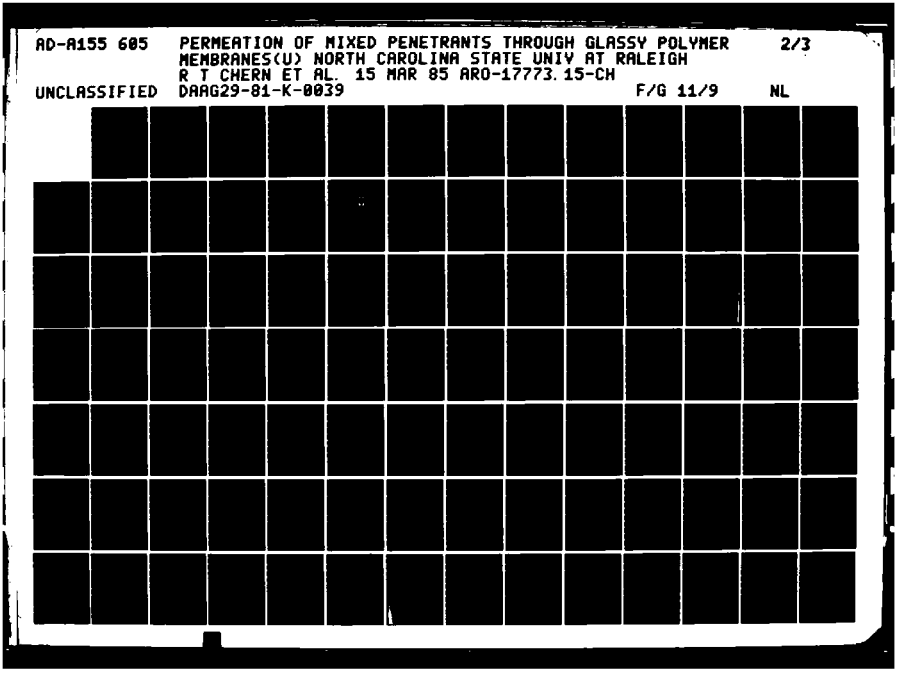
AD-A155 605 PERMEATION OF MIXED PENETRANTS THROUGH GLASSY POLYMER 2/3
MEMBRANES(U) NORTH CAROLINA STATE UNIV AT RALEIGH
R T CHERN ET AL. 15 MAR 85 ARO-17773.15-CH
UNCLASSIFIED DAAG29-81-K-0039 F/G 11/9 NL

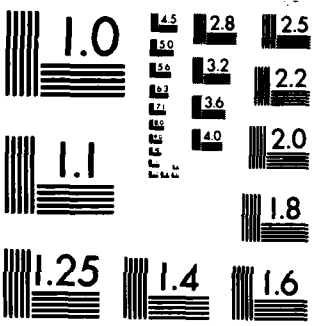

MICROCOPY RESOLUTION TEST CHART
NATIONAL BUREAU OF STANDARDS-1963-A

using a method that does not depend on the dual mode model in any way (22). Interestingly, however, the line through the data points corresponds to the predictions of $D_{eff}(C)$ using Eq (6) along with the independently determined dual mode parameters for this system (21,23). It is also important to note that the form of data in this plot which exhibits a tendency to asymptote at high pressures is not typical of plasticization. Finally, if one considers the low concentration region of Figure 6, it is clear that the diffusion coefficient is surprisingly concentration dependent. For example, $D_{eff}(C)$ increases by more than 35% as the local sorbed concentration rises from 0.142 cc(STP)/cc polymer (or 0.00020 wt. fraction) at 50 mm Hg to 1.7 cc(STP)/cc polymer (or 0.0025 wt. fraction) at 760 mm Hg. The above concentrations are extremely dilute, corresponding to less than 1 CO_2/1200 PET repeat units and 1 CO_2/98 repeat units respectively (4).

An even more dramatic case corresponds to CO_2 in PVC in which $D_{eff}(C)$ rises by 86% as the local concentration increases from 1 CO_2/4400 repeat units at 100 mm Hg to 1 CO_2/1300 repeat units at 500 mm Hg at 40°C (24). The above values of CO_2 solubility are based on measurements by Toi (24) and Tikhomorov et al. (25) which are in good agreement.

At such extraordinarily low penetrant concentrations, plasticization of the overall matrix is certainly not anticipated. Motions involving relatively few repeat units are believed to give rise to most short term glassy state properties. In rubbery polymers, on the other hand, longer chain concerted motions occur over relatively short time scales, and one expects plasticization to be easier to induce in these materials. Interestingly, no known transport studies in rubbers have indicated plasticization at the low sorption levels noted above for PVC and PET.

The discussion directly following Eq (6) provides a simple, physically reasonable explanation for the preceding observations of marked concentration dependence of $D_{eff}(C)$ at relatively low concentrations. Clearly, at some point, the assumption of concentration independence of D_D and D_H in Eq (6) will fail; however, for our work with "conditioned" polymers at CO_2 pressures below 300 psi, such effects appear to be negligible. Due to the concave shape of the sorption isotherm, even at a CO_2 pressure of 10 atm, there will still be less than one CO_2 molecule per twenty PET repeat units at 35°C. Stern (26) has described a generalized form of the dual mode transport model that permits handling situations in which non-constancy of D_D and D_H manifest themselves. It is reasonable to assume that the next generation of gas separation membrane polymers will be even more resistant to plasticization than polysulfone, and cellulose acetate, so the assumption of constancy of these transport parameters will be even more firmly justified.

Although not necessary in terms of phenomenological applications, it is interesting to consider possible molecular meanings of the coefficients, D_D and D_H. If two penetrants exist in a polymer in the two respective modes designated by "D" and "H" to indicate the "dissolved" (Henry's law) and the "hole" (Langmuir) environments, then the molecules can execute diffusive movements within their respective modes or they may execute intermode jumps.

"D" →	"D"	"dissolved" to "dissolved" jump
	"H"	"dissolved" to "hole" jump
"H" →	"H"	"hole" to "hole" jump
	"D"	"hole" to "dissolved" jump

Clearly, the true character (activation energy, entropy and jump length) of the phenomenologically observed D_D will be a weighted average of the relative frequency of "D"→"D" and "D"→"H" jumps, and likewise for D_H in terms of "H"→"H" and "H"→"D" jumps. Given the relatively dilute overall volume fraction associated with the non equilibrium gaps which comprise the "H" environment (< 4 to 5% on a volume basis), one may to a first approximation assume that most diffusive jumps of a penetrant from a "D" environment result in movement to another "D" environment and most diffusive jumps from "H" environments result in movement to a "D" environment. The observed activation energies, entropies and jump lengths, therefore, have fairly well-defined meanings on a molecular scale.

One can easily show that the appropriate equation derived from the dual mode sorption and transport models for the steady state permeability of a pure component in a glassy polymer is given by Eq (7) (18) when the downstream receiving pressure is effectively zero and the upstream driving pressure is p.

$$P = k_D D_D \left[1 + \frac{FK}{1 + bp} \right] \qquad (7)$$

The first term in Eq (7) describes transport related to the Henry's law environment, while the second term is related to the Langmuir environment. The tendency for the permeability to asymptotically approach the limiting value of $k_D D_D$ at high pressures derives from the fact that after saturation of the upstream Langmuir capacity at high pressures, additional pressure increases result in additional flux contributions only from the term related to Henry's law which continues to increase as upstream pressure increases.

The remarkable efficacy of the dual mode sorption and

transport model for description of pure component data has been illustrated by plots of the linearized forms of Eq (2) and Eq (7) for a wide number of polymer/penetrant systems (4,5,9, 10,22,24). These linearized plots are stringent tests of the ability of the proposed functional forms to describe the phenomenological data. Assink (27) has also investigated the dual mode model using a pulsed NMR technique and concluded that:

> "We have been able to demonstrate the basic validity of the assumptions on which the dual mode model is based and we have shown the usefulness of NMR relaxation techniques in the study of this model."

Whereas the dual sorption and transport model described above unifies independent dilatometric, sorption and transport experiments characterizing the glassy state, an alternate model offered recently by Raucher and Sefcik provides an empirical and fundamentally contradictory fit of sorption, diffusion and single component permeation data in terms of parameters with ambiguous physical meanings (28). The detailed exposition of the dual mode model and the demonstration of the physical significance and consistency of the various equilibrium and transport parameters in the model in the present paper provide a back drop for several brief comments presented in the Appendix regarding the model of Raucher and Sefcik.

Mixed Component Sorption and Transport

Arguments similar to those presented above for pure components have been extended to generalize the expressions given in Equations 2 and 7 to account for the case of mixed penetrants (29,30). The appropriate expressions are given below:

$$C_A = k_{DA}P_A + \frac{C'_{HA}b_AP_A}{1 + b_AP_A + b_BP_B} \qquad (8)$$

$$P_A = k_{DA}D_{DA}\left[1 + \frac{F_AK_A}{1 + b_AP_A + b_BP_B}\right] \qquad (9)$$

In the above expressions, "A" refers to the component of primary interest while "B" refers to a second "competing" component.

The permeability of a polymer to a penetrant depends on the multiplicative contribution of a solubility and a mobility term. These two factors may be functions of local penetrant concentration in the general case as indicated by the dual mode model. Robeson (31) has presented data for CO_2 permeation in

polycarbonate in which both solubility and diffusivity are reduced due to antiplasticization caused by the presence of the strongly interacting 4-4' dichloro diphenyl sulfone. On the other hand, sorption of a less strongly interacting penetrant, such as a hydrocarbon, may affect primarily only the solubility factor without significantly changing the inherent mobility of the penetrant in either of the two modes. Flux reduction in this latter context occurs simply because the concentration driving force of penetrant A is reduced. This results from the exclusion of A by component B from Langmuir sorption sites which were previously available to penetrant A in the absence of penetrant B.

Consistent with the preceding discussion concerning sorption and flux reductions by relatively non interacting penetrants, the data shown in Figure 7 clearly illustrate the progressive exclusion of CO_2 from Langmuir sorption sites in poly(methyl methacrylate) (PMMA) as ethylene partial pressure (p_B) is increased in the presence of an essentially constant CO_2 partial pressure of $p_A = 1.53 \pm 0.04$ atm (32). The tendency of the CO_2 sorption shown in Figure 7 to decrease monotonically with ethylene pressure provides impressive support for the "competition" concept on which Eq (8) and Eq (9) are based. Permeation data are not available for this system to determine if changes in the value of D_D and D_H occur in the mixed penetrant situation; however, for the case of the relatively non interacting ethylene at the pressures studied, any such effects are expected to be minor.

The data shown in Figure 8 illustrate the reduction in permeability of polycarbonate to CO_2 caused by competition between isopentane and CO_2 for Langmuir sorption sites (33). The flux depression shown in Figure 8 was found to be reversible, with the permeability returning to the pure CO_2 level after sufficient evacuation of the isopentane-contaminated membrane. Even at the low isopentane partial pressure considered (117 mm Hg) the tendency is clear for the CO_2 permeability to be depressed from its pure component level toward the the limiting value ($P_A = k_{DA}D_{DA}$) corresponding to complete exclusion of CO_2 from the Langmuir environment. Further increases in the isopentane partial pressure in the feed should eventually complete the depression of CO_2 permeability to its limiting value of 4.57 Barrers unless plasticizing effects set in at the higher isopentane levels. This suggests, for example, that the effective CO_2 permeability at a CO_2 partial pressure of 2 atm could be reduced by as much as 36% due to small amounts of such hydrocarbons in the feed stream.

The lines drawn through the data in Figure 8 were calculated from Eq (7) and Eq (9) for the pure and mixed penetrant feed situations, respectively, using the same CO_2 model parameters in both cases. The affinity constant of

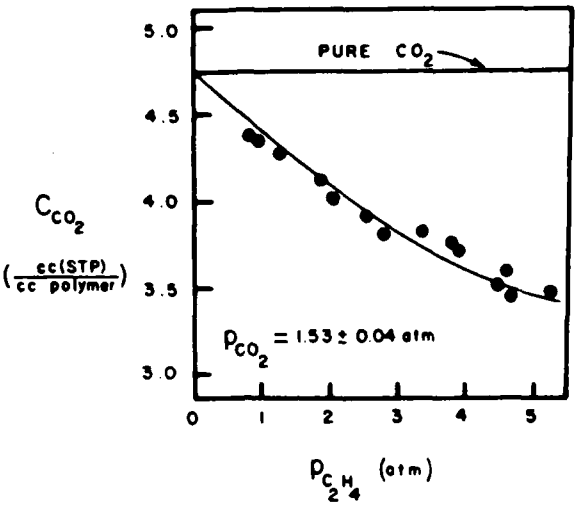

Figure 7. The effect of ethylene on the sorption level of carbon dioxide in poly(methyl methacrylate) at 35 °C.

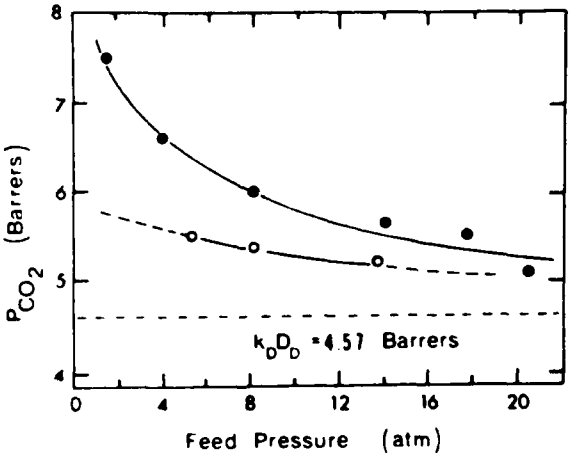

Figure 8. Permeability of Lexan polycarbonate to carbon dioxide at 35 °C as a function of CO_2 partial pressure. [O, in the presence of 117 mm. Hg of isopentane in the feed. ●, pure CO_2 .]

isopentane was estimated for use in Eq (9) to be 13.8 atm^{-1} (33). The excellent fit of the data suggests that D_D and D_H for CO_2 in the mixed feed case are not affected measurably by the presence of the relatively non-interacting isopentane. The sorption and transport parameters for CO_2 in the polycarbonate sample used in the above study are reported in Table 2.

Conclusions

The confluence of current views of the glassy state with recent data for sorption and transport of mixed penetrants in glassy polymers provides a complementary framework useful in both areas. Specifically, the concept of "unrelaxed volume" invoked to explain concavity in the sorption isotherm may eventually be valuable in rationalizing different creep, impact strength and physical aging behavior of glassy polymers. The dual mode sorption and transport model provides a valuable basis for both qualitative and quantitative analysis of gas separator operation in the preplasticizing regime. Although plasticizing effects are likely to be of considerable importance at high pressures in gas separators with the present generation of membrane materials, one might anticipate that the next generation of materials based on very high T_g , highly rigid backbone polymers will minimize sensitivity to such deleterious effects. If such stiff-chain materials can be formulated into useful membranes, phenomena associated with dual mode sorption and transport will be of primary importance over the full range of operating pressures, since the transition to plasticizing behavior shown in Figure 1 would presumably require very high sorbed concentration levels. Such plasticization-resistant membranes might even maintain reasonable selectivity in liquid/liquid permeation separations such as pervaporation.

Appendix: Comments Concerning The "Matrix" Model For Sorption and Difffusion in Glassy Polymers

In the preceding discussion we have presented a model with physically interpretable parameters to explain sorption data for penetrants in glassy polymers. The basis of the model, the concept of "unrelaxed volume" is also useful in understanding many other properties of glassy polymers such as impact strength, physical aging and creep, which are related to the non equilibrium nature of these materials. Moreover, this model yields a physically consistent expression for the local effective diffusion coefficient, $D_{eff}(C)$, which shows concentration dependence at sorbed concentrations well below the point at which substantial interaction of one penetrant with the matrix is generally expected to significantly facilitate the movement of another penetrant.

Table 2

Sorption and transport parameters of CO_2 in Lexan polycarbonate at 35°C

k_D $\frac{cc(STP)}{cc\text{-}atm}$	0.6751
b atm^{-1}	0.2563
C_H' $\frac{cc(STP)}{cc\ polymer}$	17.61
D_D cm^2/sec	5.1484×10^{-8}
D_H cm^2/sec	5.8266×10^{-9}

The dual mode model assumes that the heterogeneity that characterizes the glassy polymer state can be treated in a physically reasonable fashion using the concept of two basically different environments in the polymer. One environment corresponds to that in which a penetrant molecule is sorbed between chain segments that have achieved essentially their equilibrium conformations and interchain distances (perhaps with the aid of the invading penetrant during the "conditioning" step shown in Figure 3). A second environment corresponds to that in which a penetrant molecule finds itself sorbed in a region of localized lower density (perhaps due to local chain kinks or other impediments to rapid relaxation). The model requires, however, that the local concentrations of C_D and C_H in Eq (1) adjust themselves consistent with the requirement that there is only one chemical potential applicable to the penetrant, and at sorption equilibrium this chemical potential is also identical to that of the penetrant in the external gas phase. Any significant energetic heterogeneity associated with sorption in the nonequilibrium gaps regions should manifest itself as a failure in the Langmuir form to fit the deviation from the simple Henry's law model, since the Langmuir form assumes a uniform site affinity. Repeated tests of the linearized form of the Langmuir contribution to sorption have shown excellent conformity to the model. Any such energetic heterogenity is, therefore, of negligible importance with respect to sorption modeling. In their recent paper, Raucher and Sefcik interpret Dr. R. Assink's pulsed NMR study of ammmonia sorption in polystyrene (27) and indicate that: "Spectroscopic analyses of gas molecules within polymer matrices are consistent with all of the gas molecules being in a single state" (28). One is given the indirect and erroneous impression from Raucher's and Sefcik's reference to Assink's work that the Assink study did not support the concepts of the dual mode model. On the contrary, the conclusions of Dr. Assink with regard to this issue completely support the dual mode model premises as shown below in a direct quote of the complete conclusions from the Assink paper (27):

> "We have been able to critically examine the dual mode model by pulsed NMR relaxation techniques. The pressure dependence of the concentration of sorbed gas was consistent with the dual mode model while the relaxation data addressed itself to the validity of the assumptions made by the model. The assumption of rapid interchange was found to be valid for this system while the assumption of an immobile adsorbed phase could introduce a small error in the analysis. It should be possible to reduce this error by more exact measurements of the concentration of sorbed gas as classical pressure experiments could

provide. We have been able to demonstrate the basic validity of the assumption on which the dual mode model is based and we have shown the usefulness of NMR relaxation techniques in the study of this model."

The only "small error", suggested in Assink's statement concerning the dual mode model's assumptions, deals with the earlier approximation by Vieth and Sladek (34) that D_H was equal to zero. The work of Assink was performed prior to the formulation of the dual mobility model which eliminates this approximation and accomodates values of $D_H > 0$ (17,18).

In the present symposium, Dr. Raucher argued that the observed curvature in gas sorption isotherms does not arise from a site saturation mechanism such as we have described in the preceding discussion. The form of the sorption isotherm and local concentration dependent diffusion coefficient proposed by Raucher and Sefcik are given below:

$$C = \frac{\sigma_o P}{1 + \alpha C} \qquad \text{(A-1)}$$

$$D_{eff}(C) = D_o[1 + \beta C] \qquad \text{(A-2)}$$

where D_o was identified as the zero concentration limit of the diffusion coefficient and β was identified as a plasticization-related parameter which indicates the relative sensitivity of the local diffusion coefficient, $D_{eff}(C)$ to the presence of other penetrants in the vicinity. While no physical interpetation was given to the sorption parameters, the σ_o parameter is clearly equal to the limiting slope of the concentration versus pressure isotherm. During a question and answer period following his presentation, Dr. Raucher explicitly ruled out an interpretation of the parameter α in terms of a site saturation mechanism similar to the Langmuir model.

Drs. Raucher and Sefcik have stated: "The apparent concentration dependence of the sorption capacity in the matrix model results from a decrease in a Henry's law-like constant as the polymer adjusts to the sorbate" (28). The extent of the interpretation of α offered by these authors is that: "α is a parameter indicating the magnitude of the change in solubility arising from changes in the gas-polymer matrix". Specifically, what is missing from their discussion is a statement as to what the nature of the hypothetical polymer/penetrant interactions are that cause the concavity in the isotherm. In other words, what change is induced in the nature of the polymer in the presence of the penetrant? The "model" comprised of Eq (A-1) and (A-2) has a strictly empirical basis. It seems incumbent upon these authors to explain how the change in the polymer matrix makes it more difficult to insert another penetrant

[Eq (A-1)], but at the same time makes it easier for the penetrant to move through the matrix [Eq (A-2)]. The dual mode model offers the physical interpretation that concavity in the isotherm arises from a site saturation mechanism related to filling of unrelaxed gaps--a phenomenon which is not only easily visualized and understood, but also has been tested explicitly with independently obtained dilatometric data (See Figure 5).

In an attempt to justify the assumption of plasticization put forth in their interpretation of β in Eq (A-2), Kaucher and Sefcik compare transport data and ^{13}C NMR data for the CO_2/PVC system. This comparison has several questionable aspects. To relate local molecular chain motions to the diffusion coefficient of a penetrant, one should use the so-called local effective coefficient, $D_{eff}(C)$, such as shown in Figure 5 rather than an average or "apparent" diffusion coefficient as was employed by these authors. $D_{eff}(C)$ describes the effects of the local sorbed concentration on the ability of the average penetrant to respond to a concentration or chemical potential gradient in that region.

Raucher and Sefcik, on the other hand, base their comparisons between NMR data and transport data on the so-called "apparent" diffusion coefficient defined by:

$$D_a = \ell^2/6\theta \qquad (A-3)$$

where θ is the observed time lag and ℓ is the membrane thickness. D_a does not have a simple meaning equivalent to a true molecular mobility unless both the time lag and permeability are independent of upstream pressure. Since this situation is not typically observed in glassy polymers, one must use $D_{eff}(C)$ for comparison with complementary techniques that probe molecular motion.

The seriousness of this oversight is apparent in Sefcik and Schaefer's analysis of Toi's transport data (24) in terms of their NMR results (28). The value of the so-called "apparent" diffusion coefficient calculated from Toi's time lag data increases by ~25% for an upstream pressure range between 100 mm Hg and 500 mm Hg. On the other hand, the value of $D_{eff}(C)$ calculated from Toi's data changes by 86% over the concentration range from 100 to 500 mm Hg. The difference in the two above coefficients arises from the fact that D_a is an average of values corresponding to a range of concentrations from the upstream value to the essentially zero concentration downstream value in a time lag measurement. $D_{eff}(C)$, on the other hand, has a well-defined point value at each specified concentration and is typically evaluated (independent of any specific model other than Fick's law) by differentation of solubility and permeability data (22).

A second issue clouding the NMR interpretation of Toi's

40°C transport data lies in the fact that the cited NMR data were collected at 26°C rather than 40°C. If one neglects this fact, Sefcik and Schaefer suggest that the 5.7% increase in the average rotating frame relaxation rate, $\langle R_{1\rho}(C)\rangle$ over the pressure range (100 mm Hg to 500 mm Hg) corresponding to Toi's measurements validate their claims concerning plasticization. This suggestion neglects the fact that the 25% increase in D_a does not match the 5.7% increase in $\langle R_{1\rho}(C)\rangle$. Moreover, recall that D_a is actually not even the correct coefficient to compare with $\langle R_{1\rho}(C)\rangle$. The observed 86% increase in $D_{eff}(C)$ is in poor agreement with the 5.7% increase in the NMR parameter over the range of pressures where both types of data are available.

The considerable discrepancy between the changes in the two parameters $D_{eff}(C)$ and $\langle R_{1\rho}(C)\rangle$ is not impressive proof for plasticiation at such low concentrations. This observation is especially true since part of the observed 5.7% increase in $\langle R_{1\rho}(C)\rangle$ may be accounted for by spin-spin effects. The value of $\langle R_{1\rho}(C)\rangle$ requires cautious interpretation in terms of bulk polymer properties such as the effective diffusion coefficient; especially in light of the preceding discussion concerning Toi's data. It is important to remember that even at 500 mm Hg, there is only one CO_2 molecule for every 1300 PVC repeat units in the above situation and yet an increase of 86% occurs in the value of $D_{eff}(C)$ between 100 mm Hg and 500 mm Hg. These conditions are extraordinarily dilute, and the observed concentration dependence of $D_{eff}(C)$ is perfectly consistent with a site saturation type behavior inherent in the dual mode model. We have always acknowledged that concentration dependence of D_D and D_H may become important factors at elevated pressures for plasticization prone polymers. Such effects, if present have been of second order importance in our work which is generally performed on "conditioned" polymers at CO_2 pressures no greater than 300 psi. Eventual concentration dependence of D_D and D_H is, however, not related to the views of Raucher and Sefcik summarized by Eq (A-1) and Eq (A-2). These equations require that the seemingly mutually exclusive processes of antiplasticization (Eq A-1) and plasticization (Eq A-2) occur simultaneously.

Finally, it was suggested by Raucher and Sefcik that the equations derived from their analysis were essentially as effective as the dual mode model for describing existing data. This statement requires some strong qualification, since no linear equation can describe the inflected form of the $D_{eff}(C)$ plot shown in Figure 6 which was evaluated by graphical differentiation of the permeability and solubility data without reference to any particular model other than Fick's law (21,22). The curve through the data, nevertheless, corresponds to the dual mode model and provides a very good description of the data. The form of these data is not at all consistent with

plasticization. This same argument will apply for essentially all of the cases in which the dual mode model has been shown to fit the form of the local diffusivity. The data points can at best be made to "snake" around the linear fit of the expression in Eq (A-2) and the linear model becomes seriously in error as D_{eff} begins to asymptote. Limited data for two gas/polymer systems were shown by Dr. Raucher which indicated that the descriptions of permeabilities and time lags using the dual mode and matrix models is not very different for the systems checked. If this is true, it is surprising since the different forms of $D_{eff}(C)$ would be expected to give rise to somewhat different time lag results when integrated according to Frisch's method (35). A similar conclusion pertains to the permeablity, since even if the solubility data were perfectly described, the misfit of $D_{eff}(C)$ suggests that there should be a misfit in permeability as well. It is possible that a misfit of $D_{eff}(C)$ versus C and of C versus p could offset each other.

In one of their comparisons between the matrix model and the dual mode model, a somewhat misleading presentation of data is unintentionally offered in Figure 4 of the Raucher and Sefcik paper: "Matrix Model of Gas Sorption and Diffusion in Glassy Polymers" (28). What should be compared in the left hand side of this plot is the dual mode model with refitted parameters over the same pressure range as the "Matrix model" parameters were refitted over. Clearly, a detailed statistical comparison of the permeability and time lag predictions arising from Eq (A-1) and Eq (A-2) must be made with the large body of experimental data available for glassy systems before a conclusion can be reached regarding the efficacy of the "matrix" model for phenomenologically describing such data in general.

On a more basic level, since the matrix model implicitly requires a somewhat inconsistent interpretation for the various model parameters in Eq (A-1) and Eq (A-2), it becomes primarily an empirical means of reproducing the observed pure component data with no fundamental basis for generalization to mixtures. One could, of course envision several extensions based on additional α terms in the denominator of Eq (A-1) and additional β terms in Eq (A-2). Such an approach to mixture permeation analyses would be completely empirical and mimic the generalization of Eq (2) and Eq (7); however, without any physical justification. The generalizations of Eq (2) and Eq (7) were natural outgrowths of the fundamental physical basis of the Langmuir isotherm. The fact that the mixture data are so consistent with Eq (7) and Eq (9) provides strong support for the physical basis of the dual mode model.

An important value of a permeation model is not simply its ability to correlate experimental data, but rather to provide a framework for understanding the principal factors controlling membrane performance. The dual mode model is derived from

consistent, physical descriptions of the glassy state and yields parameters which make unambiguous molecular scale statements regarding the general nature of glassy, amorphous materials.

In summary, the two expressions offered in Eq (A-1) and Eq (A-2) provide empirical forms for correlating the general trends in pure component sorption and transport data. These expressions are not offered in terms of internally consistent physical arguments and appear to offer no fundamental basis for understanding general glassy state behavior. Furthermore, no fundamental approach is apparent for the treatment of the critically important mixed penetrant problem using the model, since the various parameters in the model lack the well-defined significance provided by the dual mode model.

Nomenclature

b_i Affinity constant of component i for the polymer (atm^{-1})
D_D Diffusion coefficient of the Henry's law species (cm^2/sec)
D_H Diffusion coefficient of the Langmuir species (cm^2/sec)
F Ratio of Langmuir and Henry's law diffusion coefficients
k_D Henry's law constant (cm^3 gas (STP)/cm^3 polymer-atm)
K $C'_H b/k_D$ where C'_H is the capacity of Langmuir mode (cm^3 gas (STP)/cm^3 polymer)
p_i Upstream driving pressure for penetrant i (atm)
P_i Permeability of i (cm^3 gas(STP)-cm/cm^2-sec-cmHg)
V_g Specific volume of the glassy polymer (cm^3/g)
V_ℓ Specific volume of the densified glassy polymer (cm^3/g)

Acknowledgments

The authors gratefully acknowledge support of this work under NSF Grant No. CPE-79-18200 and ARO Contract No. DAAG29-81-K-0039. Also the assistance of Mrs. Leslie Edgerton in typing the manuscript is acknowledged.

Literature Cited

1. Stannett, V. T.; Koros, W. J.; Paul, D. R.; Lonsdale, H. K. and Baker, R. W.; Adv. in Polymer Sci., 1979, 32, 69.
2. Barrer, R. M. and Barrie, J. A.; J. Polym. Sci., 1957, 23, 331.
3. Pye, D. G.; Hoehn, H. H. and Panar, M.; J. Appl. Polym. Sci., 1976, 20, 287.
4. Koros, W. J. and Paul, D. R.; J. Polym. Sci.-Polym. Phys. Ed., 1978, 16, 1947.
5. Wonders, A. G. and Paul, D. R.; J. Membr. Sci., 1979, 5, 63.
6. Fechter, J. M.; Hopfenberg, H. B. and Koros, W. J.; Polym. Engr. and Sci., 1981, 21, 925.

7. Koros, W. J. and Paul, D. R.; J. Polym. Sci., Polym. Phys. Ed., 1981, 19, 1655.
8. Horiuti, J.; Sci. Papers of the Inst. of Phy. and Chem. Res. (Tokyo); 1931, 17, 126.
9. Chan, A. H. and Paul, D. R., Polym. Engr. and Sci., 1980, 20, 87.
10. Huvard, G. S.; Stannett, V. T.; Koros, W. J. and Hopfenberg, H. B., J. Membr. Sci., 1980, 6, 185.
11. Chen, S. H., M.S. Thesis, North Carolina State University, 1982.
12. Lewis, O. G.; "Physical Constants of Linear Homopolymers," Springer Verlag, New York (1968).
13. Kolb, H. J. and Izard, E.; J. Appl. Phys., 1949, 20, 564.
14. Matuska, S. and Ishida, Y.; J. Polym. Sci., Pt. C., 1960, 14, 247.
15. Mercier, J. P.; Aklonis, J. J.; Litt, M.; and Tobolsky, A. V.; J. Appl. Polym. Sci., 1965, 9, 447.
16. Sandler, Stanley I.; "Chemical and Engineering Thermodynamics," J. Wiley and Sons, New York, 1977, pg. 435.
17. Petropoulos, J. H.; J. Polym. Sci., Pt. 2-A, 1970, 8, 1797.
18. Paul, D. R. and Koros, W. J.; J. Polym. Sci.-Polym. Phys. Ed., 1976, 14, 675.
19. Koros, W. J.; Chan, A. H. and Paul, D. R.; J. Membr. Sci., 1977, 2 165.
20. Barrie, J. A.; Williams, M. L. and Munday, K.; Polym. Engr. and Sci., 1980, 20, 20.
21. Koros, W. J., Ph.D. Dissertation; "Sorption and Transport of Gases in Glassy Polymers," The University of Texas (Austin), 1977.
22. Koros, W. J.; Paul, D. R. and Rocha, A. A.; J. Polym. Sci., Polym. Phys. Ed., 1976, 14, 687.
23. Koros, W. J. and Paul, D. R.; J. Poly. Sci., Polym. Phys. Ed., 1978, 16, 2171.
24. Toi, K.; Polym. Engr. and Sci., 1980, 20, 30.
25. Tikhomorov, B. P.; Hopfenberg, H. B.; Stannett, V. T. and Williams, J. L.; Macromol. Chem., 1968, 118, 177.
26. Stern, S. A. and Saxena, V.; J. Membr. Sci., 1980, 7, 47.
27. Assink, R. A.; J. Polym. Sci.-Polym. Phys. Ed., 1975, 13, 1665.
28. Raucher, D. and Sefcik, M.; Paper presented in this symposium.
29. Koros, W. J.; J. Polym. Sci.-Polym. Phys. Ed., 1980, 18, 981.
30. Koros, W. J.; Chern, R. T.; Stannett, V. T. and Hopfenberg, H. B.; J. Polym. Sci.-Polym. Phys. Ed., 1981, 19, 1513.
31. Robeson, L. M.; Polym. Engr. and Sci., 1969, 9, 277.

32. Sanders, E. S.; Koros, W. J.; Hopfenberg, H. B. and Stannett, V. T.; "Mixed Gas Sorption in Glassy Polymers: Equipment Design and Considerations and Preliminary Results," Submitted for Publication, J. Polym. Sci.- Phys. Ed.
33. Chern, R. T.; Koros, W. J.; Hopfenberg, H. B. and Stannett, V. T.; "The Effects of Low Partial Pressures of Isopentane on the Permeability of Polycarbonate to CO_2," accepted by J. Polym. Sci.- Phys. Ed.
34. Vieth, W. R. and Sladek, K. J.; J. Coll. Sci., 1965, 20, 1014.
35. Frisch, H. L.; J. Phys. Chem., 1957, 61, 93.
36. Smith, G. N.; M.S. Thesis, North Carolina State University, 1980.

RECEIVED December 27, 1982

Reprinted from ACS SYMPOSIUM SERIES, No. 223
INDUSTRIAL GAS SEPARATIONS
Thaddeus E. Whyte, Jr., Carmen M. Yon and Earl H. Wagener, Editors
Copyright 1983 by the American Chemical Society
Reprinted by permission of the copyright owner

Reprinted from I&EC PRODUCT RESEARCH & DEVELOPMENT, 1984, 23, 317.
Copyright © 1984 by the American Chemical Society and reprinted by permission of the copyright owner.

A Simple Apparatus for Measurement of Liquid Permeabilities through Polymeric Films

A concise description of the evolutionary design of a simple apparatus for measurement of the steady-state permeability of polymer films to penetrating liquids is presented. The cell eliminates inherently leaky polymeric seals (O-rings or gaskets) by using opposing metal O-rings which produce uniform deformation and seal of the experimental polymer film by the metal O-rings which are opposing and in perfect register. The permeability cell weighs approximately 125 g, is constructed entirely from off-the-shelf components, and permits gravimetric characterization of steady-state permeabilities by using a conventional analytical balance and a forced-air, constant-temperature convection oven.

Background and Introduction

The estimation of permeation rates of liquids through polymeric films is a problem often encountered by packaging engineers. Relatively few data exist to guide the practicing engineer in this regard for typical polymer/penetrant systems due to the difficulty of performing such

0196-4321/84/1223-0317$01.50/0 © 1984 American Chemical Society

measurements economically.

The present note describes briefly the shortcomings in an early cell design which, while seemingly adequate in principle, was not effective for measuring losses through low flux barriers. We then present an extremely simple and effective alternate design which can be constructed from off-the-shelf components and permits measurement of steady-state permeabilities even in relatively low permeation (high barrier) systems.

The permeation of a solvent through a polymer in the absence of cracks, pores, or other compromising defects is conveniently interpreted as a stepwise solution–diffusion process (Salame and Steingiser, 1977) involving: (1) dissolution of the solvent into the polymer film, (2) diffusion through the film, driven by a concentration gradient, and (3) desorption from the outer film surface.

By definition, for liquid permeation through a polymer film the permeability, P, is the steady-state flux of a penetrant through a polymer membrane, J_s, normalized by the activity change, Δa, across the sample thickness, l (Petropoulos, 1974)

$$P = J_s/[\Delta a/l] \qquad (1)$$

Measurement of liquid permeation through polymers can be performed by a weight loss method. Goebel et al. (1982) used heat-sealed polyolefin bottles filled with the desired penetrant and determined the weight loss due to permeation through the bottle wall. In trying to calculate solvent permeability from the Goebel data, Koros et al. (1982) were confronted with the problem of defining the exact diffusion area and the uniformity of the polymer thickness comprising the bottle wall.

To eliminate such uncertainty, associated with diffusion area and film thickness, we decided to use a simple flat membrane cell. The first version of the cell was made of glass to ensure inertness to all conventional organic solvents. To minimize leaks we used a Viton O-ring joint. Delrin brackets were used to provide a tight seal. Delrin is a tough material, yet it is soft enough not to break the glass cell. Initial tests indicated that a small but unacceptable amount of solvent loss was occurring through the O-ring seal. Teflon tape was wrapped around the exterior of the O-ring joint and a heat shrinking tube was employed over the Teflon sealed O-ring joint before mounting the brackets to minimize leaks.

Even with all of these precautions, reproducibility was still rather poor when the Viton O-ring seal was used. It appears that deformation of the thick polyethylene film (20 mils) by the rubber O-ring was not satisfactory to form a reproducibly good seal and the degree of sealing changed slightly from run to run, thereby causing vary... ...ults for the same nominal run conditions. Additionally, some actual permeation loss through the O-ring is anticipated.

Description of the New Cell Design

To circumvent the difficulties encountered with the first cell described above, a basically different design using two symmetrically opposed *metal* O-rings integral to the top and bottom sealing surfaces was adopted. The two O-rings deform the film slightly, and uniformly, to provide an extraordinarily tight seal. Essentially no weight loss (<-0.0001 g/day) was observed in a cell with three layers of standard aluminum foil replacing the membrane in a protracted run of 8 days. On the other hand, loss rates from the Viton O-ring sealed glass cell in such leak tests were erratic and sometimes approached 0.040 g/day. Typical losses in these runs were in the range of 0.005 to 0.020 g/day for the glass cell.

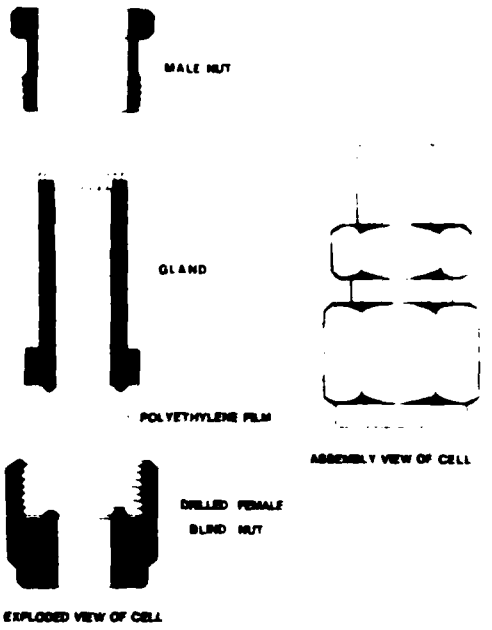

Figure 1. Schematic diagram of permeation cell.

A schematic of the successful cell design is presented in Figure 1. The cell is inexpensive, being comprised of $^1/_2$-in. stainless steel CAJON VCR fittings modified to meet the needs of the experiment. The low cost of the apparatus permits procurement of a large number of the cells for studying many solvent/polymer pairs in large-scale tests. The cell shown in Figure 1 contains three parts. A drilled blind female nut, a male nut, and a gland. A $^5/_8$-in. hole was drilled in the blind nut to match the opening of the gland. The inner part of the gland was drilled to match the upper wall thickness of the gland and was sealed from the top with silver solder to hold the stainless steel cap. The detailed fabrication procedure is described in the Appendix.

The polymer film serves as a gasket and the seal is made by tightening the gland to the blind nut using the male nut. A torque wrench was used to apply a reproducible torque of 50 in.-lb_f to ensure that the film is not cut by the O-rings while it is being sealed. Our experience to date has been confined to tough polyolefins and we anticipate the possibility of problems with brittle polymers such as polystyrene because the metal O-ring might crack rather than uniformly seal the rigid polymer.

The advantages of the new cell design are summarized as follows: (1) It insures an essentially perfect seal around the desired film area which enables accurate measurement of the weight loss through the film. (2) The weight of the cell does not exceed 125 g when loaded and is, therefore, within the 160 g limit of most sensitive analytical balances. (3) The VCR metal O-rings provide a very well-defined diffusion area for the purpose of calculating permeabilities. (4) CAJON VCR connectors are readily available in different sizes as an off-the-shelf component, so the cells are inexpensive and easy to construct.

The cells were cleaned after each run in an ultrasonic cleaner using dionized water, followed by a drying step at 40 °C for 48 h. For the solvents studied in our work, a typical run using 20-mil high density polyethylene film requires from 10 to 12 days under controlled temperature conditions. Higher molecular weight solvents or "tighter" barrier films would presumably require longer run times to reach steady state and to permit characterization of the

Table I

penetrant	$P \times 10^7$,[a] this study	$P \times 10^7$,[a] from data of Goebel et al.	[(P) Goebel et al.]/[(P) this study]
heptane	14.6 ± 0.3	19.2	1.32
isooctane	1.4 ± 0.1	3.24	2.31

[a] Permeability units = [cm³ (STP) cm]/[cm² s].

steady-state permeation rate, but this is not a serious restriction.

An analytical balance with five-decimal accuracy is needed to detect the extremely low loss rates of some solvents (0.0001 g/day). With low flux solvents for certain polymers the accuracy of the balance determines the accuracy of the results. A Mettler Model H10W balance (accurate to ±0.0001 g) was used in our work. A small flow rate of air is focused on the downstream membrane face to eliminate concentration polarization which could bias permeation results.

Discussion

Typical data for isooctane and heptane permeation through 20 mil thick high-density polyethylene films are shown in Figure 2 for both the earlier (unsuccessful) and the latest (successful) designs. The original cell design provides irreproducible weight loss results for both high flux and low flux solvents due to irreproducibility of seal formation. For both solvents, however, the new cell design provides reproducible results. Note that the results for the new cell lie below those of the glass cell by an amount equal to the leak through and around the rubber O-ring seal.

As mentioned before, the sensitivity of the balance can compromise the accuracy of the measurement. In fact, we encountered this problem in our work. The steady-state weight loss of isooctane was found to be 0.0017, 0.0018, and 0.0019 g/day in three similar cells. The uncertainty in the last digit is determined by the basic measurement capabilities of the balance we employed. The problem is not as serious in the case of heptane, where the steady-state permeation rate is an order of magnitude higher, so measurement uncertainties of ±0.0001 g associated with the balance are negligible.

One can, for example, calculate the permeability for the penetrants given above using the preceding average weight loss data in conjunction with eq 1. The diffusion area for the cell shown in Figure 1 was 1.50 cm², and the film thickness used in this work was 0.051 cm. The activity difference across the membrane (Δa) in eq 1 was equal to unity, because pure liquid was in contact with the film at the upstream face ($a_2 = 1$) and a quickly moving air stream swept the downstream face ($a_1 = 0$). Therefore, inserting the data for the average loss rate for the two penetrants into eq 1, the permeabilities reported in Table I can be calculated as shown in Table II for isooctane.

Table I also shows a comparison between the permeabilities of heptane and isooctane obtained by this study

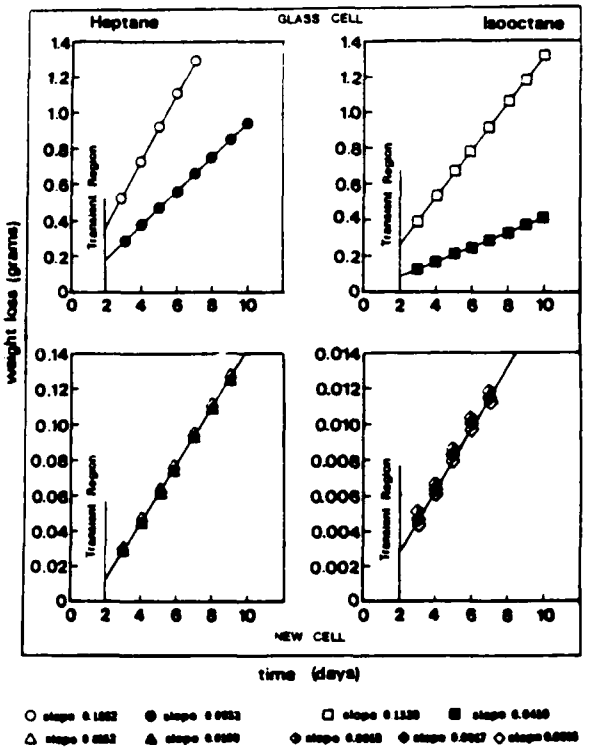

Figure 2. Reproducibility of results for the glass cell and the new cell.

and permeabilities reported by Koros et al. based on the work done by Goebel et al. Various factors are believed to cause the difference in results shown in Table I, mainly, sample to sample variation. Other factors which could contribute to the observed differences are possible inaccuracies in approximating the diffusion area and the nominal wall thickness of the bottles used by Goebel et al. These geometrical effects, however, are expected to be of rather minor importance since the ratio of the permeabilities in the present study to those calculated from the whole package tests of Goebel are quite different for the two solvents. Clearly, if only area or thickness differences dominated, the ratio of permeabilities should be essentially the same for both solvents; thus the cause of the discrepancy is most likely a result of sample-to-sample variation.

Conclusions

It is far more effective to seal the cell by deforming a test film with the symmetrical metal O-ring arrangement from top and bottom rather than sealing the film using a standard, elastomeric O-ring seal. The cell based on the metal O-ring concept will most likely be unsuitable for brittle polymers such as polystyrene. Except for this limitation, the cell is very versatile and effective for measuring both low and high flux penetrants with acceptable reproducibility. Even relatively ductile, glassy polymers such

Table II. Sample Calculations for Isooctane

Data:	average weight loss	0.0018 g/day	
	diffusion area	1.5 cm²	
	film thickness	0.051 cm²	

$$P = \frac{0.0018\ \text{g}}{\text{day}} \cdot \frac{\text{g mol}}{114.23\ \text{g}} \cdot \frac{22400\ \text{cm}^3(\text{STP})}{\text{g mol}} \cdot \frac{1\ \text{day}}{86400\ \text{s}} \cdot \frac{0.051\ \text{cm thickness}}{1.5\ \text{cm}^2\ \text{area}}$$

$$P = 1.1 \times 10^{-7}\ \left(\frac{\text{cm}^3(\text{STP})\ \text{cm}}{\text{cm}^2\ \text{s}}\right)$$

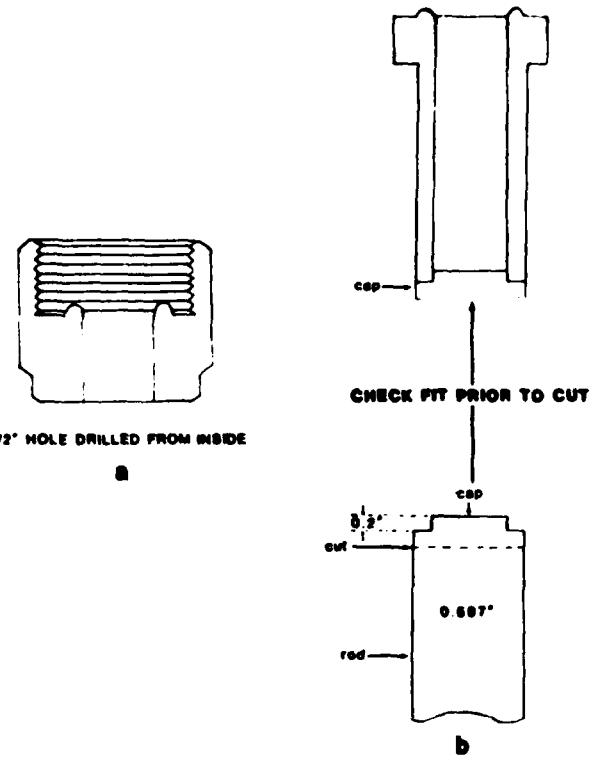

Figure 3. VCR fittings modifications.

as poly(ethylene terephthalate) and polycarbonate should also be suitable for use with the cell.

Acknowledgment

The authors are grateful to Air Products for supplying the films and to the Army Research Office for funding part of the project under contract number DAAG 29-81-K-0039. We also wish to acknowledge Ms. Sally Lloyd for typing the manuscript.

Appendix

Detailed Procedure Recommended for Modification of VCR Fittings. The VCR male nut requires no modification for use in the cell; however, the blind female nut and gland must be altered slightly. Using a metal lathe equipped with a three-jawed chuck, center the VCR blind female nut with a countersink, and drill a $^1/_2$-in. hole as shown below. It is best to drill from the inside of the nut to the outside, since this enables deburring the edge without damaging the polished metal O-ring inside the nut. (See Figure 3a.)

After completing the female nut, the VCR gland should be mounted in the lathe and drilled from the collared end along the entire length to an inside diameter of $^1/_2$-in. Again, care should be taken to avoid damage to the polished metal O-ring on the collared end of the gland during drilling and deburring.

To complete the gland modification, stainless steel bar stock is used to make an end cap. The stock should be turned down to the outer diameter of the VCR gland (0.597 in.). A small length (0.2 in.) of the bar should then be turned down to the inner diameter of the gland (0.500 in.) (See Figure 3b).

Caps should be individually fitted for each VCR gland for best results. After the preliminary forming operation, proper fit of the cap can be checked before cutting off the workpiece to allow easy filing and deburring. Both the gland and mating cap should be cleaned and degreased prior to welding.

Although a variety of welding options exist, we found it convenient to use a stainless steel brazing material (Eutectic 1020) with a standard oxy-acetylene torch. Following cleaning of the internal surfaces by reaming, the cell is ready to assemble. The fabrication time, exclusive of set-up procedures, is approximately 1 h for each cell.

Literature Cited

Goebel, K. A.; Janas, V. F.; Waytek, A. G. *Polym. News* **1982**, *8*, 37.
Koros, W. J.; Stannett, V. T.; Hopfenberg, H. B. *Polym. Eng. Sci.* **1982**, *22*, 738.
Petropoulos, J. H. *J. Polym. Sci. Phys. Ed.* **1974**, *12*, 35.
Salame, M.; Steingiser, S. *Polym. Plast. Technol. Eng.* **1977**, *8*(22), 155.

Department of Chemical Engineering
North Carolina State University
Raleigh, North Carolina 27650

Haitham S. A. Al-Hussaini
William J. Koros
Michael Howard
Harold B. Hopfenberg*

Received for review August 25, 1983
Accepted January 9, 1984

Selective Permeation of CO_2 and CH_4 through Kapton® Polyimide: Effects of Penetrant Competition and Gas-Phase Nonideality

R. T. CHERN, W. J. KOROS,* B. YUI, H. B. HOPFENBERG, and V. T. STANNETT, *Department of Chemical Engineering, North Carolina State University, Raleigh, North Carolina 27650*

Synopsis

Sorption isotherms for pure CO_2 and pure CH_4 in Kapton H® polyimide films at 60°C are reported for pressures up to 20 atm and are analyzed in terms of the dual-mode sorption model. An experimental scheme for the measurement of steady-state permeabilities of both pure and mixed gas feeds is described. Permeabilities of Kapton to the individual components at 60°C are presented for a mixture comprised of 32.2% CO_2 in CH_4 as functions of feed pressure up to 590 psi (absolute). The permeabilities for the individual penetrants in the mixed feed are lower than the respective pure-component values at the corresponding partial pressures. Furthermore, the permeabilities of both penetrants drop as the feed pressure is increased at constant composition. The dual-mobility transport model used to analyze the data postulates that the observed pressure and composition dependence of the permeabilities is due to competition between penetrants for a limited microvoid sorption capacity in the glassy polymer. It is demonstrated that in addition to flux depressions due to dual-mode effects, nonideality of the gas phase must be accounted for to explain the substantial flux depressions observed for the CO_2/CH_4 mixtured used in this study.

INTRODUCTION

Sorption and Transport of Pure Gases

The sorption isotherms of gases and vapors in glassy polymers have been analyzed by many authors using the dual-mode sorption model given by

$$C = C_D + C_H = k_D p + C'_H bp/(1 + bp) \quad (1)$$

Physical interpretations of the three parameters appearing in eq. (1) have been offered previously.[1] Besides the normal dissolution of penetrants in the polymer matrix, which follows the form of Henry's law, this model postulates that a second mode of sorption is operative. This additional sorption mode corresponds to the filling of excess unrelaxed volume present in glassy polymers and is described well by a Langmuir isotherm with total capacity C'_H and affinity constant b. This model has been shown to be satisfactory for moderate pressures in the absence of strong interactions between penetrants and polymer molecules, which may cause plasticization or swelling.[1-5]

® Registered trademark, E.I. Du Pont Company.

* The Center for Energy Studies, The University of Texas at Austin, Austin, TX 78712.

Journal of Polymer Science: Polymer Physics Edition, Vol. 22, 1061-1084 (1984)
© 1984 John Wiley & Sons, Inc
CCC 0098-1273/84/061061-24$04.00

Under the above conditions, the diffusive fluxes of pure gases in glassy polymers can be analyzed in terms of the dual-mobility model[1,3,6,7] given by

$$N = -D_D \frac{dC_D}{dx} - D_H \frac{dC_H}{dx} \tag{2}$$

This model assumes instant local equilibrium of penetrant concentrations between the two environments and accounts explicitly for diffusion of penetrants through the two types of environment with potentially different mobilities D_D and D_H. Although these two diffusivities may, in principle, depend on concentration,[8] many experimental observations[1-3,9] indicate that for simple gases the two coefficients are essentially concentration independent when the penetrant concentration in the polymer is relatively low. When the downstream pressure is maintained at approximately zero, the permeabilities of pure gases have the following form:

$$P = k_D D_D [1 + FK/(1 + bp)] \tag{3}$$

where $K = C'_H b/k_D$ and $F = D_H/D_D$.

Transport of Gas Mixtures

For cases involving only weak penetrant–penetrant and penetrant–polymer interactions, Koros et al.[10] showed that the dual-mobility model can be generalized to describe the transport of mixed gases in glassy polymers. The following expression was derived for the permeability of component A in a binary-component feed when the downstream pressure can be approximated as zero:

$$P_A = k_{DA} D_{DA} [1 + F_A K_A/(1 + b_A p_A + b_B p_B)] \tag{4}$$

Compared with eq. (3), the additional term appearing in the denominator of the second term of eq. (4) reflects the competition of the "second" component for the unrelaxed regions present in glassy polymers.[10,11] This term results in a predicted permeability decrease of component A owing to the competition of component B for sorption and transport pathways in the membrane. Chern et al.[12] demonstrated experimentally that the permeability of Lexan polycarbonate at 35°C to CO_2 was indeed reduced by more than 15% when a small amount (<3.5 mol %) of isopentane was introduced into a pure CO_2 feed stream. It was shown that these data are consistent with the form of eq. (4). Moreover, it was later reported by Chern et al.[13] that the permeability of Kapton H polyimide to CO_2 was depressed by up to 11% by the presence of H_2O at low relative humidities (5.5 and 9.3%). Similar effects have been reported for water and hydrocarbons in polyimides by Pye et al.[14] and by Robeson[15] for CO_2 in the presence of 4,4'-dichlorodiphenylsulfone in polysulfone. This paper is a continuation of these previous studies to test the general validity of the provocative implication of eq. (4) that the presence of a second component in a mixed feed will lower the permeability of the other component in the absence of overriding plasticizing effects. In that regard, steady-state permeability data of Kapton H polyimide to a CO_2 and CH_4 mixture and the respective pure gases are presented as functions of feed pressure at 60°C. The important effects of temperature and feed composition are under investigation and will be presented in a later publication.

EXPERIMENTAL

Materials

Gases

Coleman-grade CO_2 (99.999%), instrument-grade CH_4 (99.7%), and research-grade N_2 (99.9995%) were used. The mixture (32.2% CO_2, 67.8% CH_4) and the calibration gas (202 ppm CH_4, 2040 ppm CO_2 in N_2) were purchased from Air Products and Chemicals, Tamaqua, PA. The composition of the CO_2/CH_4 mixture was determined by using the relative response factor generated in our laboratory.[16]

Film

The 0.3-mil Kapton H polyimide films were kindly supplied by the E. I. Du Pont Company. Kapton has the following structure as its repeat unit:

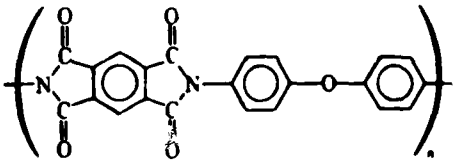

which provides a balance between stiffness through the aromatic diimide and flexibility through the ether linkage.

The films were degassed at 60°C for 48 h before permeation measurements. DSC (differential scanning calorimeter) data generated in our laboratory indicated no trace of a glass transition up to 500°C, although Du Pont reported evidence of a transition between 400 and 500°C for Kapton H, depending on the method of measurement.[17]

Apparatus

Permeation

All tubing, connections, valves, and the permeation cell are either 314 or 316 stainless steel. The permeation cell was custom made and the other cell components were purchased from Raleigh Valve and Fitting Co., Raleigh, NC. The detailed dimensions of the permeation cell and a schematic diagram of the apparatus are shown in Figures 1 and 2, respectively. The effective area available for permeation is 9.6 cm^2.

To minimize concentration polarization on the feed side, the feed flow rate was adjusted to values such that the maximum stage cut was less than 0.01% of the feed. An approximate estimation scheme is provided in Appendix A, which indicates that the concentration polarization was, indeed, negligible even at the highest permeation fluxes studied.

Matheson model 9 two-stage regulators were used to deliver and maintain feed pressures up to 260 psi (absolute) and a Matheson model 4 one-stage regulator with stainless-steel diaphragm was used for pressures higher than 260 psi (absolute). An Airco model 18 two-stage pressure regulator was used to drive an

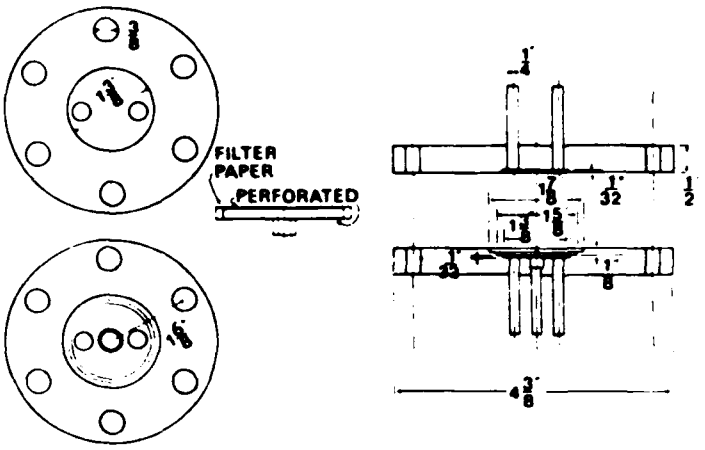

Fig. 1. Dimensions of the permeation cell.

Air Products gas flow controller which has an instantaneous precision of 0.3%. The actual flow rate of the N_2 pickup stream was measured using a bubble flow meter kept at constant temperature with a reproducibility of approximately 0.5%. The pressure of the N_2 pickup stream was monitored by a Kulite ITQS pressure transducer and was maintained at less than 0.1 psi (gauge). The permeation apparatus was immersed in an insulated constant-temperature air bath. A base load variable heater was used to compensate the continuous heat loss to the environment and another variable heater, together with a Fisher RotoStat mercury thermoregulator and a relay, kept the bath temperature within ±0.05°C of the set value.

The calibration gas was used as an external standard for the analysis of the permeant samples. A Varian 3700 GC (gas chromatograph) with dual TCD

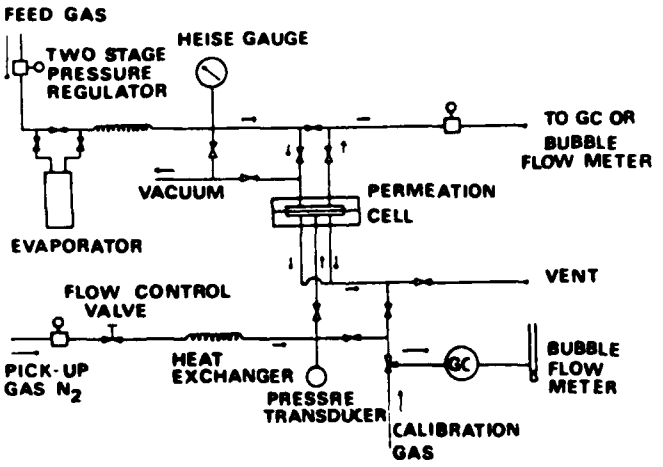

Fig. 2. Schematic diagram of the permeation apparatus.

(thermal conductivity detector) and a Shimazu GC with single FID (flame ionization detector) were used respectively for determining the concentrations of CO_2 and CH_4 in the permeate. This arrangement was necessary because the tail of the N_2 peak overlapped the CH_4 peak and the concentrations of CH_4 in the permeate were near the limit of TCD sensitivity. Four and one-half feet of 100/120 carbosieve S columns were used for both GCs with sample loops of 1 and 0.25 cm^3, respectively.

It was found that the permeability was independent of the N_2 pickup flow rate, ranging from 8 to 25 m^3/min. This observation indicates that the responses of both detectors are indeed linear with respect to the concentrations of the penetrants. Since responses of the detectors may vary slightly with time, calibrations were performed daily to minimize uncertainties in the final calculations.

Sorption

Isotherms of pure CO_2 and CH_4 were determined by using very sensitive pressure decay procedures and an apparatus which has been described in detail in earlier publications by our group.[16,18-21] This procedure involves rigorous material balance calculations using pertinent equations of state for the various gases. The sorption parameters in eq. (1) were determined by a nonlinear regression algorithm.[16,18,19]

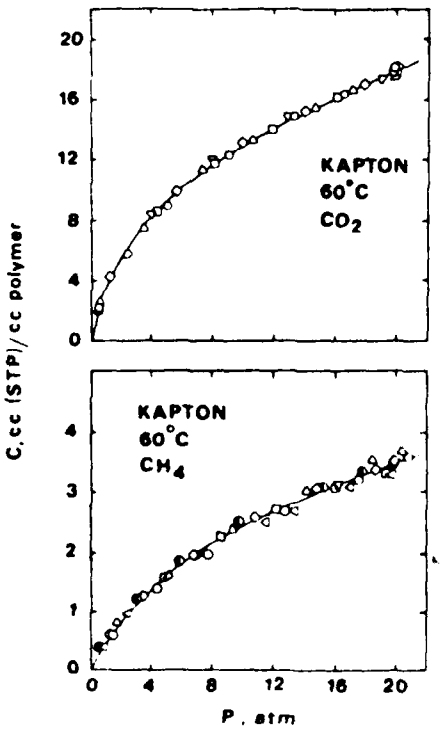

Fig. 3. Sorption isotherms at 60°C: (a) CO_2, (b) CH_4, in Kapton H polyimide. Different symbols stand for different runs.

TABLE I
Dual-Mode Sorption Parameters for Pure CO_2 and Pure CH_4 in Kapton Polyimide at 60°C

	Based on pressure			Based on fugacity		
	$k_D \left(\frac{\text{cm}^3\,(\text{STP})}{\text{cm}^3\,\text{atm}}\right)$	$C'_H \left(\frac{\text{cm}^3\,(\text{STP})}{\text{cm}^3}\right)$	$b\ (\text{atm}^{-1})$	$k'_D \left(\frac{\text{cm}^3\,(\text{STP})}{\text{cm}^3\,\text{atm}}\right)$	$C'_H \left(\frac{\text{cm}^3\,(\text{STP})}{\text{cm}^3}\right)$	$b^{\#}\ (\text{atm}^{-1})$
CO_2	0.380 ± 0.054	12.480 ± 1.48	0.296 ± 0.023	0.439 ± 0.058	11.817 ± 1.486	0.316 ± 0.069
CH_4	0.070 ± 0.011	2.684 ± 0.376	0.174 ± 0.032	0.073 ± 0.011	2.653 ± 0.384	0.175 ± 0.034

RESULTS AND DISCUSSION

Sorption and Permeation of Pure Gases

Sorption

Sorption isotherms of pure CO_2 and pure CH_4 in Kapton H polyimide at 60°C are shown in Figures 3(a) and 3(b). Each isotherm includes at least four consecutive series of runs in which the penetrant pressure was increased stepwise from low to high values. In both cases, virgin films which had been degassed

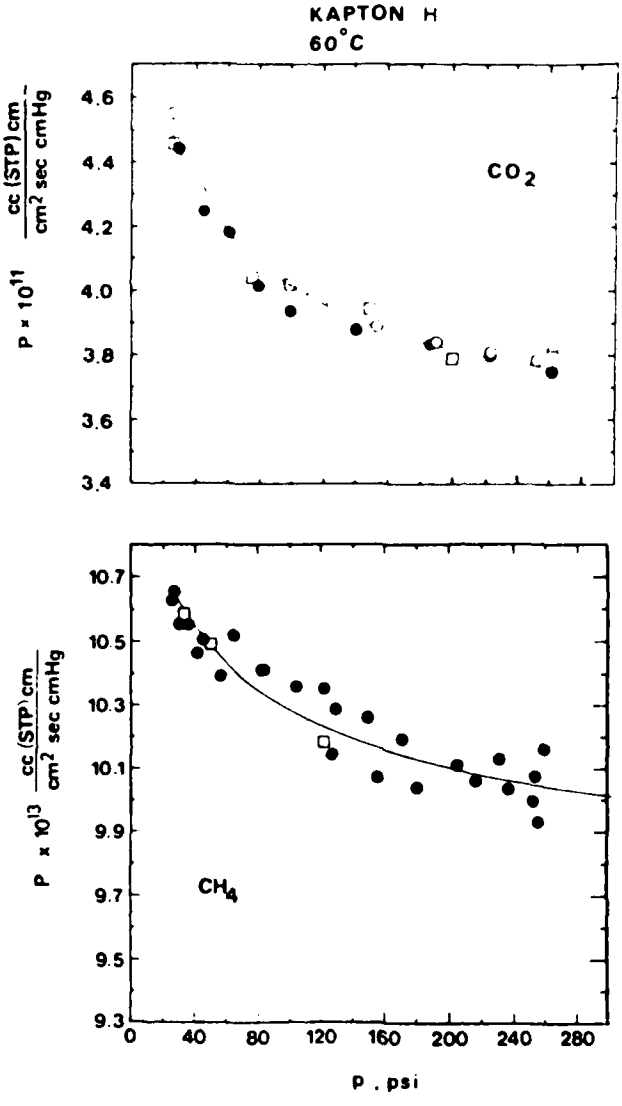

Fig. 4. Permeability of Kapton H polyimide at 60°C: (a) CO_2; order of measurement (○) 10/1982, (□) 12/1982, and (●) 1/1983. (b) CH_4, (●, □) measured two months apart.

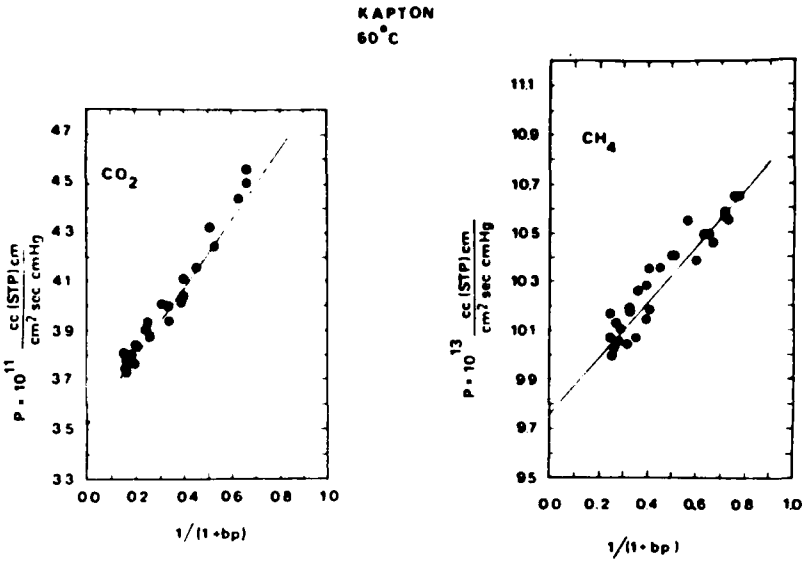

Fig. 5. Permeability of Kapton H at 60°C plotted according to eq. (3): (a) CO_2, (b) CH_4.

at 60°C for 120 h were used. An initial "conditioning" effect during the first sorption cycle, which has been observed consistently for other glassy polymers,[1-3,9,18,19,21] appears to be absent for Kapton. The conditioning effect is pronounced, for example, when Lexan polycarbonate is exposed to CO_2 at 35°C.[22]

The sorption isotherms were analyzed in terms of the dual-mode sorption model [eq. (1)] using nonlinear least-squares regression[2,18] and yielded the dual-mode parameters k_D, C'_H, and b in Table I. These parameters were then used to generate the solid lines in Figures 3(a) and 3(b).

Permeation

Steady-state permeabilities at 60°C for both pure CO_2 and pure CH_4 decrease with increasing pressures as shown in Figures 4(a) and 4(b). These data are replotted in Figures 5(a) and 5(b) according to eq. (3), and from the slopes and intercepts, transport parameters in Table II are calculated. The solid lines in Figures 4(a) and 4(b) are calculated values based on the dual-mobility model with parameters in Tables I and II. The reproducibility of the permeability measurement is within 1% even over a long period of time during which the film has been exposed to CO_2/CH_4 mixtures of various compositions and over a wide range of pressures. This observation is illustrated in Figure 4(a) where CO_2 permeabilities, measured approximately three months apart for the same film, fall essentially on the same curve. Furthermore, no high-pressure "conditioning" effect on permeability was observed for a film exposed to 300 psi (absolute) CO_2 continuously for 48h. Only slight increases (<2%) in CO_2 permeability were observed for a film exposed to 450 psi (absolute) (30 atm) CO_2 for 24 h.

The diffusion coefficient D_{eff}, defined as

TABLE II
Transport Parameters of Pure CO_2 and Pure CH_4 in Kapton Polyimide at 60°C

	Based on pressure			Based on fugacity		
	D_D (cm²/s)	D_H (cm²/s	F	D_D^f (cm²/s	D_H^f (cm²/s	F
CO_2	7.044×10^{-9}	2.899×10^{-10}	0.0412	6.567×10^{-9}	2.075×10^{-10}	0.0316
CH_4	1.061×10^{-9}	1.844×10^{-11}	0.0174	1.042×10^{-9}	1.318×10^{-11}	0.0126

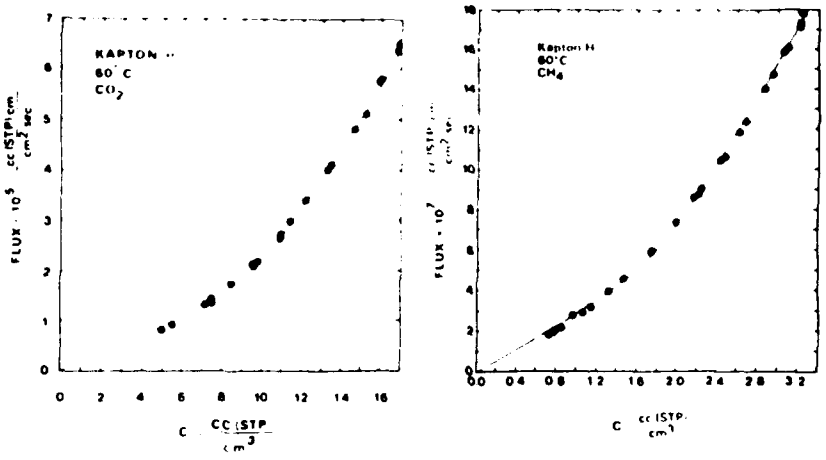

Fig. 6. Permeation flux versus penetrant concentration at the upstream surface position of the membrane: (a) CO_2, (b) CH_4. The lines are drawn to assist reading only.

$$N = -D_{\text{eff}} \frac{dC}{dx} \tag{5}$$

can be obtained by differentiating the steady-state flux shown in Figures 6(a) and 6(b) with respect to the sorbed penetrant concentration C_2 evaluated at the feed side, $x = L$:

$$D_{\text{eff}}(C_2) = \left.\frac{d(NL)}{dC}\right|_{C_2} \tag{6}$$

Instead of performing the differentiation graphically,[1] a secant method was applied to points in Figures 6(a) and 6(b) to determine the derivatives. The detailed procedure is illustrated in Appendix B. The results are included in Figures 7(a) and 7(b).

Alternatively, D_{eff} may be calculated from the independently determined dual-mode sorption and transport parameters according to eq. (7). The derivation of eq. (7) has been presented by Paul et al.[7]

$$D_{\text{eff}}(C_2) = D_D \frac{1 + FK/(1 + bp_2)^2}{1 + K/(1 + bp_2)^2} \tag{7}$$

The calculated values are represented by the solid lines in Figures 7(a) and 7(b). The agreement between the experimental values and model calculations is clearly quite satisfactory.

Permeation of Mixed Gases

Permeabilities

Permeabilities of CO_2 and CH_4 for a 32.2% CO_2 in CH_4 mixture, determined as functions of pressure up to roughly 590 psi (absolute) (40.2 atm), are presented

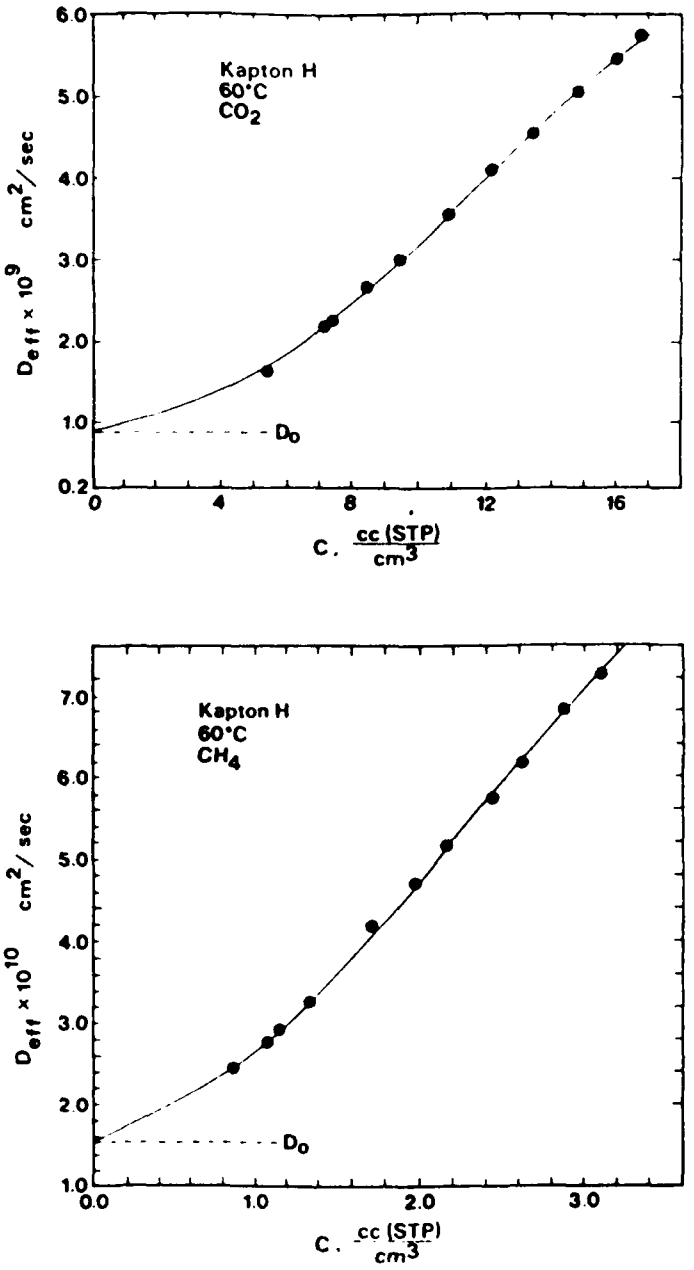

Fig. 7. Effective diffusion coefficient as defined in eq. (5) versus penetrant concentration: (a) CO_2, (b) CH_4. The solid line represents model predictions using fugacity-based parameters.

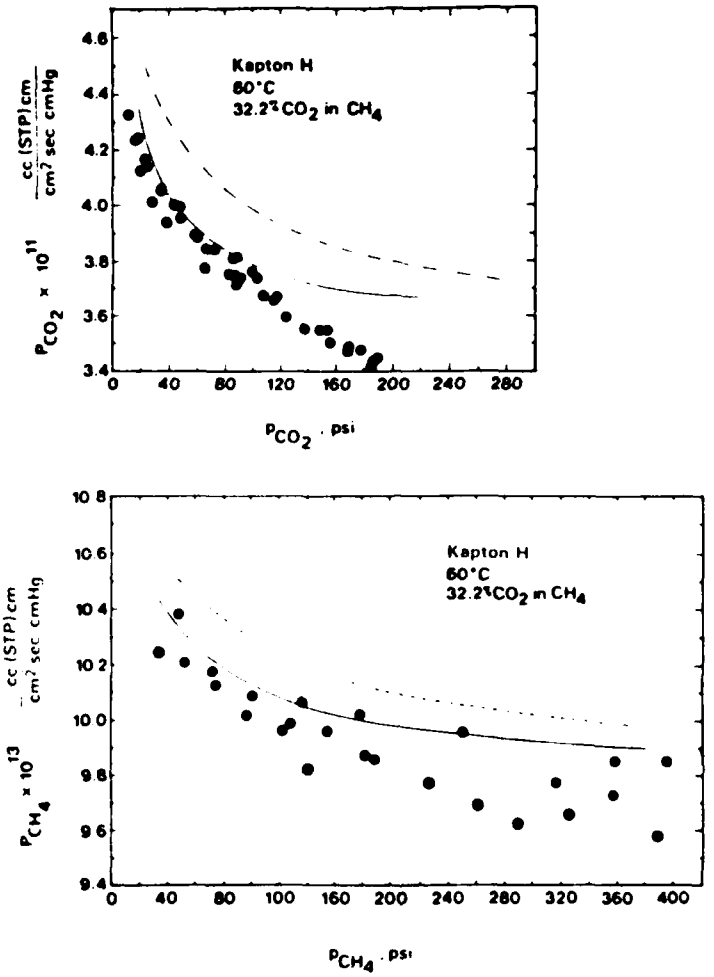

Fig. 8. Permeability of Kapton H to a CO_2/CH_4 mixture, mole fractions CO_2 = 32.2%, CH_4 = 67.8% versus penetrant partial pressure: (a) CO_2, (b) CH_4. The solid lines represent model calculations.

in Figures 8(a) and 8(b). The reproducibilities of the data were roughly ±1% and ±0.5% for CH_4 and CO_2, respectively. The somewhat worse reproducibility of the CH_4 data may be caused by the instability of the single FID detector used for CH_4 analysis. A discussion of the errors associated with the permeability data reported in this article is included in Appendix C.

Each point in Figures 8(a) and 8(b) represents the average value of at least four repeated measurements. The solid lines in the figures are calculated on the basis of eq. (4) using the sorption and transport parameters of the respective pure gases shown in Tables I and II. The broken lines represent values calculated from the dual-mobility model [Eq. (3)] based on the respective partial pressures but neglecting competition between CO_2 and CH_4 for the limited number of microvoid sorption sites in Kapton H.

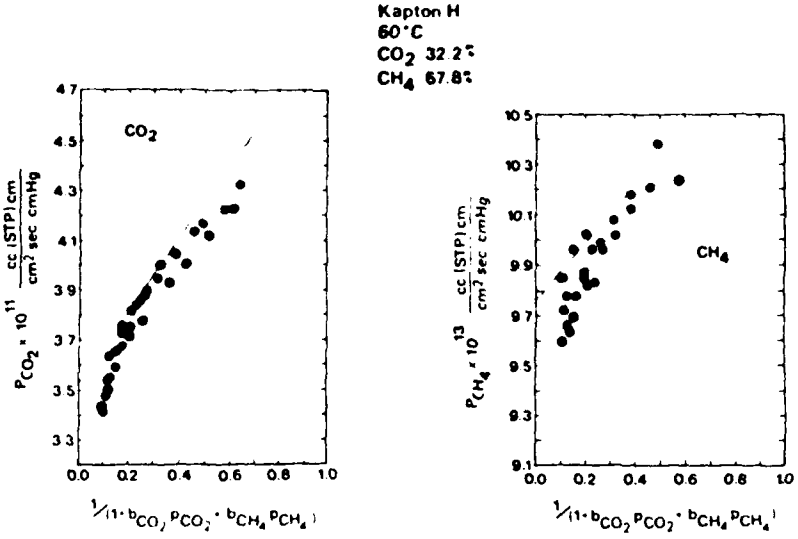

Fig. 9. Permeability versus $1/(1 + b_{CO_2}p_{CO_2} + b_{CH_4}p_{CH_4})$, according to eq. (4): (a) CO_2, (b) CH_4. The solid lines represent model calculations.

Apparently, individual permeabilities are reduced significantly by the presence of the other penetrant. This observation supports the point of view that penetrants compete for a limited number of sorption sites and thus the associated diffusion pathways in the glassy polymer. Therefore, the two penetrants do not permeate independently, even when strong specific intermolecular interactions are absent.

On the other hand, deviations between model calculations and experimental data increase as the feed pressure increases and become significant for total pressures above 300 psi (absolute). According to eq. (4), there is a linear relation between P_A and $1/(1 + b_Ap_A + b_Bp_B)$. As an alternative test of the validity of the model, the permeability data are replotted according to this scheme in Figures 9(a) and 9(b), where the lines are model calculations, using the sorption and transport parameters of the respective pure gases shown in Tables I and II.

Clearly, additional considerations other than simple competition for the microvoid sorption sites have to be included to explain the substantial depression of mixture permeabilities, particularly at higher pressures. This effect, related to gas-phase nonidealities at high upstream pressures is discussed in detail below.

Separation Factors

Conventionally, the separation factor is defined as $(y_A/y_B)/(x_A/x_B)$, where y_i's and x_i's are the mole fractions of the penetrants in the product and feed streams, respectively. When the pressure of the product stream is negligibly small compared with the feed pressure, the separation factor will be approximately equal to the ratio of permeabilities P_A/P_B, which is sometimes called the

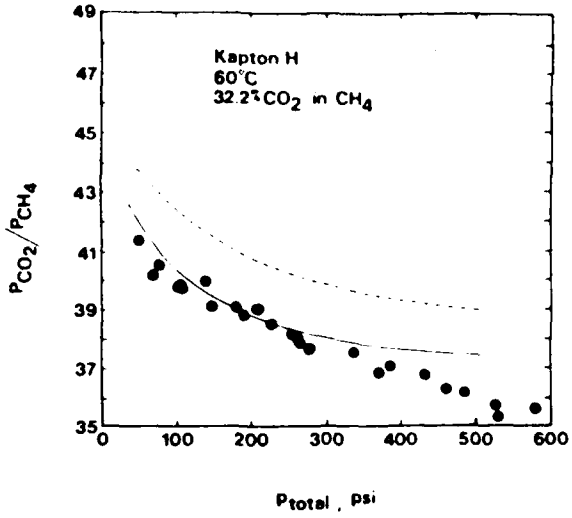

Fig. 10. Ideal separation factor versus total feed pressure.

"ideal separation factor."[23,24] The solid line in Figure 10 represents values calculated from the dual-mode model using the respective forms of P_A and P_B from eq. (4). The broken line, on the other hand, corresponds to model predictions without considering the competition effect discussed above. Again, the effects of competition are evident and have to be accounted for when assessing the selectivities of glassy polymers. As discussed below, this apparent pressure dependence of the ideal separation factors actually arises from the combined contributions of both competition effect and the effect of the gas-phase nonideality.

Effects of Nonideality of the Gas Phase

Conventionally, the permeability of component i (P_i) is defined in terms of Δp_i, the difference in partial pressures of component i at the upstream and downstream faces of the membrane of thickness L:

$$P_i = \frac{N_{ssi}}{\Delta p_i/L} \cong \frac{N_{ssi}}{p_{i2}/L} \tag{8}$$

where N_{ssi} is the steady-state flux of component i through the membrane. The approximation noted is well satisfied when the downstream pressure p_1, is close to zero, as it is in the present work. In cases where p_2 differs significantly from the fugacity, it is reasonable to define an alternative permeability P_i^* in terms of the fugacity difference of the penetrant across the film:

$$P_i^* = \frac{N_{ssi}}{\Delta f_i/L} \cong \frac{N_{ssi}}{f_{i2}/L} \tag{9}$$

Clearly, for gases that show negligible nonideal gas behavior, the two definitions coincide. For a gas such as CO_2, however, $P^*_{CO_2}/P_{CO_2} = p_2/f_2 = 1/\phi$, where ϕ is

the gas-phase fugacity coefficient of CO_2 at the upstream temperature and pressure.

Such considerations become even more significant in mixed gas situations for which one may hold p_2 constant but cause f_2 to change markedly owing to the addition of a high-pressure second component. To permit decoupling permeability reductions caused by this gas-phase effect from the polymer-phase effect associated with saturation of the microvoid sorption sites, we shall recast eqs. (1) and (3) in terms of fugacity and redetermine the pertinent coefficients. An alternative approach to this problem has been suggested by Petropoulos[6]; however, we have chosen the current approach for simplicity and for ease of extension to multicomponent situations. The resulting equations are similar to eqs. (1), (3), and (4) except fugacities instead of partial pressures are used:

$$C = k'_D f + C'_H b' f/(1 + b' f) \tag{10}$$

$$P' = k'_D D'_D [1 + F' K'/(1 + b' f)] \tag{11}$$

$$P' = k'_{DA} D'_{DA} [1 + F'_A K'_A/(1 + b'_A f_A + b'_B f_B)] \tag{12}$$

Pure Gases

Since fugacity is the fundamental property that must be equal in the gas phase and polymer phase, the parameters in eqs. (10) and (11) should be more appropriate for mixed gas calculations. As noted above, it is possible to reduce the fugacity of component A at constant partial pressure by introducing another component B in a high-pressure gas mixture. By basing calculations on fugacity, any gas-phase complexities can be treated independently of the dual-mode effects that are of principal interest in this study.

The dual-mode sorption parameters for CO_2 and CH_4 based on eq. (10) are included in Table I. The transport parameters and fit of the data to eq. (11) are displayed in Table II and Figures 11(a) and 11(b). For CH_4, this treatment apparently does not significantly affect the fit of data and parameter values as

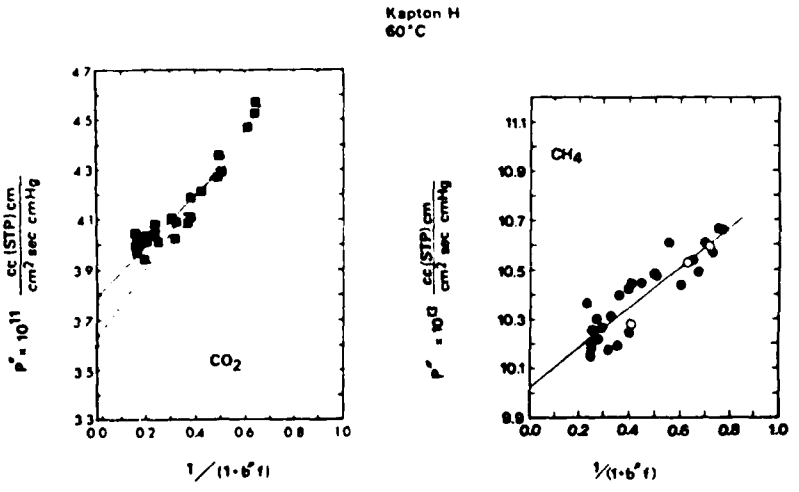

Fig. 11. Permeability versus $1/(1 + b'f)$ according to eq. (11): (a) CO_2, (b) CH_4.

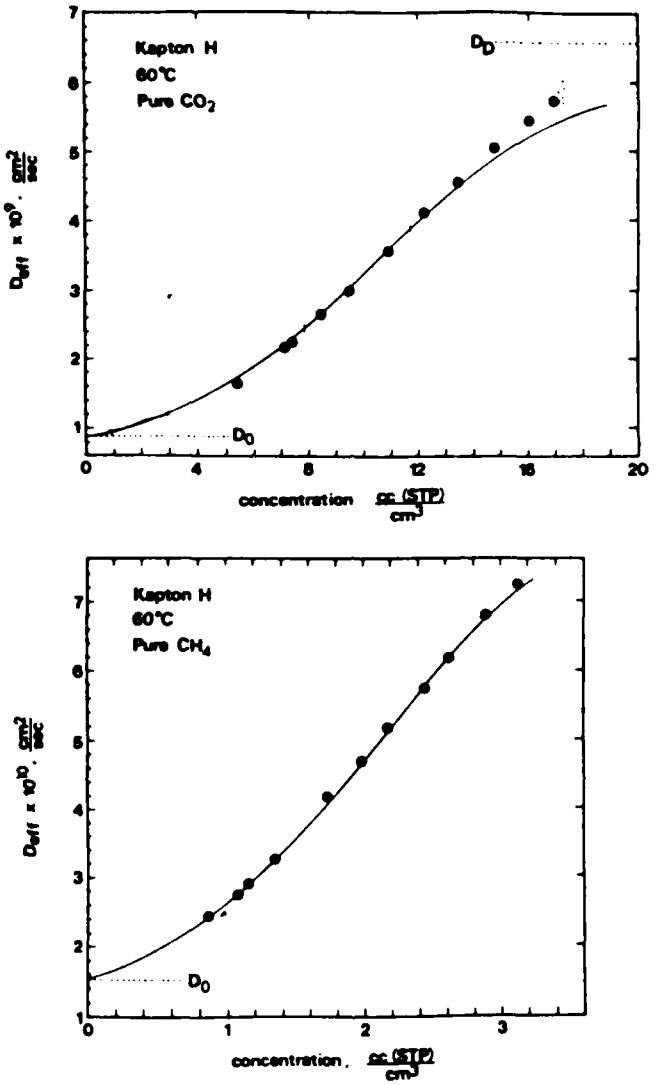

Fig. 12. Effective diffusion coefficient versus penetrant concentration: (a) CO_2, (b) CH_4. The solid line represents model predictions using fugacity-based parameters.

is consistent with the fact that CH_4 is roughly an ideal gas under the experimental conditions. On the other hand, for CO_2, the fit of the data to eq. (12) is slightly less satisfactory than its counterpart in Figure 5(a), which was discussed in a previous section. In fact, there seems to be a slight curvature in Figure 11(a), suggesting that a small amount of plasticization may have taken place at higher CO_2 concentrations and caused a minor change in D_D'. In the present case, however, even if the nonlinear relation is attributed completely to an increase in D_D', less than 5% change in D_D' is apparent, as indicated by the intercepts of

the solid and dashed lines in Figure 11(a). The fit of the data to the fugacity-based model for both CO_2 and CH_4 is still quite good.

A tentative treatment may include allowing a small increase in D_{ij}° with concentration in order to fit the data at higher CO_2 concentrations (corresponding

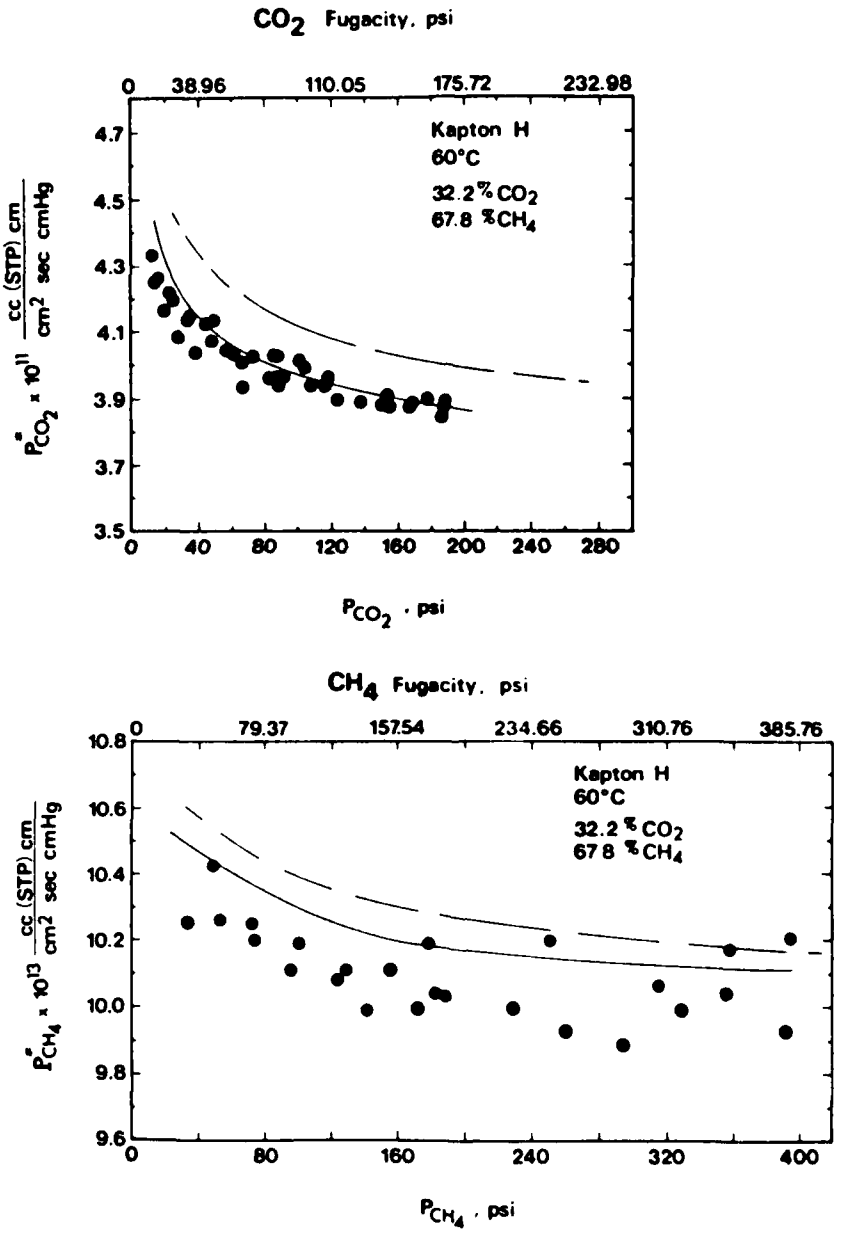

Fig. 13. Permeability as defined in eq. (10) versus penetrant partial pressure: (a) CO_2, (b) CH_4. The solid lines represent model calculations.

to $p_{CO_2} > 13$ atm). This approach could proceed along the lines suggested by Stern and Saxena[8] and seems to provide a reasonable explanation for the data available. To corroborate these preliminary findings, a more detailed investigation regarding the sorption and permeation of gases in glassy polymers at pressures higher than those covered in this study is currently under way in our laboratory.

Concentration-Dependent Local Diffusion Coefficient

To investigate the concentration dependence of the fugacity-based permeability further, we resort to eqs. (6) and (7), following the same procedures as discussed above. The results are included in Figures 12(a) and 12(b), where the circles are experimental values evaluated according to the method described in Appendix B and the solid line represents values calculated based on eq. (13):

$$D'_{\text{eff}}(C_2) = D'_{l_0} \frac{1 + F'K'/(1 + b'f_2)^2}{1 + K'/(1 + b'f_2)^2} \tag{13}$$

Again, the fit between experimental data and model predicted values is reasonably good. For CH_4, no plasticizing effects are evident as pointed out previously. The dotted circle in Figure 12(a) is an extrapolated value based on experimental data which together with the last few points at higher concentrations seems to support the suggestion discussed previously that D'_{l_0} may increase slightly with penetrant (CO_2) concentration at the high end of the concentration range.

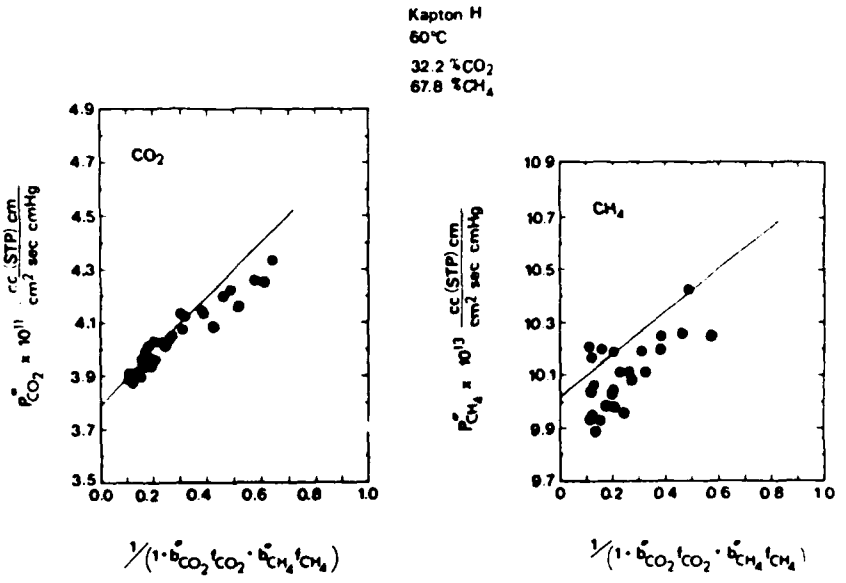

Fig. 14. Permeability versus $1/(1 + b'_{CO_2}f_{CO_2} + b'_{CH_4}f_{CH_4})$ according to eq. (12): (a) CO_2, (b) CH_4. The solid lines represent model calculations.

Mixed Gases

A treatment similar to that leading to eq. (4) but instead based on fugacity may be applied to the mixture data according to eqs. (9) and (12). The results are included in Figures 13(a), 13(b), 14(a), and 14(b). The solid lines in these figures correspond to model calculations using eq. (12) with sorption and transport parameters reported in Tables I and II. The broken lines in Figures 13(a) and 13(b) correspond to the pure-component permeabilities at the same partial pressures. The magnitude of the depression apparent from comparison of the points and the broken lines is on the order of 5% for CO_2 and 2% for CH_4. In Figures 13(a) and 13(b), both pressure and fugacity are included as abscissas for reference purposes. Evidently, the fit between experimental data and model predictions for CO_2 is improved as compared with their counterparts in Figures 8 and 9, particularly at higher total pressures where nonideality of the gas phase is comparable with or even dominant over the competition effect. For CH_4, little improvement is evident compared with the previous approach. This result is reasonable since CH_4 is relatively ideal. Moreover, the permeability of CH_4 exhibit less pressure dependence than that of CO_2, and there is a larger percentage scatter in the CH_4 data due to the measurement difficulties noted above. This hinders efforts to assess the degree of misfit between the data and model calculations.

The ratios of the fugacity-based permeabilities are plotted in Figure 15, where the solid and the broken lines represent model predictions with and without competition considerations, respectively.

Interestingly, the data in Figure 15 have a much milder pressure dependency than their counterparts shown in Figure 10.

The physical meaning of the ratio of the fugacity-based permeabilities P'_A/P'_B is apparent from its definition:

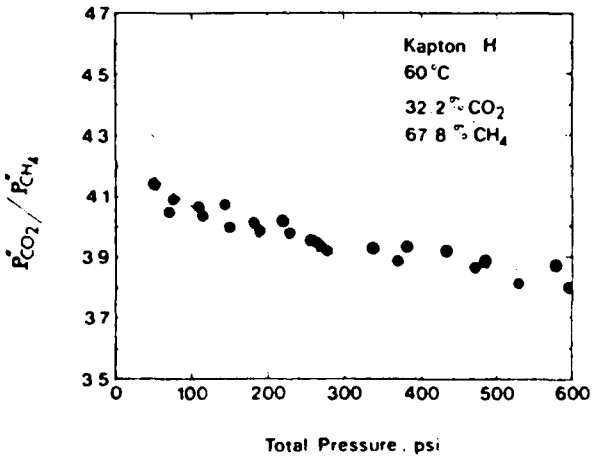

Fig. 15. Ratios of fugacity-based permeabilities [eq. (12)] versus total feed pressure. The solid line represents model calculations.

$$\frac{\text{(flux of A)/(fugacity difference of A across the film/film thickness)}}{\text{(flux of B)/(fugacity difference of B across the film/film thickness)}}$$

Clearly, this ratio serves as an index of the intrinsic selectivity of the polymer for the two gases since the nonideality of the gas phase has been explicitly accounted for in the above expression. On the other hand, the ratio of the pressure-based permeabilities gives the "actual" separation factor $(y_A/y_B)/(x_A/x_B)$ which can be achieved when the downstream pressure approaches zero. This latter parameter reflects the combined effects of both the intrinsic polymer permselectivity and the gas-phase nonideality. A comparison between Figures 10 and 15 demonstrates the importance of decoupling gas-phase nonideality from experimental flux data for gas mixtures which otherwise could lead to erroneous conclusions concerning transport phenomena in the polymer phase. The reasonable success of the proposed interpretation of the CO_2/CH_4 mixture permeabilities also indicates that extra complexities due to compaction of the rigid polymer phase are not present, at least under the experimental conditions covered in this study (cf. ref 25).

CONCLUSION

Sorption and transport of pure CO_2 and pure CH_4 in Kapton H polyimide at 60°C, like many other gas/polymer pairs, are described well by the dual-mode models. Permeabilities of individual penetrants in a mixed gaseous feed are significantly lower than the corresponding pure-gas values at the same partial pressures. This difference becomes larger when the total feed pressure is increased. At lower total pressures, which correspond to a relatively ideal gas phase, the observed phenomena are amenable to the interpretations of the generalized dual-mobility model based on partial pressures. However, as the total feed pressure increases, the effects of gas-phase nonideality increase and become comparable or even more important than the proposed competition mechanism. To differentiate and facilitate analysis of these two factors, an alternative dual-mode model based on fugacity is proposed. The fit between experimental data and model predictions is quite satisfactory. Small apparent deviations between model and experimental results for pure CO_2 can be attributed to a minor (<5%) increase which occurs at pressures above 10–15 atm for the so-called Henry's-law mode diffusion coefficient D_D.

These findings together with previous studies of the effects of condensible vapors[12,13] provide quantitative support for the proposition that simple gases compete for the limited microvoid sorption sites in glassy polymers and cause reduced sorption concentrations and permeation rates of the individual penetrants. The effect of competition on the fugacity-based permeabilities of both CO_2 and CH_4 in Kapton H polyimide is relatively small under the conditions covered in the present study. For example, according to eq. (12), the permeability of CO_2 at 60°C and 20 psi (absolute) partial pressure will be lowered by roughly 10% from its pure-component value of 4.51×10^{-11} to 4.08×10^{-11} cm^3 (STP) cm/cm^2 s cm Hg as 180 psi (absolute) of CH_4 is introduced. On the other hand, for polymers which exhibit higher Langmuir capacities C'_H, it is expected that the competition effect will be even more prominent.[10]

Moreover, this analysis points out that gas-phase nonideality should be accounted for at high pressures if the mixtures of interest are highly nonideal. The

present approach thus provides a useful tool for determining the relative magnitude of the competition factor and the nonideality factor under given physical conditions. Further tests of the proposed treatment will be pursued using the same polymer/gas system as in the present study but at other temperatures and higher pressures where plasticization is expected to further complicate the mixed gas permeation behaviors.

The authors gratefully acknowledge support of this work under NSF Grant No. CPE-79-18200 and ARO Grant No. DAAG29-81-K-0039. The assistance of Mr. M. Headinger in providing word processor programs is also acknowledged.

APPENDIX A: ESTIMATION OF CONCENTRATION POLARIZATION IN THE PERMEATION CELL

Gas transport through a nonporous membrane involves the following steps:

(1) diffusion through the upstream gaseous phase boundary layer
(2) sorption into the membrane
(3) diffusion through the membrane
(4) desorption from the downstream face
(5) diffusion through the downstream gaseous phase boundary layer

Under normal conditions, equilibria are assumed to prevail at the membrane surfaces; consequently only the resistances associated with steps 1, 3, and 5 which are included in Figure 16 will be considered.

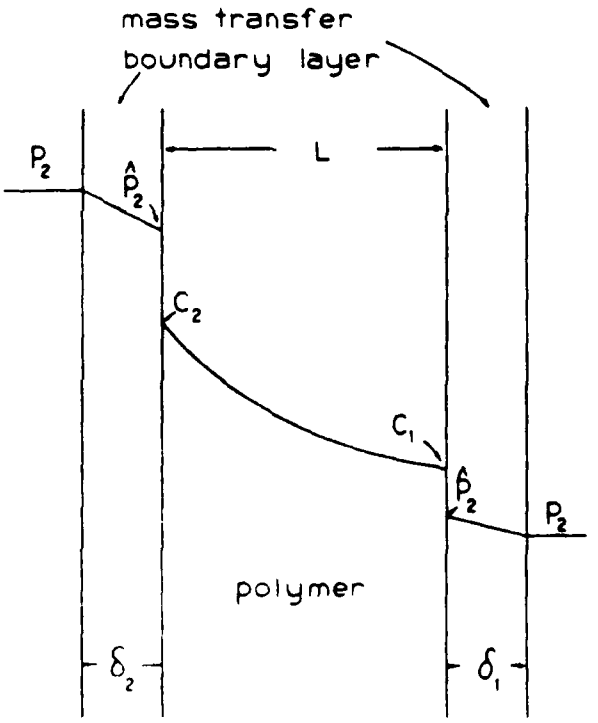

FIG. 16. Schematic diagram of the various resistances associated with gas transport through a nonporous membrane

At steady state, it can be shown that[29]

$$N = (p_2 - \hat{p}_2)/r_2 = (\hat{p}_1 - p_1)/r_1 = \bar{P}(p_2 - p_1)/L = \bar{D}(C_2 - C_1)/L \quad \text{(A1)}$$

where N is the permeation flux, $\bar{P}$ is the observed permeability, p_i's are the partial pressures in the bulk gaseous phase, $\hat{p}_i$'s are the partial pressures at the membrane surfaces, C_i's are the penetrant concentrations corresponding to $\hat{p}_i$'s, r_i's are the gas-phase resistances to mass transfer, and $\bar{D}$ is the average diffusion coefficient in the polymer film defined as

$$\bar{D} = \int_{C_1}^{C_2} \frac{D(C)dC}{C_2 - C_1}$$

It is assumed that an apparent solubility coefficient S can be used to relate the gas pressure and its concentration in the polymer, i.e., $C = Sp$. For simplicity, S will be assumed to be constant since we are only interested in an order-of-magnitude estimate here. Equation (A1) can be simplified to the following form:

$$\bar{P} = \frac{1}{1/S\bar{D} + (r_1 + r_2)/L} \quad \text{(A2)}$$

Assuming molecular diffusion dominates in the gas phase boundary layer and the convection term is negligible, then

$$r_1 = \delta_1 Z_1 RT/D_{g1} \text{ and } r_2 = \delta_2 Z_2 RT/D_{g2}$$

where δ_i's are the thickness of the gaseous films, Z_i's are the compressibilities of the gases, R is the universal gas constant, T is the gas temperature, and D_{gi}'s are the diffusion coefficients in the gas phase.

For the present system, the following set of numbers are believed to correspond to the worst case. $\delta_1 = 0.25$ cm, $\delta_2 = 0.25$ cm, $D_{g2} = 1.0E-3$ cm^2/s,* $D_{g1} = 1.0E-1$ cm^2/s,* $Z_2 = 0.9$, $Z_1 = 0.98$, $T = 333$ K, $L = 0.3$ mil. Under these conditions, the combined resistance of the gas phases can be calculated using the denominator of eq. (A2).

$$\frac{r_1 + r_2}{L} = 2.8E7 \frac{\text{cm Hg cm}^2\text{ s}}{\text{cm}^3\text{(STP) cm}}$$

However, for systems under consideration in this paper, the following numbers, which correspond to the resistance of the polymer phase, are typical for CO_2 and CH_4, respectively.

$$\frac{1}{S\bar{D}} = 2.8E9 \frac{\text{cm Hg cm}^2\text{ s}}{\text{cm}^3\text{(STP) cm}}$$

$$\frac{1}{S\bar{D}} = 1.0E12 \frac{\text{cm Hg cm}^2\text{ s}}{\text{cm}^3\text{(STP) cm}}$$

Apparently, concentration polarization is negligible under these conditions, since the resistance associated with the polymer film is close to 100–10^4 times larger than those of the gaseous films even under the rather thick boundary layer conditions assumed.

APPENDIX B.: A SECANT METHOD USED FOR EVALUATING THE EFFECTIVE LOCAL DIFFUSION COEFFICIENT D_{eff} IN Eq. (5)

As pointed out in the Results and Discussion section, eq. (5) is useful for determining the concentration dependence of an effective diffusion coefficient D_{eff} without referring to any specific diffusion model other than Fick's law. At steady state, eq. (5) can be integrated to give

$$\int_0^l N\,dx = NL = -\int_{C_1}^{C_2} D_{eff}\,dC \quad \text{(B1)}$$

* Estimated from Eqs. (11-4.1) and (11-6.2) in ref. 27.

and hence

$$\left.\frac{dNL}{dC}\right|_{C=C_2} = D_{eff}(C_2) \tag{B2}$$

where $D_{eff}(C_2)$ is the effective diffusion coefficient at concentration C_2, C_i's correspond to the penetrant concentrations in the membrane at the upstream and downstream surface positions, and N is the measured permeation flux at steady state. A series of experimental values of N measured at upstream pressures p_2's are tabulated with the corresponding upstream sorbed concentrations C_2's obtained from sorption isotherms. According to eq. (B2), the effective diffusion coefficient D_{eff} at any concentration, say α_f, can be evaluated by taking the derivative of N at α_f multiplied by L.

In order to evaluate the slope of C_2 vs. N at $C_2 = \alpha_f$, a plot of $(\beta_i - \beta_f)/(\alpha_i - \alpha_f)$ vs C_2 is prepared, where $i \neq f$, and α_i's and β_i's are experimental numerical values of C_2 and N, respectively. The slope at x_f can then be read directly from the plot, or a regression algorithm may be used to determine the best-fit curve and from that relation the slope at α_f can be calculated. This method is useful and introduces little bias when no abrupt changes in the slopes are present in the original data. In the present case, the relationship between N and C_2 is smooth and the incremental changes in both N and C_2 are relatively small, so the resultant values for D_{eff} should be quite accurate.

APPENDIX C: PROPAGATION-OF-ERRORS ANALYSIS

A propagation-of-errors analysis was performed to estimate the experimental uncertainties of the reported permeability data. It was found that roughly 90% of the error was contributed by uncertainties associated with (i) film thickness, (ii) concentration of the calibration gas, (iii) concentration of the feed gas, (iv) effective permeation area, and, for lower pressure measurements, (v) upstream pressure.

Errors of the measured chromatogram areas were roughly ±0.5 and ±1.0% for CO_2 and CH_4, respectively. The errors of N_2 flow rate and the upstream penetrant pressure were roughly ±0.5% and ±0.5 psi, respectively. Film thickness measured by micrometer, optical microscopy, and weighing agreed within 0.01 mil; this was assumed to represent an approximate standard error, i.e., ca. ±3%. The nominal permeation area is 9.6 ±0.02 cm^2, but the effective permeation area may deviate somewhat from this value owing to errors introduced during the film mounting step which can only be estimated to be ca. ±1%. The concentration of the feed gas was determined in our laboratory to have an error of ±1%. The error associated with the concentration of the calibration gas was not determined in our laboratory owing to equipment limitations, and was assumed to be ±3% of the assay given by the supplier.

Based on the above information, the standard error of the absolute values of the reported permeabilities can be estimated. For example, the standard error of the permeability of pure CO_2 at 26 psi (absolute) and 60°C is roughly ±6%, and that of pure CH_4 at 27 psi (absolute) is roughly ±10.7%. At 580 psi (absolute) and 60°C, the errors are ±10.5% for CO_2 and ±10.7% for CH_4, for the 32.2% CO_2/CH_4 mixture.

References

1. W. J. Koros, A. H. Chan, D. R. Paul, *J. Membr. Sci.*, **2**, 165 (1977).
2. W. J. Koros and D. R. Paul, *J. Polym. Sci. Polym. Phys. Ed.*, **16**, 1947 (1978).
3. P. Masi, D. R. Paul, and J. W. Barlow, unpublished.
4. A. S. Michaels, W. R. Vieth, and J. A. Barrie, *J. Appl. Phys.*, **34**, 1 (1963).
5. V. T. Stannett, W. J. Koros, D. R. Paul, H. K. Lonsdale, and R. W. Baker, *Adv. Polym. Sci.*, **32**, 69 (1979).
6. J. H. Petropoulos, *J. Polym. Sci. A-2*, **8**, 1979 (1970).
7. D. R. Paul and W. J. Koros, *J. Polym. Sci. Polym. Phys. Ed.*, **14**, 675 (1976).
8. S. A. Stern and V. Saxena, *J. Membr. Sci.*, **7**, 47–59 (1980).
9. A. J. Erb and D. R. Paul, *J. Membr. Sci.*, **8**, 11 (1981).
10. W. J. Koros, R. T. Chern, V. T. Stannett, and H. B. Hopfenberg, *J. Polym. Sci. Polym. Phys. Ed.*, **9**, 1513 (1981).
11. W. J. Koros, *J. Polym. Sci. Polym. Ed.*, **18**, 981 (1980).

12. R. T. Chern, W. J. Koros, H. B. Hopfenberg, and V. T. Stannett, *J Polym Sci Polym Phys Ed* ., **21**, 753 (1983).
13. R. T. Chern, W. J. Koros, E. S. Sanders, and R. E. Yui, *J. Membr. Sci* , **15**, 157 (1983).
14. D. G. Pye, H. H. Hoehn, and M. Panar, *J. Appl. Polym. Sci.*, **20**, 287-301 (1976).
15. L. M. Robeson, *Polym Eng Sci* , **9**, 277 (1969).
16. E. S. Sanders, W. J. Koros, H. B. Hopfenberg, and V. T. Stannett, *J Membr. Sci* , **13**, 161 (1983).
17. "Kapton Polyimide Film—Summary of Properties," E.I. du Pont Company, 1981.
18. W. J. Koros, G. N. Smith, and V. T. Stannett, *J. Appl. Polym. Sci.*, **26**, 159 (1981).
19. S. Chen, M. S. Thesis, North Carolina State University, 1982.
20. W. J. Koros and D. R. Paul, *J. Polym. Sci. Polym. Phys. Ed.*, **14**, 1903 (1976).
21. W. J. Koros and D. R. Paul, *Polym. Eng. Sci.*, **1**, 14 (1980).
22. A. G. Wonders and D. R. Paul, *J. Membr. Sci.*, **5**, 63 (1979).
23. F. P. McCandless, *Ind Eng Chem. Prod. Res. Dev.*, **11**, 470 (1972).
24. S. A. Stern and W. P. Walawender, Jr., *Sep. Sci.*, **4**, 129 (1969).
25. S. M. Fang and S. A. Stern, *Chem. Eng. Sci.*, **30**, 773 (1975).
26. S. T. Hwang and K. Kammermeyer, *Membrane in Separations*, Interscience, New York, 1975.
27. R. C. Reid, J. M. Prausnitz, and T. K. Sherwood, *The Properties of Gases and Liquids*, 3rd ed., McGraw-Hill, New York, 1977.

Received July 25, 1983
Accepted December 6, 1983

MATERIAL SELECTION FOR MEMBRANE-BASED GAS SEPARATIONS

R. T. Chern, W. J. Koros[1], H. B. Hopfenberg
and V. T. Stannett
Department of Chemical Engineering
North Carolina State University
Raleigh, N. C. 27650

High membrane permselectivity for a gas mixture is well-known to correlate with low permeability of the desired product through the membrane. Exceptions to this rule exist, however, and this suggests the possibility of improved membranes for a number of important applications. This paper suggests possible polymer structural changes which may allow control over the magnitudes of permeabilities and selectivities. These suggestions result from considering the permeability and selectivity in terms of their separate thermodynamic solubility and kinetic mobility contributions. The two contributions vary markedly with changes in the polymer structure and correlate with variations in penetrant and polymer physical properties. The feasibility of developing extremely selective high flux membrane materials is explored in terms of these correlations. The potential for such developments is shown to be fairly high for cases in which the permeant molecule is substantially more compact than the nonpermeant molecule if the resulting mobility advantage is not eliminated by a large solubility advantage favoring the nonpermeant. Several important examples of such systems are discussed including H_2/CH_4 and CO_2/CH_4. A short discussion of approaches to assess membrane materials for resistance to attack by components in the process stream is also presented.

Introduction

Membrane-based gas separations have emerged as important chemical engineering unit operations for hydrogen recovery from purge and recycle streams (1-4) and for carbon dioxide and water removal from natural and land fill gases (5-9). Using asymmetric structures in high surface area modules permits the use of higher selectivity, lower permeability glassy polymers in the place of rubbery materials.

[1]Current address: The Center for Energy Studies, The University of Texas, Austin, TX 78712

The first generation of gas separators has achieved an impressive penetration into markets traditionally dominated by cryogenic, chemical and physical sorption processes. Competition from these processes is strong. Membranes with higher permeabilities, selectivities and resistance to penetrant attack are required to meet challenges from these traditional processes and to permit expansion into additional application areas.

Although no commercial examples exist currently in the gas separation field, thin film composite membranes such as those pioneered by Cadotte and co-workers (10) may ultimately permit the use of novel materials with unique transport properties supported on standard porous membranes. Therefore, the focus in this paper will be on suggesting a basis for understanding differences in the permeability and selectivity properties of glassy polymers. Presumably, if such materials prove to be difficult to fabricate into conventional monolithic asymmetric structures, they could be produced in a composite form. Even if thin film composite structures are used, however, the chemical resistance of the material remains an important consideration. For this reason, a brief discussion of this topic will be offered.

Typically, membrane research efforts focus upon the determination of the permeability and selectivity of candidate polymers without explicit consideration of the solubility and mobility terms comprising the permeability (11-13). This approach is reasonably effective for screening available polymers for a particular application but not optimum for providing guidelines to improve membrane performance by scientific alteration of the polymer structure. Moreover, it may lead one to an overly pessimistic view of the selectivity and permeability properties achievable as a result of polymer structural variations. As an adjunct to this typical approach, correlations of the penetrant diffusion coefficients and solubilities with the physical and chemical natures of the polymers and penetrants will be discussed. These correlations rationalize the generally observed relationship between high selectivity and low permeability. They also provide a partial basis for understanding reports of several deviant cases in which high selectivity and permeability are observed for H_2/CH_4 and CO_2/CH_4 systems. It is these deviant cases that may lead the way to a new generation of more productive and selective membranes.

Background and Theory

One-dimensional diffusion through a flat membrane will be treated in the following discussion. The effects of membrane asymmetry will be neglected since the process of permselection occurs in the thin dense layer of effective thickness, ℓ, at the membrane surface. In such a case, the expression for the local flux of a penetrant at any point in the dense layer can be written as shown in Equation 1 (14):

$$N = - D \frac{dC}{dx} \qquad (1)$$

where the diffusion coefficient, D, may be a function of local concentration, C, in the membrane. The diffusion coefficient may be interpreted in terms of a preexponential factor, D°, and an exponential term that depends upon the activation energy for the diffusion process, E_D (14).

$$D = D^\circ \exp[- E_D/RT] \tag{2}$$

To a first approximation, E_D is the average energy that must be localized next to the penetrant to generate an opening large enough to permit the molecule to execute a jump. If concentration dependence of the diffusion coefficient exists, both D° and E_D may be functions of the amount of penetrant present. At low concentrations, the activation energy should be related strongly to the minimum cross section of the penetrant, since this defines the critical opening size necessary for a jump to occur. The large effect on molecular mobility caused by differences in penetrant size or shape is illustrated in Figure 1 for a typical rubbery and glassy polymer, respectively. The larger nonspherical penetrants tend to approach a plateau diffusivity because the cross-sectional area of the molecule as well as its volume determine its ability to find a gap of sufficient size to permit a jump. Presumably, nonspherical penetrants move in a somewhat oriented fashion, and the individual jump lengths may be only fractions of the total length of the molecule. Associated with the more highly restrictive glassy environment comes a greater ability to perform size or shape discrimination between penetrants. This difference between the glassy and rubbery state is illustrated clearly by the much larger spread in diffusion coefficients in the glassy polymer compared to the rubbery one. Recognition of the preceding facts often leads to the generalization that low membrane permeability is necessary for high selectivity. Although the two generally correlate, there appear to be attractive exceptions to the rule that are worthy of serious investigation (11,13).

The permeability of a membrane to a penetrant is defined by Equation 3:

$$P = \frac{N \ell}{[p_2 - p_1]} \tag{3}$$

where p_2 and p_1 are the upstream and downstream pressures of the component acting across the effective membrane thickness, ℓ. Clearly, the permeability of the membrane is not only determined by the mobility of the penetrant discussed above but also by its solubility, because the higher the solubility difference across the membrane, the higher will be the observed flux and permeability. The contributions of the two factors can be seen clearly for the case where the downstream pressure, p_1, is negligible. Substituting Equation 1 into Equation 3 and integrating leads to Equation 5:

$$P = - \left(D \frac{dC}{dx} \right) \left(\frac{\ell}{p_2} \right) \tag{4}$$

so $$\int_0^{\ell} \frac{P}{\ell}\, dx = \int_0^{C_2} \left(\frac{D\, dC}{C_2}\right)\left(\frac{C_2}{p_2}\right) = \bar{D}\,\bar{S} \qquad (5)$$

where $\bar{D} = \left(\int_0^{C_2} D\, dC \Big/ \int_0^{C_2} dC\right)$ defines an average measure of the penetrant's mobility in the membrane between the upstream concentration, C_2, and downstream concentration, $C_1 \approx 0$ (14). The parameter, $\bar{S} = C_2/p_2$, equal to the secant slope of the sorption isotherm evaluated at the upstream conditions, is a measure of the solubility of the penetrant in the membrane. The mobility factor in Equation 5 is kinetic in nature and largely determined by polymer-penetrant dynamics as discussed in the context of Equation 2. The solubility factor in Equation 5 is thermodynamic in nature and is determined by polymer-penetrant interactions and the amount of excess interchain gaps existing in the glassy polymer (17).

When the downstream pressure, p_1, is negligible compared to the upstream pressure, p_2, the separation factor, α_{AB}, defined by Equation 6 can be related to the ratio of the permeabilities of components A and B (18) as shown in Equation 7:

$$\alpha_{AB} = [y_A/y_B]\,[x_A/x_B] \qquad (6)$$

$$\alpha^*_{AB} = P_A/P_B \qquad (7)$$

where x_i's and y_i's are the local mole fractions of components A and B at the upstream and downstream membrane faces, respectively. The superscript * in Equation 7 indicates that α^* is the so-called "ideal separation factor" which applies under the conditions described above. The ratio of the component permeabilities in such a case provides a useful measure of the intrinsic permselectivity of a membrane material for mixtures of A and B.

When the interaction between one penetrant and the polymer is not affected by the presence of another penetrant, the pure-component permeabilities of the two penetrants in the mixture can be used in Equation 7. For rubbery polymers at low penetrant partial pressures, this assumption of independent-permeation appears satisfactory (19-20). It does not, however, appear to hold in general for glassy polymer membranes (12,13,21-25). Moreover, it also has been shown that plasticization of both rubbery (26) and glassy (27) polymers can occur at higher penetrant activities.

Based on the recent study of the permeabilities of Kapton polyimide to CO_2/CH_4 mixtures (21,22), it is expected that for systems which can be described by the generalized dual mode model (17), the permeability ratio of CO_2 over CH_4 in a mixture can be approximated to within about 20% by using the respective pure component permeabilities. Consequently, for the present general discussion, pure-component values will be used in Equation 7 in the following sections for discussing this important system.

Discussion

General Considerations. Representative CO_2 permeabilities for several glassy polymers at 35°C are plotted as a function of the upstream penetrant pressure in Figure 2 (8). Except for cellulose acetate, the permeabilities decrease monotonically with upstream pressure, consistent with the dual mode model predictions (17). The behavior of cellulose acetate in terms of plasticization arguments will be addressed in a later section. The ideal separation factors for CO_2/CH_4 at 20 atm, calculated using the pure-component permeabilities, are plotted in Figure 3 versus the solubility parameters of the various polymers. The solubility parameters of polymers (28-32) and the permeability data (5,6,33-35) were taken from a number of sources. A simple interpretation of Figure 3 might be that the higher intersegmental interactions associated with high solubility parameter polymers create a mobility selecting environment by making it more difficult to form a transient gap of sufficient size to pass a bulky, spherical CH_4 molecule compared to a streamlined, linear CO_2 molecule. As illustrated in later discussion of the separate mobility and solubility factors in Equation 5, this argument based solely on mobility selectivity appears to be oversimplified. Especially in the case of cellulose acetate, it will be shown that solubility considerations are of considerable importance.

Examination of Figures 2 and 3 supports the previous observation that low permeability and high selectivity are generally related. For example, the CO_2 permeability of poly(phenylene oxide) (PPO) is over twelve times higher than that of polysulfone, but its CO_2/CH_4 selectivity is less than half that of polysulfone. Kapton, on the other hand, is over twenty-five times less permeable to CO_2 than polysulfone, yet its CO_2/CH_4 selectivity is more than twice as high as that of polysulfone.

Such trends suggest that increases in permselectivity could be achieved by substituting a polar or hydrogen-bonding group on the phenylene ring of PPO to increase its cohesive energy density at the expense of its high CO_2 permeability. Alternatively, one could introduce irregularities into the Kapton backbone through the use of one or more comonomers along with the standard bis-4(aminophenyl ether) used as the diamine in Kapton production. Such modifications should inhibit packing and thereby lower the effective cohesive energy density. This "opening up" of the polymer structure would tend to markedly increase the CO_2 permeability but on the basis of Figure 3, may also reduce the selectivity. These concepts are derivative of those pioneered by H. Hoehn of DuPont in his work on the development of reverse osmosis membranes from aromatic polyamides (36).

Solubility and Diffusivity Considerations. The preceding general discussion has been largely conjectural in terms of the specific reasons for the relationship between variations in the cohesive energy density and variations in the cohesive energy density and variations in selectivity and permeability. To pursue these issues in a more quantitative fashion, it is useful to consider the separate

solubility and mobility contributions, $\bar{D}$ and $\bar{S}$, for the various polymers shown in Figure 3.

The sorption isotherms for most gases in glass polymers tend to have concave shapes like those shown in Figure 4. As a result, the apparent solubility ($\bar{S} = C_2/p_2$) is a decreasing function of the upstream penetrant pressure. On the other hand, the diffusion coefficients, $\bar{D}$, of gases in glassy polymers typically increase with sorbed concentration even in the absence of plasticization (17). Such increases are moderate for all of the materials in Figure 2 except cellulose acetate and can be explained in terms of saturation of excess volume in the polymer as concentration increases. Strong plasticization, on the other hand, produces dramatic upswings in the apparent mobility as appears to be the case with cellulose acetate. The observed pressure dependence of the permeabilities shown in Figure 2 are the net result of these two effects related to $\bar{D}$ and $\bar{S}$. In the case of cellulose acetate, the sorption isotherm for CO_2 has the same type of concave shape as shown in Figure 4, so a sharp increase in $\bar{D}$ apparently overpowers the effect of the decreasing apparent solubility coefficient. The reason for cellulose acetate's greater tendency to be plasticized compared to the other polymers in Figure 2 is currently not well understood. Since plasticization tends to produce a more rubbery material, it is to be expected that selectivity losses may attend the large upswing in CO_2 permeability, but no published data are available to corroborate this suggestion.

The apparent solubilities and average diffusivities, $\bar{S}$ and $\bar{D}$, for CO_2 and CH_4 in a number of glassy polymers at 30°C and 20 atm are shown in Table I. The values reported for cellulose acetate were estimated from various sources in the literature (5,6,37). In the case of cellulose acetate where CO_2 plasticization is apparently significant, it was assumed that the CH_4 permeability in CO_2/CH_4 mixtures will increase by at least the same percentage as the CO_2 permeability. This assumption seems reasonable since the plasticized matrix becomes more rubber-like and less discriminating for penetrants of different sizes and shapes (see Figure 1).

According to Equation 7, the ratio of permeabilities is given by Equation 8 after substitution from Equation 5 for components A and B:

$$\alpha^*_{AB} = P_A/P_B = [\bar{S}_A/\bar{S}_B]\,[\bar{D}_A/\bar{D}_B] \qquad (8)$$

Equation 8 demonstrates that the ideal separation factor can be separated into a so-called "solubility selectivity", $[\bar{S}_A/\bar{S}_B]$, and a "mobility selectivity", $[\bar{D}_A/\bar{D}_B]$. These two ratios are also reported in Table I. Evidently, the contribution of the "mobility selectivity" is the dominant factor for all of the polymers considered except cellulose acetate in which the opposite is observed. The CO_2 plasticization tendency of cellulose acetate may, in fact, be related to this polymer's apparent high "solubility selectivity". Clearly, the available data do not justify more than a tentative suggestion at this point that high "solubility selectivity" such as that seen in cellulose acetate may be associated with a tendency to be plasticized with a subsequent loss in glass-like selectivity. More detailed sorption and diffusion measurements using a single

preclude the need to rely upon mobility regulating mechanisms to aid in the separation process. This is the basis for solvent extraction and liquid membrane systems. The problems and considerations in such cases are quite different from those in standard bulk polymer systems and will not be discussed here.

Manipulation of the structure of standard bulk polymers to alter their mobility selectivity can be guided somewhat by correlations such as those shown in Figures 6 and 7. Figure 6 shows a correlation of $\bar{D}$ for various penetrants in a number of different glassy polymers. The correlating variable, the kinetic diameter of the gas, is related to the zeolite window dimension that will just permit passage of the penetrant of interest (39). For molecules that are essentially spherical, such as methane, argon and helium, this dimension is similar to the Lennard-Jones diameter. For asymmetric molecules such as carbon dioxide and nitrogen, however, the kinetic diameter corresponds more closely to the minimum diameter of the molecule. This figure shows clearly the extremely strong effect on the penetrant mobility caused by small differences in minimum penetrant diameter. A difference of less than 1.5 A distinguishes the kinetic diameters of helium and methane; however, there is almost three orders of magnitude difference in their mobility in polycarbonate. The spread in the various diffusivity values for a given penetrant in different polymers can be partially understood in terms of Figure 7. This figure shows the effects of variations in the specific volume of the polymer on the observed diffusion coefficients, $\bar{D}$. While this correlation is useful and intuitively satisfying, it undoubtedly oversimplifies the true differences in molecular-scale environments sampled by a penetrant as it moves through the polymers. The tendency for glassy polymers to exhibit local variations in the amount and distribution of molecular scale intersegmental gaps trapped during the quenching process from the rubbery state has been discussed in detail (17). Nevertheless, the correlation in Figure 7 is useful in depicting relative differences between extremes such as that represented by the highly open PPO environment and the rather compact Kapton environment. It is clear that the mobility selectivity is substantially higher for Kapton than for PPO. The ratios of the apparent diffusivities of CO_2 and CH_4 increase from 6.9 for PPO to 15.4 for Kapton; however, the permeability for CO_2 drops by more than two hundred fold in going from PPO to Kapton. Such a dramatic penalty in productivity certainly tends to confirm the general point of view that one cannot have both high selectivity and high productivity in the same membrane material.

Fortunately, encouraging exceptions to such a point of view can be found in the literature for both H_2/CH_4 and CO_2/CH_4 systems (11,13). These studies suggest the possibility of increasing the product permeability while maintaining or even increasing selectivity by proper design of the polymer molecular architecture. Examples of such exceptional polymers are given in Table II. Polymers A and B are generically classified as polyimides and were formed by condensation of 4,4'- hexafluoroisopropylidene diphthalic anhydride with 3,5-diaminobenzoic acid and with 1,5-diaminonaphthalene, respectively (13). Note that the high permselectivities of polymers A and B are consistent with correlations such as that in Figure 3, since polyimides typically exhibit high coehesive energies similar

preclude the need to rely upon mobility regulating mechaniams to aid in the separation process. This is the basis for solvent extraction and liquid membrane systems. The problems and considerations in such cases are quite different from those in standard bulk polymer systems and will not be discussed here.

Manipulation of the structure of standard bulk polymers to alter their mobility selectivity can be guided somewhat by correlations such as those shown in Figures 6 and 7. Figure 6 shows a correlation of $\bar{D}$ for various penetrants in a number of different glassy polymers. The correlating variable, the kinetic diameter of the gas, is related to the zeolite window dimension that will just permit passage of the penetrant of interest (39). For molecules that are essentially spherical, such as methane, argon and helium, this dimension is similar to the Lennard-Jones diameter. For asymmetric molecules such as carbon dioxide and nitrogen, however, the kinetic diameter corresponds more closely to the minimum diameter of the molecule. This figure shows clearly the extremely strong effect on the penetrant mobility caused by small differences in minimum penetrant diameter. A difference of less than 1.5 A distinguishes the kinetic diameters of helium and methane; however, there is almost three orders of magnitude difference in their mobility in polycarbonate. The spread in the various diffusivity values for a given penetrant in different polymers can be partially understood in terms of Figure 7. This figure shows the effects of variations in the specific volume of the polymer on the observed diffusion coefficients, $\bar{D}$. While this correlation is useful and intuitively satisfying, it undoubtedly oversimplifies the true differences in molecular-scale environments sampled by a penetrant as it moves through the polymers. The tendency for glassy polymers to exhibit local variations in the amount and distribution of molecular scale intersegmental gaps trapped during the quenching process from the rubbery state has been discussed in detail (17). Nevertheless, the correlation in Figure 7 is useful in depicting relative differences between extremes such as that represented by the highly open PPO environment and the rather compact Kapton environment. It is clear that the mobility selectivity is substantially higher for Kapton than for PPO. The ratios of the apparent diffusivities of CO_2 and CH_4 increase from 6.9 for PPO to 15.4 for Kapton; however, the permeability for CO_2 drops by more than two hundred fold in going from PPO to Kapton. Such a dramatic penalty in productivity certainly tends to confirm the general point of view that one cannot have both high selectivity and high productivity in the same membrane material.

Fortunately, encouraging exceptions to such a point of view can be found in the literature for both H_2/CH_4 and CO_2/CH_4 systems (11,13). These studies suggest the possibility of increasing the product permeability while maintaining or even increasing selectivity by proper design of the polymer molecular architecture. Examples of such exceptional polymers are given in Table II. Polymers A and B are generically classified as polyimides and were formed by condensation of 4,4'- hexafluoroisopropylidene diphthalic anhydride with 3,5-diaminobenzoic acid and with 1,5-diaminonaphthalene, respectively (13). Note that the high permselectivities of polymers A and B are consistent with correlations such as that in Figure 3, since polyimides typically exhibit high coehesive energies similar

to Kapton. Surprisingly, however, both polymers A and B exhibit not only the expected high selectivities but also permeabilities that are markedly higher than those of cellulose acetate or polysulfone.

A similarly encouraging exception to the general trend in selectivity and productivity is found in the poly(aryl ether) family to which the standard polysulfone material belongs. Polymers C and D in Table II are also classified as polysulfones and are referred to as poly(tetramethyl bis-A sulfone) and poly(tetramethyl bis-L sulfone), respectively (11). One would have overlooked this group of materials if an oversimplified correlation such as that shown in Figure 3 were the only guideline used in candidate selection. As shown in Table II, polymers C and D are roughly five and fifteen times respectively more permeable to CO_2 than standard polysulfone. The CO_2/CH_4 selectivities of these two polymers are roughly 2.4 and 0.9 times respectively, that of standard polysulfone.

In both the polyimides and the aryl ether cases, the backbones are comprised of bulky structures that resist compact packing of segments. The intersegmental separations in these rigid bulky polymers may be large enough to permit relatively free movement of penetrants below a certain critical size. On the other hand, the separations may be small enough and local chain motions restricted enough to provide a substantial size- and shape-discriminating ability for slightly less compact molecules. Although solubility and diffusivity data are not available for these materials, the above interpretation appears to be reasonable. In the case of polymer D, the presence of the flexible cycloalkyl group presumably offsets the stiffening effect due to methylation and the selectivity is actually slightly lower than that of standard polysulfone. Pilato et al (11) suggested that densities of polymers C and D (1.15 and 1.10 g/cc, respectively) compared to standard polysulfone (1.24 g/cc) results in the higher permeabilities of these complex sulfones compared to the standard material. Such a suggestion is clearly consistent with the trends shown in Figure 7.

The preceding observations suggest that a loosely packed glassy polymer with sufficient cohesive energy and a rigid plasticization-resistant backbone is conducive to both high flux and high selectivity. Following this conclusion, even without synthesizing generically new polymers, relatively high permeabilities and selectivities may be achievable by structural modifications of poly(aryl ethers) polyimides, polyamides, polycarbonates, polyesters and polyurethanes.

Environmental Factors. Clearly, discovery of an extraordinarily permeable and selective material that can survive only weeks or months in the required operating environment will be unacceptable. The present brief discussion suggests approaches to consider in evaluating environmental challenges to a candidate material. Such tests should be performed in parallel with detailed sorption and transport measurements soon after a candidate material is found to have desirable selectivity and permeability properties.

Complex stress distributions can exist in quenched glassy polymers and can make them subject to microscopic failure. This is especially true in the presence of thermal and penetrant level cycling because surface layer expansion can induce substantial tensile

stresses. Under tensile stresses, many glassy polymers develop a dense network of fine surface cracks or "crazes". Load bearing fibrils, composed of bundles of chains, and having void volumes in the 50% range (40), traverse the crazes. The basic sorption and transport properties of such a material are drastically changed with essentially complete loss of selectivity in the crazed region.

A simple method for evaluating the stress cracking tendency of materials by environmental agents can be used as a screening test. The test sample is used in the form of a cantilevered beam loaded with a weight as shown in Figure 8 (41). By exposing the sample to a test environment containing various partial pressures of agents such as CO_2, H_2S and H_2O, the potential for stress-cracking of the polymer can be determined in a quantitative manner. Because the stress in the bar varies from the maximum at the clamped end to zero at the free end, a stress-cracking agent will cause cracking down to the point where the stress is insufficient to produce a local failure of the secondary bonds between polymer segments. This test can be performed as a function of temperature as well as composition to identify operating conditions where potential problems can be anticipated. The critical stress, S_c, is calculated from Equation 9 where F is the total force applied (clip plus weight), L is the distance along the bar between the free end and the stress crack closest to it. The dimensions b and d are the width and thickness of the bar in Figure 8.

$$S_c = \frac{6\,FL}{b\,d^2} \qquad (9)$$

The surface crazes observed are typically on the order of a micron in depth, so the entire sample bar thickness does not to be invaded for the test to be useful. Even rather large molecules can penetrate to the depth of a micron in a matter of hours or days, and smaller molecules like CO_2 can do so in a matter of minutes or seconds.

True chemical attack, as opposed to the above physical process of crazing, can be predicted somewhat on the basis of known liability of chain backbone groups. For example, it is known that ester linkages are particularly susceptible to hydrolytic attack. Imide groups are, on the other hand, quite hydrolytically stable but are subject to aggressive attack by Lewis bases. A combined infrared spectroscopic and gravimetric sorption study has been used to follow the progressive attack of ammonia on the imide ring of Kapton (42). The severity of the attack suggests that one should be cautious in using materials such as the highly selective imides in Table II for separations where Lewis bases are present.

The focus of this paper and the multiplicity of environment hazards faced by a candidate membrane material make it impossible to enumerate specifics in greater detail than that discussed above. If strong stress-cracking tendencies are observed in the tests described above (that is, low values of S_c observed), plasticization tendencies may exist for the polymer-penetrant pair. In such a case, care should be exercised to study the candidate material under conditions that include the most demanding environment anticipated in actual use.

Conclusions

There appears to be reasons for cautious optimism concerning the possibility of developing more permeable and selective membranes in spite of the general inverse relationship between these two variables. Control of chain backbone rigidity and intersegmental packing density may provide a means of selectively permitting the passage of a relatively compact permeant molecule while substantially restricting the nonpermeant. Reliance on solubility selectivity to provide the major means of discriminating between gas penetrants in dense polymer films may be less promising. Cellulose acetate, the only material considered that is strongly selective for CO_2 compared to CH_4 on the basis of solubility, appears to exhibit a strong plasticizing response to increasing CO_2 pressures. Such an effect is expected to further reduce the mobility selectivity of cellulose acetate and thereby cause it to lose overall selectivity as CO_2 partial pressure increases. A similar trend may be observed for other glassy materials that rely strongly upon solubility as the principal basis for its selectivity, however, considerably more research is required before this tentative conclusion can be verified.

A correlative approach such as that shown in Figure 3 for the overall selectivity (or permeability) is useful in some senses but insufficient because it would have led one to overlook the extremely interesting family of poly(aryl ethers) which in some cases have both high selectivity and high permeabilities. A detailed analysis of the mobility and solubility contributions to the permeability and selectivity properties of an homologous series of candidate materials can be extremely valuable in membrane material selection. Such an approach permits one to assess the true cause of changes in the observed permeability and selectivity and can more effectively guide a systematic program to optimize membrane material transport properties.

Environmental sensitivity of candidate materials must be assessed under conditions of temperature, pressure and composition that simulate actual usage. Facilure of a material in this context can severely limit the range of applicability of a membrane that otherwise has outstanding properties.

Acknowledgments

The authors gratefully acknowledge support of this work under NSF Grant No. CPE08319285 and ARO contract No. DAAG29-81-0039. Also Dr. E. S. Sanders is acknowledged for providing his data on the solubility of various gases in PMMA for use in Fig. 5. Ms. Maxwell's assistance in typing this manuscript is also acknowledged.

Literature Cited

1. Gardner, R. J.; Crane, R. A.; Hannan, J. F. CEP 1977, 73, 11, 76.
2. Bollinger, W. A.; MacLean, D. L.; Narayan, R. S. CEP 1982, 78, 10, 27.
3. Schell, W. J.; Houston, D. D. CEP 1982, 78, 10, 33 and Hydrocarbon Proces. 1982, 61, 9, 249.
4. Lane, V. O. Hydrocarbon Proces. 1983, 62, 8, 56.

5. Mazur, W. H.; Chan, M. C. CEP 1982, 78, 10, 38.
6. Coady, A. B.; Davis, J. A. CEP 1982, 78, 10, 45.
7. Schendel, R. L.; Mariz, C. L.; Mak, J. Y. Hydrocarbon Proces. 1983, 62, 8, 58.
8. Koros, W. J. "Membrane-Based Gas Separations: Data Base and Models for Glassy Polymers", paper presented at Sunriver Membrane Conference, Sunriver, Oregon, September 1983.
9. Koros, W. J. "Gas Separation Technology", International Membrane Technology Conference, Sydney, Australia, November 1983.
10. Cadotte, J. E.; King, R. S.; Majerle, R. J., Petersen, R. J. J. Macromol. Sci.-Chem. 1981, A15, 725.
11. Pilato, L.; Litz, L.; Hargitay, B.; Osborne, R. C.; Farnham, A.; Kawakami, J.; Fritze, P.; McGrath, J. Polym. Prepr., Am. Chem. Sci., Div. Polym. Chem. 1975, 16. 41.
12. McCandless, F. P. I&EC Process Des. Develop. 1972, 11, 470.
13. Pye, D. G.; Hoehn, H. H.; Panar, M. J. Appl. Polym. Sci. 1976, 20, 287.
14. Crank, J. "The Mathematics of Diffusion", Clarendon, Oxford Press, 2nd Ed., 1975.
15. Van Amerongen, G. J. Rubber Chem. & Techn. 1964, 37, 1065.
16. Berens, A. R. J. Vinyl. Technol. 1979, 1, 38.
17. Chern, R. T.; Koros, W. J.; Sanders, E. S.; Chen, S. H.; Hopfenberg, H. B. *ACS Symposium Series No. 233, Industrial Gas* Separations, Whyte, T. E.; Yon, C. M.; Wagner, E. H. Eds; 1983; p. 47.
18. Stern, S. A.; Walawender, W. P. Separ. Sci. 1969, 4, 129.
19. Rogers, C. E. In "Physics and Chemistry of the Organic Solid State"; Fox, D.; Labes, M. M.; Weissberger, A. Eds.; Interscience: New York 1965.
20. Yi-Yan, N.; Felder, R. M.; Koros, W. J. J. Appl. Polym. Sci. 1980, 25, 1755.
21. Chern, R. T.; Koros, W. J.; Hopfenberg, H. B.; Stannett, V. T. J. Polym. Sci., Phys. Ed. in press.
22. Chern, R. T. Ph.D. Dissertation, North Carolina State University, Raleigh, NC, 1983.
23. Chern, R. T.; Koros, W. J.; Hopfenberg, H. B.; Stannett, V. T. J. Polym. Sci.,Phys. Ed. 1983, 21, 753.
24. Chern, R. T.; Koros, W. J.; Sanders, E. S.; Yui, R. E. J. Membr. Sci. 1983, 15, 157.
25. Antonson, C. R.; Gardner, R. J.; King, C. F.; Ko, D. Y. Process Des. Develop. 1977, 16, 463.
26. Stern, S. A.; Mauze, G. R.; Frisch, H. L., J. Polym. Sci., Phys. Ed. 1983, 21, 1275.
27. Saxena, V.; Stern, S. A. J. Membr. Sci. 1982, 12, 65.
28. Hay, A. S.; Shenian, P.; Gowan, A. C.; Erhardt, P. F.; Haaf, W. R.; Therberge, J. E. In "Encyclopedia of Polymer Science and Technology"; Mark, H.; Gaylord, N. G.; Bikales, N. M. Eds.; Interscience, NY, 1964.
29. Schnell, H. "Chemistry and Physics of Polycarbonate", Interscience, NY, 1964.
30. Johnson, R. N.; Farnham, A. G.; Clendinning, R. A.; Hale, W. F.; Merriam, C. N. J. Polym. Sci., 1967, A-1, 2375.
31. Lewis, O. G. "Physical Constants of Linear Homo-polymers", Springer-Verlag, NY. 1968.

32. Burrell, H. In "Polymer Handbook"; Bandrup, J.; Immergut, E. H. Eds.; John Wiley and Sons, NY, 1975.
33. Koros, W. J.; Chan, A. H.; Paul, D. R. J. Membr. Sci. 1977, 2, 165.
34. Erb, A. J.; Paul, D. R. J. Membr. Sci. 1981, 8, 11.
35. Morel, G.; Paul, D. R. J. Membr. Sci. 1982, 10, 273.
36. Hoehn, H.; Richter, J. W., US Patent Reissue, 1980, 30, 351.
37. Stern, S. A.; DeMeringo A. J. Polym. Sci., Phys. Ed. 1978, 16 735.
38. Heyd, R. L.; McCandless, F. P. J. Membr. Sci. 1977, 2, 375.
39. Breck, D. W. "Zeolite Molecular Sieves"; John Wiley and Sons, NY, 1974; p. 636.
40. Kambour, R. P. J. Polym. Sci. 1964, A2, 4159.
41. "Selecting Pastics for Chemical Resistance", Modern Plastics Encyclopedia, 1981-1982, p. 499.
42. Iler, L. R.; Laundon, R. C.; Koros, W. J. J. Appl. Polym. Sci. 1982, 27, 1163.

Figure Captions

1 Diffusion coefficients for a variety of penetrants in natural rubber at 25°C and rigid poly(vinyl chloride) at 30°C. The van der Waals' volumes are quoted from Handbook of Chemistry and Physics, 35 ed., 1953-54, page 21-24 to 21-26, CRC, Cleveland, Ohio.

2 Pressure dependence of CO_2 permeability in a variety of glassy polymers at 35°C. The cellulose acetate data are estimated from a number of sources including References 5 and 6 and "The Science and Technology of Polymer Films", ed. by O. J. Sweeting, Vol. II, Wiley Interscience, NY, (1971).

3 Correlation between the solubility parameter of several glassy polymers and the ideal separation factors for the CO_2/CH_4 system calculated using the pure component permeabilities at 35°C for a 20 atm upstream pressure of each component.

4 Sorption isotherms for various gases in polycarbonate at 35°C.

5 Correlation of the apparent solubility at 20 atm and 35°C with the critical temperatures of various penetrants in a number of glassy polymers. ● polycarbonate, ○ poly(phenylene oxide), □ polysulfone, ■ Kapton, ◇ cellulose acetate, ◆ PMMA.

6 Correlation of the average diffusion coefficient, $\bar{D}$, and the kinetic diameters of several penetrants in a number of glassy polymers at 35°C for an upstream penetrant pressure of

20 atm. ● polycarbonate, ○ poly(phenylene oxide), □ polysulfone, ■ Kapton, ◇ cellulose acetate.

7 Correlation of the average diffusion coefficients of several penetrants with the specific volumes of the polymers for an upstream penetrant pressure of 20 atm at 35°C.

8 Simple apparatus for evaluating stress cracking potential of candidate membrane materials.

Figure 1: Diffusion coefficients for a variety of penetrants in natural rubber and rigid PVC (vinyl chloride) at 25 to 35 and 30°C.

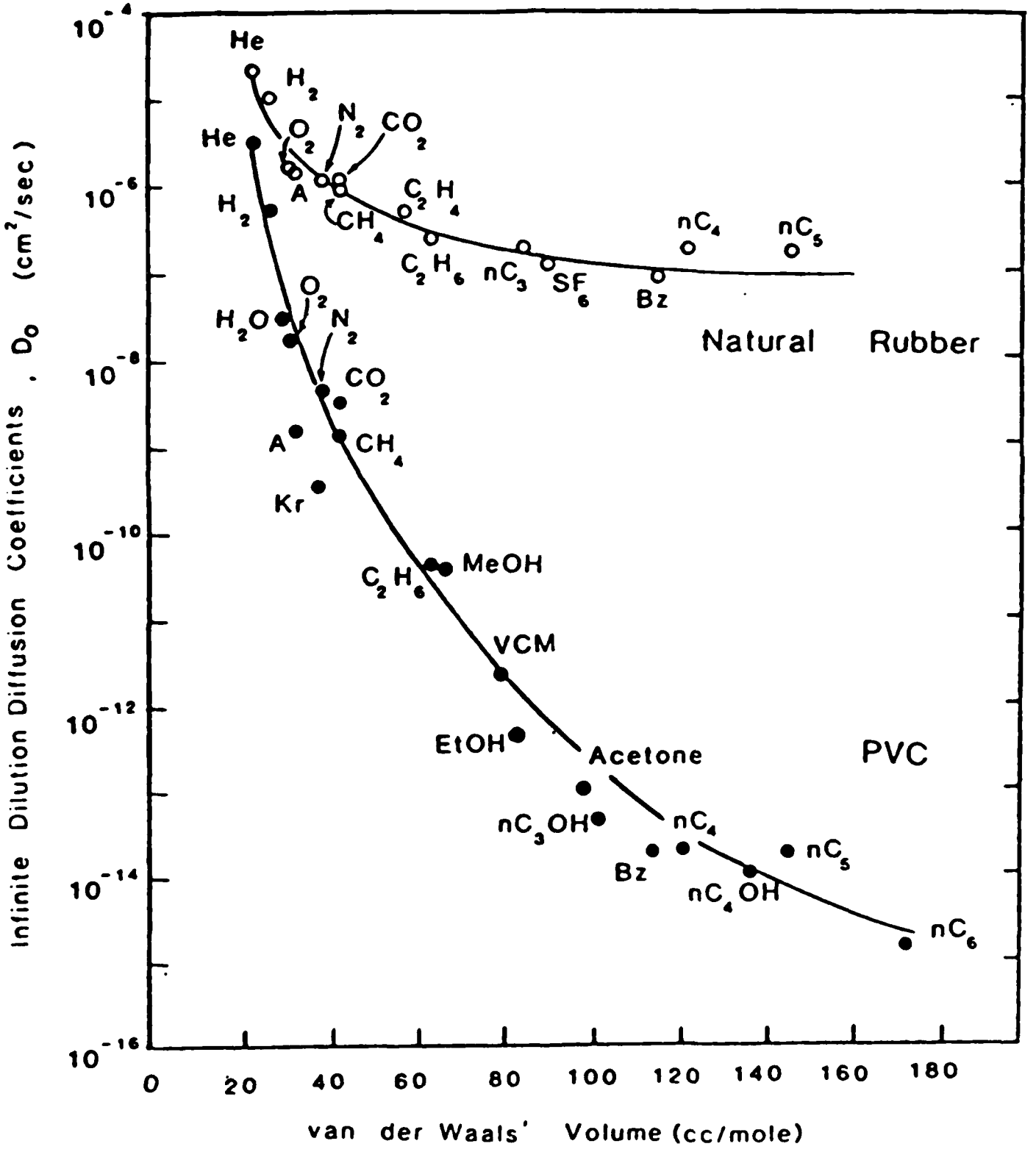

Figure 2. Pressure dependence of CO_2 permeability in a variety of glassy polymers at 35°C. The cellulose acetate data are estimated from a number of sources including References 5 and 6 and "The Science and Technology of Polymer Films", ed. by O. J. Sweeting, Vol. II, Wiley Interscience, NY, (1971).

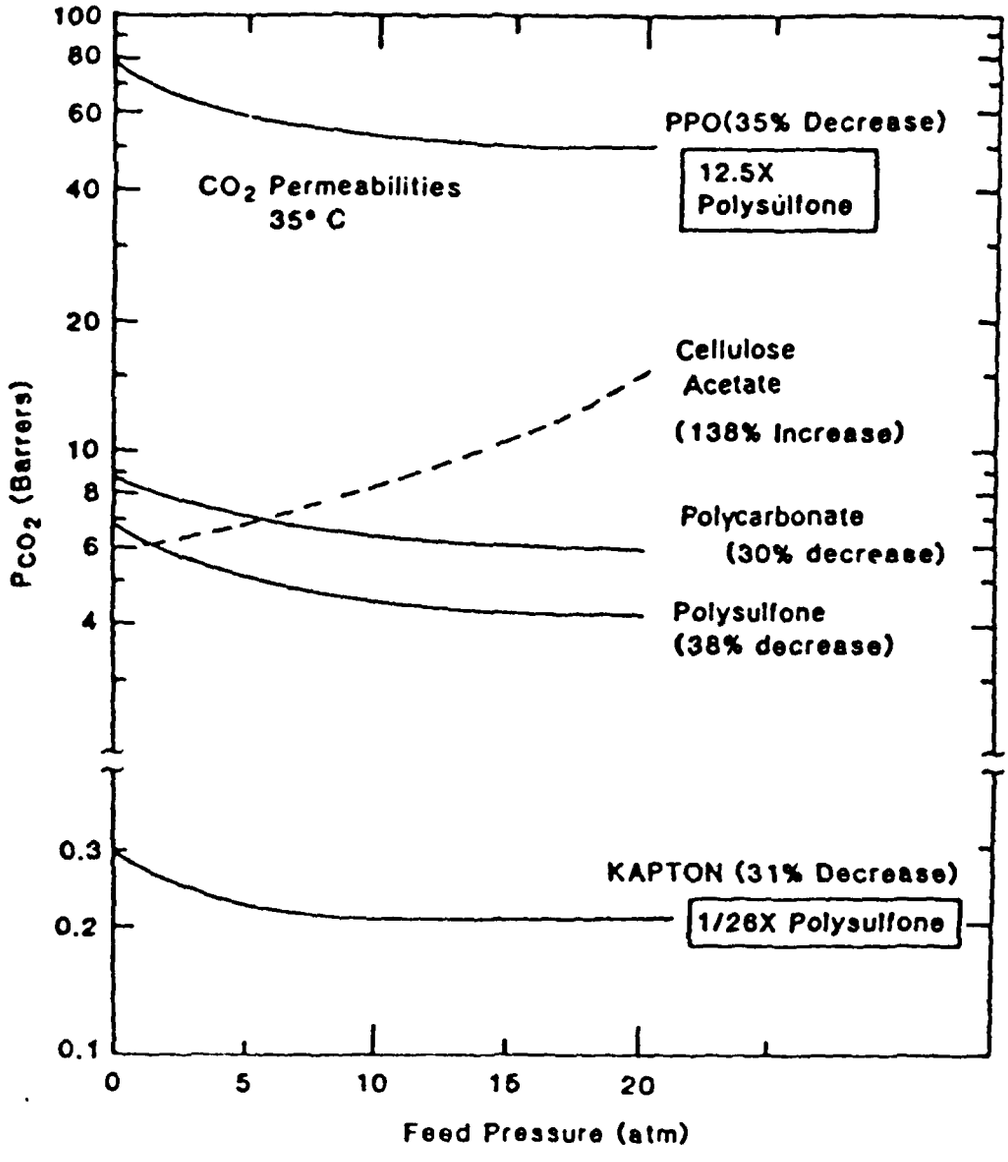

Figure 3. Correlation between the solubility parameter of several glassy polymers and the ideal separation factors for the CO_2/CH_4 system calculated using the pure component permeabilities [2] at 35°C for a 20 atm upstream pressure of each component.

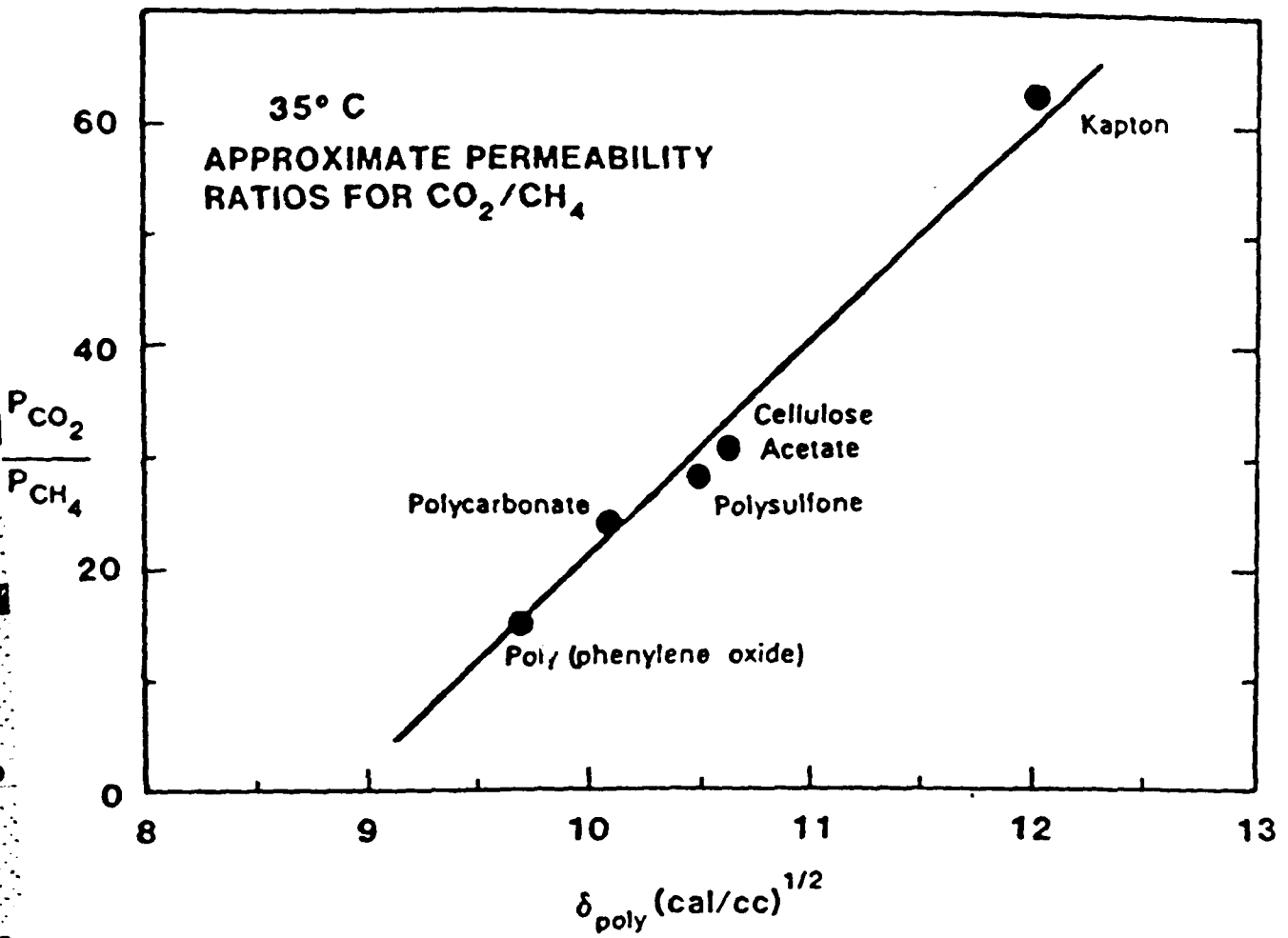

Figure 4: Sorption isotherms for various gases in polycarbonate at 35°C

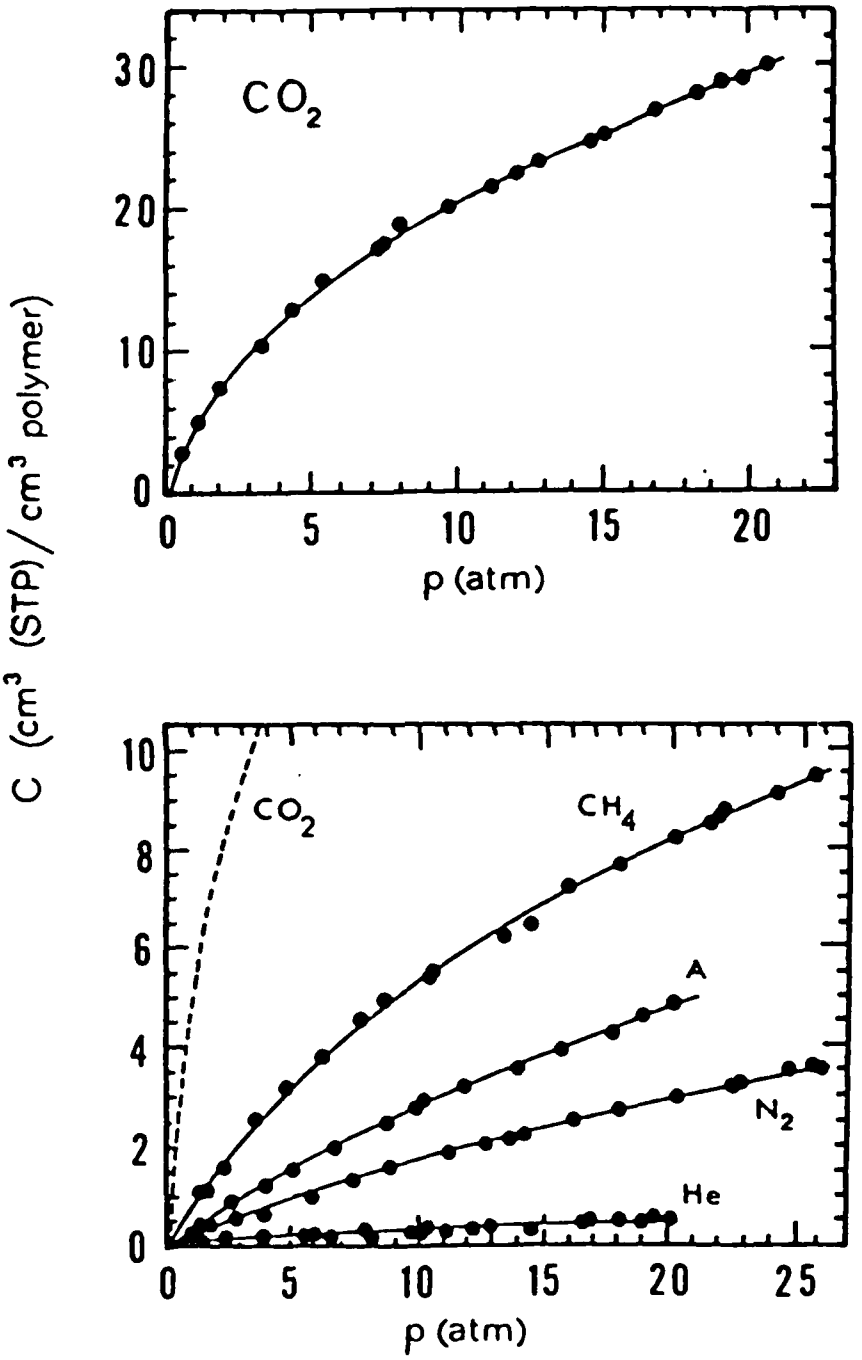

Figure 5: Correlation of the apparent solubility at 20 atm and 35°C with the critical temperatures of various penetrants in a number of glassy polymers.

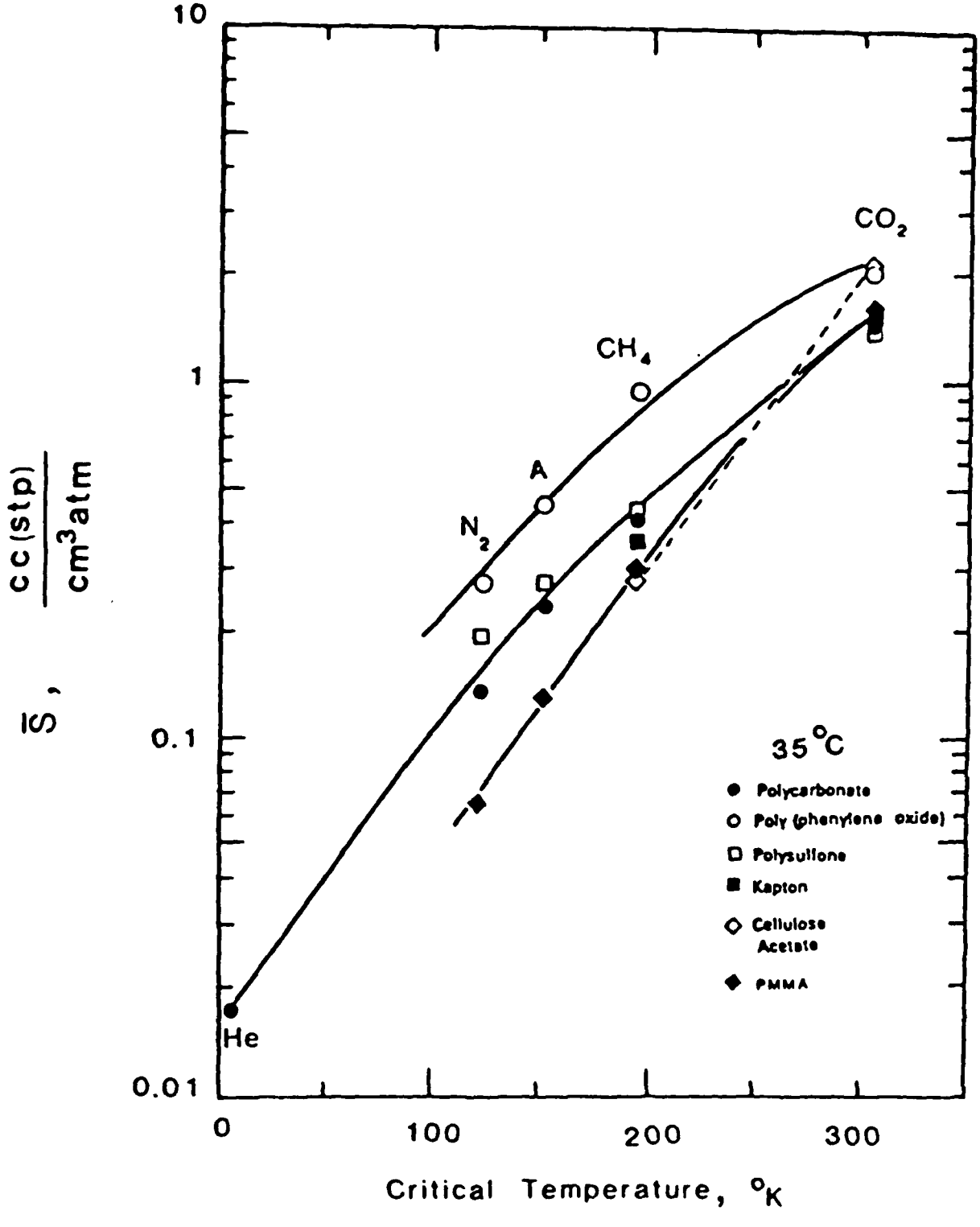

Figure 6. Correlation of the average diffusion coefficient, $\bar{D}$, and the kinetic diameters of several penetrants in a number of glassy polymers at 35°C for an upstream penetrant pressure of 20 atm.

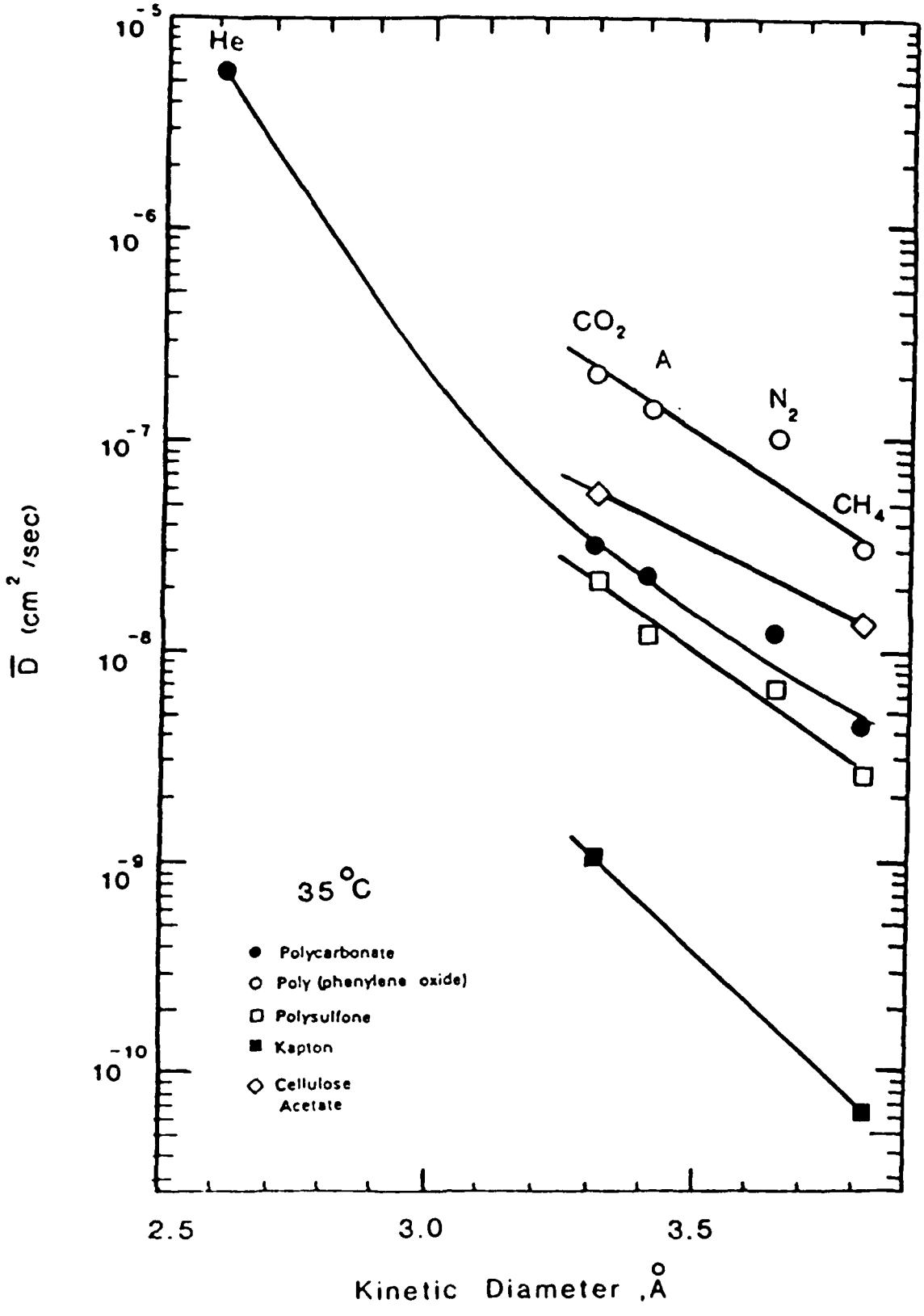

Figure 7: Correlation of the average diffusion coefficients of several penetrants with the specific volumes of the polymers for an upstream penetrant pressure of 20 atm.

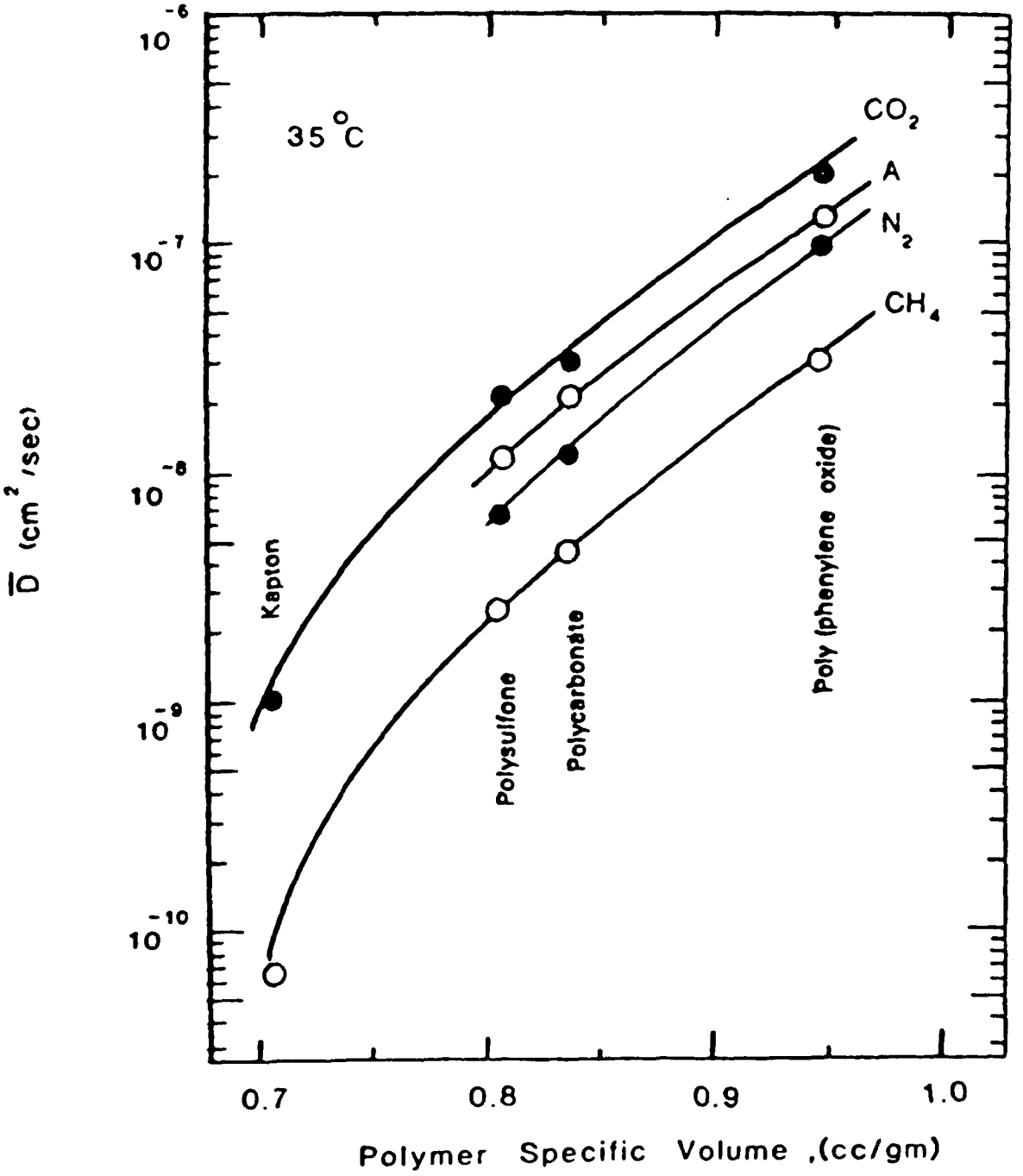

Figure 8: Simple apparatus for evaluating stress cracking potential of candidate membrane materials.

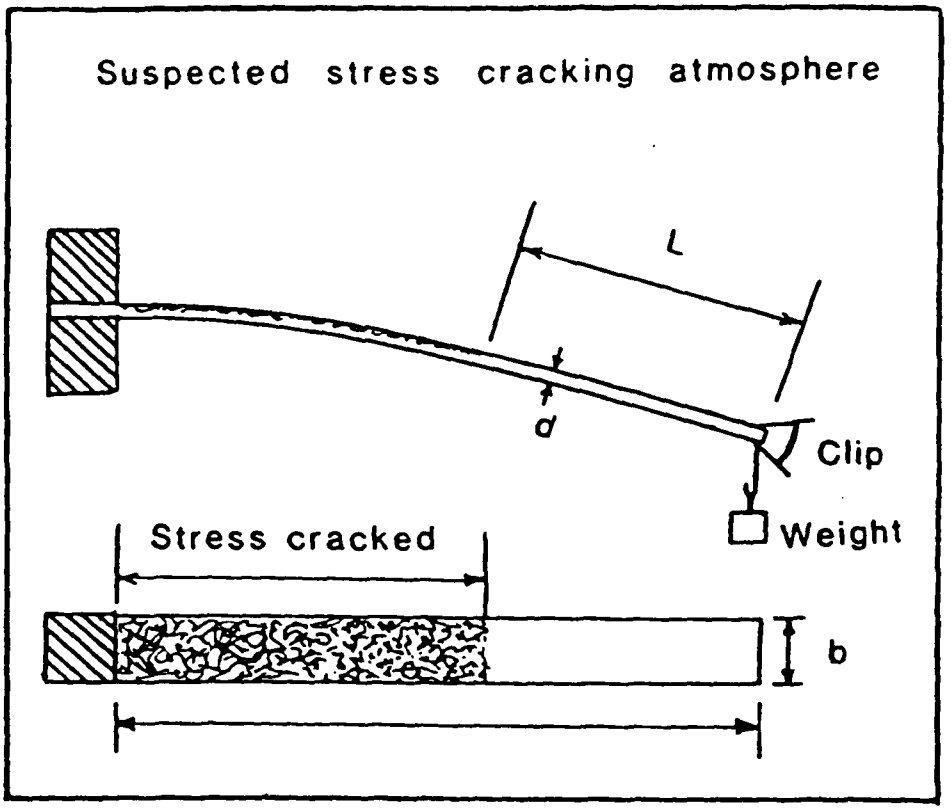

Table 1: Mobility and solubility contributions to the permeability and selectivity of typical glassy polymers at 35° C for a 20 atm pressure of both components based on pure component parameters.

POLYMER	$\bar{D}_{CO_2}$ *	$\bar{S}_{CO_2}$ **	$\bar{D}_{CH_4}$ *	$\bar{S}_{CH_4}$ **	$\frac{P_{CO_2}}{P_{CH_4}}$	$\frac{\bar{D}_{CO_2}}{\bar{D}_{CH_4}}$	$\frac{\bar{S}_{CO_2}}{\bar{S}_{CH_4}}$
POLY(PHENYLENE OXIDE) (PPO)	2.2×10^{-7}	2.10	3.2×10^{-8}	0.95	15.1	6.88	2.2
POLYCARBONATE	3.2×10^{-8}	1.47	4.7×10^{-9}	0.41	24.4	6.81	3.6
CELLULOSE ACETATE ***	5.9×10^{-8}	2.05	1.4×10^{-8}	0.28	30.8	4.21	7.3
POLYSULFONE	2.3×10^{-8}	1.44	2.6×10^{-9}	0.45	28.3	8.85	3.2
KAPTON	1.0×10^{-9}	1.53	6.5×10^{-11}	0.37	63.6	15.38	4.1

* $\bar{D}$ has units of [cm^2/sec].
** $\bar{S}$ has units of [cc(STP)]/[cc of polymer- atm].
*** Estimated values as indicated in the caption of Figure 2.

Sorption and Transport of Benzene in Poly(ethyl . Terephthalate)

C. J. PATTON,* R. M. FELDER, and W. J. KOROS,† *Department of Chemical Engineering, North Carolina State University, Raleigh, North Carolina 27650*

Synopsis

The kinetics and equilibria of benzene sorption in poly(ethylene terephthalate) were measured at 40°C, 50°C, and 60°C, with benzene activities ranging from 0.02 to 0.3. At most experimental conditions, diffusion was found to be Fickian; however, evidence of non-Fickian transport was found at the highest activity levels. Values of the diffusion coefficient of benzene range from 10^{-14} cm^2/s at 40°C to 10^{-12} cm^2/s at 60°C in the limit of low concentrations. Nonlinear isotherms observed for benzene sorption were successfully interpreted in terms of the dual mode model for sorption in glassy polymers, whereby the sorbed penetrant exists as two populations: one sorbed according to Henry's law and the other following a Langmuir isotherm. Non-Fickian transport data were correlated with a model that superimposes diffusion of both the Henry's law and Langmuir populations (the "partial immobilization" model) upon first-order relaxation of the polymer matrix.

INTRODUCTION

A common method of monitoring ambient air pollution levels involves trapping an air sample in a bag made of a relatively impermeable glassy polymer, and subsequently subjecting the sample to gas chromatographic analysis. The fraction of the collected sample which is lost by sorption into the bag wall is seldom considered, due in part to a scarcity of data regarding the sorption and transport characteristics of pollutants in bag materials. The focus of the present study is the demonstration of a method for obtaining such data. Benzene was chosen as the representative pollutant and poly(ethylene terephthalate) (PET) was selected as the representative sample bag material.

The study of the sorption and transport of large condensable penetrants such as benzene in glassy polymers is complicated by the prohibitively long times that are often required to reach equilibrium at ambient and near ambient temperatures. To overcome this problem, a gravimetric sorption rate measurement technique was adopted,[1] using extremely thin film samples of PET. Even under these conditions, transport rates at ambient temperatures were too slow to permit the acquisition of the desired data in a reasonable period of time. Consequently, data were obtained at temperatures in the range 40–60°C. The resulting sorption, transport, and equilibrium parameter values may be extrapolated to ambient temperatures with a reasonable degree of accuracy.

* Currently employed with Monsanto Co., Research Triangle Park, NC.

† To whom correspondence should be addressed: The Center for Energy Studies, University of Texas, Austin, Texas 78712.

Journal of Applied Polymer Science, Vol. 29, 1095–1110 (1984)
© 1984 John Wiley & Sons, Inc.
CCC0021-8995/84/041095-16$04.00

EXPERIMENTAL

Materials. All PET film samples used in this study, other than 1.0-mil films, were provided by the DuPont Co. The 1.0-mil films were National Bureau of Standards reference materials. The benzene used was obtained from Fisher Scientific Co., and contained less than 1% impurities. The as-received benzene was frozen in liquid nitrogen, placed under vacuum for several minutes, and then allowed to thaw. Three such freeze thaw cycles were carried out to remove any noncondensable contaminants before the benzene was used in the sorption experiments.

Sorption Apparatus and Procedure. The sorption system used was a quartz spring balance enclosed in a fluid-jacketed glass cell. Details of the cell construction and operating procedures are given by Felder et al.[2] The polymer films were degassed for 24–48 h. before use.

Koros et al.[3] have shown that the previous history of glassy polymers can affect their sorption characteristics. To insure consistent sorption behavior and avoid possible anomalies due to slow relaxation, the PET samples were equilibrated at the highest benzene activity to be studied and thoroughly evacuated before any sorption data were taken. Experiments at 60°C indicated that such preswelling protocols were not necessary at the low activities used in this study, but they were, nevertheless, followed as insurance against any subtle conditioning effects which might otherwise confound results at the lowest experimental temperature. Runs were carried out at 60°C, 50°C, and 40°C, in that order.

Sorption runs were performed in an "integral" fashion. After the preconditioning treatment discussed above, the films were systematically exposed to lower benzene activities, and the sorption kinetics and equilibria were measured. Equilibrium was assumed to occur when no uptake of penetrant by the film was observed for at least 96 h. Desorption data were also routinely obtained following each sorption run, and care was taken that all the benzene sorbed was subsequently desorbed before further experiments were performed.

SORPTION EQUILIBRIA

Data and Model. Sorption isotherms for benzene in PET are shown in Figure 1. The isotherms are concave to the pressure axis. This behavior may be interpreted in terms of the so-called dual mode sorption model, which postulates that the sorbed penetrant exists in two populations: one dissolved according to Henry's law (concentration = C_D), and the other held in unrelaxed gaps between polymer chains and sorbed according to a Langmuir isotherm (concentration = C_H). This model has been found by several authors to provide a satisfactory description of the equilibrium sorption of gases and low activity vapors in glassy polymers.[4-7] Vieth[8] gives a detailed review of systems described by the dual sorption model.

The dual mode sorption isotherm is given by

$$C = C_D + C_H = k_D p + C'_H bp/(1 + bp) \tag{1}$$

where k_D [cc (STP)/cc polymer·atm] is the Henry's law constant, p (atm) is the penetrant partial pressure at equilibrium, b (atm^{-1}) is the affinity constant of

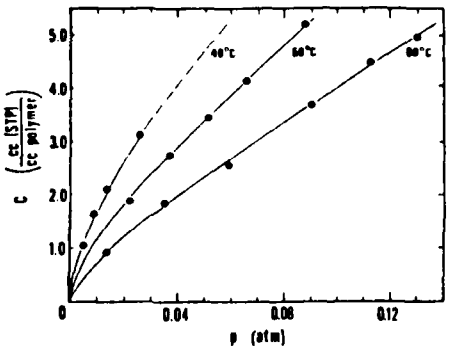

Fig. 1. Sorption isotherm for benzene in 0.10 mil poly(ethylene terephthalate).

the gas for the Langmuir sites, and C'_H [cc (STP)/cc polymer] is the maximum capacity of the polymer for the penetrant in the Langmuir sorption mode.

The data shown in Figure 1 were fit by nonlinear regression, using a Fletcher–Powell function minimization algorithm[9] to minimize the sum of squares of the unweighted residuals at each temperature. The model parameters determined in this manner are listed in Table I. The solid curves shown in Figure 1 were generated from eq. (1) using these parameters.

Henry's Law Constant and Langmuir Affinity. The values of the Henry's law constant k_D and the Langmuir affinity constant b, shown in Table I, are much larger than corresponding values found for CO_2 in PET over the same temperature range.[10] This seems reasonable, since at 50°C, CO_2 is at a reduced temperature of 1.06 while benzene has a reduced temperature of only 0.57. Clearly, benzene has a much greater tendency than CO_2 to exist in a condensed phase due to its significantly higher critical temperature.

The solubility parameters b and k_D are each amenable to standard van't Hoff analysis, as shown in Figure 2. The van't Hoff formulas determined by fitting the data are given in Table I. The slopes of these semilogarithmic plots multiplied by $-R$, where R is the gas constant, equal the enthalpy changes for transferring one mole of benzene from the gas phase into the dissolved Henry's law (ΔH_D) and Langmuir (ΔH_b) populations, respectively. The values of ΔH_D and ΔH_b determined in this manner are −32.8 kJ/mol and −34.1 kJ/mol. The enthalpy of benzene in the Henry's law mode is thus approximately 1300 J/mol

TABLE I
Dual Mode Sorption Parameters for the PET/Benzene System

Temp (°C)	k_D[a] [cc (STP)/ cc polymer·atm]	C'_H [cc (STP)/ cc polymer]	b[b] (atm^{-1})	K[c] = $C'_H b/k_D$
40	67.33	1.73	150.1	3.85
50	44.42	1.42	100.2	3.20
60	31.57	1.00	68.2	2.17

[a] $k_D = 2.275 \times 10^{-4} \exp[3945/T\ (°K)]$, $\Delta H_D = -32.8$ kJ/mol.
[b] $b = 3.079 \times 10^{-4} \exp[4102/T\ (°K)]$, $\Delta H_b = -34.1$ kJ/mol.
[c] $C'_H = 0.043\ [83.0 - T\ (°C)]$.

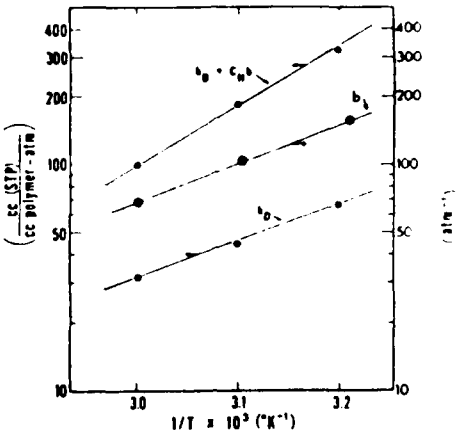

Fig. 2. Van't Hoff plots of the true Henry's law equilibrium sorption parameter (k_D), the Langmuir affinity parameter (b), and the apparent Henry's law parameter ($k_D + C'_H b$) for benzene in poly-(ethylene terephthalate).

higher than that of benzene sorbed in the molecular gaps between chains. The difference is less than that reported by Koros et al.[10] for CO_2 in PET (5020 J/mol).

The latter results may be interpreted in light of a suggestion of Michaels et al.[4] that more energy is needed for a molecule to enter the Henry's law mode since separation of polymer chains is needed for dissolution by this mechanism, whereas molecules in the Langmuir mode sorb in preexisting gaps. This accounts for the positive difference between ΔH_D and ΔH_b. The argument also implies that as the size of the penetrant molecule increases, the energy needed to sorb into the gaps should increase correspondingly, since an expansion or coalescence of existing gaps may be necessary to accommodate the larger penetrant molecules. Thus, the magnitude of the difference in enthalpies of the sorbed molecules in each environment should decrease with increasing molecular size, in agreement with the results given above.

The apparent Henry's law constant k_D^*, which equals the low-pressure limiting slope of the sorption isotherm, is from eq. (1) equal to $k_D + C'_H b$, and can also be represented by an effective van't Hoff expression, as shown in Figure 2. The apparent sorption enthalpy at low pressures, ΔH_D^*, was determined to be −51.2 kJ/mol. This quantity does not have a simple physical interpretation, since it includes temperature-dependent contributions from C'_H which are not truly energetic in nature.[10]

Langmuir Capacity. Information about the "gaps" in the polymer in which the Langmuir population is sorbed is provided by the magnitude and temperature dependence of the Langmuir capacity C'_H. Koros[11] proposed that regions of localized lower density are frozen in glassy polymers when the polymers are quenched to a state below T_g from the rubbery region. They further asserted that the difference between the actual specific volume of the glass, v_g, and the limiting specific volume, v_l, obtained by extrapolating the v vs. T curve from the rubbery region through T_g, provides a direct measure of the volume of the gaps

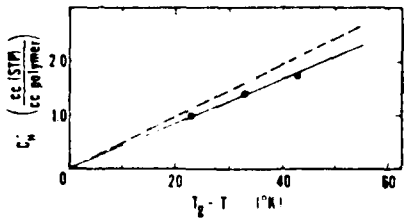

Fig. 3. Comparison of experimentally measured points of the Langmuir capacity parameter, C_H, with predicted values (·····) calculated using eq. (2).

between chain segments. The latter quantity is in turn related to the Langmuir capacity, as follows:

$$C_H' = \frac{[(v_g - v_l)]}{v_g} \rho^* \tag{2}$$

where ρ^* is the molar density of the sorbate at the saturation point of the Langmuir isotherm. The amount of unrelaxed volume, and thus C_H', should decrease with increasing temperature, finally disappearing near the glass transition.

If the specific volumes of the polymer in both the rubbery and glassy regions each vary approximately linearly with temperature, then, from eq. (2), over a reasonably small temperature interval, C_H' should vary linearly with the difference between the actual temperature T and the glass transition T_g.[10] A plot of C_H' vs. $(T_g - T)$ for benzene in PET, shown in Figure 3, confirms this expectation. The equation of the line that fits the data is given in Table I.

Values of C_H' were predicted from eq. (2), using the density of pure liquid benzene for ρ^*, values for dilatometric expansion coefficients for PET from the literature,[12] and a value $T_g \approx 83°C$ obtained from differential scanning calorimetry measurements.[13] The results are shown as the dotted line along with the measured values in Figure 3. The agreement between the predicted and measured values is gratifying.

SORPTION RATES

Uptake Rates and Diffusion Coefficients. Figures 4 and 5 show plots of the cumulative mass of benzene sorbed, $M_t(t)$, normalized by the uptake at equilibrium, M_∞ vs. $\sqrt{t}$ for a 1.0-mil and a 0.1-mil film, respectively. Effective Fickian diffusion coefficients were determined from the formula

$$\bar{D} = 0.04919\, h^2/t_{1/2} \tag{3}$$

where h is the polymer thickness and $t_{1/2}$ is the time required for the sorption of half the equilibrium uptake of penetrant.[1] The coefficients determined in this manner were substituted into the solution of the diffusion equation for sorption into flat membranes[14]:

$$M_{t,F} = M_{\infty,F}\left\{1 - \frac{8}{\pi^2}\sum_{n=0}^{n=\infty}\frac{\exp[-\bar{D}(2n+1)^2\pi^2 t/h^2]}{(2n+1)^2}\right\} \tag{4}$$

The results are shown as the solid curves through the data in Figures 4 and 5.

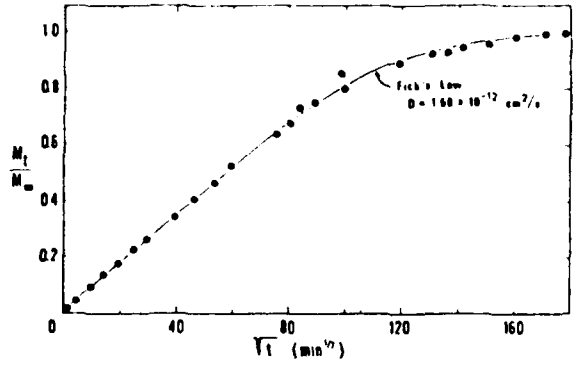

Fig. 4. Sorption kinetic run for benzene sorption in 1.0 mil thick poly(ethylene terephthalate) at 60°C for a vapor activity equal to 0.25; l = 1.0 mil.

The model of purely Fickian diffusion is seen to provide an excellent representation of the sorption of benzene into a 1.0-mil PET film at 60°C, but deviations from this ideal model appear for the thinner (0.1-mil) membrane at the same and a lower temperature, even at lower vapor activities. For the thin film, the Fickian model describes the data well only at 40°C for the lowest activity studied (p/p_0 = 0.02).

The above observations suggest that a relaxation process is superimposed on the Fickian diffusion process. At very low vapor activities, penetrant-induced relaxations are relatively minor, explaining why the sorption curves are described most effectively by the Fickian model at low activities. In fact, any small relaxational effects present in the low activity case (p/p_0 = 0.02) at 40°C cannot be distinguished from experimental error.

This interpretation is consistent with the ability of the pure Fickian diffusion model to correlate the kinetic data for the thicker (1.0-mil) film. Since the diffusion and relaxation processes superimpose (no distinct two-stage sorption is observed) in the 0.1-mil film, the characteristic relaxation time of the polymer under the conditions studied is presumably of the same magnitude as the characteristic diffusion time (h^2/D) for this film. For the thick film, the characteristic diffusion time is 100 times larger than that of the thin film, while the characteristic relaxation times are about the same for both films. It follows that the diffusion process in the thick film is roughly 2 orders of magnitude slower than the relaxation process, so that a model which neglects relaxation effects in this film should provide a good correlation of sorption kinetic data, as is, in fact, the case.

Enscore[15] measured rates of sorption of *n*-hexane in polystyrene microspheres, and found that the uptake after long times proceeded more slowly than the Fickian model predicted. The measured responses were similar to those observed in most of the sorption runs for the thin film presented in Figure 5. Enscore analyzed his data in terms of a phenomenological model proposed by Berens and Hopfenberg[16] that permits separation of diffusion and relaxation effects. A similar approach will be used in the present study for the thin film samples.

Berens-Hopfenberg Model. According to the Berens-Hopfenberg model, penetrant uptake can be described as the linear superposition of a Fickian dif-

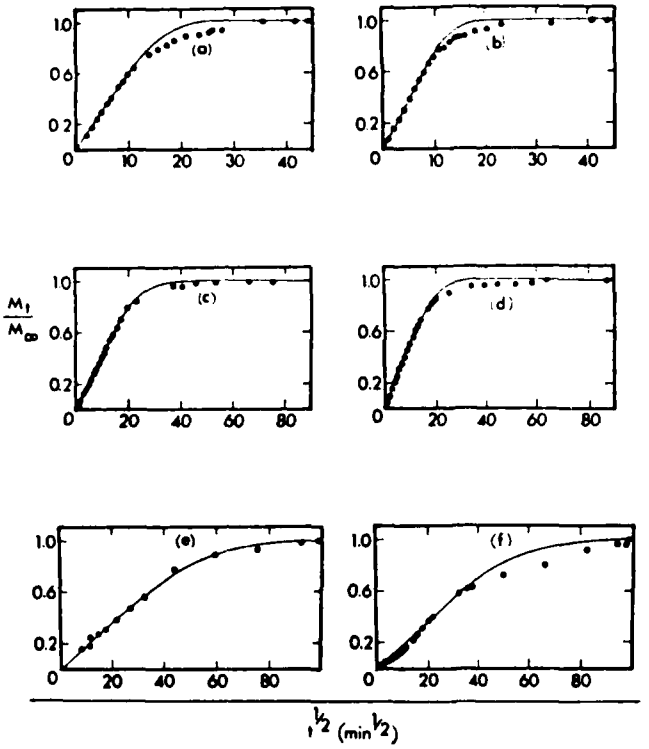

Fig. 5. Sorption kinetic runs for benzene in 0.10 mil PET under a variety of conditions. The lines are the Fickian model [(eq. (4)] using diffusion coefficients estimated from the half-time formula [(eq. (3)]: (a) $p/p_0 = 0.07$, 60°C; (b) $p/p_0 = 0.22$, 60°C; (c) $p/p_0 = 0.06$, 50°C; (d) $p/p_0 = 0.30$, 50°C; (e) $p/p_0 = 0.02$, 40°C; (f) $p/p_0 = 0.11$, 40°C.

fusion term and a first-order relaxation term.[16] The total uptake at a given time is given by

$$M_t = M_{t,F} + M_{t,R}, \tag{5}$$

where $M_{t,F}$ is the amount that would be sorbed by the Fickian process proceeding alone, given by eq. (4), and $M_{t,R}$ is the corresponding term for the relaxation process. The uptake due to relaxation is

$$M_{t,R} = M_{\infty,R}[1 - \exp(-kt)] \tag{6}$$

where k is a first-order rate constant for the relaxation process, and $M_{\infty,R}$ represents the equilibrium uptake due to relaxation.

Substitution of eqs. (4) and (6) into eq. (5) and division by the total quantity of dissolved penetrant at equilibrium, M_∞, yields

$$\frac{M_t}{M_\infty} = \varphi_F \left\{1 - \frac{8}{\pi^2} \sum_{n=0}^{n=\infty} \frac{\exp[-\bar{D}(2n+1)^2\pi^2 t/h^2]}{(2n+1)^2}\right\} + (1 - \varphi_F)[1 - \exp(-kt)] \tag{7}$$

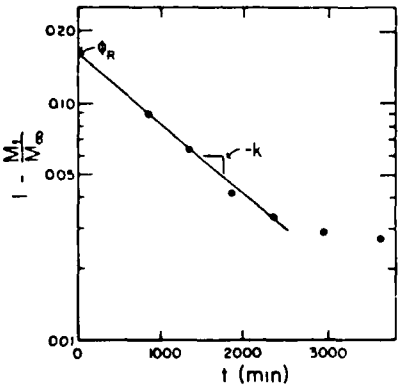

Fig. 6. Illustration of approximate graphical method for evaluation of the Berens-Hopfenberg model parameters for use in eq. (7); $p/p_0 = 0.11$, 60°C.

where

$$\varphi_F = M_{\infty,F}/M_\infty \tag{8}$$

is the fraction of the equilibrium sorption contributed by the diffusion process.

The expression of eq. (7) is seen to contain three adjustable parameters: the effective diffusion coefficient $\bar{D}$; the relaxation rate parameter k; and the fraction of the equilibrium sorption due to diffusion, φ_F. The values of k and φ_F are first estimated by analyzing the uptake data at times sufficiently long for the summation in eq. (7) to be negligible. When this is the case, the simplified equation may be rewritten as

$$1 - M_t/M_\infty = (1 - \varphi_F)\exp(-kt) \tag{9}$$

In view of eq. (9), it might be anticipated that a semilogarithmic plot of $(1 - M_t/M_\infty)$ vs. t would be linear over some intermediate range of times—long enough for the summation of eq. (7) to be negligible, but not long enough for the closeness of the approach to equilibrium to make the data imprecise. The slope of the line would equal $-k$, and the intercept would equal $(1 - \varphi_F)$. A representative plot of this type is shown in Figure 6. The plot is indeed close to linear for times in the range 800–2000 min, thus allowing the estimation of k and $\varphi_R = 1 - \varphi_F$.

Once the two relaxation process parameters have been estimated, it is a straightforward matter to estimate the effective Fickian diffusion coefficient $\bar{D}$. The asymptotic limit of the uptake due to diffusion alone is by definition φ_F. If $t_{1/2}$ is the time required for the fractional uptake (M_t/M_∞) to reach half of this limiting value, the effective diffusion coefficient $\bar{D}$ may be estimated from eq. (3).

While the above procedure yields reasonable estimates of the three parameters of the Berens–Hopfenberg model, its neglect of the interactions between the diffusion and relaxation processes must inevitably lead to estimation errors. Improved parameter estimates were obtained by applying nonlinear regression to the sorption rate data, simultaneously determining the values of k, φ_F, and

TABLE II
Optimum Parameter Values of D, k, and φ_F Determined from Experimental Data for Benzene Sorption in PET

p/p_0	$D \times 10^{13}$ (cm^2/s)	$k \times 10^5$ (s^{-1})	φ_F
	$T = 40°C$		
0.02	0.67	–	1.00
0.06	1.70	0.36	0.51
0.11	2.00	0.36	0.44
	$T = 50°C$		
0.06	4.67	1.31	0.85
0.10	5.04	1.43	0.85
0.14	5.70	1.43	0.79
0.19	5.90	0.90	0.85
0.25	6.50	1.00	0.87
0.30	6.80	0.90	0.88
	$T = 60°C$		
0.03	10.70	4.04	0.89
0.07	12.0	3.20	0.80
0.11	14.5	4.59	0.84
0.17	14.9	3.57	0.65
0.22	15.5	2.05	0.88

$\bar{D}$. A pattern search (Hooke–Jeeves) function minimization algorithm[9] was used to determine the parameter values that minimized the unweighted sum of squares of residuals between the data points and the predictions of eq. (7).[13] The procedure described in the preceding paragraphs was used to obtain the initial parameter estimates provided as input to the search routine, and convergence was usually quite rapid.

Values of the three model parameters determined for the sorption of benzene into 0.1-mil PET film at 40°C, 50°C, and 60°C are given in Table II. Correlations of the sorption data for several representative runs (corresponding to those of Fig. 5) are shown in Figure 7, which illustrates both the adequacy of the Berens–Hopfenberg model and the inadequacy of the simple Fickian model to represent the sorption of benzene in thin PET films at the higher penetrant activities considered in these thin films.

As shown by the results given in Table II, the diffusion coefficient $\bar{D}$ increases with increasing concentration (or vapor activity), as is often observed in glassy polymer systems. The relaxation rate parameter k appears to increase significantly with increasing temperature, but at a given temperature little systematic variation of k with penetrant activity is observed. The fraction of sorption controlled by diffusion, φ_F, did not vary systematically with either temperature or penetrant activity under the conditions studied. However, it is quite likely that significant variations in both k and φ_F would be observed if a broader range of conditions were examined.

The value of the true Fickian diffusion coefficient for a given temperature and penetrant activity should be independent of film thickness. Results obtained in two runs carried out at 60°C confirm this expectation. In one run, performed with a 1.0-mil film and a benzene activity of 0.25, transport was almost entirely

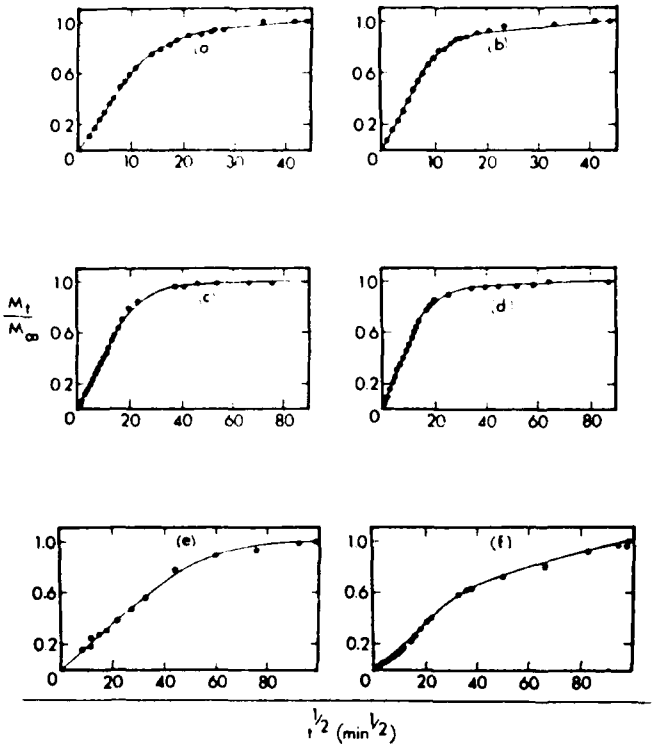

Fig. 7. Sorption kinetic runs for benzene shown in Figure 5. The lines are the Berens-Hopfenberg equation fit to the data using the parameters in Table II: (a) $p/p_0 = 0.07$, 60°C; (b) $p/p_0 = 0.22$, 60°C; (c) $p/p_0 = 0.06$, 50°C; (d) $p/p_0 = 0.30$, 50°C; (e) $p/p_0 = 0.02$, 40°C, (f) $p/p_0 = 0.11$, 40°C.

by pure Fickian diffusion (see Fig. 4), with $\bar{D} = 1.58 \times 10^{-12}$. In another run, performed with a 0.1-mil film and a benzene activity of 0.22 (see Fig. 7), the value of $\bar{D}$ determined by fitting the data with the Berens–Hopfenberg model was 1.55×10^{-12}, statistically indistinguishable from the first value.

From Table II, the characteristic time scale for the relaxation process (k^{-1}) is 5×10^4 s, and the characteristic times for the diffusion process (h^2/D) are 10^5 s and 10^7 s for the 0.1-mil and 1.0-mil films, respectively. These results are completely consistent with the previous discussion about the relative importance of the diffusion and relaxation processes in the two films. It is clear that, in the thicker film, the 200-fold greater characteristic time scale for diffusion relative to relaxation precludes direct observation of the relaxation process.

In short, the Berens–Hopfenberg model provides an excellent phenomenological description of the sorption process. It is also worth noting, however, that the model does not by itself provide insight into the molecular source of the apparent differences between the "diffusion" and "relaxation" processes. Additional experimentation beyond the scope of the present study, possibly involving dilatometric measurements, and the formulation and validation of a nonequilibrium statistical model of the glassy state will be required to obtain such insight.

Dual Mobility (Partial Immobilization) Model. It is clear from consideration of the data in Table II that the phenomenologically determined average diffusion coefficients tend to increase with penetrant activity (or sorbed concentration). The observed diffusivities of penetrants in glassy polymers often increase with increasing penetrant concentration, even in the absence of plasticization by the penetrant.[17] Fick's law, given by eq. (10), is traditionally used to describe the migration of penetrant at low activities:

$$N = -D_{\text{eff}} \frac{\partial C}{\partial x} \tag{10}$$

where N is the observed flux, D_{eff} is an effective local concentration-dependent diffusion coefficient, C is the local sorbed concentration, and x is the direction of migration.

Paul and Koros[18] formulated a transport model based on the dual mode sorption concept, which explicitly assigns a separate mobility to penetrants in the Henry's law and Langmuir populations. This model, termed the dual mobility or partial immobilization model, expresses the flux as

$$N = -D_D \frac{\partial C_D}{\partial x} - D_H \frac{\partial C_H}{\partial x} \tag{11}$$

where D_D and D_H are the respective diffusion coefficients of the Henry's law (C_D) and Langmuir (C_H) populations. A similar model expressed in terms of gradients in chemical potential has been discussed by Petropolous.[19]

The relationship between the effective local diffusion coefficient [D_{eff} of eq. (10)] and the dual mobility model parameters is as follows[17]:

$$D_{\text{eff}} = D_D \left[\frac{1 + FK/(1 + \alpha C_D)^2}{1 + K/(1 + \alpha C_D)^2}\right] \tag{12}$$

where $K = C'_H b/k_D$, $F = D_H/D_D$, and $\alpha = b/k_D$. Clearly, if $F \neq 1$ ($D_D \neq D_H$), the local effective diffusion coefficient of all sorbed species is a function of the local penetrant concentration.

Since the value of D_{eff} in eq. (12) changes from the beginning of a sorption run (at which point the concentration is defined to be a uniform C_1, usually 0) to the end of the run (when the concentration is C_2), the actual diffusion coefficient determined from the curve-fitting procedure previously described is appropriately defined as[20]

$$\bar{D} = \frac{\int_{C_1}^{C_2} D_{\text{eff}}\, dC}{C_2 - C_1} \tag{13}$$

Substitution of eq. (12) for D_{eff} into this equation yields[21]

$$\bar{D} = D_D \left[\frac{1 + FK/(1 + bp_1)(1 + bp_2)}{1 + K/(1 + bp_1)(1 + bp_2)}\right] \tag{14}$$

where p_1 and p_2 are the equilibrium partial pressures at $t = 0$ and $t = \infty$, respectively. If p is the constant penetrant partial pressure surrounding the

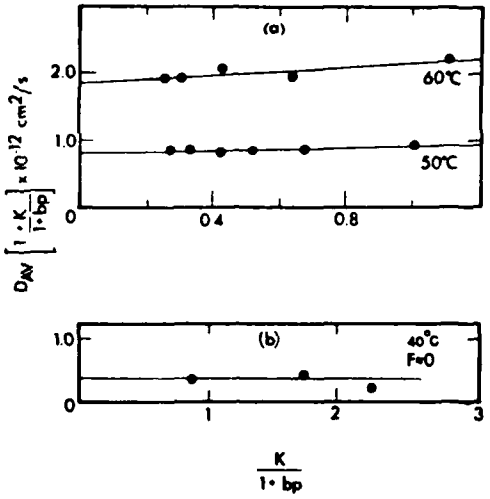

Fig. 8. Average diffusion coefficient values (see Table II) plotted according to eq. (15).

membrane during an integral sorption experiment, then $p_1 = 0$ and $p_2 = p$, and eq. (14) reduces to

$$\overline{D} = D_D \left[\frac{1 + FK/(1 + bp)}{1 + K/(1 + bp)} \right] \tag{15}$$

The last equation indicates that a plot of

$$\overline{D}\left(1 + \frac{K}{1 + bp}\right) \text{ vs. } \frac{K}{1 + bp}$$

should produce a straight line with slope D_H ($= FD_D$) and intercept D_D. Figure 8 shows such plots for the benzene–PET system at 40°C, 50°C, and 60°C, with the value of K and b taken from Table I and those of $\overline{D}$ from Table II. The values of D_D and D_H determined in this manner are listed in Table III.

The results show that the Langmuir-sorbed species is between 10% and 20% as mobile as the Henry's law population at 50°C and 60°C, and therefore that neglecting the mobility of the former species (as was routinely done in early analyses of dual-mode transport in glassy polymers) could lead to substantial errors in data correlation. At 40°C, on the other hand, it appears that, within the accuracy of the data available, the assumption $F \approx 0$ is a reasonable *mathematical* approximation. Physically, of course, $D_H \neq 0$, or else the assumption

TABLE III
Kinetic Parameters D_D, D_H, and F for Benzene in 0.10 mil PET Film

Temp (°C)	D_D[a] × 10^{13} (cm²/s)	D_H × 10^{13} (cm²/s)	$F = D_H/D_D$
40	3.5	$\ll D_D$	$\simeq 0$
50	8.14	1.06	0.13
60	18.5	3.43	0.185

[a] $D_D = 0.395 \exp[-8691/T\,(°K)]$, $E_D = 72.3$ kJ/mol.

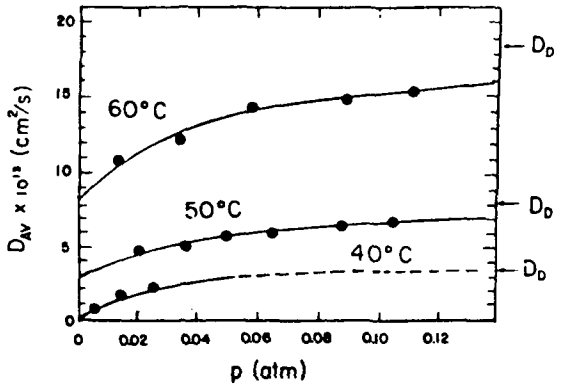

Fig. 9. Comparison of observed average diffusion coefficients (see Table II) to the values calculated from eq. (15) using the parameters in Tables I and III.

of local equilibrium between the two sorption modes could not be satisfied.

The values of D_D shown in Table III are well correlated by an Arrhenius formula. The formula is also given in Table III; the activation energy for diffusion of the Henry's law-sorbed species is 72.7 kJ/mol. Since the diffusion coefficient of the Langmuir-sorbed species is negligible at the lowest of the three temperatures studied, a similar analysis for D_H cannot meaningfully be done.

A direct illustration of the variation of the effective diffusion coefficient with penetrant partial pressure is given in Figure 9, which plots $\bar{D}$ vs. p for the three temperatures studied. Also shown on this figure are the curves predicted from eq. (15), using the dual mobility model parameters given in Table III.

Since the glassy polymer matrix undergoes swelling at the same time diffusive transport is occurring, the Henry's law solubility coefficient k_D and diffusion coefficient D_D change slightly during a sorption run, so that application of the given equations for $\bar{D}$ is not rigorously justified. However, the excellent correlation of the $\bar{D}$ vs. p data shown in Figure 8 indicates that, at the conditions of the present experiments, swelling was slight enough for its effect on the calculated value of $\bar{D}$ to be neglected.

Prediction of Permeabilities and Time Lags. The transport properties reported thus far can be determined by either sorption rate measurements, as was done in this study, or by permeation experiments.[1] The latter approach involves the determination of the steady-state permeability and diffusion time lag.

Koros and Paul[18] derived analytical expressions for the permeability and time lag for systems described by the partial immobilization model. Substitution of the parameters for the benzene/PET system given in Tables I and II into these expressions yields the plots of permeability and time lag vs. penetrant partial pressure shown in Figures 10 and 11. In the absence of non-Fickian effects, both the permeability and the time lag are seen to be decreasing functions of upstream partial pressure.

The effects of relaxational contributions to the transport process should be relatively unimportant in the case of the steady-state permeability, and so the accuracy of the predictions in Figure 10 is expected to be quite satisfactory, even

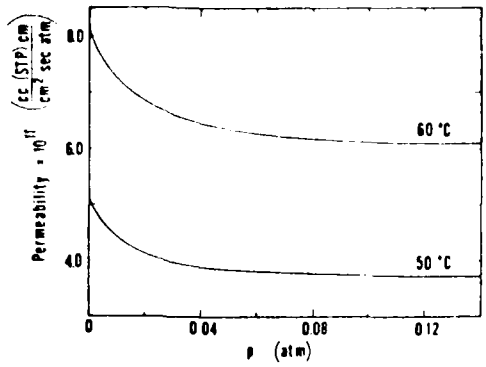

Fig. 10. Prediction of the steady state permeability of benzene for poly(ethylene terephthalate) at 50°C and 60°C.

for thin films. On the other hand, time-dependent relaxations during the transient period could protract the approach to steady-state, thereby causing the predictions of θ to be underestimated for the 0.1-mil film except at very low vapor activities. For the thicker film, time lags should be 100 times greater than those shown in Figure 11, since the lags vary as the square of the film thickness.

For the same reason that the Fickian model successfully described sorption in the thick film but failed to do so for the thin film, one would expect the predictions of time lags determined by scaling the results of Figure 11 to describe the behavior of thick films, but to fail for thin films. This is a fortunate result, in that it suggests that the behavior of thick barrier films ($\geq$1 mil) can be deduced by studying thin films over more convenient time scales. This is the topic of a current study in our laboratory.

Desorption Kinetics. Desorption rates were measured routinely after benzene sorption had reached equilibrium. Data from a representative desorption run at 50°C are shown in Figure 12. The line shown in this figure is the

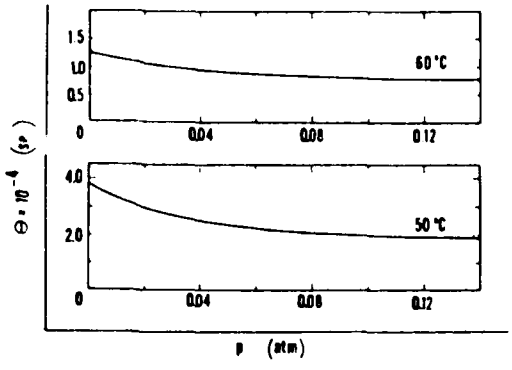

Fig. 11. Prediction of the diffusion time lag for benzene in a 0.10 mil thick film of poly(ethylene terephthalate) at 50°C and 60°C.

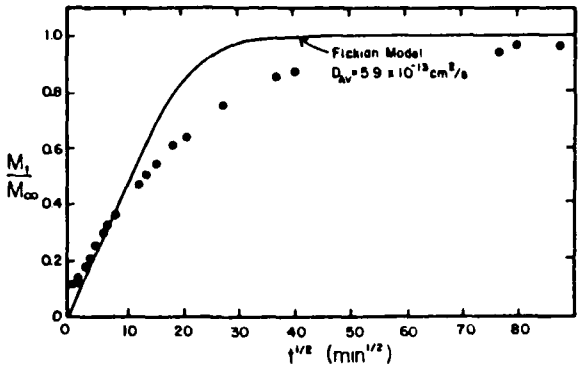

Fig. 12. Comparison of the experimentally observed normalized desorption kinetic run for benzene in poly(ethylene terephthalate) with the simple Fickian model line [eq. (4)]. The average diffusion coefficient for this system, determined from the Berens–Hopfenberg analysis of the sorption data (see Table II), was used in the calculation: $T = 50°C$, $p/p_0 = 0.19$, $l = 0.1$ mil.

prediction of the Fickian transport model using the diffusion coefficient determined from the corresponding sorption run.

The results indicate that rapid desorption occurs initially, followed by a slower desorption process. Such non-Fickian behavior is presumably due to consolidation of distended polymer chains over the same time scale as that of the diffusion process for the thin film samples. Due to equipment failure, a formal desorption experiment was not performed on the 1.0-mil film. One would expect, however, that desorption from the thicker film would more closely approximate Fickian behavior, again because the characteristic time scale for diffusion is substantially longer than for chain relaxation in the thick sample.

CONCLUSIONS

The dual mode sorption and partial immobilization models provide good correlations of data for benzene sorption in PET at low vapor activities. This result is particularly significant in that these models have heretofore been used primarily for noncondensable gases. The occurrence of relaxation in the polymer during sorption was treated successfully with the Berens–Hopfenberg model.

The diffusional mobility of the Langmuir-sorbed component is significantly lower than the mobility of the Henry's law component for benzene in PET. This result is consistent with previous results which suggest that the relative mobility of penetrants in the Langmuir and Henry's law environments ($F = D_H/D_D$) decreases as the critical temperature of the penetrant increases.[2] Benzene has a high critical temperature[22] (562K), so that low values of F were anticipated and observed.

The temperature dependence of the Langmuir capacity, C_H', was qualitatively and quantitatively consistent with the interpretation of this parameter in terms of unrelaxed volume frozen in the polymer below T_g. The predictions of C_H' from dilatometric data for PET and the density of liquid benzene were gratifyingly accurate.

The results also indicate that the sorption anomalies seen in this study are less

apparent when dealing with the thicker films. This suggests that these anomalies will be of minor consequence in the prediction of benzene sorption into air bags (3–5 mils thick), even through significant quantities of benzene may in fact be sorbed into the bag wall.

The authors gratefully acknowledge support of this work by EPA Cooperative Agreement CA 805194010, and ARO Contract DAAG29-81-K-0039. Thanks are extended to Dr. M. Katz of the E. I. DuPont Company, Circleville, Ohio, and Dr. J. Barnes of the National Bureau of Standards, for providing PET film samples for use in this study. Although the research described in this paper has been funded in part by the United States Environmental Protection Agency, it has not been subjected to the Agency's required peer and policy review, and therefore does not necessarily reflect the views of the Agency, nor does mention of trade names or commercial products constitute endorsement or recommendation for use.

References

1. R. M. Felder and G. S. Huvard, in *Methods of Experimental Physics*, R. Fava, Ed., Academic, New York, 1980, Vol. 16c, Chap. 17.
2. R. M. Felder, C. J. Patton, and W. J. Koros, *J. Polym. Sci., Polym. Phys. Ed.*, **19**, 1895 (1981).
3. W. J. Koros, D. R. Paul, and A. Rocha, *J. Polym. Sci., Polym. Phys. Ed.*, **14**, 687 (1976).
4. A. Michaels, W. R. Vieth, and J. A. Barrie, *J. Appl. Polym. Sci.*, **34**, 1 (1963).
5. R. M. Barrer, J. A. Barrie, and J. G. Slater, *J. Polym. Sci.*, **27**, 315 (1958).
6. W. R. Vieth, P. M. Tam, and A. S. Michaels, *J. Colloid Interface Sci.*, **22**, 360 (1966).
7. V. Stannett, W. J. Koros, D. R. Paul, H. K. Lonsdale, and R. W. Baker, "Recent Advances in Membrane Science," in *Advances in Polymer Science*, H. J. Canton et al., Eds., Springer-Verlag, Berlin, 1974, Vol. 32.
8. W. R. Vieth, J. M. Howell, and J. H. Hsieh, *J. Membr. Sci.*, **1**, 177 (1976).
9. J. L. Kuester and J. H. Mize, *Optimization Techniques with Fortran*, McGraw-Hill, New York, 1973, p. 355.
10. W. J. Koros, D. R. Paul, and G. S. Huvard, *Polymer*, **20**, 956 (1979).
11. W. J. Koros, "Dual Mode Sorption and Transport of Gases in Glassy Polymers," final report, N. S. F. Research Initiation Grant No. ENG 78-05577, 1978.
12. H. J. Kolb and E. F. Izard, *J. Appl. Phys.*, **20**, 564 (1949).
13. C. J. Patton, M.S. thesis, North Carolina State University, 1980.
14. J. Crank, *The Mathematics of Diffusion*, 2nd ed., Oxford University Press, London, 1975.
15. D. J. Enscore, Ph.D. dissertation, North Carolina State University, Raleigh, 1977.
16. A. R. Berens and H. Hopfenberg, *Polymer*, **19**, 489 (1978).
17. W. J. Koros, D. R. Paul and R. Rocha, *J. Polym. Sci., Polym. Phys. Ed.*, **14**, 687 (1976).
18. D. R. Paul and W. J. Koros, *J. Polym. Sci., Polym. Phys. Ed.*, **14**, 675 (1976).
19. J. H. Petropolous, *J. Polym. Sci., A-2*, **8**, 1797 (1970).
20. J. Crank and G. S. Park, "Methods of Measurement," in *Diffusion in Polymers*, J. Crank and G. S. Park, Eds., Academic, London, 1975.
21. W. J. Koros, C. J. Patton, R. M. Felder, and S. J. Fincher, *J. Polym. Sci., Polym. Phys. Ed.*, **18**, 1435 (1980).
22. R. C. Reid, J. M. Prausnitz, and T. K. Sherwood, *The Properties of Gases and Liquids*, McGraw-Hill, New York, 1977.

Received June 8, 1983
Accepted October 5, 1983

From: POLYIMIDES, Vol. 1
Edited by K.L. Mittal
(Plenum Publishing Corporation, 1984)

SORPTION AND TRANSPORT OF PHYSICALLY AND CHEMICALLY INTERACTING PENETRANTS IN KAPTON® POLYIMIDE

L. Iler, W. J. Koros, D. K. Yang and R. Yui

Department of Chemical Engineering
North Carolina State University
Raleigh, North Carolina 27650

Gravimetric sorption and desorption data are reported for water and anhydrous ammonia in Kapton® at 30°C. The data for water at low activity are described well by Fick's Law with a concentration dependent diffusion coefficient. At high vapor activity, evidence of small extents of chemical reaction of the water with imide groups was discovered. Even after exposure to a relative humidity of 81.4% for two weeks, however, only 0.31% of the imide structures were affected. Anhydrous ammonia, on the other hand, at rather low relative saturations (0.012 to 0.032) interacted strongly with some of the imide structures of Kapton®. Infrared and gravimetric sorption/desorption measurements were used to characterize the locus and extent of reaction. It was found that after exposure of a 0.5 mil sample to an ammonia relative saturation of 0.0316 for 16 days, roughly 17% of the imide structures were disturbed. Analysis of the coupled diffusion and chemical reaction suggests that only a fraction of the total number of imide groups (~20%) appear to become "activated" or "labilized" during the solid state curing step in which stresses may arise. Stress relief by the limited ammonolysis reaction presumably deactivates the remaining imide groups. The possiblity of using Kapton® as a combined protective barrier and scavenger coating or film is explored briefly.

INTRODUCTION

Aromatic polyether diimides are known for their excellent high temperature resistance to degradation. Our interest in these high glass transition polymers stems from an ongoing study of permselective membranes for various sampling and separation applications [1-3]. In the course of our research, we have encountered an extremely interesting range of physical and chemical interactions which several rather common penetrants exhibit with an important commercial polyimide, Kapton®, whose repeat unit is shown below.

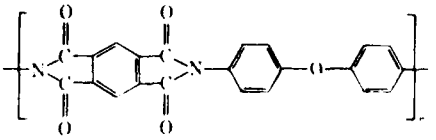

Imide linkages are known to be somewhat sensitive to attack by basic penetrants, and this fact is actually used to an advantage in the erosion of Kapton® to produce extraordinarily thin films (<0.0001 in) for electronics applications, by exposure to an alkaline etching medium. The present study will focus on much milder penetrant exposure conditions. In such cases, the small molecule acts primarily as a probe of the distribution of the physically and chemically heterogeneous environments which appear to be present in Kapton® [4].

EXPERIMENTAL

Materials

The Kapton® poly(ether-imide) used in the present study was kindly supplied by the E. I. DuPont Company, Circleville, Ohio. Films of thickness 2.0 ± 0.01 mil, 0.5 ± 0.01 mil, and 0.3 ± 0.01 mil were used.

The water used in this study was triple distilled and exposed to three freeze/thaw cycles to remove dissolved gases. The anhydrous ammonia was obtained from Air Products and Chemicals, Inc., Raleigh, North Carolina at a purity of 99.9% and was used as received.

Apparatus

The design and operation of the McBain quartz spring balance used in this study has been described previously[4]. With this system, a direct gravimetric measure of penetrant uptake within the polymer as a function of time can be determined by observing changes in the spring extension.

The sorption cell and supporting apparatus are shown in Figure 1. A quartz spring with a spring constant of 0.500±0.006 mg/mm extension was used. The polymer sample was hung at the base of the spring, and a glass reference fiber was hung parallel to the spring to compensate for small shifts in the spring support position which might occur during the experiment. A precision microscope, capable of detecting spring deflections as small as 0.005 mm, was used to observe spring extension; therefore, deflections represented by masses as small as 2.5 μg were detectable.

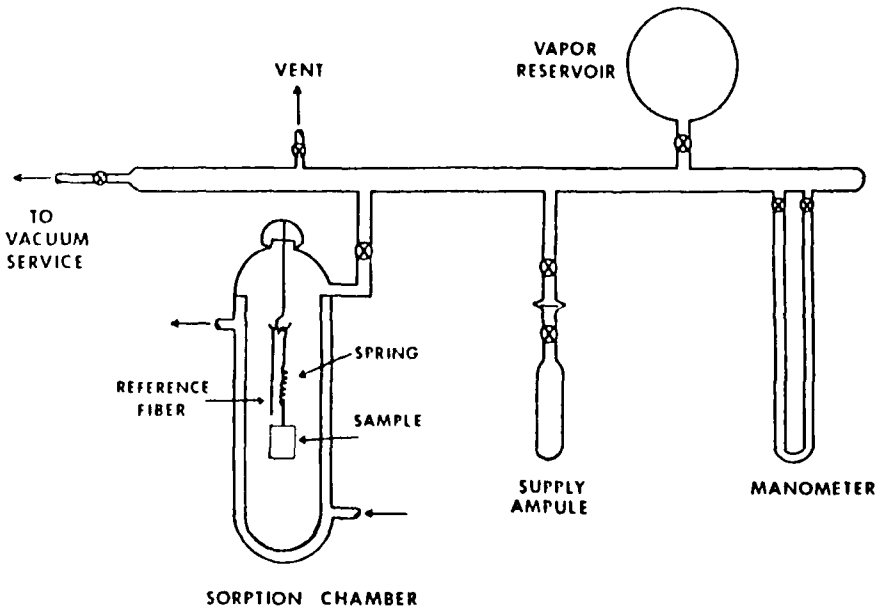

Figure 1. McBain balance apparatus used for gravimetric determination of vapor sorption data.

The sorption cell was maintained at a constant temperature by circulating a silicone fluid from a bath through a fluid jacket surrounding the cell. Brass screen was wrapped around portions of the cell and grounded to reduce static attraction between the cell wall and the polymer film. A large vapor reservoir was used to increase the total volume of the sorption system, thereby eliminating measurable fluctuations in pressure within the sorption cell.

Procedures

A Kapton® sample of known weight was hung from the quartz spring and degassed for 24 hours. A constant weight of the degassed sample was obtained within 10 hours. The system, excluding the sorption cell, was pressurized with penetrant to an empirically determined value that would give the desired sorption pressure when the stopcock to the sorption cell was opened. At time zero, the penetrant was admitted into the sorption cell, and the spring extension was measured as a function of time. The system pressure was monitored during the experiment and was permitted to vary no more than ±5 mm Hg. System pressure was adjusted by either introducing more penetrant or by raising or lowering the heating tape temperature in the exterior lines. To begin a desorption experiment, the valve connecting the sorption cell to the vacuum line was opened, and the contraction of the spring was observed as a function of time.

BACKGROUND AND THEORY

Simple Nonreactive Fickian Transport

The transport of relatively noninteracting penetrants such as N_2, CO_2 and SO_2 in glassy polymers may be described using Fick's Law (Equation (1)) for transport:

$$N = -D(C)\frac{dC}{dx} \qquad (1)$$

where N is the one-dimensional diffusional flux in the x-direction with D(C) equal to the local diffusion coefficient of the penetrant which can be a functio.. of local concentration, C. The normalized sorption or d'sorption kinetics for a slab of thickness 2ℓ can be expressed as the intinite series, shown below for the case where D is a constant, independent of concentration:

$$\frac{M_t}{M_\infty} = 4\left[\frac{Dt}{\ell^2}\right]^{1/2}\left\{\frac{1}{\pi^{1/2}} + 2\sum_{n=1}^{\infty}(-1)^n \text{ ierfc}\left[\frac{n\ell}{2(Dt)^{1/2}}\right]\right\} \quad (2)$$

where M_t and M_∞ are the mass sorbed (or desorbed) at time t and at "infinite" time, respectively[5]. The value of the constant diffusion coefficient in Equation (2) can be evaluated easily using the well-known "half-time" relation (Equation (3)) which is derived by evaluating the time ($t_{1/2}$) corresponding to $M_t/M_\infty = 0.5$ using Equation (2).

$$D = \frac{0.0492\ \ell^2}{t_{1/2}} \quad (3)$$

For simple Fickian behavior described by Equation (2), the normalized sorption and desorption responses are linear functions of $t^{1/2}$ up to at least values of $M_t/M_\infty = 0.5$ to 0.6[5]. In situations for which the diffusion coefficient is a function of local concentration (C), Equation (2) can still be used with reasonable effectiveness if one realizes that the diffusion coefficient appearing in that equation represents an average or "effective" coefficient typical of the concentration range being considered.

The gravimetric sorption/desorption kinetic runs in Figures 2 and 3 for SO_2 in Kapton® at 35°C show a simple Fickian transport process typical of a case in which D(C) increases with local concentration. Specifically, if the data in Figure 2 are plotted in the normalized form as M_t/M_∞ (shown in Figure 3), then the response is a linear function of $t^{1/2}$ up to values of M_t/M_∞ ranging from 0.5 to 0.6 for both the sorption and desorption runs. Furthermore, the sorption data lie above the desorption data indicating that the diffusion coefficient increases with increasing concentration. The lines drawn through the normalized sorption and desorption curves in Figure 3 were calculated from the standard infinite series expression (Equation (2)) for simple Fickian uptake. Effective average values for the diffusion coefficients, corresponding to 6.75×10^{-11} cm^2/sec and 4.37×10^{-11} cm^2/sec for the sorption and desorption runs, respectively, were used to obtain the fit shown. The departure from the simple Fickian model's prediction at longer times for the desorption run is presumably a consequence of the considerable concentration dependence of the SO_2 diffusion coefficient. The diffusivity approaches its "zero concentration" or infinite dilution limiting value in the last stages of desorption[3].

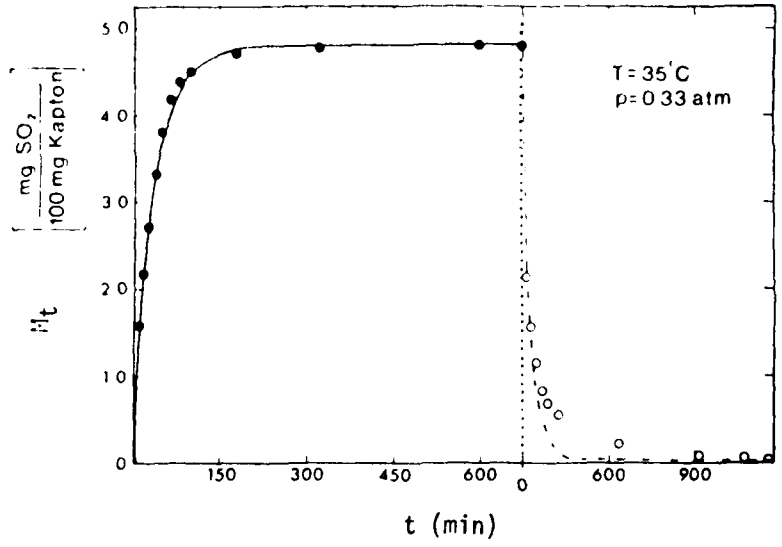

Figure 2. Sorption (●)/desorption (○) kinetic runs for a 0.5 mil Kapton® polyimide film at 35°C and at a SO_2 pressure of 0.33 atm.

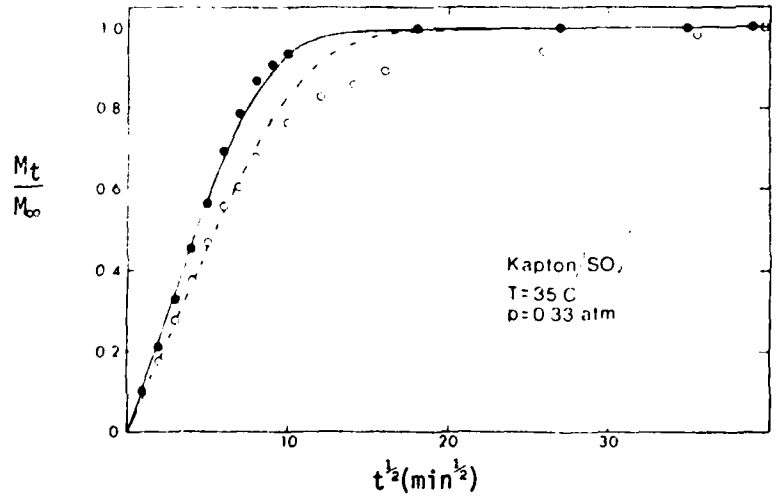

Figure 3. Normalized sorption (●)/desorption (○) kinetic runs for a 0.5 mil Kapton® film at 35°C and at a SO_2 pressure of 0.33 atm. Note that all of the SO_2 sorbed into the polymer film is removed during desorption.

As noted by Berens[6], the van der Waals volume, b, of a penetrant serves as a useful measure of the size of the molecule. The parameter, b, therefore, is a useful correlating tool for "infinite dilution" diffusion coefficients of relatively noninteracting penetrants in a given polymer, since it is more difficult to move large molecules than small molecules through a given environment. Strong interactions of the penetrant with the polymer could reduce the infinite dilution diffusion coefficient by imposing a large activation energy for execution of a typical diffusional jump. A simple correlation for infinite dilution diffusion coefficients, D_0, in terms of b is shown in Figure 4. On the basis of this plot, we anticipated a diffusion coefficient for ammonia in the range of 10^{-9} cm^2/sec. Such a diffusion coefficient would yield an equilibration time of roughly 20 minutes for a 0.5 mil film. As will be discussed, radically different behavior was observed with extremely protracted uptake. Moreover, total desorption was not possible, leading to the hypothesis of a chemical reaction. This hypothesis has been verified by infrared spectroscopy work which will also be described.

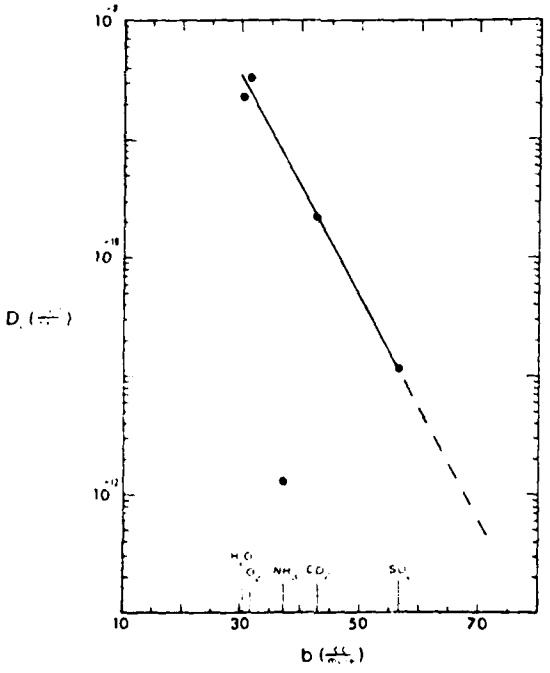

Figure 4. Correlation of diffusion coefficients at infinite dilution for various penetrants in Kapton® at 30°C, using the van der Waals volume, b, as the correlating parameter. Note that both the H_2O and NH_3 points deviate from the correlation line for the nonreactive gases.

Coupled Fickian Transport with Chemical Reaction

For cases in which a chemical reaction accompanies the diffusional invasion of the penetrant, the transient diffusion equation may be written as

$$\frac{\partial C}{\partial t} = \frac{\partial}{\partial x}\left[D(C)\frac{\partial C}{\partial x}\right] - r \qquad (4)$$

where r is the local rate of consumption of the invading penetrant by the reaction when the local penetrant concentration is C. Although the assumption of first order kinetics simplifies the analysis of the response, the pseudo first order approximation may break down and second order kinetics must be considered, when a significant fraction of the functional groups in the polymer are being consumed by the reaction. For the case where psuedo first order kinetics provides a satisfactory description of the reaction phenomenona, the approach suggested by Danckwerts[7] can be used to model the combined diffusion and chemical reaction process. The mass uptake at any time, t, per unit cross sectional area is termed M_t and can be represented by Equation (5) in such a case:

$$M_t = \left[\frac{4C_o D}{\ell}\right]\left(\sum_{n=1}^{\infty} \frac{kt}{k+\alpha_n} + \sum_{n=1}^{\infty} \frac{\alpha_n}{(k+\alpha_n)^2}\left\{1 - \exp[-t(k+\alpha_n)]\right\}\right) \qquad (5)$$

where C_o is the equilibrium solubility of penetrant in the polymer in the absence of reaction, and k and D are the local first order reaction rate constant and diffusion coefficient of the penetrant, respectively. In cases where D is concentration dependent, an average value of the coefficient, averaged over the interval from zero to C_o, may be used approximately. The film thickness, ℓ, and D and k combine to yield the composite parameter $\alpha_n = \pi^2 D(2n+1)^2/4\ell^2$. Analysis of data for M_t *vs* t permits evaluation of D and k for the system[7].

RESULTS AND DISCUSSION

Water Vapor Sorption

Sorption and desorption kinetics for water vapor in 2.0 mil Kapton® at two different activities are shown in Figures 5 and 6. The low activity run is described well by the Fickian model, and the lines through the data points were calculated using average diffusion coefficient values of 2.86×10^{-9} cm^2/sec and 2.43×10^{-9} cm^2/sec for the sorption and desorption runs, respectively. The high activity run in Figure 6 indicates that only about 98% of

the originally sorbed water could be desorbed from the film even after prolonged evacuation. The line through the sorption data in Figure 6 was calculated using Equation (5) along with a value of D = 3.609×10^{-9} cm^2/sec and k = 9.027×10^{-7} sec^{-1}. Since the concentration in the film drops rapidly in the case of desorption, relatively minor amounts of reaction should occur during penetrant removal, so the simple nonreactive desorption model represented by Equation (2) was used to calculate the line through the desorption data. For the desorption data, a value of D = 2.70×10^{-9} cm^2/sec was evaluated from the half-time formula (Equation (3)), and M_∞ was taken to be simply equal to the actual amount of penetrant desorbed from the film. Desorption times extending for very long periods (> 48 hours) failed to remove more of the sorbed water than had been removed after the 400 minutes shown in Figure 6. The effective values of the diffusion coefficients estimated from the low and high activity runs appear to be of the same magnitude. Therefore, while concentration dependence of the diffusion coefficient is clear from the fact that the normalized sorption/desorption responses do not superimpose in Figure 5, the effect is not too large. Moreover, while the diffusion

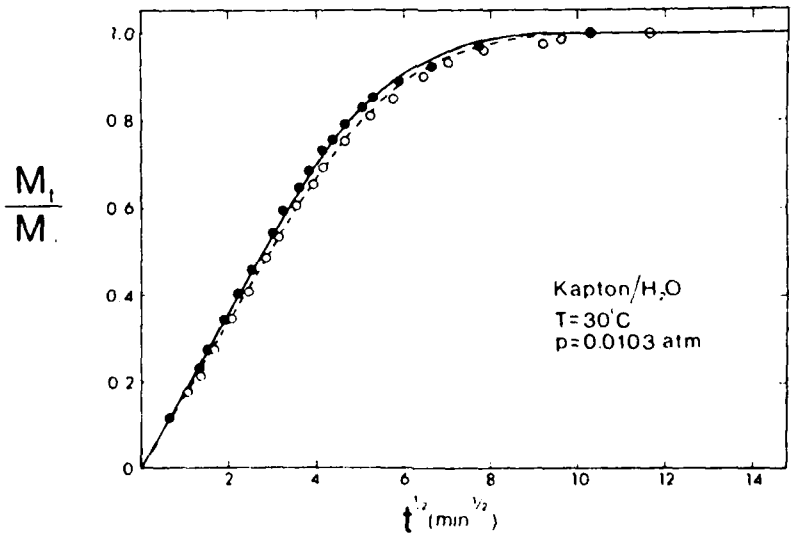

Figure 5. Low activity normalized sorption (●)/desorption (○) kinetic runs for a 2 mil Kapton® film at 30°C and at a H_2O pressure of 0.0103 atm. Note that all of the sorbed H_2O is removed during desorption.

coefficients evaluated from the low activity runs (Figure 5) are not rigorously characteristic of "zero concentration" conditions, it is clear that they do correspond to low sorbed concentration levels and their average value is reasonably consistent with the data in Figure 4 for relatively noninteracting penetrants. The fact that the diffusion coefficient for water lies somewhat below the correlation line may be due to the fact that hydrogen bonding interactions between water and imide groups tend to increase the activation energy for diffusion, thereby reducing the value of D.

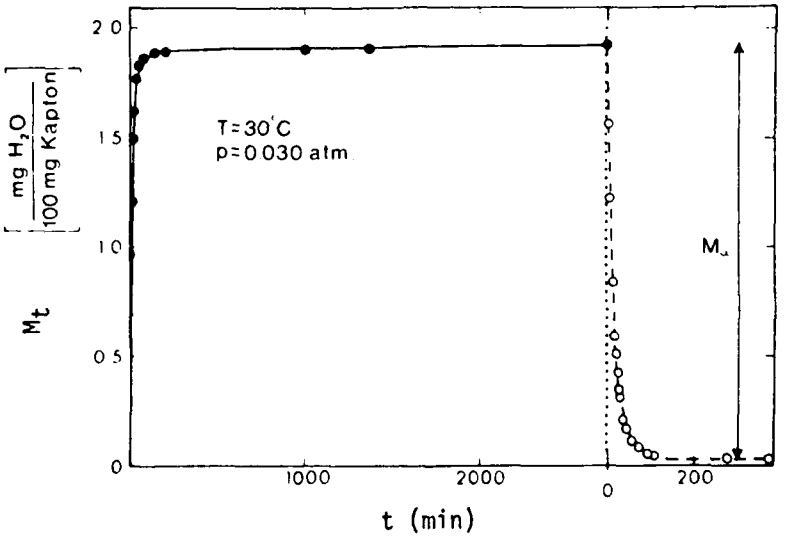

Figure 6. Sorption (●)/desorption (○) kinetic run for a 2 mil Kapton® film (high activity). Note that at desorption equilibrium (M_∞), 0.03 mg H_2O/100 mg of Kapton® remained in the film after protracted desorption under vacuum.

The small value of the reaction rate constant, k, determined from the Danckwerts analysis of the high activity run, explains why the reaction was undetectable in the low activity run. An increase in the temperature of measurement might increase the importance of the reaction significantly. These effects are currently under investigation.

Anhydrous Ammonia Sorption-0.5 mil Sample

The sorption and desorption runs shown in Figure 7 illustrates clearly that a considerably different response is observed for sorption of anhydrous ammonia in a 0.5 mil Kapton sample compared to water or SO_2. Since the van der Waals volume of ammonia is 37.1 cc/mole, one expects the effective diffusion coefficient for ammonia to be roughly 7×10^{-10} cm^2/sec on the basis of size alone. The sorption equilibration time in such a case would correspond roughly to 25 minutes (or 5 $min^{1/2}$). Clearly, the sorption process in Figure 7 is greatly protracted and is still occurring at 14,400 min (or 120 $min^{1/2}$). Furthermore, desorption for extended periods under high vacuum (approximately 12 days) is ineffective for the removal of roughly 50% of the originally sorbed penetrant.

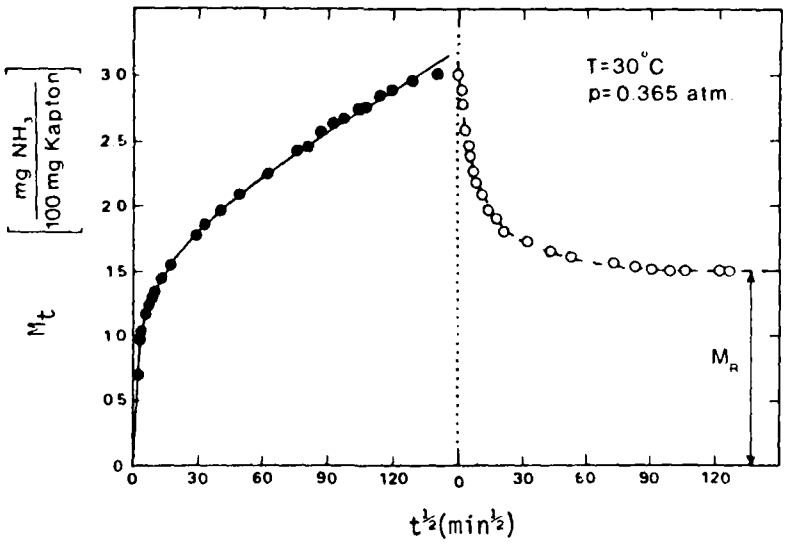

Figure 7. Sorption (●)/desorption (○) kinetic runs for a 0.5 mil Kapton® film at 30°C and at a NH_3 pressure of 0.365 atm. Note that at desorption equilibrium, 1.49 mg NH_3/100 mg of Kapton® (M_R) remained in the polymer after protracted desorption under vacuum.

As discussed earlier[4], the point of attack of ammonia appears to be the imide linkage, as illustrated below:

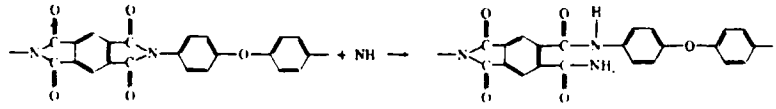

Based on the magnitude of the undesorbable component in Figure 7 (M_R), it appears that approximately 17% of the total imide groups in the sample have been attacked over the time scale of the experiment. A similar, but much less extensive reaction involving H_2O is presumably responsible for the small amount of undesorbable penetrant shown in Figure 6. In the case of water, only 0.31% of the imide groups were affected over the time scale of the experiment.

The infrared spectra shown in Figure 8 suggest that in the case of ammonia, the long term uptake leading to the undesorbable component is primarily due to random imide scission according to the above reaction. The presence of the increased absorbances in

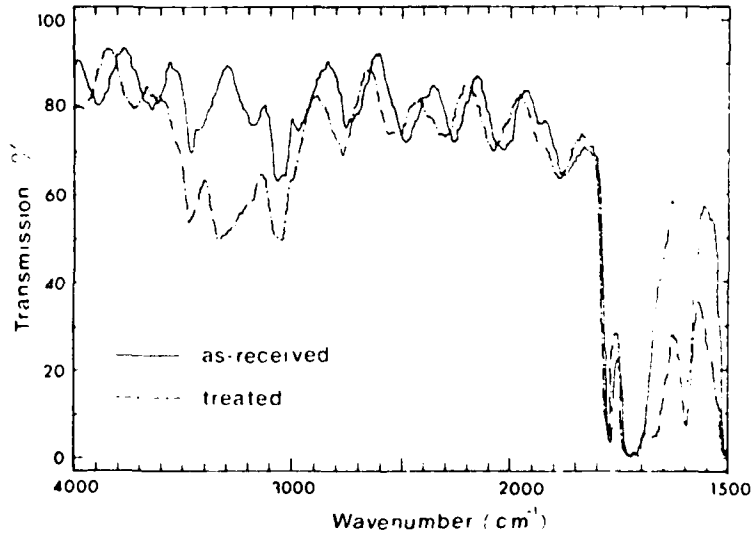

Figure 8. Infrared spectra of the as-received and the NH_3 exposed Kapton® samples. Note the increased absorbance in both the 1630-1700 cm^{-1} and 3200-3500 cm^{-1} regions, consistent with the postulated reaction between NH_3 and the imide structures.

AD-A155 605 PERMEATION OF MIXED PENETRANTS THROUGH GLASSY POLYMER 1/3
MEMBRANES(U) NORTH CAROLINA STATE UNIV AT RALEIGH
R T CHERN ET AL. 15 MAR 85 ARO-17773.15-CH
UNCLASSIFIED DAAG29-81-K-0039 F/G 11/9 NL

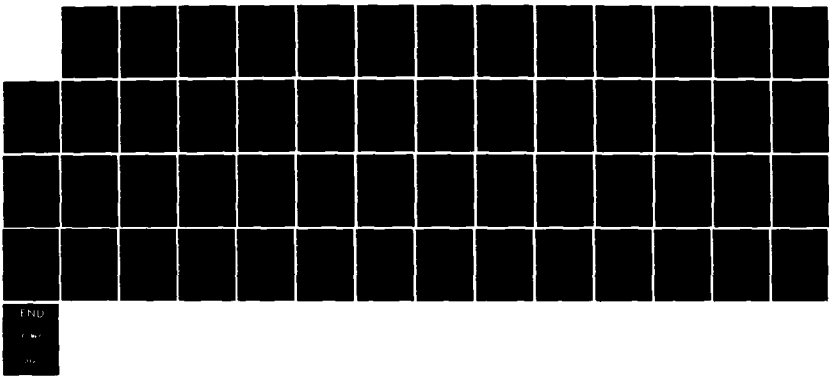

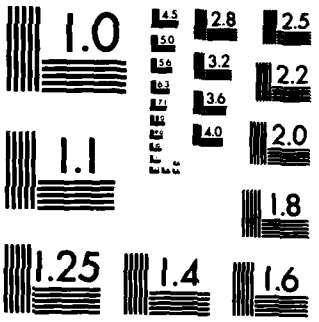

MICROCOPY RESOLUTION TEST CHART
NATIONAL BUREAU OF STANDARDS-1963-A

the range 1630-1700 cm^{-1} and 3200-3500 cm^{-1} are characteristic primary and secondary amides, consistent with the above reactic Similar infrared scans on the sample corresponding to Figure 6 revealed no significant difference from the as-received film, presumably since only 0.31% of the imide structures were affect by the water exposure.

A Danckwerts analysis of the sorption run in Figure 7 according to Equation (5) produced values for $D = 1.29 \times 10^{-12}$ cm^2/sec and $k = 3.46 \times 10^{-6}$ sec^{-1}. Again, one may assume that si the sorbed concentration drops rapidly during desorption, any continued reaction occurring during penetrant removal may be neglected to a first approximation. In this case, a value of D 2.35×10^{-11} cm^2/sec can be evaluated from the half-time formula f desorption (Equation (3)) using the actual amount of penetrant desorbed from the film for the value of M_∞.

Although the above two estimates of diffusion coefficients are not in very good agreement, it is clear that both estimates suggest that the mobility of NH_3 lies substantially below the level expected on the basis of simple size related factors. The extraordinarily low values of the NH_3 diffusion coefficient relative to water and the other "noninteracting" components in Figure 4 may arise from diffusional resistance caused by specific NH_3/polymer interactions. Such interactions may increase the effective activation energy for diffusion, thereby hampering diffusive motion.

In an attempt to resolve the reason for the large difference (a factor of 18) between the above estimates of the ammonia diffusion coefficient based on the Danckwerts analysis and the simple desorption analysis, an additional study of this system was undertaken using thin (0.3 mil) films for comparison with the 0.5 mil case.

Anhydrous Ammonia-0.3 mil Samples

As shown in Figure 9, replicate ammonia sorption runs on identical as received samples of 0.3 mil Kapton® films are highly reproducible. The desorption run for sample I in Figure 9 indicates clearly that considerable reaction has occurred even after 200 minutes for the 0.3 mil sample, since a substantial amount of ammonia (designated as $(M_R)_I$) is irreversibly retained in the film after prolonged evacuation times. By continuing the sorption experiment for 11,500 minutes with sample II and then desorbing, the irreversibly retained ammonia, $(M_R)_I$, is not increased proportionally to the reaction periods for sample I and II. It is clear, therefore, that the rate of reaction slows markedly as time progresses although only a small fraction (<14%)

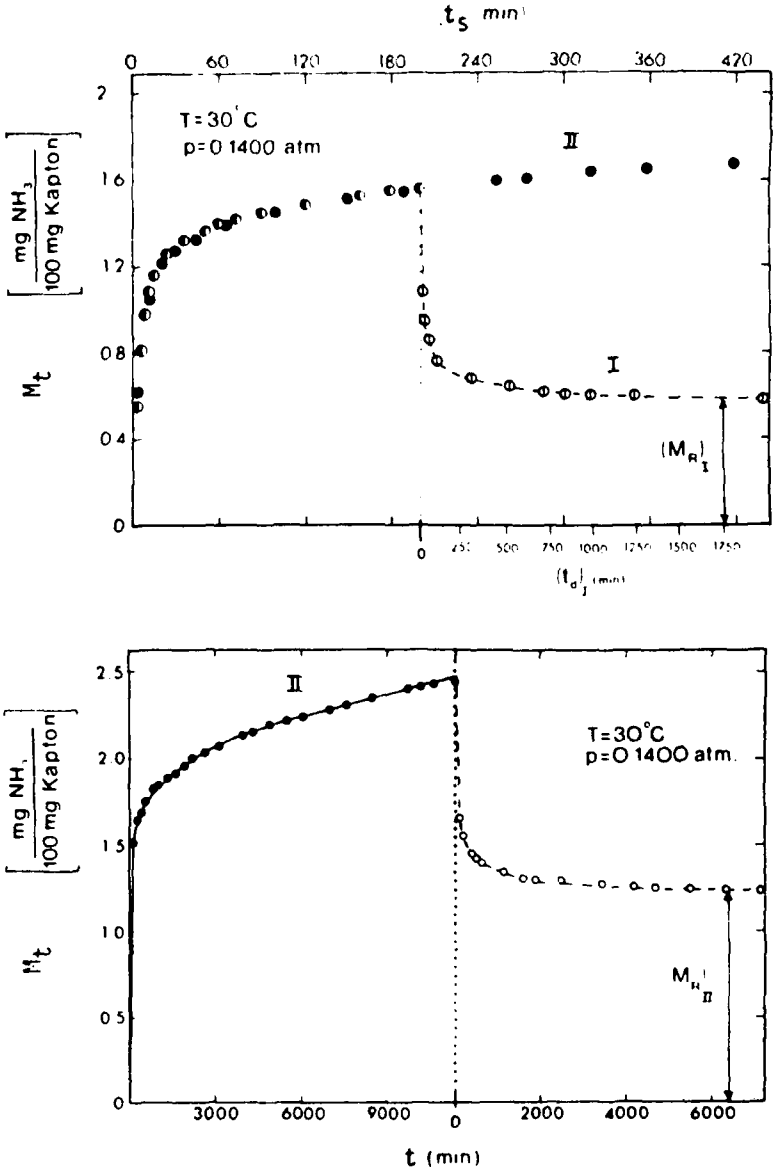

Figure 9. Replicate NH_3 sorption/desorption kinetic runs on identical as-received 0.3 mil Kapton® films (sample I - sorption (◐)/desorption (Φ); sample II - sorption (●)/desorption (○)). Note that as sorption time (t_s) is increased from 200 min (I) to 11,500 min (II), the undesorbable NH_3 increases from 0.584 mg NH_3/100 mg of Kapton® ($(M_R)_I$) to 1.234 mg NH_3/100 mg of Kapton® ($(M_R)_{II}$), respectively.

of the originally present imide groups have been attacked even for sample II.

If one performs a simple Danckwerts analysis of the short time data for sample I & II (≤200 min), values of $D = 2.9 \times 10^{-11}$ cm^2/sec and $k = 191 \times 10^{-6}$ sec^{-1} are obtained, in rather poor agreement with the 0.5 mil Danckwerts' results at higher activity. On the other hand, if one performs a Danckwerts analysis on the long term run for sample II, values of $D = 0.48 \times 10^{-12}$ cm^2/sec and $k = 3.2 \times 10^{-6}$ sec^{-1} are obtained which are in reasonable agreement with the long term run at the higher activity for the 0.5 mil sample. The k values are in very good agreement, and the somewhat higher value of the diffusion coefficient at the higher activity for the 0.5 mil sample may simply be a manifestation of the increase in D(C) with concentration (or activity). As will be discussed later, however, it is believed that the short term values of D and k are more representative of physically meaningful coefficients rather than the long term values derived for both the 0.5 and 0.3 mil samples.

From consideration of the "locked-in" concentrations shown in the short time ($(M_R)_I$) and long time ($(M_R)_{II}$) desorption plots for the 0.3 mil film, one can show that approximately 6.6% of the total imide groups have been attacked after 200 min, while 13.8% of the total imide groups have been attacked after 11,500 minutes. It appears that in both the 0.3 and 0.5 mil film the imide group reactivity drops dramatically when close to 20% of the groups have been reacted. Recall that 17% of the groups have reacted in the 0.5 mil film after close to 15,000 minutes (Figure 7), and the M_t vs t plot had flattened out greatly at that point. The above suggestion is reasonable in light of the fact that during the curing process, involving closure of the imide rings, the solid polyamic acid precursor film becomes a very rigid material whose effective Tg rises to 400°C, which is well above the 150°C curing temperatures. In such a case, the final curing process is likely to introduce a considerable amount of unrelaxed stress in the glassy polymer and thereby "labilize" a selected fraction of the imide groups. Exposure of the polymer to an agent such as NH_3 then provides a means of stress relaxation via selective imide scission. It has been shown earlier that reheating the sample to 120-150°C under vacuum causes reimidization as proven by IR spectroscopy[4].

Kapton®, therefore, has an interesting ability to combine a good barrier property with a limited, but nontrivial, capacity for scavenging of undesirable basic pollutants or residuals which might otherwise damage the component being covered by the film. The change in properties such as modulus and Tg resulting from the degradation of 5-20% of the imide groups is likely to be rather modest since the main polymer chain stays intact. This topic is

currently under study and will be reported in a later paper.

The disagreement between the values of D estimated from desorption using Equation (1) and from the standard Danckwerts analysis for the long term sorption runs in the 0.3 and 0.5 mil samples may arise from a breakdown in the accuracy of the assumed pseudo first order kinetics. If the initial concentration of "labilized" groups, C_{I_o}, amounts to only 20% of the total imide groups present, the pseudo first order expression in Equation (4) could begin to fail seriously when ammonolysis reaches 5% of the total groups (i.e., 25% of the active groups). The correct form for the reaction expression in such a case would be given by Equation (6):

$$r = k^* C_I C \qquad (6)$$

where k^* is a true intrinsic rate constant for reaction of a stress activated imide, C is the local concentration of ammonia, and C_I is the time and position dependent concentration of stress activated imide groups in the polymer. Interestingly, the instantaneous values of C_I in a reacting system does not necessarily equal the difference between the initial number of stress activated groups (C_{I_o}) and the number of reacted groups, since stress relaxation accompanying the ammonolysis may aid in deactivating some of the groups that originally would be candidates for attack. Conversely, if the film is exposed to a macroscopic external stress, additional imides may be activated compared to the unstressed film. The situation is, therefore, potentially very complex and the challenge is to simplify it to the point where useful approximate calculations are possible, at least for an unstressed film. Note from Table I that in the limit as $t \to 0$, the D's estimated from the Danckwerts' analysis and those from the desorption half time analysis become similar (200 min. run), thereby suggesting that the diffusion coefficients estimated by the two methods ($3\text{-}4 \times 10^{-11}$ cm^2/sec) are physically reasonable and consistent. It appears that the effect noted earlier (with respect to an activation energy increase due to NH_3/polymer interaction) still causes the diffusion coefficient for ammonia to fall considerably below the corrresponding line of the noninteracting penetrants in Figure 4.

The above conclusions are reasonable since it is clear that by considering only short time cases (such as in Figure 9) using the Danckwerts analysis, the psuedo first order reaction assumptions become valid. Evaluation of $k^* C_I$ for a series of short run times, followed by extrapolation of the values back to $t=0$ will then permit estimation of $k^* C_{I_o}$, characteristic of the inherent as-received film. The value of C_{I_o} initially can be estimated independently by performing a series of long term measurements and noting the asymptotic limit to which the

undesorbable component appears to be approaching. On the basis of the limited measurements performed here, it appears that this number corresponds to roughly 20% of the originally present imide links at 30°C. This corresponds to $C_{I_o} = 1.5 \times 10^{-3}$ mole activated imides /cc. If one assumes that the value of $k = k^* C_I$ determined from the 200 minute Danckwerts' run is reasonably representative of the initial value, then the value of the intrinsic rate constant, k^*, can be calculated to be 0.13 cc/mole sec. Clearly, using these parameters (or more carefully determined ones as outlined above), the complete M_t vs t response can be derived by straightforward numerical methods for any film thickness or external vapor activity of interest. Similarly, by evaluation of the temperature dependence of D and k^* (and C_{I_o} if necessary), the analysis can be extended to cover a wide range of temperatures as well. These numerical calculations are underway and will be described in a future paper.

Table I: Kinetic Parameters $D_{Danckwerts}$, k and $D_{Desorption}$ for H_2O and NH_3 Sorption in Kapton® Polyimide at 30°C.

Penetrant	Film Thickness (mils)	$t_{SORPTION}$ (min)	$D_{DANCKWERTS}$ (cm^2/sec)	k (sec^{-1})	$D_{DESORPTION}$ (cm^2/sec)
H_2O	2.0	2750	3.6×10^{-9}	9.03×10^{-7}	2.7×10^{-9}
NH_3	0.5	14,400	1.29×10^{-12}	3.46×10^{-6}	2.35×10^{-11}
	0.3	200	2.9×10^{-11}	191×10^{-6}	3.97×10^{-11}
		11,500	0.48×10^{-12}	3.2×10^{-6}	1.25×10^{-11}

CONCLUSIONS

Kapton® polyimide displays an interesting range of transport behaviors at 30°C ranging from simple Fickian diffusion to coupled diffusion with chemical reaction. The relatively noninteracting penetrants, SO_2, CO_2 and O_2 exhibit diffusion coefficients whose magnitudes can be correlated well on the basis of the relative molecular sizes of the penetrants. In the case of water, some evidence for physical (hydrogen bonding) and weak chemical interactions were observed. These interactions appeared to reduce the effective diffusion coefficient slightly for water in the film compared to the coefficient expected strictly on the basis of size alone. Polymer/penetrant interactions can, in principle, reduce the effective diffusion coefficient by increasing the average activation energy required for the penetrant to execute a diffusional jump. Based on the Eyring theory of rate processes, an increase in activation energy will tend to reduce the diffusion coefficient.

In the case of ammonia sorption into Kapton®, substantial chemical interactions are apparent. Infrared spectroscopy and gravimetric sorption/desorption measurements were effective for monitoring the ammonolysis reaction. The point of ammonia attack appears to be selected imide groups which comprise a relatively small fraction (~20%) of the total imide group population present in the initially cured film. It is suggested that a fraction of the imide groups become "activated" or "labilized" during the final solid state curing step in which unrelieved stresses may be introduced. The ammonolysis reaction serves to relieve these stresses and thereby deactivate the remaining imide groups substantially. It appears, therefore, that Kapton® has a useful ability to combine good barrier properties (low D's (Figure 1)) with an additional nontrivial capacity for scavenging undesirable basic pollutants or other residuals that might otherwise damage the component being protected. A complementary approach might be used to protect against the invasion of an acidic component (e.g., H_2S) by using a film with a stress-activated acid sensitive group.

ACKNOWLEDGEMENT

The authors gratefully acknowledge the financial support of this project by the Army Research Office under Grant Number DAA29-81K-0039.

REFERENCES

1. W. J. Koros, C. J. Patton, R. M. Felder and S. J. Fincher, J. Polym. Sci.: Phys. Ed., 18, 14 (1980).
2. W. J. Koros, J. Wang and R. M. Felder, J. Appl. Polym. Sci., 19, 2805 (1981).
3. R. M. Felder, C. J. Patton and W. J. Koros, J. Polym. Sci.: Phys. Ed., 19, 1895 (1981).
4. L. R. Iler, R. C. Laundon and W. J. Koros, J. Appl. Polym. Sci. 27, 1163 (1982).
5. J. Crank, "The Mathematics of Diffusion", Second Edition, Clarendon Press, Oxford, 1975.
6. A. R. Berens, J. Vinyl Technol., 1(1), 8 (1979).
7. P. V. Danckwerts, Trans. Faraday Soc., 47, 1014 (1951).

SIMULATION OF A HOLLOW FIBER GAS SEPARATOR: THE EFFECTS OF PROCESS AND DESIGN VARIABLES

by

Rey. T. Chern*, William. J. Koros and Peter. S. Fedkiw

Department of Chemical Engineering
North Carolina State University
Raleigh, NC 27695

ABSTRACT

A model is developed for simulating the performance of an isothermal hollow fiber gas separator. The model equations are solved numerically as a boundary-value problem. Permeate pressure build-up has been considered explicitly and concentration dependence of the permeabilities are taken into account using the dual-mode sorption and transport models. The effects of possible penetrant competition according to the generalized dual mode model are also examined. Utility of the computational results for separator module design is emphasized for various case studies using "characteristic curves" which represent the relation between degree of separation and fast-gas recovery. The effects on separator performance caused by changes in fiber dimensions (inside diameter, outside diameter and length), feed pressure, membrane area (number of fibers), feed composition and feed flow rate are presented. A triple-separator arrangement for the separation of a 12 %/88 % CO_2/CH_4 mixture is also discussed to illustrate how the results of single-stage studies can be readily extended to multistage design considerations.

---

* Author to whom correspondence should be addressed.

INTRODUCTION AND BACKGROUND

Successful application of membranes for separation purposes depends upon discovery of economically competitive membranes with high permselectivities and permeabilities. On the other hand, engineering considerations such as membrane configurations and flow patterns of the feed and permeate streams are also important in determining the performance of the final separator system. Recognition of this fact is reflected by the numerous modeling studies reported in the literature, Weller and Steiner (1950), Naylor and Backer (1955), Oishi et al. (1961), Stern et el. (1965), Breuer and Kammermeyer (1967), Walawender and Stern (1972), Blaisdell and Kammermeyer (1973), Pan and Habgood (1974), Hwang and Kammermeyer (1975), Stern (1976), Antonson et el. (1977), Stern and Wang (1978), Pan and Habgood (1978), and Stern (1979). In most studies, however, emphasis has been focused primarily on the calculation techniques and comparison between different idealized flow patterns. The present paper will emphasize the effects of various design and process variables on separator performance and consider the implications for optimal hollow fiber separator design. Due to the large number of possible flow arrangements, the discussion in this paper will be confined to a countercurrent, shell-feed, hollow fiber separator. However, the general approach can be applied, with slight modifications, to other situations including spiral-wound or flat membrane systems.

Hollow fibers

The inside (ID) and outside (OD) diameters of typical fibers are in the ranges of 80 to 300 μm and 300 to 1000 μm, respectively, and the length has been reported to be up to 16 ft, Gerow (1974), Klein et al. (1977). Due to the small cross section, a large number of fibers can be packed into separators with moderate diameters to provide a large membrane area per unit volume (>10,000 m^2/m^3), Gerow (1974). In contrast to flat membranes, hollow fibers are self-supporting. The maximum external or internal pressures at which they can be operated are determined by the modulus of the membrane material, the ratio of fiber OD and ID, and the detailed structure of the asymmetric membrane. An approximate analysis can be made by assuming the hollow fiber to be a homogeneous and isotropic elastic tube as suggested by Stern et al. (1977), Varga (1966) and Thorman et al. (1978).

The selective dense layer on the outside region of the hollow fiber is normally very thin (<1,500Å) and fragile. Unless the elastic modulus of the material is large, the dense layer may be ruptured by the dilation action when the fiber is pressurized internally. The shell-feed mode in which the fiber is pressurized externally, consequently is of most commercial interest.

When operated at high permeation rates, pressure build-up in the fiber bore is substantial for smaller fibers(e.g. <100 μm). The increase in bore-side pressure will deminish the permeation driving pressure differences across the membrane wall and will lower the overall production rate and undermine selectivities compared to cases with milder

pressure profiles even if the operating conditions are the same. Optimization of fiber dimensions (diameter and length) becomes particularly important for these systems.

Permeability

The permeability and selectivity of an asymmetric membrane can be affected not only by the dense layer, but also by the porous sublayer. Moreover, even the permeability of the dense layer is subject to complications caused by gas phase pressure and composition variations particularly when the selective layer of the membrane is made of glassy polymers, Chern et al. (1983, 1984). Time dependent behavior, presumably associated with compaction of the porous support layer of the spiral-wound asymmetric membrane, has been observed by Coady and Davis (1982). These effects are likely to be equally important for both flat membranes and hollow fibers. Well characterized experimental data regarding the effect of asymmetry of membrane structures are generally lacking although a useful simplified mathematical description has been performed by Sirkar (1977). For simplicity, in the following model development, the effect of asymmetry will be neglected, and the dual-mode transport model will be used to represent the apparent permeability of penetrant i. The dual-mode transport model postulates that the diffusive flux of a penetrant is the sum of two contributions: one contributed by the concentration gradient of the dissolved mode, the other is due to the concentration gradient of the additional mode in the microvoids of the glassy polymer. The observed pressure and composition dependency of the

permeabilities of gas mixtures can be attributed to competition between penetrants for the limited microvoid sorption capacity in the glassy polymer. The local permeation flux of penetrant A according to this model is:

without competition

$$N_A = \frac{D_{DA}}{(\frac{ID}{2})\ln\frac{OD}{(OD-2\ell)}} \left[k_{DA}(p_2y_{2A}-p_1y_{1A}) + F_A\left(\frac{C'_{HA}b_Ap_2y_{2A}}{1+b_Ap_2y_{2A}} - \frac{C'_{HA}b_Ap_1y_{1A}}{1+b_Ap_1y_{1A}}\right)\right] \quad (1)$$

with competition

$$N_A = \frac{D_{DA}}{(\frac{ID}{2})\ln\frac{OD}{(OD-2\ell)}} \left[k_{DA}\left(p_2y_{2A}-p_1y_{1A}\right) + F_A\left(\frac{C'_{HA}b_Ap_2y_{2A}}{1+b_Ap_2y_{2A}+b_Bp_2y_{2B}} - \frac{C'_{HA}b_Ap_1y_{1A}}{1+b_Ap_1y_{1A}+b_Bp_1y_{1B}}\right)\right] \quad (2)$$

Definition of terms is summarized in the NOTATION Section. Of course, other empirical or theoretical expressions for the pressure and composition dependence of the permeability could also be used.

MODEL DEVELOPMENT

Major assumptions made in the development of the model equations are:

1. Isothermal operation with shell-feed and negligible pressure drop in the shell side.
2. The differential form of the Hagen-Poiseuille equation is valid for

describing the permeate stream pressure variation inside the fiber bore. This is based on Berman's study of incompressible laminar flow in permeable tubes with constant injection at the tube wall, Berman (1953). Pan and Habgood (1978) suggested that as long as the parameter (tube ID)(local permeate flux)/(viscosity) is smaller than one, it is a reasonable approximation. This assumption was also adopted by Antonson et al. (1977) and Chern (1983). On the other hand, Thorman and Hwang (1978) have combined expressions for compressible flow in an impermeable tube and incompressible flow in a permeate tube using a first-order perturbation technique to describe the momentum balance. Direct experimental verification of the above two approaches has, however, not been reported.

3. The permeability of the selective layer to each penetrant obeys the dual-mode transport model (Eqs 1 and 2). Eq 1, with $p_1=0$, has been used successfully to describe pressure dependent permeabilities generally observed for pure gas permeation in glassy polymers in the absence of strong plasticization effects, Chern et al. (1983). Eq 2 will be used to evaluate the importance of penetrant-competition for a binary mixture.
4. The porous sublayer has a negligible resistance to permeation.
5. Negligible gas-phase concentration gradients exist in the permeation direction; i.e., no concentration polarization.
6. Both the feed and the permeate streams are plug-flow and rapid radial mixing occurs such that the gas phase composition next to the permselective membrane is equal to that in the bulk stream.

Pan (1983) has raised some doubts regarding the validity of assumption 6 when high flux asymmetric membranes are used. He proposed that local fluxes should be similar to the characteristics of cross flow pattern for the high flux asymmetric membrane used in his experiment; i.e., the local flux is not affected by the bulk composition of the permeate. For a He/CH_4 mixture with Y_{He}= 0.82%, Pan (1983) reported that the performance of a separator operated at low stage cut (< 3%) are roughly the same for countercurrent and cocurrent flow arrangements.

Slight modifications in the following model equations will be required if the validity of assumption 6 is in doubt. However, due to the unavailability of quantitative information regarding the resistance of the porous support layer, no further discussion will be pursued in this paper. Although the computational results will be different from those presented below if assumption 6 is not valid, similar parametric analyses could be adopted for generating useful information for design purposes.

The highly idealized picture in accord with assumptions 1, 2 and 3 is depicted in Figure 1. It is equivalent to postulating that different asymmetric hollow fibers with different ID can be prepared with a fixed "effective" thickness of the dense layer possessing the same permeability characteristics. As a result, for a fixed driving pressure across the fiber wall, the "permeation rate" depends on the effective thickness of the dense layer, but is not affected by the value of ID. This idealization will allow an independent investigation of the effects of fiber ID, free from complications due to changes in permeation resistance

of the fiber wall.

Model Equations

Antonson et al. (1977) and Pan and Habgood (1978) have developed model equations for constant-permeability systems and solved them as an initial-value problem for design calculations where the length of the separator was to be determined. However, the length of fibers normally is predetermined by other design considerations such as permeate pressure build-up and module fabrication cost. The advantage of being able to treat the fiber length as a dependent variable for determining the overall membrane area requirement is, consequently, largely diminished. That is, practically, membrane area for a given separation task will be provided by controlling the total number of fibers of predetermined length in a separator module and the number of modules to be used.

Since the material and momentum balances for the countercurrent arrangement is intrinsically a boundary-value problem, Chern (1983) has proposed an alternative approach using a boundary-value algorithm for finite-difference equations as developed by Newman (1973). This latter method can be readily extended to multicomponent systems without rearranging the original material and momentum balances (c.f. Pan Habgood (1978)). According to the schematic diagram shown in Figure 2, the following equations can be written:

Bore-side material balance

$$\frac{d\, m_{pA}}{dz} = [N_A \pi ID][1 - H(z-z_w)] \quad (3)$$

$$\frac{d\, m_{pB}}{dz} = [N_B \pi ID][1 - H(z-z_w)] \quad (4)$$

where $H(z-z_w)$ is the unit step-function which is needed since there is no permeation in the potted section of the fiber; N_A and N_B are as given in Equations 1 or 2 depending on whether competition effect is considered or not.

Bore-side momentum balance (Hagen-Poiseuille equation)

$$\frac{d(p_l^2)}{dz} = \frac{256\, R\, T\, m_p\, \mu}{ID^4\, \pi} \quad (5)$$

The local molar flow rate of component i in the permeate and in the shell side per fiber are represented by m_{pi} and m_{fi}, respectively; m_p is the total molar flow rate in the fiber; R is the gas constant; and μ is the viscosity of the gas mixture which is calculated according to the expressions suggested by Reid et al. (1977)

The boundary conditions for equations (3) and (4) are set at $z = 0$, yet that for equation (5) is set at $z = z_L$

$$z = 0 \qquad m_{pA} = m_{pB} = 0 \tag{6}$$

$$z = z_L \qquad p_1 = p_{1,L} \tag{7}$$

The overall material balances for components A and B at any location z in the fiber are the remaining balance equations required

$$m_{fA} = m_{fA,0} + m_{pA} \tag{8}$$

$$m_{fB} = m_{fB,0} + m_{pB} \tag{9}$$

Equations (8) and (9) are used to determine the local shell-side partial pressures of A and B for use in N_i since $Y_{2i} = m_{fi}/(m_{fi} + m_{fj})$.

Equations (3), (4) and (6) with equations (5) and (7) constitute a boundary-value problem. However, since the equations are coupled and since the shell-side molar flowrates are known only at z_L, two additional, trivial ordinary differential equations are introduced to utilize Newman's procedure.

$$\frac{d(m_{fA,0})}{dz} = 0 \tag{10}$$

$$\frac{d(m_{fB,0})}{dz} = 0 \tag{11}$$

which are subject to the boundary condition at z_L, respectively:

$$m_{fA,0} + m_{pA,z_L} = m_{fA,f} \tag{12}$$

$$m_{fB,0} + m_{pB,z_L} = m_{fB,f} \tag{13}$$

Equations (10) and (11) along with (3), (4) and (5) were solved as a coupled boundary-value ordinary differential equation system of 5 unknowns after non-dimensionalization and linearization. The detailed operations were described by Newman (1973) and White (1978).

The linearized forms of Eqs 3 through 11 together with the boundary conditions listed above can be used directly for solving the typical performance-evaluation problem. Namely, the pressure, composition and flow rate of the feed stream and the premeate pressure are assigned. The task is to determine the flow rate and composition of the residue and the permeate streams for a given separator. For design calculations, for example, if membrane area is unknown but the ratio of the permeate flow rate to the feed flow rate is assigned, one needs to include either an interpolation or an optimization scheme in the main program since a systematic variation of the coefficients in these equations will be required.

Note that the potted length (z_L-z_w) does not contribute to the separation but instead provides extra length for permeate pressure build-up. Clearly, it should be made as short as allowed by module integrity and leak-free considerations.

COMPUTATIONAL RESULTS AND PARAMETRIC STUDIES

Separator specifications used in the calculation are shown in Table 1 unless stated otherwise. Experimental permeability data in terms of the dual-mode parameters which have been reported by Toi et al. (1982), Erb and Paul (1981), and Koros et al. (1977) are summarized in Table 2.

Characteristic Curves A very informative presentation of the performance of a given type of separator is to plot the fast-gas (the

higher permeability penetrant) concentration in the permeate product and the slow-gas concentration in the residue product as functions of the fractional fast-gas recovery into the permeate product. These curves will be called the "characteristic curves" and will be used to indicate the effects of varying one of the several important design and operating variables.

Fiber Dimensions and Pressure Build-up in the Fiber Bore As apparent from Eq 5, friction loss in the fiber bore can be significant if the bore diameter is small and the permeate flow rate (m_p) is high. In Figure 3(a), the "driving" pressure ($\Delta p_i = p_{2i} - p_{1i}$) profiles of CO_2 for three different fiber bore sizes (ID=50, 100 and 150 μm) are compared with the case where permeate pressure is constant. Permeability data for polysulfone are used in the calculation; the separator dimensions are shown in the figure caption and in Table 1. Except for fiber ID, all the other operating variables are the same for the four cases. The constant-permeate-pressure results can easily be obtained by letting Eq 5 equal to zero while keeping all the other equations intact; it corresponds to the most favorable driving pressure profile at the given operating conditions. The loss of CO_2 driving pressure toward the residue end for this latter case is due solely to depletion of CO_2 from the feed stream as more and more CO_2 molecules permeate to the bore side of the fiber. Partial pressure profiles of CO_2 in the shell and the tube sides are contrasted in Figure 3(b) for two extreme cases; one with significant permeate pressure build-up, the other with negligible pressure build-up.

The deleterious effects of diminished CO_2 partial pressure difference are reflected in the characteristic curves shown in Figure 4. If the feed is lean in CO_2, the separator with ID=150 μm produces much higher purity permeate product at the same CO_2 recovery. The difference is not as great when the feed stream is rich in CO_2. This is understandable since the permeate purity is determined by the relative permeation fluxes of the fast- and the slow- gases. If the feed is originally rich in CO_2 and the feed pressure is reasonably high, the said ratio will not be drastically decreased in the presence of permeate pressure build-up.

Due to reduction in the driving force when smaller fiber is used, much larger membrane area is needed to affect the same CO_2 recovery from a given feed rate even if the feed is rich in CO_2, as shown in Figure 5. For the system in Table 3, more than two-fold decrease in the permeate production rate results from a change in ID from 150 to 50 μm while the permeate and the residue purities are lowered by 5.7% and 27%, respectively. This reduction in permeate production capacity is caused mainly by the decrease in CO_2 recovery. There is also dramatic increases in the CH_4 driving pressure (Δp_{CH_4}) across the fiber wall as shown in Figure 6 when larger fiber ID is used. However, due to the much lower permeability of CH_4, the ratio of the CH_4 recovery to the CO_2 recovery is actually decreased with increasing ID values, even if the CH_4 recovery itself increases from 3.8 to 5.2% as indicated in the last column of Table 3.

Smaller fiber outside diameters with a fixed ID will lower the permeate flow rate per fiber roughly proportionally with a concomitant decrease in permeate pressure build-up if the characteristic thickness remains the same. It will also increase more than proportionally the number of fibers which can be accomodated in a module of a given diameter. The net result is higher permeate production capacity per unit volume and higher permeate purity at the same fast-gas recovery. Clearly, in principle, fibers with small OD and large ID should be used. The absolute values of these two dimensions will depend on the magnitude of the expected permeate flow rate per fiber and certainly the fabrication technology and mechanical strength considerations.

Whenever the permeate pressure build-up is expected to be nontrivial, care should be taken to avoid excessive fiber length. This is illustrated in Table 4 where a fiber with ID=50 μm is used. Due to the permeate pressure build-up, doubling the total membrane area by increasing the fiber length results in no significant improvement in module performance. On the other hand, for the case with no permeate pressure build-up, a two-fold increase in fiber length results in roughly 60% more permeate with a slight deterioration in its purity as also shown in Table 4.

Feed Composition The effects of feed composition variations on separator characteristics are illustrated in Figure 7. The permeate product purity is sensitive to the initial fast-gas mole fraction particularly when the feed is relatively lean in the fast-gas as

indicated by the significant change from curve 1 to curve 2 in Figure 7. The residue characteristic curves converge towards unity as the CO_2 recovery approaches one while the permeate characteristic curves asymptote to their respective limiting values at zero CO_2 recovery. This limiting permeate product purity is determined by the feed composition, operating conditions, separator dimensions and membrane selectivity.

Membrane area required to effect the same fractional fast-gas recovery is also sensitive to feed stream composition as shown in Figure 8. There is little difference in area requirement for feeds with CO_2 mole fraction greater than 0.45 when the separator is operated at smaller than 0.3 CO_2 recovery. However, the difference increases significantly at higher recoveries because Δp_{CO_2} along the fiber length is higher for a more concentrated feed. Together with higher attainable permeate product purity discussed earlier, this explains largely why available reports indicate that the membrane process is more competitive with conventional processes when the feed has a higher fast-gas concentration, Youn et al. (1982), Goddin (1982).

Feed Pressure The effects of feed pressure on the performance of a separator is shown in Figure 9. Raising the feed pressure results in a higher purity permeate product at the same CO_2 recovery, although the extent of the increase diminishes at higher feed pressures. Interestingly, the residue characteristic curve of CH_4 is rather insensitive to the feed pressure at fixed CO_2 recoveries. Due to the low permeability of polysulfone to CH_4, the amount of CH_4 lost to the

permeate is low enough such that higher feed pressure does not significantly change the residue composition at the same fractional CO_2 recovery. The relative membrane area requirement for different feed pressures is compared in Figure 10. Clearly, less membrane area is needed to affect the same CO_2 recovery whenever higher feed pressure is used.

The Effects of Composition Dependent Permeability There are some experimental data indicating the existence of competition between penetrants in accordance with the postulations of the generalized dual-mode transport model (Eq 2), Chern et al. (1983). It is of interest then to examine the magnitude of this competition effect on the overall performance of an actual separator. This is illustrated in Tables 5 and 6 where the performance of the same separator is evaluated based on both the "competition" and "no-competition" assumptions (Eqs 2 and 1, respectively). As expected, competition of penetrants for the available sorption sites in the polymer results in lower permeate production rate.

In Table 5, competition actually results in higher permeate purity which is also indicated by the local CO_2/CH_4 wall flux ratios. The change in separator performance as reflected in the values of stage-cut, permeate purity, residue purity and permeate production rate is, however, relatively small (<5%) for the CO_2/CH_4 mixture/polysulfone system shown in Table 5. The effects are somewhat more significant for the He/CH_4 mixture/polycarbonate system. Roughly a 14% decrease in the permeate

purity results from competition when the feed is dilute in He (such as many natural gases). For a feed containing relatively higher concentration of He, the change returns to the 5 to 6% level as shown in Table 6.

Application of the Single Stage Analyses Although multiple-separator design is not the main theme of this paper, the following discussion is intended to illustrate the utility of the previous single-stage analyses. Typical of all rate-determined unit operations, membrane separation suffers the depletion of separating driving force (i.e. partial pressure difference) along the unit. As shown in Figures 4, 7 and 9, even with a fairly permselective membrane, high purity permeate product can not be produced using a single-stage separator unless CO_2 partial pressure in the feed stream is maintained sufficiently large.

For systems such as in helium recovery from natural gas where the initial concentration of He is normally <1%, multiple-compression stages are often necessary. Moreover, if both high-purity permeate and residue products are desirable, additional stripping stages would be required, though not necessarily compression stages. The "continuous" membrane column originated by Pfefferle (1964) and refined by Hwang and Thorman (1980) and Thorman (1979) is an exception (where each unit includes one stripping module and one enriching module with very large permeate product recycle).

Since systems with more than three compression stages have been reported to be unattractive with respect to both capital and operating cost, a conventional cascade design with three stages will be discussed. Figure 11 is an example of one of many possible schemes for producing high-purity CH_4 and CO_2 products from a CO_2/ CH_4 mixture with $Y_{CO_2} = 0.12$. Permeability data of dense polysulfone at 35° C are used in the calculation. Other pertinent data are indicated in the figure and Tables 1 and 2.

Feed pressures of the various stages are determined according to the characteristic curves similar to those shown in Figure 9 for different feed compositions. For the enriching section, the objective is to find the minimum feed pressure needed to produce permeate product of desired purity when the separator is operated at a reasonable CO_2 recovery, given the anticipated range of feed rate. This procedure can be carried out as long as the dimensions of the hollow fibers are predetermined, which is a typical case. As indicated in Figure 9, except for low feed pressure ranges (or more precisely, the ratio p_{2f}/p_{1L}) and very high CO_2 recoveries, the permeate product purity is not very sensitive to the feed pressure. Consequently, it is not difficult to choose this near-optimal feed pressure and membrane area for a given feed and fiber dimensions.

For the stripping section, the objective is to minimize area requirement and CH_4 loss to the permeate stream. As already shown in Figures 9 and 10, higher feed pressure lowers the membrane area requirement while affecting only slightly the residue purity. The residue purity is primarily dependent on the feed composition as

indicated in Figure 7, but higher feed pressure will hasten the depletion of CO_2 and thus decrease the loss of CH_4 to the permeate stream for a target residue purity. The feed pressures of the stripping stages are then determined by a balance between costs associated with membrane area, compression and CH_4 losses.

The two parallel modules in the feed stage are used to strip as much CO_2 as possible while producing a permeate product of slightly more than 60 mole % CO_2. This target CO_2 mole fraction is determined from the characteristic curve (curve 3) in Figure 7. Clearly, at the given conditions, a feed stream of at least 60 % CO_2 is needed for producing a final permeate product of greater than 95% CO_2 from the second compression stage at a reasonably high CO_2 recovery . On the other hand, no further compression is required in the stripping section where it is relatively easy to produce a residue product of greater than 98% CH_4. Again we resort to the characteristic curves and choose the minimum CO_2 recovery to minimize CH_4 loss while keeping the residue purity above 98% CH_4.

In general, the feed-stage in a cascade should be operated at maximum recovery of the most permeable component(s) while maintaining a high enough purity such that few enriching stages will be required to satisfy the final permeate purity. This would maximize fast-gas production, and minimize waste of membrane area and recompression of the recycled permeate stream(s) in the stripping section.

To ensure reasonable process flexibility for handling feed rate and composition fluctuations, several optional designs may be included; for example, (A) feed pressures to the various stages may be allowed to change over a range of values, (B) part of the final permeate product may be recycled to the feed port of the last enriching stage to boost its feed concentration as reported by Pan and Habgood (1978) and Teslik and Sirkar (1981), and (C) some limited independent manipulation of stage cut may be provided by using several parallel smaller modules in each stage which can be turned on or off according to process requirements. The last option may not be very desirable because of increased module cost. Option (B) is a viable means of increasing the purity of the final permeate product but it also causes significant reductions in the overall permeate production rate and increases in the compression load. Option (A) appears to be the most effective approach for providing process flexibility. However, a combination of these options may be needed if the feed rate and composition fluctuate significantly.

CONCLUSIONS

Treating the model equations as a boundary-value problem is shown to be an effective approach for membrane separator design calculations. Other than the obviously important variables such as the thickness of the selective layer and membrane permeability, fiber ID, OD and length are shown to be very important in determining the performance of the final separator module. In particular, for a given fiber outside diameter it

is clear that large fiber ID should be used in order to minimize permeate pressure build-up which is deleterious in terms of both productivity and selectivity. The mechanical strength certainly must be considered as well, but even with moderately permeable membranes, an inside diameter smaller than 100 microns can be undesirable. This consideration is even more important for membranes with higher permeabilities. Pressure and composition dependence of the penetrant permeabilities as described by the dual-mode transport model (Eqs 1 and 2) has been included in the model equations. Under the same operation conditions, inclusion of penetrant-competition (Eq 2) results in roughly 5 to 14% change in most of the dependent variables compared with the "no competition" case (Eq 1) for the systems examined. Finally, an example of a multiple-separator system is given to emphasize the importance of the single stage analyses.

ACKNOWLEDGEMENT

The authors gratefully acknowledge support of this work under ARO Grant No. DAAG29-81-K-0039.

REFERENCES

1. Antonson C.R., Gardner R.J., King C.F. and Ko D.Y., Ind. Eng. Chem., Process Des. Dev., 1977, 16(4), 463.

2. Berman A.S., J. Appl. Phys., 1953, 24(9), 1232.

3. Blaisdell C.T. and Kammermeyer K., Chem. Eng. Sci., 1973, 28, 1249.

4. Breuer M.E. and Kammermeyer K., Separ. Sci., 1967, 2(3), 319.

5. Chern R.T., Koros W.J., Sander E.S. and Yui R., J. Membr. Sci., 1983, 15, 157.

6. Chern R.T., Koros W.J., Sanders E.S., Chen S.H. and Hopfenberg H.B., ACS Symposium, "Industrial Gas Separations", 1983, 223, 47.

7. Chern R.T., Measurement and Modeling of Mixed Gas Permeation in Glassy Polymers", Ph.D. dissertation, North Carolina State University, Raleigh, 1983.

8. Chern R.T., Koros W.J., Yui B., Hopfenberg H.B. and Stannett V.T., J. Polym. Sci., Phys. Ed., 1984, 22(6), 1061.

9. Coady A.B., Davis J.A., Chem. Eng. Progress, 1982, 78(10), 44.

10. Erb A.J. and Paul D.R., J. Membr. Sci., 1981, 8, 11.

11. Gerow J.A., US Patent 3,832,830, Sep. 3, 1974.

12. Goddin C.S., Hydrocarbon Process, 1982, 61(5), 125.

13. Hwang S.T. and Kammermeyer K., "Membranes in Separations", Wiley-Interscience, NY, 1975.

14. Hwang S.T., Thorman J.M. and Yuen K.M., Separ. Sci. Technol., 1980, 15(4), 1069.

15. Hwang S.T. and Thorman J.M., AIChE J., 1980, 26(4), 558.

16. Hwang S.T. and Ghalchi S., J. Membr. Sci., 1982, 11, 187.

17. Klein E., Smith J.K. and Morton F.C., US Patent 4,051,300, Sep. 27, 1977.

18. Koros W.J., Chan A.H. and Paul D.R., J. Membr. Sci., 1977, 2, 165.

19. Naylor R.W. and Backer P.O., AIChE J., 1955, 1, 95.

20. Newman J.S., "Electrochemical systems", Prentice-Hall, NJ, 1973, p.414.

21. Oishi J., Matsumura Y., Higashi K. and Ika C., J. Atomic Energy Soc.(Japan), 1961, 3, 923.

22. Pan C.Y. and Habgood H.W., Ind. Eng. Chem. Fundam., 1974, 13(4), 323.

23. Pan C.Y. and Habgood H.W., Can. J. Chem. Eng., 1978, 56, 197.

24. Pan C.Y., Jensen C.D., Bielech C. and Habgood H.W., J. Appl. Polym. Sci., 1978, 22, 2307.

25. Pan C.Y., AIChE J., 1983, 29(4), 545.

26. Pan C.Y. and Habgood H.W., Can. J. Chem. Eng., 1978, 56, 210.

27. Pfefferle W.C., US Patent 3,144,313, 1964.

28. Reid R.C., Prausnitz J.M. and Sherwood T.K.,"The Properties of Gases and Liquids", 3rd Ed., McGraw-Hill, 1977.

29. Sirkar K.K., Chem. Eng. Sci., 1977, 32, 1137.

30. Stern S.A., "Gas Permeation Processes", in "Industrial Processing with Membranes", Lacey R.E., Loeb S., and R.E. Krieger, Ed., Huntington NY, 1979; Chap.13.

31. Stern S.A. and Wang S.C., J. Membr. Sci., 1978, 4, 141.

32. Stern S.A., "The Separation of Gases by Selective Permeation", in "Membrane Separation Processes", Mears P., Ed., Elsevier Scientific, NY, 1976, Chap. 8.

33. Stern S.A. and Walawender W.P., Separ. Sci., 1969, 4(2), 129.

34. Stern S.A., Sinclair T.F., Gareis P.G., Vahldieck N.P. and Mohr P.H., Ind. Eng. Chem., 1965, 57, 49.

35. Stern S.A., Onorato F.J. and Libove C., AIChE J., 1977, 23(4), 567.

36. Teslik S. and Sirkar K.K., paper presented at 182nd ACS National Meeting, NY, 23-28 August 1981.

37. Thorman J.M. and Hwang S.T., Chem. Eng. Sci., 1978, 33, 15.

38. Thorman J.M., "Engineering Aspects of Capillary Gas Permeators and the Continuous Membrane Column", Ph.D. Thesis, University of Iowa, Iowa City, Iowa, 1979.

39. Toi K., Morel G. and Paul D.R., J. Appl. Polym. Sci., 1982, 27, 2997.

40. Varga O.H., "Stress-Strain Behavior of Elastic Materials", Interscience, NY, 1966.

41. Walawender W.P. and Stern S.A., Separ. Sci., 1972, 7, 553.

42. Weller S. and Steiner W.A., Chem. Eng. Progress, 1950, 46(11), 585.

43. White R. E., Ind. Eng. Chem. Fundam., 1978, 17(4), 369.

44. Youn K.C., Blytas G.C. and Wall H.H. III, paper presented at GPA Regional Meeting, Houston, Nov. 17, 1982.

LIST OF FIGURES

7 Effects of feed composition on the characteristic curves. Fiber ID= 150 μm. OD= 300 μm. NF= 9×10^5. p_{1L}= 44.1 psia.

8 Effects of feed composition on membrane area requirement relative to NF= 9×10^5. Fiber ID= 150 μm. OD= 300 μm. p_{1L}= 44.1 psia.

9 Effects of feed pressure on characteristic curves. Fiber ID= 150 μm. OD= 300 μm. NF= 9×10^5. p_{1L}= 44.1 psia.

10 Effects of feed pressure on membrane area requirement relative to NF= 9×10^5. Fiber ID= 150 μm. OD= 300 μm. NF= 9×10^5. p_{1L}= 44.1 psia.

11 Example of a two-compression-stage separator system.

LIST OF TABLES

NOTATION

a	total membrane area in a separator module
D_{DA}, k_{DA}, F_A, C'_{HA}, b_A	dual-mode parameters of A, see Table 2
ID, OD	inside and outside diameter of the hollow fiber
$H(z-z_w)$	the unit step-function
ℓ	the "effective" thickness of the asymmetric fiber wall
$m_{fA,f}$	initial molar flow rate of A in the feed per fiber
m_{pA}	local molar flow rate of A in the fiber bore per fiber
m_p	local total permeate molar flow rate per fiber
MT	membrane type
N_A	local permeation flux of component A
NF	total number of fibers in the module
p_1	local permeate total pressure in the fiber bore
p_{1L}	total permeate pressure at the open end of the fiber
p_2	feed side total pressure
R	universal gas constant
T	temperature
Y_{1A}	local mole fraction of A in the permeate stream
Y_{2A}	local mole fraction of A in the shell stream (feed side)
z	distance from the closed end of the fiber
z_w	the effective length of the fiber
z_L	total length of the fiber
μ	viscosity

subscript 0 indicates the residue end of the module
L indicates the permeate exit end of the module
1 the permeate side
2 the shell side (feed side)
A or B indicates component A or B

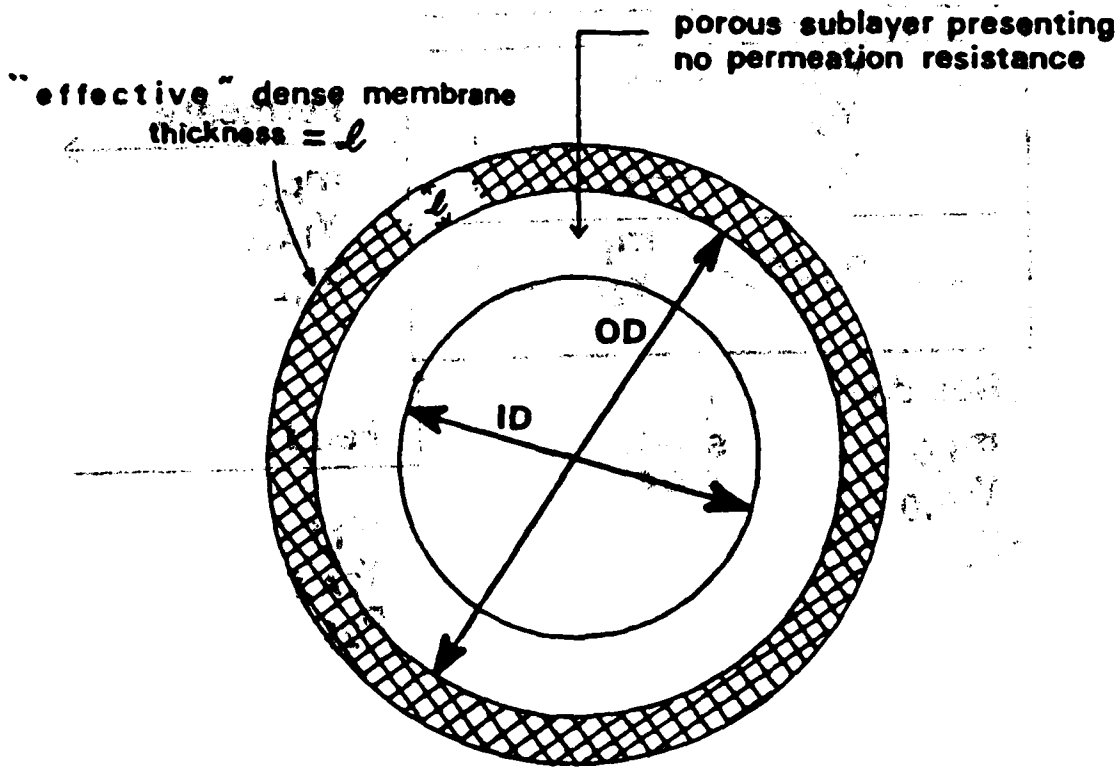

cross section of an asymmetric hollow fiber

Figure 1 A highly simplified description of the permeation resistance of a hollow fiber wall.

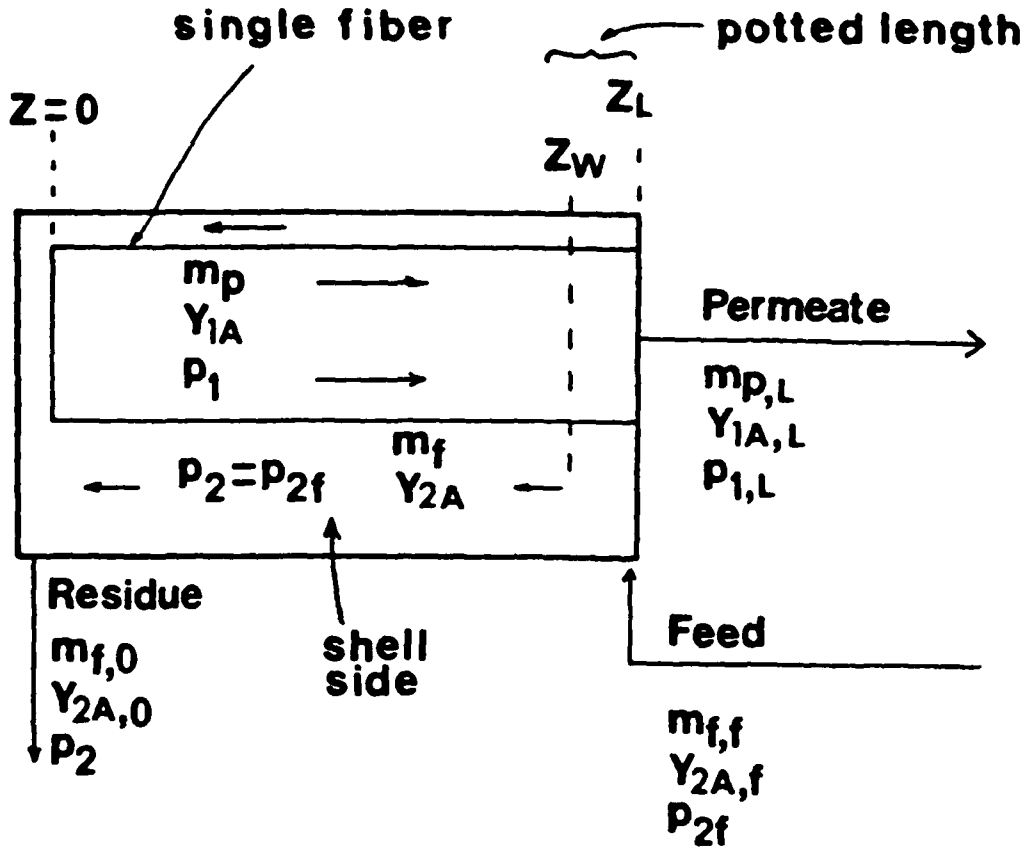

Figure 2 Notation used for the development of model equations.

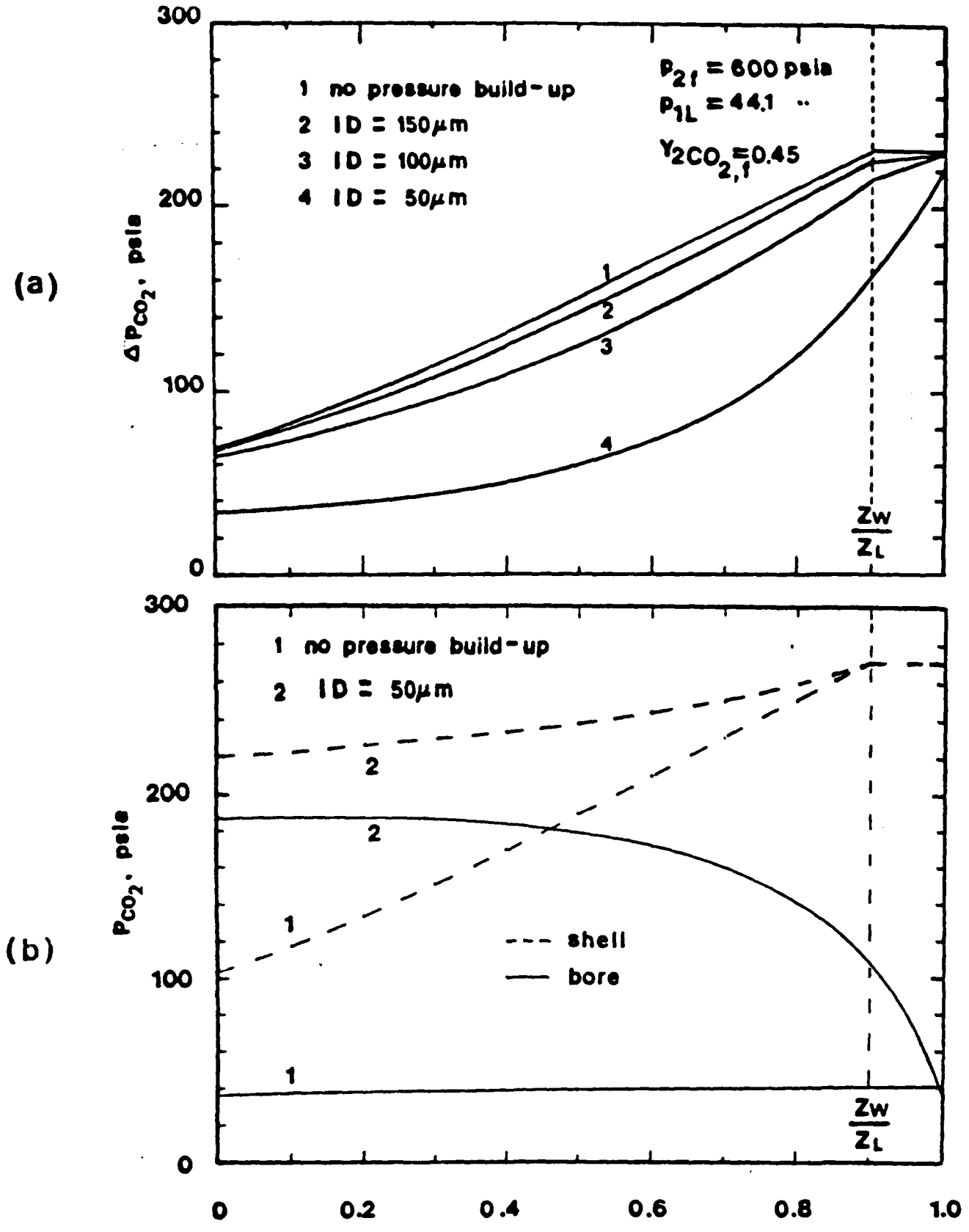

Figure 3 Effects of fiber ID on CO_2 (the fast gas)
(a) Partial pressure difference across the fiber wall.
(b) Shell-and tube-side partial pressure.
Fiber OD = 300μm, NF=9x10^5, feed rate = 126,374 SCFH.

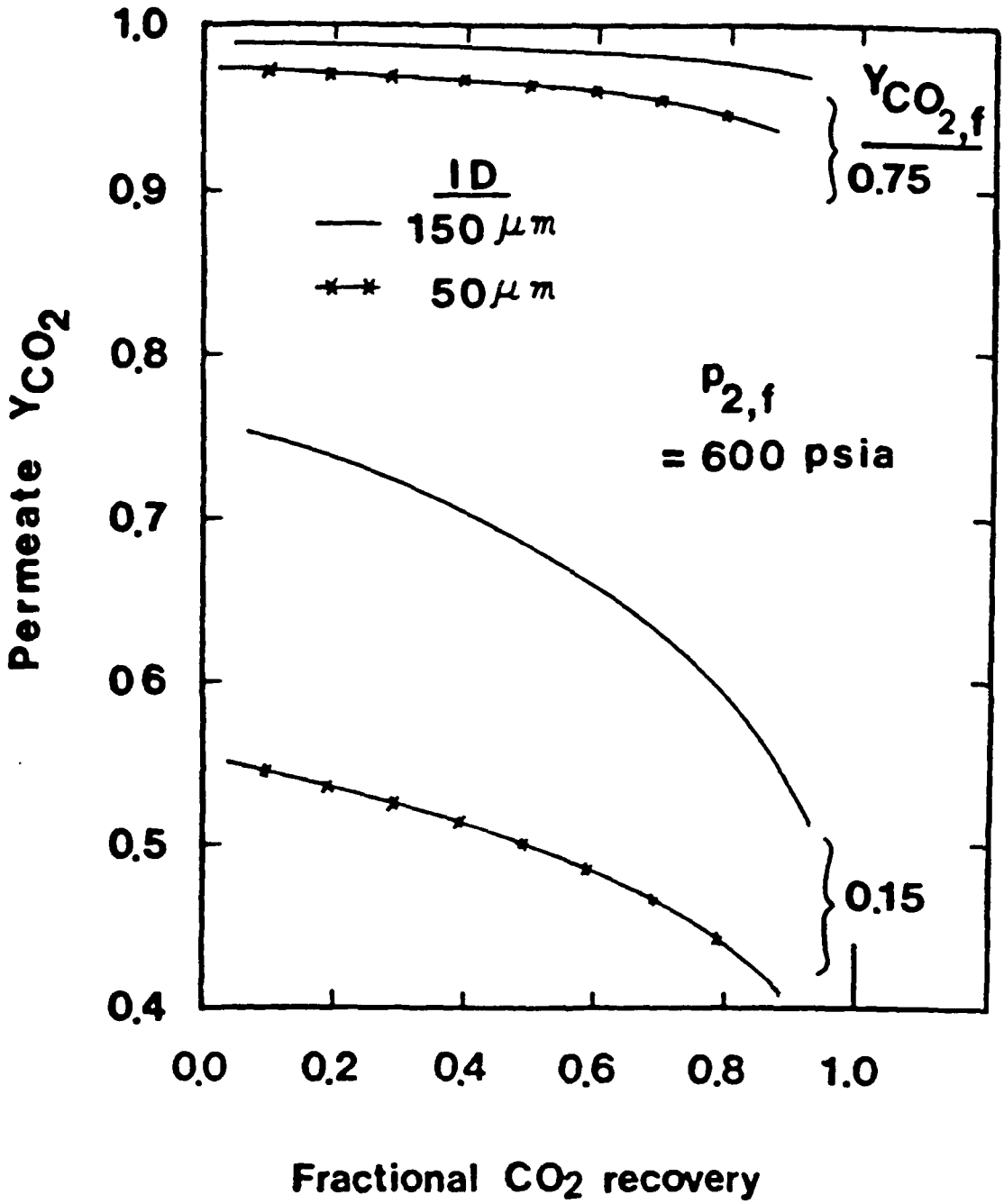

Figure 4 Effects of fiber inside diameter on the characteristic curves. OD= 300 μm, NF=9×10^5, feed rate= 126,374 SCFH. p_{1L}= 44.1 psia.

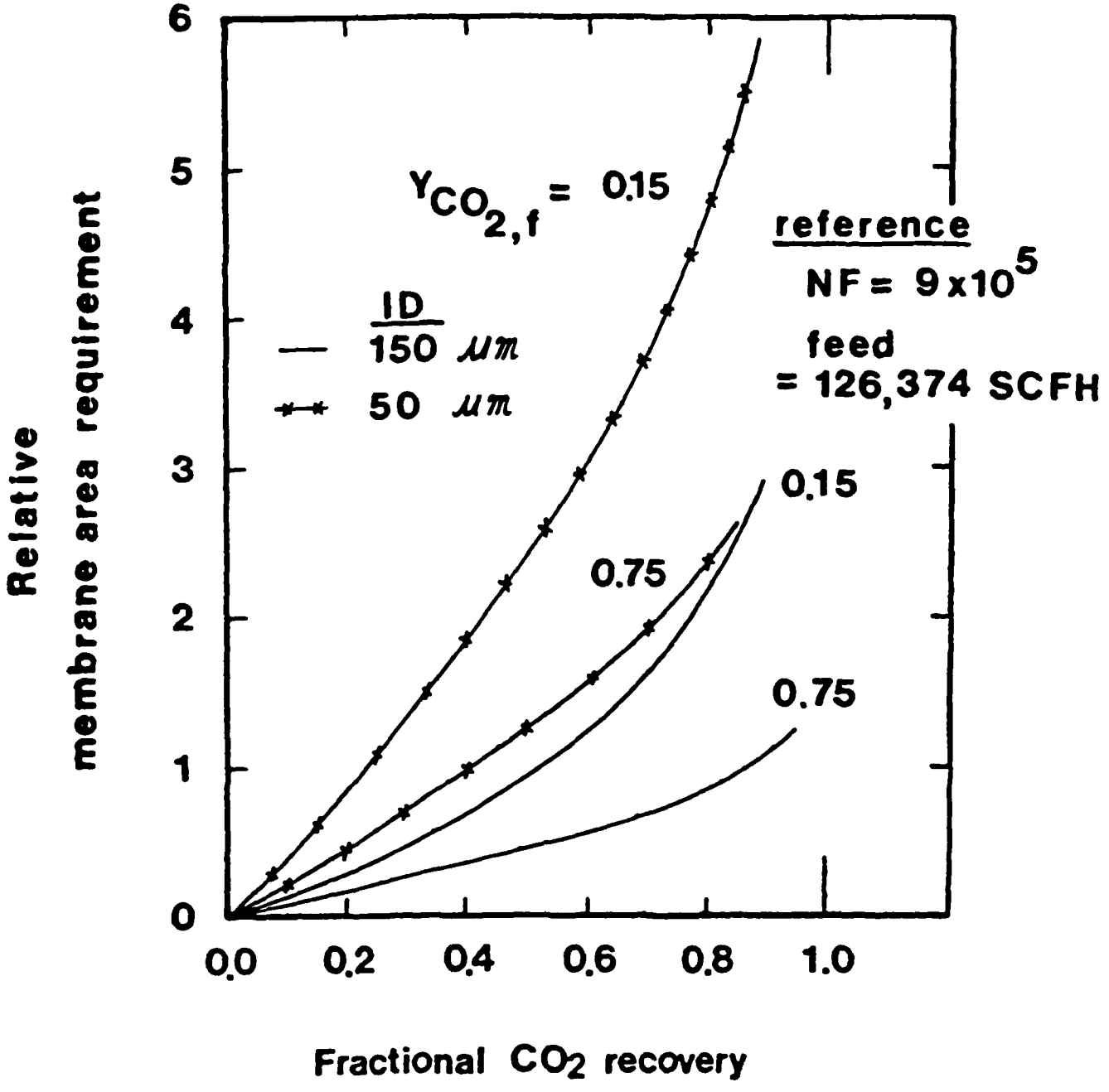

Figure 5 Effects of fiber inside diameter on membrane area requirement relative to NF=9×10^5. Feed rate = 126,374 SCFH. p_{1L} = 44.1 psia.

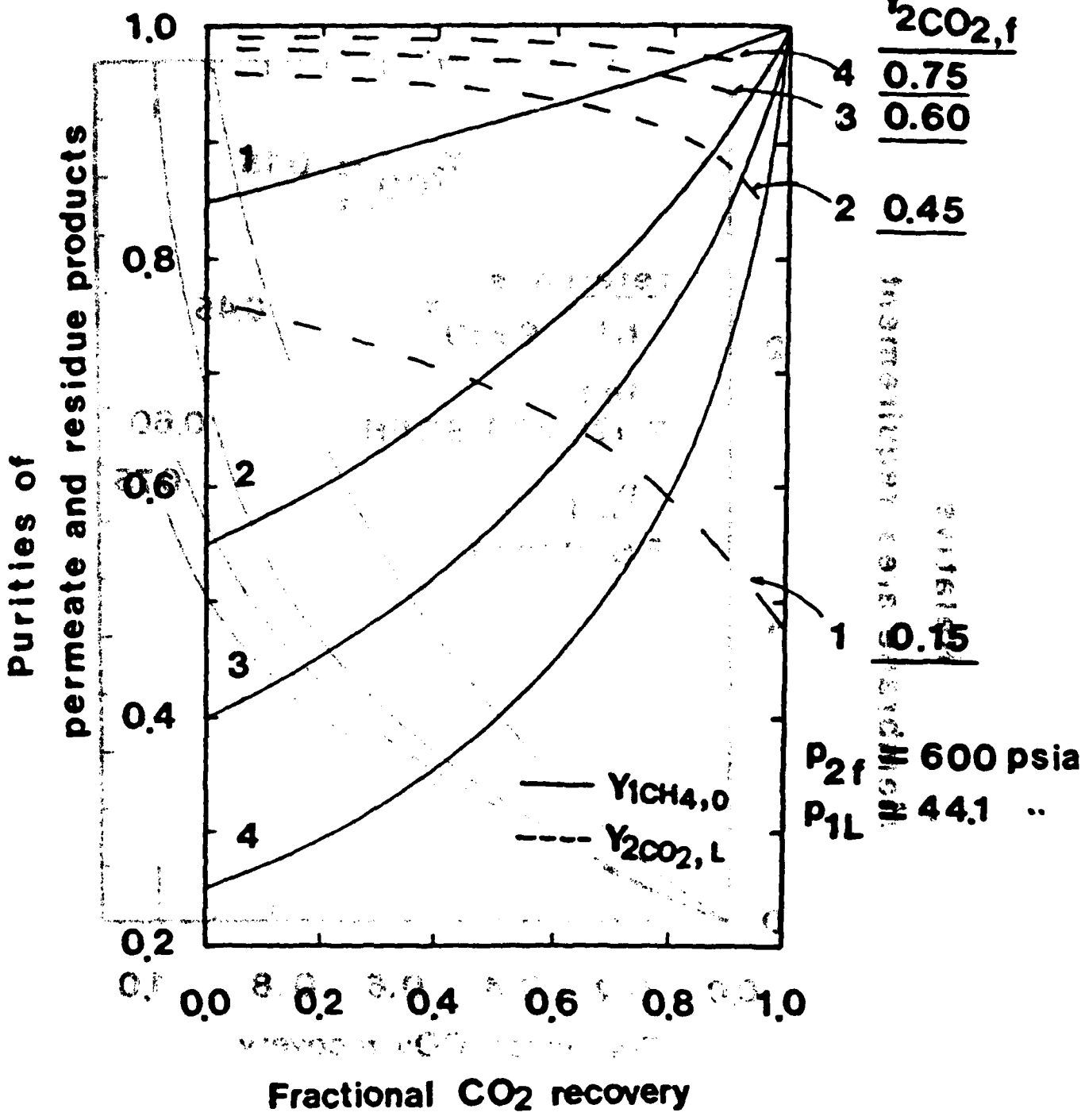

Figure 7 Effects of feed composition on the characteristic curves. Fiber ID= 150μm, OD= 300μm, NF= 9×10^5.

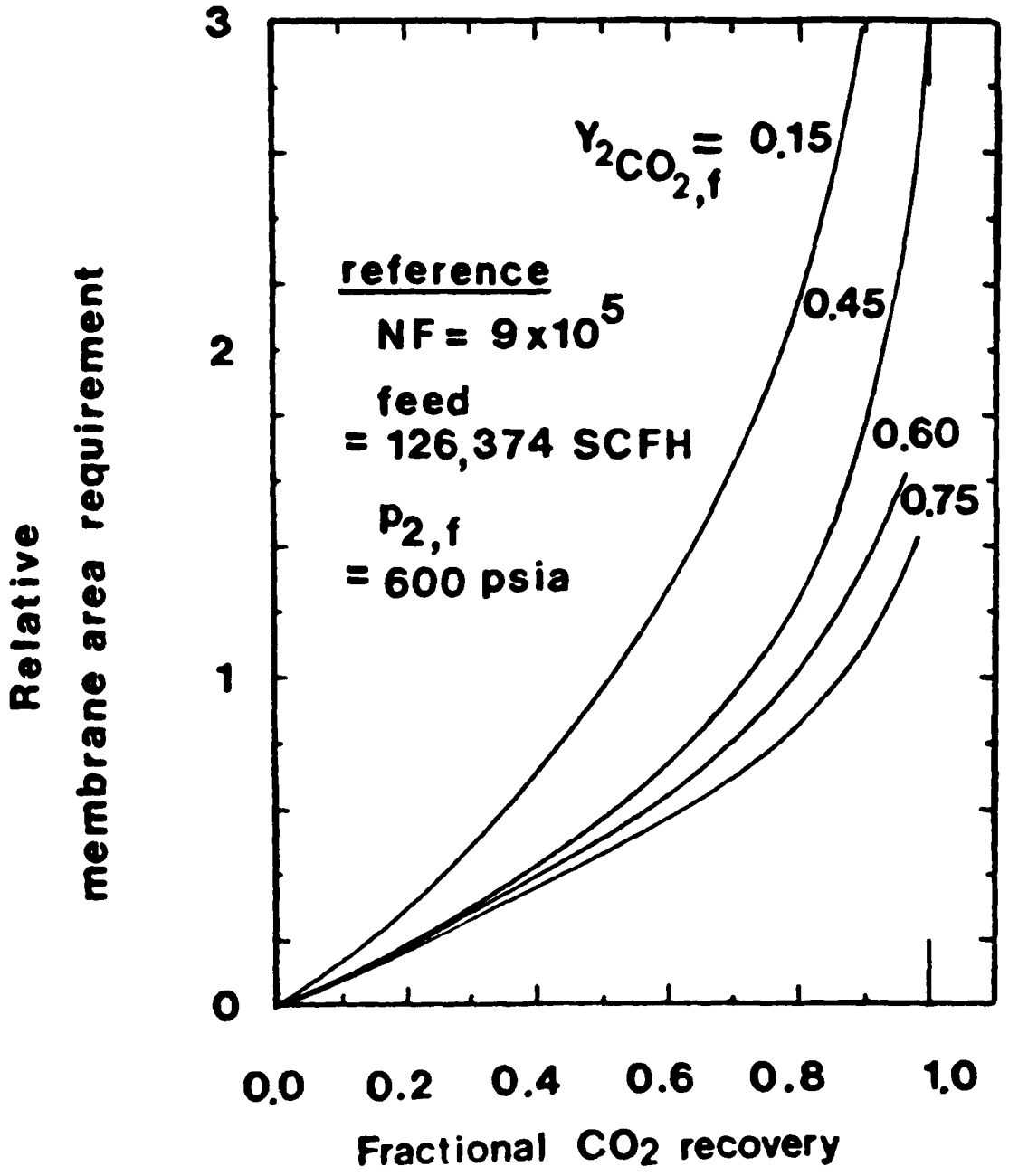

Figure 8 Effects of feed composition on membrane area requirement relative to NF= 9×10^5. Fiber ID= 150 μm. OD= 300 μm. P_{1L} = 44.1 psia.

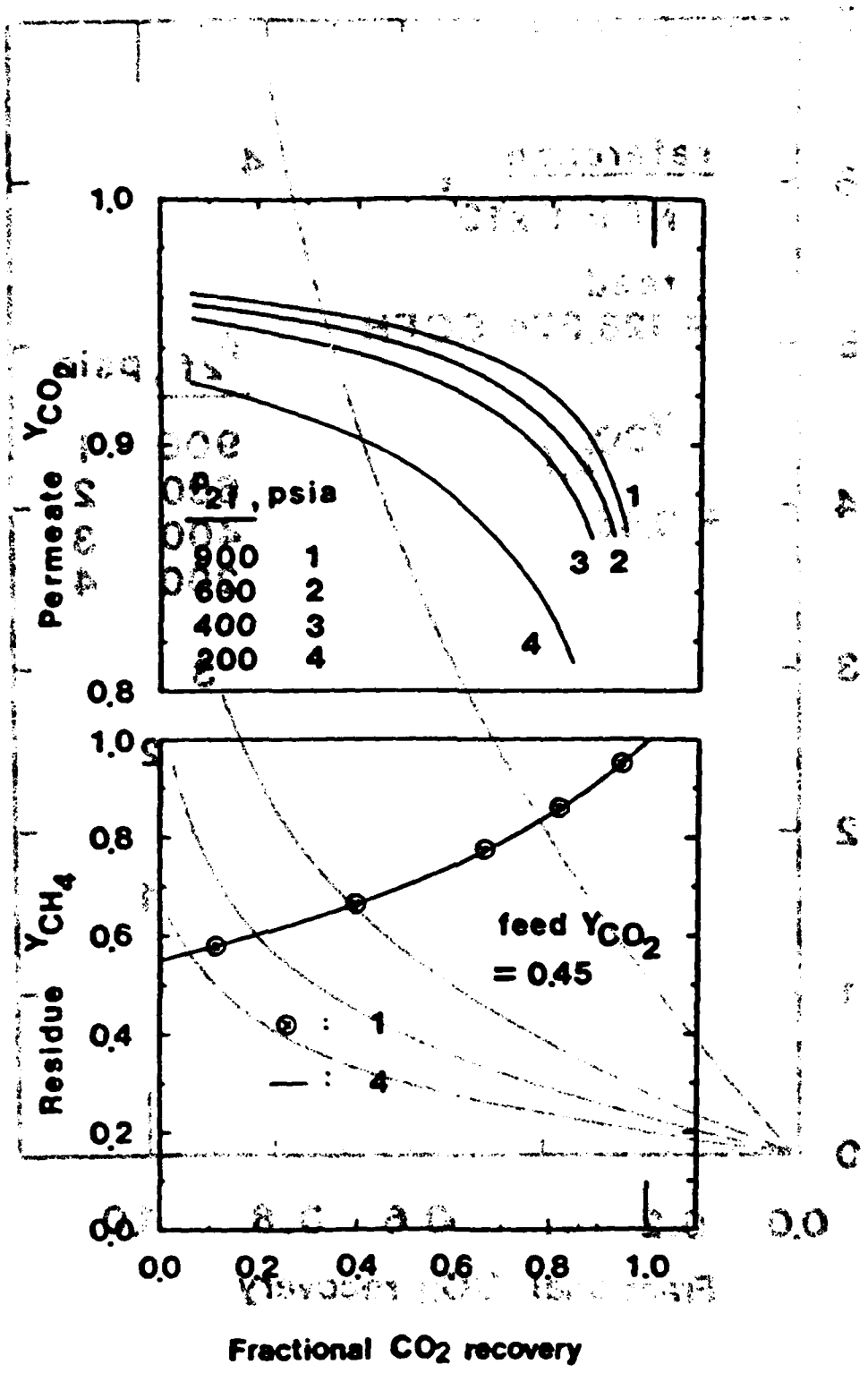

Figure 9. Effects of feed pressure on characteristic curves. Fiber ID= 150μm, OD= 300μm, NF= 9×10^5, p_{1L}= 44.1 psia.

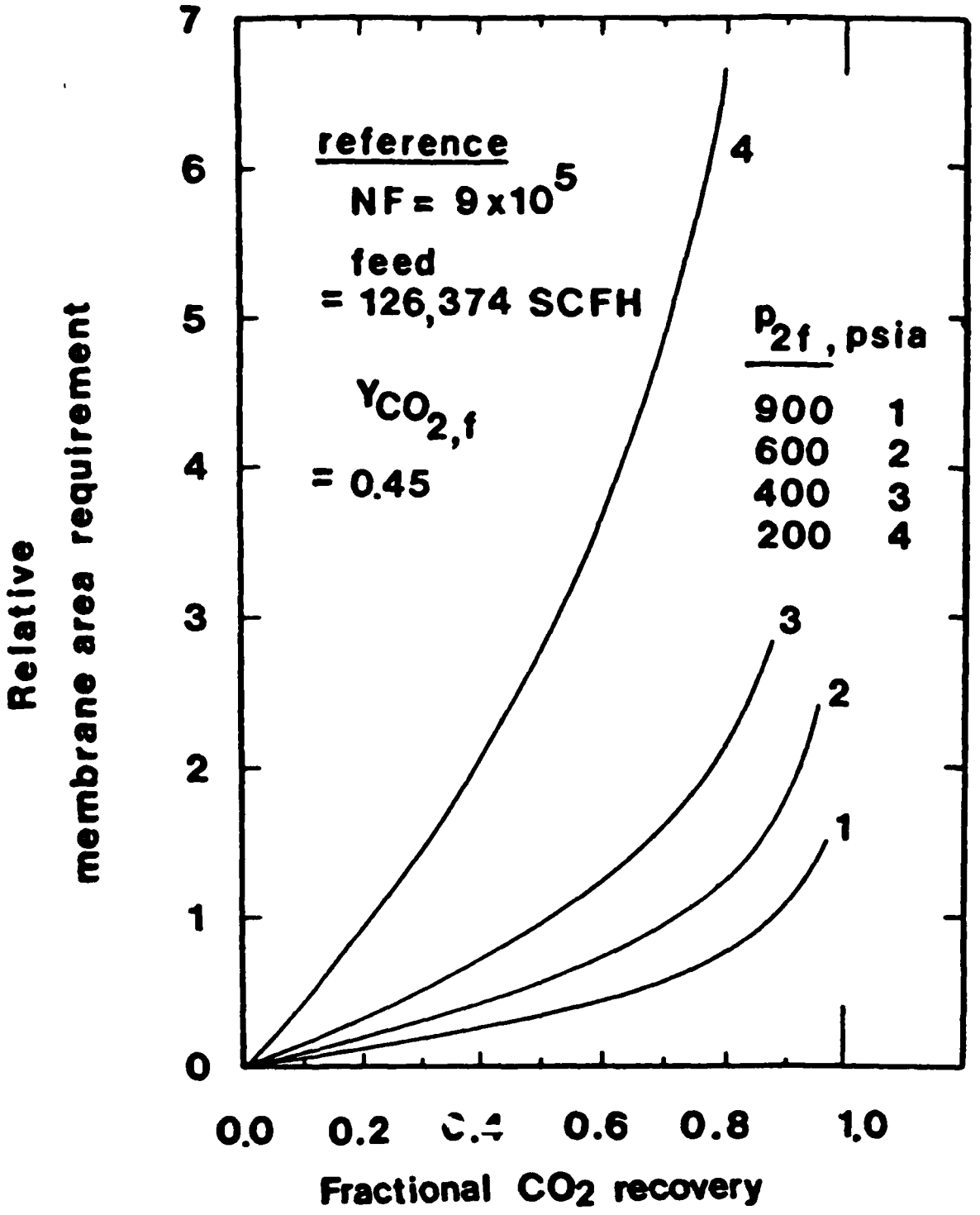

Figure 10 Effects of feed pressure on membrane area requirement relative to NF= $9x10^5$. Fiber ID= 150 μm. OD=300 μm. p_{1L}= 44.1 psia.

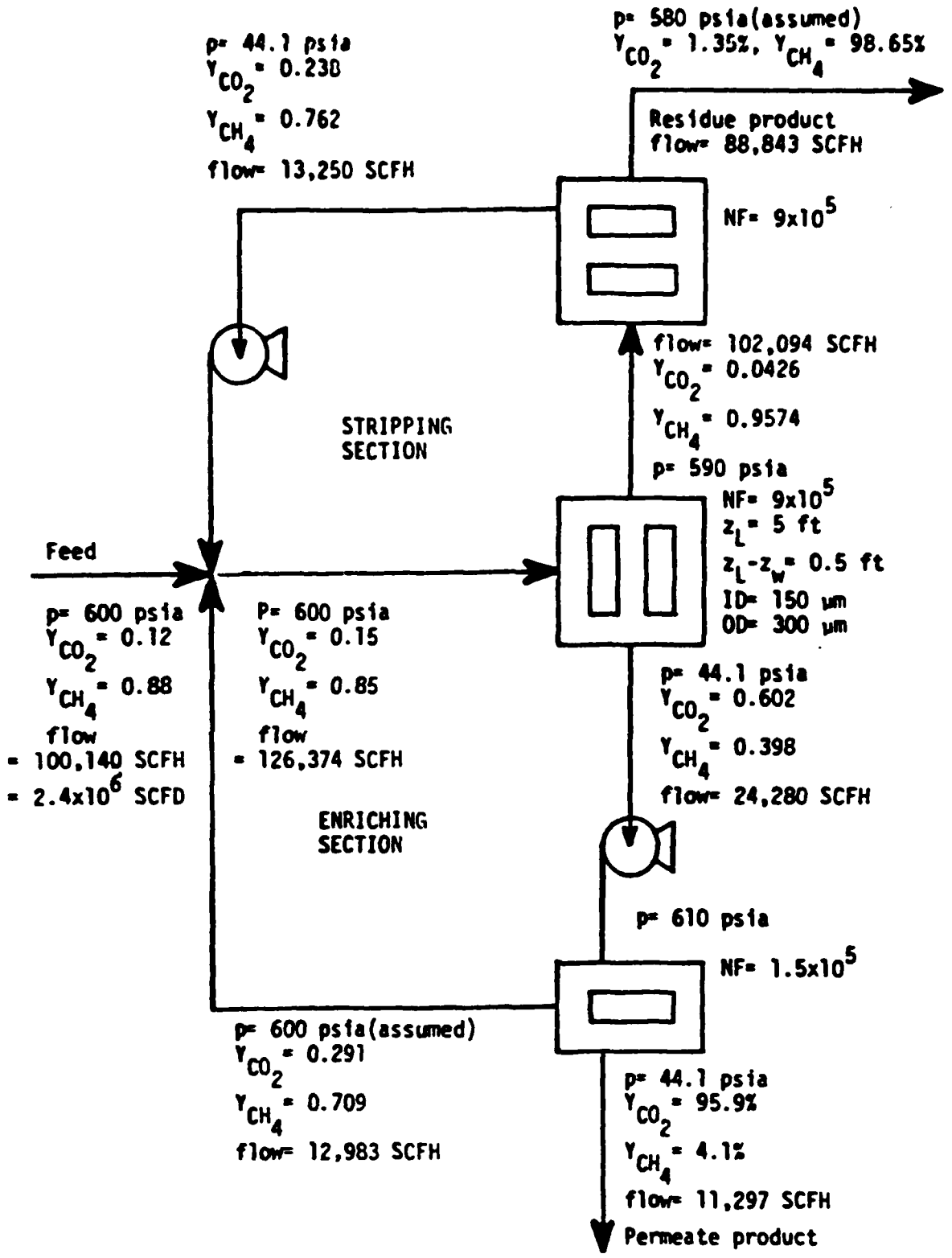

Figure 11 Example of a two-compression-stage separator system.

Table 1 Separator dimension and operation condition ranges used in the calculation.

Polymer	Polysulfone or Polycarbonate
Temperature	$35^{o}C$
Feed	Pressure e.g. 600 psia Composition e.g. CO_2/CH_4 mixture, $Y_{2CO_2f} = 0.45$
Permeate	Pressure 44.1 psia
Fiber dimensions	ID e.g. 50 μm OD 300 μm z_L 152.4 cm $(z_L - z_w)$ 15.2 cm Number of fibers (NF) e.g. 9×10^5 Effective membrane thickness ℓ = 1000 Å

Table 2 Dual-made parameters* of pure gases at 35°C.

Polymer	Penetrant	k_D, $\frac{CC(STP)}{cm^3\ atm}$	C_H', $\frac{CC(STP)}{cm^3}$	b, atm^{-1}	$D_D \times 10^8$ $\frac{cm^2}{sec}$	F
Polysulfone	CO_2	0.664	17.90	0.326	4.40	0.105
	CH_4	0.161	9.86	0.070	0.444	0.349
Polycarbonate	H_e	0.0145	0.313	0.0121	550	1.33
	CH_4	0.147	8.38	0.0841	1.09	0.115

*According to the dual-mode model, the diffusive flux $N = -D_D \frac{dC_D}{dx} - D_H \frac{dC_H}{dx}$;

Total sorption concentration $C = C_D + C_H$, and

$$C_D = k_D p$$

$$C_H = \frac{C_H' b p}{1 + bp}$$

$F = D_H/D_D$, where p is the pressure of the penetrant in the gas phase.

Table 3 Effects of permeate pressure build-up on the performance of a hollow fiber separator.

	permeate CO_2 mole fraction	residue CH_4 mole fraction	permeate production rate, SCFH	% recovery overall CO_2 %	% recovery CH_4 %
no pressure buildup	0.924	0.827	46766	37.0 / 75.8	5.2
fiber ID = 150μm	0.922	0.806	44594	35.3 / 72.2	5.0
100μm	0.916	0.762	39622	31.4 / 63.7	4.8
50μm	0.872	0.633	20918	16.6 / 32.0	3.8

feed rate = 126,374 SCFH
p_{2f} = 600 psia
$Y_{r\eta_2}$ = 0.45
permeate p_{1L} = 44.1 psia
NF = 9×10^5
ID = 150 μm
OD = 300 μm
z_L = 5 ft
$z_L - z_w$ = 0.5 ft
Polysulfone, 35°C

Table 4 The effect of fiber length on separator performance.*

	fiber length, cm	fractional CO_2 recovery	permeate product $Y_{CO_2,L}$	residue product $Y_{CH_4,O}$	total stage cut
ID = 50μm	304.8 (10 ft)	0.27	0.86	0.62	0.14
	152.4 (5 ft)	0.22	0.90	0.61	0.11
No permeate pressure build-up	304.8	0.778	0.920	0.838	0.381
	152.4	0.490	0.946	0.700	0.233

*At the same operating conditions as shown in Table 3.

Table 5 Effects of dual-mode competition on CO_2/CH_4 separation.*

CO_2/CH_4 mixture, $Y_{CO_2,f}$ = 0.45 , Polysulfone at 35°C			
		competition	no competition
CO_2 recovery to the permeate		0.722	0.750
CH_4 recovery to the permeate		0.050	0.062
permeate product Y_{CO_2}		0.922	0.908
residue product Y_{CH_4}		0.806	0.820
permeate production rate SCFH		44,594	47,023
	Z		
local CO_2/CH_4	0.2	6.83	5.99
flux ratio	0.4	10.27	8.73
	0.6	15.06	12.32
	0.8	21.50	16.85

*At the same operating conditions as shown in Table 3.

Table 6 Effect of dual mode competition on He/CH_4 separation.*

Lexan Polycarbonate, 35°C. CH_4/He mixture				
feed	Y_{He} = 0.01		Y_{He} = 0.1	
	competition	no competition	competition	no competition
He recovery to the permeate	0.579	0.669	0.733	0.817
CH_4 recovery to the permeate	0.069	0.069	0.075	0.075
permeate product Y_{He}	0.078	0.089	0.522	0.547
permeate production rate, SCFH	10,572	10,709	20,004	21,275

*At the same operating conditions as shown in Table 3.

20. SEPARATION OF GASEOUS MIXTURES USING POLYMER MEMBRANES

W. J. Koros
Center for Energy Studies
The University of Texas
at Austin
Austin, Texas

and

R. T. Chern
Department of Chemical
Engineering
North Carolina State University
Raleigh, North Carolina

Contents

END

FILMED

7-85

DTIC